

**CHARACTERIZATION, VISUALIZATION AND QUANTIFICATION  
OF SOIL MACROPORES AND PREFERENTIAL FLOW USING  
SPECT AND X-RAY CAT SCANNING**

by

**JOHAN S. PERRET**

A thesis submitted to the Faculty of Graduate  
Studies and Research in Partial Fulfilment  
of the requirements for the degree of

**DOCTOR OF PHILOSOPHY**

Department of Agricultural and Biosystems Engineering  
Macdonald Campus of McGill University  
Montreal, Quebec, Canada

© J.S. Perret, August, 1998



# ABSTRACT

Johan Perret

Ph.D. (Agr. Eng.)

The presence of soil macropores provides an opportunity for water and associated chemicals to move preferentially through the vadose zone. Most studies on the characterization of macropore flow consider the soil system to be a “black-box”. Thus, efforts to describe macropores in quantitative terms have not yet resulted in a comprehensive theoretical framework that allows for a complete representation of their geometry and their effect on preferential flow.

Macropore networks in four large undisturbed soil columns (850 mm x 77 mm diameter), were quantified and visualized, both in 2-D and 3-D, using X-ray Computer Assisted Tomography (CAT). Macropore quantification included two-dimensional parameters (i.e., number of macropores, macropore size, hydraulic radius, rectangularity and circularity), and three-dimensional and topological parameters (i.e., macropore length, volume, 3-D hydraulic radius, tortuosity, numerical density, coordination number, and connectivity). Pores larger or equal to 1.0 mm in equivalent diameter were readily detected, visualized and quantified. It was found that the average macroporosity of four soil columns varied between 2.1 and 3.8 %. From the hydraulic radius distribution, it was inferred that about 20 % of macropore throats have a diameter of 1.6 mm. It was found that the majority of macropore networks had a length of 40 mm, a volume of 60 mm<sup>3</sup> and a wall area of 175 mm<sup>2</sup>.

Breakthrough of potassium iodide was monitored with X-ray CAT scanning. This approach allowed for real-time examination of flow mechanisms through the macropore and matrix flow domains at various depths along the soil column. Flow in the matrix domain suggested that part of the matrix contains small pores (mesopores) that were connected to macropore networks. It is suggested that the matrix domain should be subdivided into two regions: mesopores and micropores. In addition, the macropore domain should be defined both in terms of macropore geometry and its ability to convey the tracer preferentially.

Single Photon Emission Computer Tomography (SPECT) was also used for the real-time analysis, both in 2-D and in 3-D, of radioactive tracer flow patterns in four soil columns. Our results characterized preferential flow very clearly in soil columns. This technique has never been applied to soil physics and opens new avenues for tracer studies in soils.

Efforts were made to relate the 3-D geometry of macropores to their water and solute conveying abilities. A new multi-region modeling approach was developed to simulate macropore flow in a soil under saturated conditions using an analogy between macropore flow and pipe flow. The macropore domain was divided into two regions, namely the laminar and turbulent regions. A modified version of Poiseuille's law was used to model solute breakthrough in the laminar region. For the turbulent region, a new formula was derived, based on Manning's equation. Modifications were made so that these models took into account macropore tortuosity and the distribution density functions of macropore size and hydraulic radius. This approach provides a reliable approximation of the overall tendency for breakthrough in the macropore domain.



# RÉSUMÉ

Johan Perret

Ph.D. (Génie Agr.)

La présence de macropores entraîne une infiltration rapide, dite préférentielle, de composés chimiques, tels les pesticides, à travers la zone vadose du sol. La plupart des études visant à caractériser le phénomène d'écoulement préférentiel à travers les macropores considèrent le sol tel une "boîte-noire". Ainsi, il n'a pas encore été possible de décrire de façon quantitative l'effet de la géométrie des macropores sur cet important phénomène hydrologique.

Quatre colonnes de sol (850 mm x 77 mm de diamètre) ont été prélevées intactes pour visualiser et quantifier la structure des macropores à l'aide d'un CAT scanner. La quantification des macropores a permis de déterminer leurs morphologies en deux dimensions (diamètre cylindrique équivalent, rayon hydraulique, rectangularité et circularité), ainsi que plusieurs paramètres tri-dimensionnels et topologiques (longueur, volume, rayon hydraulique en 3-D, tortuosité, densité numérique, coordination, et connectivité). Les pores ayant un diamètre cylindrique équivalent supérieur ou égal à 1.0 mm (c.-à-d., les macropores) furent détectés et visualisés sans problème. Nos résultats indiquent que la macroporosité moyenne des quatre colonnes de sol fluctue entre 2.1 et 3.8%. Après avoir étudié la distribution des rayons hydrauliques des macropores, il a été conclu qu'environ 20% des gorges des macropores avaient un diamètre de 1.6 mm. De plus, la majorité des réseaux de macropores avait une longueur de 40 mm, un volume de 60 mm<sup>3</sup> et une surface de parois de 175 mm<sup>2</sup>.

L'infiltration d'iodure de potassium a été suivie par CAT scanning. Cette approche a permis de caractériser en temps réel les mécanismes d'écoulement préférentiel à travers les macropores. L'infiltration à travers la matrice du sol suggère la présence de petits pores (mésopores) connectés aux réseaux de macropores. Pour modéliser l'écoulement dans la matrice du sol, il est recommandé de diviser cette région en deux domaines: les mésopores et les micropores. De plus, nos résultats indiquent que

le domaine des macropores devrait être défini en tenant compte de leurs géométries et de leurs capacités à transmettre un soluté de façon préférentielle.

La technique de SPECT scanning (Single Photon Emission Computed Tomography) a aussi été utilisée pour visualiser en 2-D et 3-D et pour analyser en temps réel l'écoulement d'une solution radioactive à travers les quatre colonnes de sol. Nos résultats indiquent très clairement la présence d'écoulement préférentiel. Cette technique n'avait jamais été introduite jusqu'à lors, dans le domaine de la physique des sols. Cette première ouvre de nouvelles portes pour les études d'infiltration dans le sol.

Les résultats de la quantification des macropores ainsi que ceux obtenus lors des tests d'infiltration nous ont permis de développer un nouveau modèle "multi-régions" pour simuler l'écoulement préférentiel dans un sol saturé. Le domaine des macropores a été divisé en deux régions, à savoir la région laminaire et la région turbulente. Une version modifiée de la loi de Poiseuille a été utilisée pour modéliser l'infiltration du soluté dans la région laminaire. Pour la région turbulente, une nouvelle formule a été dérivée à partir de l'équation de Manning. Les modifications ont été faites afin que ces modèles prennent en considération la tortuosité, la fonction de densité de la dimension des macropores et du rayon hydraulique. Cette approche permet d'obtenir une bonne approximation du phénomène d'écoulement préférentiel.

## ACKNOWLEDGEMENTS

Without the support and confidence of many people, I would not have had the privilege, motivation and courage to undertake this research project. Most certainly, the first person who deserves acknowledgement is my thesis supervisor, Dr. Shiv O. Prasher. I thank Dr. Prasher for his enthusiasm in my research and his confidence in me, which were tremendous sources of motivation throughout the course of my doctoral studies. He committed countless hours of consultation, manuscript revisions and guidance for preparation of this thesis dissertation. Dr. Prasher always made time to thoroughly discuss the issues at hand. My thanks to Dr. Prasher go beyond his supervisory role since for many occasions, he opened the door to his house and shared memorable moments with the rest of our research team and his family.

I wish to express my sincere appreciation to the TIPM laboratory team in Calgary. In particular, I would like to express my special gratitude and appreciation to Dr. A. Kantzas for granting the privilege of access to scanning equipment in his imaging laboratory and for his numerous suggestions. Many thanks go to Kelly Hamilton, who helped me tremendously during the SPECT scanning experiments, and to Daniel Marentette and Kevin Allsopp for their help, great sense of humor and friendship.

Appreciation is also extended to the members of my supervisory committee, consisting of Dr. V. Raghavan, Dr. P. Dutilleul, Dr. P. Schuepp and Dr. R. Broughton, all of whom made useful suggestions during the initial stages of my research.

I would like to thank Steve Hall, Annie Tremblay, Peter Alvo and Preeti Prasher for their editorial comments and useful suggestions for the preparation of my thesis dissertation. I wish also to express my sincere appreciation to Luciano Germani for his friendship and very useful suggestions during the preparation of my presentations.

I wish to convey my gratitude to Dr. C. Langford, who was the principal investigator of this project's funding source, and to the Natural Sciences and Engineering Research Council of Canada (NSERC) who funded this research. I also gratefully acknowledge the additional financial support provided by ESTAC (Environmental Science and Technology Alliance Canada).

Many other people have provided me with help and support during the course of my doctoral studies. Unfortunately, it is not possible to name them all here, but I am sure that they will recognize themselves in these words. Thank you all.

And finally, I wish to thank the people close to my heart who, in an indirect manner, were my strength and true source of motivation. This thesis is dedicated to you, mes chers parents, frères et amis. Annie, merci pour ton aide et la chaleur de ton amour tout au long de mon parcours.

# CONTRIBUTIONS TO KNOWLEDGE

The following are the original contributions to knowledge:

1. In this research project, the capabilities of Single Photon Emission Computed Tomography (SPECT) for visualizing preferential flow in soil were investigated. It was the first time that SPECT was introduced to soil physics. This technique opens new avenues, both in 2-D and in 3-D, for real-time tracer studies in a porous medium, such as soil.
2. A reliable technique was developed to isolate and characterize flow domains in the soil using CAT scanning. This method allowed us to divide the flow field into two domains: (i) the macropore flow domain where rapid transport occurs preferentially, and (ii) the micropore flow domain where solute transport occurs at a much slower rate. To date, demarcation criteria between flow domains were rather arbitrarily defined and difficult to establish.
3. A new multi-region modeling approach, using X-ray CAT scanning to model macropore flow in a soil under saturated conditions, was developed. Efforts were made to relate the 3-D geometry of macropores to their water and solute conveying abilities. Water and solute transport in the macropore domain was modeled using an analogy between macropore flow and pipe flow. The macropore domain was divided into two regions, namely the laminar and turbulent regions. Modeling results suggest

that this approach provides a good approximation for overall breakthrough of solutes in the macropore domain.

4. Several algorithms were developed for the visualization and quantification of soil macropores directly from matrices produced by the CAT scanner. The visualization part of this work allowed us to generate 3-D views of macropore structure to an unprecedented level. Macropore quantification not only included two-dimensional parameters (i.e., number of macropores, macropore size, hydraulic radius, rectangularity and circularity) for each scan, but also took into account three-dimensional parameters that have rarely been computed for soils (i.e., macropores length, volume, 3-D hydraulic radius and tortuosity).
5. Topological macropore properties (i.e., numerical density, coordination number, connectivity and genus) were investigated. Although, in recent years, in the field of petroleum recovery, these topological concepts have been given increased attention, they have not yet been used to describe the spatial characteristics of soil macropore networks.

# TABLE OF CONTENTS

<b>ABSTRACT .....</b>	<b>i</b>
<b>RÉSUMÉ .....</b>	<b>iii</b>
<b>ACKNOWLEDGEMENTS .....</b>	<b>v</b>
<b>CONTRIBUTIONS TO KNOWLEDGE .....</b>	<b>vii</b>
<b>LIST OF TABLES.....</b>	<b>xv</b>
<b>LIST OF FIGURES .....</b>	<b>xvi</b>
<b>LIST OF SYMBOLS, ABBREVIATIONS AND ACRONYMS .....</b>	<b>xxii</b>
<b>CONTRIBUTIONS OF AUTHORS .....</b>	<b>xxv</b>
<b>CHAPTER 1 .....</b>	<b>1</b>
<b>INTRODUCTION .....</b>	<b>1</b>
1.1 Nature and Statement of Problem .....	2
1.2 Need for Further Experimental Studies.....	4
1.3 Objectives.....	5
1.4 Originality of Research Project .....	6
1.5 Scope .....	7
1.6 Thesis Organization.....	8
<b>CHAPTER 2 .....</b>	<b>12</b>
<b>REVIEW OF LITERATURE .....</b>	<b>12</b>
2.1 Soil Pores.....	12
2.1.1 Origins of soil pores .....	13
2.1.1.1 Physiopores.....	13
2.1.1.2 Biopores.....	14
2.1.2 Classification of pores.....	17
2.2 Soil Macropores .....	22
2.2.1 Definition of macropore .....	22
2.2.2 Impacts of soil macropores.....	22
2.2.2.1 Impact on water flow and solutes transport .....	23
2.2.2.2 Impact of macropores on root penetration.....	28
2.2.2.3 Impact of macropores on soil aeration.....	28
2.3 Macroporosity: Physical Characterization .....	29

2.3.1	Indirect approaches.....	30
2.3.2	Direct approaches.....	33
2.4	X-ray Computer Assisted Tomography.....	40
2.4.1	X-ray interaction with matter .....	40
2.4.2	Theory of X-ray attenuation.....	43
2.4.3	Principles of assisted tomography .....	45
2.5	Application of CAT Scanning to Soil Studies.....	49
2.5.1	Conversion of CAT scan data to physical properties .....	50
2.5.2	Bulk density mapping.....	51
2.5.3	Porosity mapping.....	51
2.5.4	Tracer analysis and real-time scanning .....	53
2.6	Single Photon Emission Computed Tomography .....	53
2.6.1	Introduction to single photon emission computed tomography .....	54
2.6.2	Radiopharmaceuticals .....	55
2.6.3	Basic principles and instrumentation .....	56
2.6.4	Image acquisition and processing.....	59
2.6.4.1	Planar imaging .....	59
2.6.4.2	Tomographic imaging.....	60
2.6.5	Application of SPECT scanning.....	61
2.7	Modeling of Water and Solute Transport.....	64
2.7.1	Stochastic approaches.....	64
2.7.2	Phenomenological approaches .....	65
2.7.2.1	Classical approach: convection dispersion models.....	65
2.7.2.2	Multi-region modeling.....	66
2.7.2.3	Pipe flow in the macropore domain.....	68
2.8	Concluding Remarks .....	70
<b>PREFACE TO CHAPTER 3 .....</b>		<b>73</b>
<b>CHAPTER 3 .....</b>		<b>75</b>
<b>3-D VISUALIZATION OF SOIL MACROPOROSITY USING X-RAY CAT</b>		
<b>SCANNING.....</b>		<b>75</b>
3.1	Abstract .....	75
3.2	Résumé .....	76
3.3	Introduction .....	77



3.4	Materials and Methods .....	82
3.4.1	Soil columns .....	82
3.4.2	Computer tomography process.....	85
3.4.3	Matrix conversion and selection of region of interest .....	86
3.4.4	Selection of programming language.....	87
3.4.5	Visualization of soil macroporosity.....	88
3.4.6	Quantification of soil macroporosity.....	92
3.5	Results and Discussion.....	95
3.6	Summary and Conclusions.....	104
<b>PREFACE TO CHAPTER 4 .....</b>		<b>106</b>
<b>CHAPTER 4 .....</b>		<b>108</b>
<b>CHARACTERIZATION OF MACROPORE MORPHOLOGY IN A SANDY LOAM SOIL USING X-RAY COMPUTER ASSISTED TOMOGRAPHY AND GEOSTATISTICAL ANALYSIS .....</b>		<b>108</b>
4.1	Abstract .....	108
4.2	Résumé .....	109
4.3	Introduction .....	111
4.3.1	Soil macropore .....	111
4.3.2	Characterization of macroporosity in soil .....	112
4.4	Materials and Methods .....	115
4.4.1	Columns extraction and soil properties .....	115
4.4.2	Soil column preparation .....	116
4.4.3	CAT scanning.....	117
4.4.4	Calibration and data conversion .....	118
4.4.5	Image generation and visualization of soil macropores .....	120
4.4.6	Characterization of soil macroporosity .....	123
4.4.7	Geostatistical analysis .....	126
4.5	Results and Discussion.....	129
4.5.1	Changes in macroporosity and number of macropores with depth .....	129
4.5.2	Macropore-size distribution with respect to depth .....	132
4.5.3	Hydraulic radius and circularity of soil macropores .....	134
4.5.4	Results of the geostatistical analysis .....	138
4.6	Summary and Conclusions.....	139

<b>PREFACE TO CHAPTER 5 .....</b>	<b>142</b>
<b>CHAPTER 5 .....</b>	<b>144</b>
<b>THREE-DIMENSIONAL QUANTIFICATION OF MACROPORE NETWORKS IN UNDISTURBED SOIL CORES.....</b>	<b>144</b>
5.1 Abstract .....	144
5.2 Introduction .....	145
5.3 Need for 3-D Analysis.....	147
5.4 Terminology .....	148
5.4.1 Macropore .....	148
5.4.2 Macropore network .....	151
5.4.3 Branch .....	151
5.4.4 Tortuosity .....	151
5.4.5 Hydraulic radius in three-dimensions.....	152
5.4.6 Topology of macropore networks .....	153
5.4.6.1 Numerical density of networks .....	153
5.4.6.2 Coordination number .....	153
5.4.6.3 Connectivity and genus of macropore networks .....	154
5.5 Materials and Methods .....	156
5.5.1 Soil cores .....	156
5.5.2 X-ray CAT scanning .....	157
5.5.3 3-D reconstruction of macropores .....	159
5.6 Results and Discussion .....	165
5.6.1 Numerical density, relative position and length of macropore networks .....	165
5.6.2 Volume, wall area and hydraulic radius .....	168
5.6.3 Inclination and tortuosity.....	172
5.6.4 Number of branches, branch-node chart and connectivity .....	174
5.7 Summary and Conclusions .....	179
5.8 Acknowledgements .....	180

<b>PREFACE TO CHAPTER 6 .....</b>	<b>181</b>
<b>CHAPTER 6 .....</b>	<b>184</b>
<b>DEVELOPMENT OF A TWO-DOMAIN SIMULATION APPROACH USING X- RAY CAT SCANNING TO MODEL SOLUTE TRANSPORT IN A SOIL WITH PREFERENTIAL FLOW PATHWAYS .....</b>	<b>184</b>
6.1 Abstract .....	184
6.2 Introduction .....	187
6.2.1 Modeling approaches .....	188
6.3 Materials and Methods .....	192
6.3.1 Soil column .....	192
6.3.2 CAT scanning and macropore characterization .....	193
6.3.3 Column saturation .....	194
6.3.4 Selection of non-reactive solute .....	195
6.3.5 Breakthrough measured by X-ray CAT scanning .....	196
6.3.6 Analysis of the solute breakthrough and recognition of the flow domains .....	198
6.4 Results and Discussion .....	200
6.4.1 Overall breakthrough .....	201
6.4.2 Breakthrough in the matrix domain .....	203
6.4.3 Breakthrough in the macropore domain .....	205
6.4.4 Modeling .....	209
6.5 Summary and Conclusions .....	220
6.6 Acknowledgements .....	222
<b>PREFACE TO CHAPTER 7 .....</b>	<b>223</b>
<b>CHAPTER 7 .....</b>	<b>226</b>
<b>SOIL-CORE BREAKTHROUGH IN INTACT SOIL COLUMNS MEASURED BY SPECT SCANNING .....</b>	<b>226</b>
7.1 Abstract .....	226
7.2 Introduction .....	227
7.3 Single Photon Emission Computed Tomography .....	228
7.4 Materials and Methods .....	230
7.4.1 Soil core extractions and column preparation .....	231
7.4.2 Breakthrough measured by SPECT scanning .....	231

7.4.3	SPECT scanning.....	232
7.4.3.1	Collimator.....	233
7.4.3.2	NaI crystal and photomultiplier tubes.....	233
7.4.3.3	Transformation of the output signal.....	235
7.4.3.4	Dynamic scanning .....	235
7.4.3.5	Planar imaging.....	236
7.4.3.6	Tomographic imaging.....	236
7.4.4	Radiopharmaceutical .....	238
7.4.5	Preprocessing of gamma camera output.....	239
7.5	Results and Discussion.....	241
7.5.1	Visualization of macropore flow .....	241
7.5.2	Effluent breakthrough.....	246
7.6	Summary and Conclusions.....	247
7.7	Acknowledgements .....	247
<b>CHAPTER 8</b>	<b>.....</b>	<b>249</b>
<b>SUMMARY AND OVERALL CONCLUSIONS</b>	<b>.....</b>	<b>249</b>
8.1	2-D and 3-D Visualization and Quantification of Macropores using X-ray CAT Scanning .....	249
8.2	Breakthrough Experiments in Soil Columns Measured by X-ray CAT Scanning and SPECT Scanning.....	252
8.3	Modeling of Preferential Flow and Conservative Solute Transport.....	254
<b>CHAPTER 9</b>	<b>.....</b>	<b>256</b>
<b>RECOMMENDATIONS FOR FUTURE RESEARCH</b>	<b>.....</b>	<b>256</b>
9.1	Recommendations for Extraction, Preparation and CAT Scanning of Large Undisturbed Soil Cores.....	256
9.2	Recommendations for Working with CAT and SPECT Data.....	257
9.3	Recommendations for Improving the Modeling Approach .....	258
9.4	New Research Areas .....	260
<b>CHAPTER 10</b>	<b>.....</b>	<b>262</b>
<b>REFERENCES</b>	<b>.....</b>	<b>262</b>
<b>APPENDIX</b>	<b>.....</b>	<b>280</b>

# LIST OF TABLES

## CHAPTER 2

Table 2.1: Classification of major soil organisms according to body size (After Swift et al., 1979).....	15
Table 2.2: Dimensions of pores formed by plant roots (After Hamblin, 1985).....	17
Table 2.3: Different classifications of pores based on their Equivalent Cylindrical Diameter.....	18
Table 2.4: Studies using CAT scanning for the evaluation of pore structure of intact soil cores.....	37
Table 2.5: Types of interactions of X-rays with matter.....	41

## CHAPTER 3

Table 3.1: Studies using CAT scanning for the evaluation of pore structure of intact soil cores.....	80
Table 3.2: Selected properties of a Chicot soil under a combination of quack grass ( <i>Elytrigia Repens (L.) Nevski.</i> ), white clover ( <i>Trifolium Repens L.</i> ) and wild oat ( <i>Avena Fatua L.</i> ).....	84

## CHAPTER 4

Table 4.1: Selected properties of a Chicot soil under a combination of quack grass ( <i>Elytrigia Repens (L.) Nevski.</i> ), white clover ( <i>Trifolium Repens L.</i> ) and wild oat ( <i>Avena Fatua L.</i> ).....	116
Table 4.2: Summary of the geostatistical analysis for Column 1 based on bulk density matrices generated by X-ray CAT scanning.....	138

## CHAPTER 5

Table 5.1: Different classifications of pores based on their Equivalent Cylindrical Diameter.....	149
Table 5.2: Selected properties of macropore networks for each of the soil columns.....	165

# LIST OF FIGURES

## CHAPTER 2

Figure 2.1:Some organisms living in soil. (After Gibbons and Wilson, 1984).....	14
Figure 2.2:Illustration of flow through (a) a homogenous soil and (b) a soil containing macropores.....	26
Figure 2.3:Schematic diagram showing the breakthrough curves of three types of soil (a) flow in a macroporous soil (b) piston-type flow in a homogeneous soil, (c) flow in a heterogeneous pore system (After Bouma, 1991).....	32
Figure 2.4:Interaction of X-rays with matter in the diagnostic X-ray energy range. $\lambda_1$ and $\lambda_2$ represent the wave length of the incident and scattered radiations respectively. (After Mazziotta and Gilman 1992).....	42
Figure 2.5:Schematic representation of the X-ray attenuation of (a) homogeneous material, (b) heterogeneous material composed of discrete units, (c) heterogeneous material with a variable attenuation coefficient over distance x. (After Greenberg et al. 1983).....	44
Figure 2.6:Principle of a translation-rotation CAT Scanner.....	45
Figure 2.7:Illustration of the coordinate system for the calculation of X-ray attenuation at a given point.....	46
Figure 2.8:Schematic illustration of the CAT scan terminology.....	48
Figure 2.9:Siemens Orbitor Gamma Camera at the TIPM laboratory in Calgary (Alberta).....	56
Figure 2.10: Basic principles and components of a gamma camera.....	58
Figure 2.11:Rotation of the gamma camera around a column of soil.....	60
Figure 2.12:Schematic representation of the two-flow domain system where Q represents flow rate, K the soil's conductivity, D the coefficient of dispersion, V the average velocity in the respective flow domains.....	67

### CHAPTER 3

Figure 3.1:Schematic illustration of the design of the soil column with the artificial macropore.....	83
Figure 3.2:Position of the soil core in the CAT scanner.....	85
Figure 3.3:Cross-sectional images; (a), (b) and (c) contrast enhancement using different color tables, (d) contour map, (e) partial threshold and (f) total threshold of the soil macropores.....	88
Figure 3.4: Longitudinal views of the four soil columns.....	90
Figure 3.5: Three-dimensional reconstruction of soil macropores of the four soil columns. The artificial macropore can be observed in column 4.....	91
Figure 3.6: Partial view of the 2-D array after segmentation.....	93
Figure 3.7: Illustration of the clustering algorithm. (a) Initial matrix. (b) The first pixel is located and the four nearest neighbors are checked for values of 1. (c) The visited pixel changed to a value different than 1 (2 in this case) and the investigation moves to the neighbor having a value of 1 (if two or more neighbors have a value of 1, the algorithm puts them in “memory”). The four new neighbors are evaluated. Two neighboring pixels have a value of 1, therefore, one of them is put in memory (denoted by 1 m). (d) The previous pixel is changed to 2 so that the algorithm will ignore it. None of the four neighboring pixels has a value of 1, thus, the algorithm moves to the pixel in memory. (e) A value 2 is substituted in the previous pixels and the new neighbors are investigated. None have a value of 1 and no pixel in memory can be recalled. (f) The evaluation of this pore is completed.....	94
Figure 3.8: Dry bulk density changes with depth of the soil profile.....	97
Figure 3.9: Number of macropores with respect to depth.....	98
Figure 3.10:Areal distribution of soil macropores with respect to depth.....	99
Figure 3.11:Relative contribution of soil macroporosity with respect to depth.....	100
Figure 3.12:Average equivalent diameter of the soil macropores with respect to depth.....	101
Figure 3.13:Average circularity and rectangularity of soil macropores with respect to depth.....	102

## CHAPTER 4

Figure 4.1: Open view of the gantry of the X-ray CAT scanner (ADVENT HD200 whole body CAT scanner - TIPM laboratory, Calgary).....	118
Figure 4.2: Results of calibration tests performed at 120 kV and 50 mA to determine the relation between the CT numbers and density of various samples.....	119
Figure 4.3: Visualization of cross-sectional images generated by “Jofran.pro”. These cross-sectional images belong to Column 1 and were scanned at (a) 2 mm, (b) 50 mm, (c) 400 mm and (d) 600 mm.....	120
Figure 4.4: Three-dimensional reconstruction of the interconnected network of soil pores and cavities of Column 1. A computer program called “Rview.pro” generated this reconstructed image.....	122
Figure 4.5: Idealized semi-variogram.....	127
Figure 4.6: (a) Original bulk density matrix (262,144 elements); (b) resized matrix containing only 961 data points.....	128
Figure 4.7: Macroporosity variations of the four soil columns with respect to depth.....	129
Figure 4.8: Results of the macropore count for the four soil columns.....	131
Figure 4.9: Macropore-size distributions of four soil columns obtained for different sections of the soil profile.....	133
Figure 4.10: Relative area-size distributions of macropores for one of the four soil columns.....	134
Figure 4.11: Hydraulic radius distributions obtained for different sections of the soil profile.....	135
Figure 4.12: Circularity distributions of four soil columns obtained for different sections of the soil profile.....	137

## CHAPTER 5

Figure 5.1: Tortuosity of a soil macropore.....	151
Figure 5.2: Schematic representation of (a) pore space, (b) coordination number on a branch-node-chart (After Dullien 1992).....	154



Figure 5.3: Illustration of the concept of connectivity and genus. (From Macdonald et al., 1986).....	155
Figure 5.4: View of the rotated gantry of the Advent HD200.....	158
Figure 5.5: Illustration of (a) the “six nearest neighboring voxels and (b) twenty six neighboring voxels; (c) Superposition of consecutive 2-D matrices for the 3-D algorithm.....	161
Figure 5.6: 3-D reconstruction of macropore networks in Column 1.....	162
Figure 5.7: Flow diagram of the PV-WAVE program “Branjo.pro”.....	163
Figure 5.8: Number, relative position and vertical length of macropore networks in the four soil columns.....	166
Figure 5.9: Frequency distributions of the length of macropore networks in the four soil columns.....	168
Figure 5.10: Frequency distributions of volume of macropore networks in the four soil columns.....	169
Figure 5.11: Frequency distributions of wall area of macropore networks in the four soil columns.....	170
Figure 5.12: Hydraulic radius of macropore networks in the four soil columns.....	171
Figure 5.13: Frequency distributions of hydraulic radius of macropore networks in the four soil columns.....	172
Figure 5.14: Frequency distributions of macropore networks inclination.....	173
Figure 5.15: Frequency distributions of tortuosity of macropore networks.....	173
Figure 5.16: Frequency distributions of number of branches per macropore network.....	174
Figure 5.17: Frequency distributions of (a) length and (b) tortuosity of branches for selected Networks of Column 1.....	175
Figure 5.18: Branch-node chart for Network 6 of Column 1.....	176
Figure 5.19: Connectivity of macropore networks and their number of branches (Column 1).....	178

## CHAPTER 6

Figure 6.1: Schematic representation of the two-flow domains system; $Q$ represents flow rate.....	190
Figure 6.2: (a) 3-D view of Column 1 (b) Branch node chart of a macropore network (network 6) running from a depth of 10 to 245 mm.....	194
Figure 6.3: X-ray attenuation coefficient of sodium iodide and potassium iodide; (a) water solution, (b) soil saturated with the tracer solution.....	195
Figure 6.4: Experimental setup used to maintain a constant water head ① Constant head apparatus, ② pump activated/ deactivated with a float, ③ one-way valve, ④ water stored at higher potential energy.....	197
Figure 6.5: Three-dimensional representation of concentration of potassium iodide at different depths and times. (a) depth=50 mm, time=14.27 min; (b) depth=100 mm, time=14.78 min; (c) depth=150 mm, time=15.28 min; (d) depth=200 mm, time=15.83 min; (e) depth=250 mm, time=16.50 min; (f) depth=350 mm, time=20.03 min; (g) depth=450 mm, time=20.97 min; (h) depth=500 mm, time=21.67 min; (i) depth=650 mm, time=23.90 min.....	198
Figure 6.6: Cross-sectional views of the soil column at depth (1) 50 mm, (2), 450 mm and 650 mm; (a) dry conditions, (b) position of macropore networks and (c) tracer flux in the macropore and matrix domains.....	199
Figure 6.7: Breakthrough curves measured at thirteen depths along the soil column and in the effluent.....	201
Figure 6.8: Tracer breakthrough in the matrix domain.....	204
Figure 6.9: Tracer breakthrough in the macropore domain.....	205
Figure 6.10: 3-D reconstruction of macropore network 6 with some of its dead-end macropores.....	206
Figure 6.11: Number of macropore branches and normalized time to reach a relative concentration of 0.8 for every scanned positions.....	207
Figure 6.12: Observed and fitted breakthrough curves in the matrix flow domain for selected depths. $R^2$ is the coefficient of determination of the regression between observed versus simulated values; $V$ is the average pore-water velocity and $D$ is the hydrodynamic dispersion coefficient.....	209

Figure 6.13: Schematic representation of macropores using the analogy with tubular reservoirs.....	211
Figure 6.14: Observed and modeled breakthrough in the macropore domain at (a) depth=200 mm, (b) depth=350 mm and (c) depth=550 mm.....	217
Figure 6.15: Schematic representation of the improved multi-regions system.....	219
<b>CHAPTER 7</b>	
Figure 7.1: Siemens Orbiter Gamma Camera at the TIPM laboratory in Calgary (Alberta).....	232
Figure 7.2: Basic principles and components of a gamma camera.....	234
Figure 7.3: Rotation of the gamma camera around a column of soil.....	237
Figure 7.4: Comparison of the radioactivity level of Technetium in water and in soil at different concentrations.....	238
Figure 7.5: Schematic representation of the breakthrough of the radioactive tracer in the top region of the soil column.....	241
Figure 7.6: Three-dimensional representation of $^{99m}\text{Tc}$ flux at different times after injection; (a) 25s, (b) 50s, (c) 75s, (d) 100s, (e) 125s, (f) 150s, (g) 200s, (h) 300s, (i) 400s, (j) 500s, (k) 750s and (l) 1000s.....	243
Figure 7.7: Relation between 3-D macropore space and tracer flux. 3-D reconstructions of macropore networks are shown for (a) Column 1 and (c) Column 4; the spatial distributions of tracer were evaluated at (b) 165 seconds in Column 1 and (d) 80 seconds in Column 4 after tracer injection.....	244
Figure 7.8: Three-dimensional reconstructions of the breakthrough in Column 4 obtained by SPECT scanning. The reconstructions represent 3-D tracer distribution at different time after injection: (a) 2 min; (b) 4 min; (c) 6 min; (d) 8 min; (e) 10 min; (f) 12 min; (g) 14 min; (h) 16 min; (I) 8 min.....	245
Figure 7.9: Breakthrough curves observed in the effluent of Column 1, 2 and 3.....	246

# LIST OF SYMBOLS, ABBREVIATIONS AND ACRONYMS

$A_{\text{cross-section}}$	Cross-sectional area of macropore [ $\text{mm}^2$ ]
$A_{\text{box}}$	Area of bounding box fitted around the macropore [ $\text{mm}^2$ ]
$b$	Intercept of calibration line for CT conversion [HU]
BTC	Breakthrough Curve
$C$	Solute concentration in CDE [ $\text{g}/\text{mm}^3$ ]
$C/C_0$	Relative concentration [ $\text{g}/\text{g}$ ]
CAT	Computer Assisted Tomography
$C_{\text{circ}}$	Circularity of macropore [dimensionless]
$C_{\text{con}}$	Connectivity [dimensionless]
CDE	Convection Dispersion Equation
CEC	Cation Exchange Capacity [ $\text{cmol}/\text{kg}$ ]
CT	Computed Tomography
CTn	Computed tomography number [HU]
$D$	Sample thickness [m]
$d$	Effective pore diameter [m]
$d_{\text{eq}}$	Equivalent cylindrical diameter of pores [mm]
$D_c$	Coefficient of hydrodynamic dispersion in CDE [ $\text{m}^2/\text{s}$ ]
$d_{\text{critical}}$	Macropore diameter at which transition between laminar and turbulent occurs [m]
$D_{\text{macro}}$	Hydrodynamic dispersion in the macropore flow domain [ $\text{mm}^2/\text{s}$ ]
$D_{\text{matrix}}$	Hydrodynamic dispersion in the matrix flow domain [ $\text{mm}^2/\text{s}$ ]
$E$	energy of the incident X-ray beam [eV]
ECD	Equivalent Cylindrical Diameter [mm]
$f_r(z,r)$	Distribution density function of macropore hydraulic radius at depth $z$
$f_s(z,r)$	Distribution density function of macropore size at depth $z$

$g$	Acceleration due to gravity [ $\text{m/s}^2$ ]
$G$	Genus [dimensionless]
$h$	Hydrostatic suction or the capillary rise [m]
$h$	Lag distance [mm]
HU	Hounsfield Unit [dimensionless]
$I$	Transmitted X-ray beam intensity [eV]
I/O	Input/Output
$I_o$	Incident X-ray beam intensity [eV]
$K_{\text{macro}}$	Macropore hydraulic conductivity [m/day]
$K_{\text{matrix}}$	Matrix hydraulic conductivity [m/day]
$L$	Shortest distance measured along a pore [m]
$L_e$	Effective average path length of a pore [m]
$m$	Slope of calibration line for CT conversion [dimensionless]
MRI	Magnetic Resonance Imaging
OM	Organic Matter content [g/g]
$P$	Perimeter of macropore [mm]
$P_{(r,\phi)}$	Projection value [dimensionless]
$Q_{\text{pore}}$	Flow rate in a pore [ $\text{m}^3/\text{s}$ ]
$Q_{\text{macropore}}$	Flow rate in the macropore flow domain [ $\text{m}^3/\text{s}$ ]
$Q_{\text{matrix}}$	Flow rate in the matrix flow domain [ $\text{m}^3/\text{s}$ ]
$r$	Equivalent cylindrical radius of the capillary [m]
$R$	Retardation factor in CDE model [dimensionless]
$r_{\text{critical}}$	Macropore radius at which transition between laminar and turbulent occurs [m]
$Re$	Reynolds Number [dimensionless]
$R_h$	Hydraulic radius [mm]
ROI	Region of Interest
$R_{\text{rec}}$	Rectangularity of macropore [dimensionless]
SPECT	Single Photon Emission Tomography
$T$	Time [s]
TIPM	Tomographic Imaging and Porous Media

$V$	Average pore-water velocity in CDE [mm/s]
$V_{\text{macro}}$	Flow velocity in the macropore flow domain [m/day]
$V_{\text{matrix}}$	Flow velocity in the matrix flow domain [m/day]
$z$	Vertical position along flow path [mm]
$Z$	Coordination number [dimensionless]
$Z_n$	Atomic number

### *Greek Symbols*

$\alpha$	Klein-Nishina coefficient [ $\text{m}^2/\text{kg}$ ]
$\beta$	Constant, $9.8 \times 10^{-24}$ [ $\text{m}^2 \cdot \text{eV}^{3.2}/\text{kg}$ ]
$\Delta H$	Hydraulic potential [m]
$\phi$	Porosity [ $\text{mm}^3/\text{mm}^3$ ]
$\gamma(h)$	Semi-variance
$\lambda_1$	Wave length of the incident radiation [m]
$\lambda_2$	Wave length of the scattered radiation [m]
$\eta$	Dynamic viscosity [ $\text{kg}/\text{m} \cdot \text{s}$ ]
$\eta_r$	Roughness coefficient in Manning's equation
$\mu$	Linear attenuation coefficient [ $\text{m}^{-1}$ ]
$\mu_w$	Linear attenuation coefficient of water [ $\text{m}^{-1}$ ]
$\nu_k$	Kinematic viscosity [ $\text{m}^2/\text{s}$ ]
$\rho_g$	Mineral grain density [ $\text{kg}/\text{m}^3$ ]
$\rho$	Bulk density [ $\text{kg}/\text{m}^3$ ]
$\sigma$	Surface tension [ $\text{kg}/\text{s}^2$ ]
$\tau$	Tortuosity [m/m]
$\varpi$	Gravimetric water content [g/g]
$\omega$	Contact angle of water [degree]

## CONTRIBUTIONS OF AUTHORS

The following is a statement from the faculty of Graduate Studies and Research concerning manuscript-based theses:

Candidates have the option of including, as part of the thesis, the text of a paper(s) submitted or to be submitted for publication, or the clearly-duplicated text of a published paper(s). These texts must be bound as an integral part of the thesis.

If this option is chosen, **connecting texts that provide logical bridges between the different papers are mandatory**. The thesis must be written in such a way that it is more than a mere collection of manuscript; in other words, results of a series of papers must be integrated.

The thesis must still conform to all other requirements of the Guidelines for Thesis Preparation. **The thesis must include:** A Table of Contents, an abstract, in English and French, an introduction which clearly states the rationale and objectives of the study, a comprehensive review of the literature, a final conclusion and summary, and a thorough bibliography or reference list, at the end of the thesis, after the final conclusion and summary.

Additional material must be provided where appropriate (e.g. in appendices) and in sufficient detail to allow a clear and precise judgement to be made of the importance and originality of the research reported in the thesis.

In the case of manuscripts co-authored by the candidate and others, **the candidate is required to make an explicit statement in the thesis as to who contributed to such work and to what extent**. Supervisors must attest to the accuracy of such statement at the doctoral oral defence. Since the task of the examiners is made more difficult in these cases, it is in the candidate's interest to make perfectly clear the responsibilities of all the authors of the co-authored papers. **Under no circumstances can a co-author of any component of such a thesis serve as an examiner for that thesis.**

The candidate was responsible for designing and conducting the research experiments, developing computer codes for the visualization and analysis of data and

preparation of manuscripts and thesis dissertation. Dr. Shiv O. Prasher, professor at the Agricultural and Biosystems Engineering Department of McGill University, contributed in all aspects of this research project. He provided the necessary funds and assistance for this research, including the supervisory guidance and reviewing of manuscripts before their submission for publication. Dr. A. Kantzas, Director of the Tomographic Imaging and Porous Media (TIPM) Laboratory in Calgary, Alberta, and associate professor at the University of Calgary's Department of Chemical and Petroleum Engineering, provided access to CAT and SPECT scanning facilities of the TIPM laboratory. Dr. Kantzas also made invaluable suggestions during CAT and SPECT scanings. Ms. K. Hamilton, nuclear research technologist at TIPM laboratory, provided help and guidance during SPECT scanning. Dr. C. Langford, University of Calgary's vice-president research and professor at the Department of Chemistry, was the principal investigator for the NSERC Collaborative Project Grant which provided major funding for this project.



# CHAPTER 1

## INTRODUCTION

---

Transport of water and associated solutes through soil has always been an important subject to soil hydrologists concerned with topics such as nutrient movement through soil and water availability to plants. More recently, due to the mounting worldwide concern about groundwater contamination by toxic chemicals, a whole new interest in water movement and contaminant transport through soil has emerged.

In the last two decades, there has been an unprecedented increase in the use of pesticides and fertilizers. Between 1970 and 1989, the global use of fertilizers has almost doubled (Brown, 1989). The use of pesticides has also increased dramatically. For example, the amount of pesticides applied on farms in the U.S. increased by 170 percent between 1964 and 1982 (Lal and Stewart, 1994). About 19 billion kg of fertilizer and 450 million kg of pesticides are used annually in the US (OTA, 1990). In Canada, more than 2 billion kg of fertilizers and 33 million kg of pesticides are applied on farmlands every year (Liaghat, 1997).

Evidence of contaminated water resources is alarming, especially in developed countries where the infrastructures needed for analyses are available. Fertilizers and pesticides have been detected in both shallow and deep groundwater aquifers (Warner, 1990). Nitrates originating from fertilizers have raised groundwater concentrations of  $\text{NO}_3\text{-N}$  above the drinking water standard of 10 mg/L in countless aquifers around the

world (Follett and Walker, 1989). There is also widespread occurrence of agricultural pesticides in surface and drainage water (Lal and Stewart, 1994).

These observations have led to the much publicized public concern and criticism of reckless use of chemicals on agricultural lands. Government agencies and research organizations have started to conduct extensive field investigations and environmental impact studies of these contaminants in various ecosystems. In 1986, the US Environmental Protection Agency reported that as much as 50 to 70 percent of water resources were polluted by agricultural activities.

## **1.1 Nature and Statement of Problem**

Recognition of the potential impacts of agro-chemicals on surface and groundwater quality has motivated researchers to better understand the dynamics of water movement and contaminant transport through soil. A substantial amount of research has been conducted on the factors affecting leaching of chemicals into soil and drainage waters. However, the majority of these studies have been performed in repacked soil columns where macropore structure of the original soil has been destroyed (Jury and Flühler, 1992). Bouma (1990) asserted that most models developed to simulate water movement and solute transport assume that soils are isotropic and homogeneous. Under these assumptions, the flow follows Darcy's law which relies on proportionality between the gradient and the flux and does not take into account macropore structure. However, in natural soil, the hydraulic gradient in continuous macropores is different from that of the surrounding matrix.

This deficiency was elucidated in the 1980's as many researchers observed phenomena which could not be explained by the Darcian type of models. For example,

Steenhuis et al. (1986) reported that water movement from the soil surface to the depth of the drain was more than two orders of magnitude faster than would be predicted by Darcian flow through homogeneous soil matrix. Based on these studies, it was inferred that there were fundamental differences between flow characteristics of a homogenized repacked soil column and an intact soil core, where most of the soil heterogeneities are preserved. Beven and Germann (1982) reviewed experimental evidence indicating that water infiltration is inadequately described by theories that treat soil as a homogeneous medium and use Darcian principles of water flow through soils. As a result, most mathematical models used for water movement and chemical fate simulation through soil are unsuitable for prediction of solute transport in natural soil. Models used to simulate water movement and solute transport in natural soil profiles must take into consideration soil heterogeneities.

It is now accepted that water percolation can be greatly accentuated by the presence of macropores in the soil (Bouma, 1981; Chen et al., 1993; Dipietro and Lafolie, 1991; Li and Ghodrati, 1994; Logsdon, 1995; Moore et al., 1986; Quinsberry et al., 1994; Singh et al., 1991; Timlin et al., 1994; Trojan and Linden, 1992). Soil heterogeneity is often attributed to non-uniformities in aggregate size distribution, and in consequence, to non-uniformity of pore size distribution. Under field conditions, the variations in soil structure cause water transport to vary significantly both laterally and vertically (Beven and Germann, 1982; Jury and Sposito, 1985). The connectivity and size of soil pores play a determining role in flow characteristics of water and solute in soil (Ma and Selim, 1997). Large and continuous pores facilitate water transport. As a result, the presence of preferential flow paths (macropores) results in rapid movement of water

and associated solutes through the soil profiles. Preferential flow plays a very important role in the transport of nutrients and agricultural chemicals from surface to sub-soil and eventually, to ground water and drainage effluents that feed streams. Rapid flow has a major impact on drainage and groundwater quality since it may not allow contaminants, such as pesticides, to be adsorbed on and into the soil particles and broken down by chemical and biological actions.

## 1.2 Need for Further Experimental Studies

A number of good reviews on macropore flow have been published (Beven and Germann, 1982; Bouma, 1991; McCoy et al., 1994; White, 1985). Beven and Germann (1982) reviewed the importance of macropores on water flow in soil. In particular, they stressed the need for a coherent theory of macropore flow. White (1985) discussed the impact of macropore flow on solute and suspended matter transport through soil using the nitrate and salt leaching example for steady and unsteady states. White (1985) concluded that more quantitative information was needed on the conditions controlling macropore flow. Bouma (1991) focused on the morphological characterization of soil macropores and how it relates to water flow and chemical transport. He concluded that the implications of macropore flow on environmental quality are quite important and that:

*“ Efforts to describe preferential movement of solutes along macropores in quantitative terms have not yet resulted in a comprehensive theoretical framework that allows for the independent prediction of such phenomena.”*

McCoy et al. (1994) reviewed experimental evidence of the occurrence of macropore flow, stating that it is still not possible to quantitatively predict water and chemical movement in soils containing macropores. They concluded that both

experimental and modeling studies are needed to better understand this important soil-water process. Lal and Stewart (1994) emphasized the complexity of the macropore flow problem, which stands among research priorities of the 21<sup>st</sup> century.

Development of more effective management systems based on accurate models, which take soil macroporosity into account, is crucial in order to decrease the adverse impacts on water quality. It is now known that the number of macropores per unit area, their diameter, orientation, continuity, circularity and tortuosity directly influence preferential flow. However, our understanding of the mechanisms of water movement in soil is still limited, in part, by a lack of adequate non-destructive and quantitative techniques to measure soil macroporosity. The development of an experimental technique which is capable of directly and repetitively measuring the spatial distribution of soil macroporosity in a non-destructive manner and in particular, of monitoring flow processes through a natural soil profile, is greatly needed.

### **1.3 Objectives**

Knowledge of soil structure, along with a suitable technique for measurement of flow characteristics of water and associated solutes through soil, is essential to understanding the mechanisms of preferential flow. Unfortunately, progress in this area has been severely limited by difficulties associated with obtaining direct and non-destructive measurements of soil structure. Consequently, questions concerning the geometry, morphology and topology of soil macropores, and how these parameters affect water flow through soil, have largely remained unresolved.

This research was undertaken to quantify the macroporosity of an agricultural soil in order to examine the relationships between macropore structure and saturated water

flow. More precisely, the objectives of this research program were:

- I. To develop an innovative and effective protocol using X-ray Computer Assisted Tomography (CAT) scanning for the characterization and visualization of the interconnected pore space of an agricultural soil,
- II. To quantify the 2-D and 3-D geometry of soil macropores in a direct, repetitive and non-destructive manner,
- III. To evaluate the effect of preferential flow paths on water movement and non-reactive solute transport in saturated conditions,
- IV. To develop a modeling approach that simulates conservative solute transport in a macroporous soil under saturated conditions, and
- V. To investigate the capabilities of Single Photon Emission Computed Tomography (SPECT) for visualizing preferential flow in soil

## **1.4 Originality of Research Project**

As in many branches of science, advances in understanding have frequently had to wait for the development of techniques for measurement and observation. Computer Assisted Tomography offers considerable potential for reliable and non-destructive in-situ characterization of soil structure. CAT scanning has rarely been exploited for systematic studies in soil, in part because most of these expensive installations are fully utilized for clinical applications.

Under an ongoing agreement with the Tomographic Imaging and Porous Media Laboratory (TIPM) in Calgary, we have had a unique opportunity to utilize two CAT scanners (an EMI CT5005 full body scanner and an Advent HD200 scanner), and a Single Photon Emission Computed Tomographic scanner. Using X-ray CAT scanning techniques and with the development of computer programs in the PV-WAVE language to assess the interconnected pore space of undisturbed soil columns, this research project offers considerable potential for reliable characterization and visualization of soil macropores. The most important feature of this approach is that it provides us with an “eye” to peek into the soil in a non-destructive manner, and to learn about the in-situ hydrologic phenomena that have a major bearing on water and agro-chemical movement. To the best of our knowledge, there are no other researchers in the world investigating the transport of water and chemicals into the soil using non-destructive three-dimensional reconstruction of soil macropores. Moreover, Single Photon Emission Computed Tomography has never been applied to flow visualization and analysis of soil. This approach opens new avenues for tracer studies in non-medical fields such as soil physics. The integration of computer programming, hardware and medical imaging devices in soil studies gives us the ability to investigate the fate and transport of water and contaminants in soil at an unprecedented level.

## **1.5 Scope**

In this research project, experiments were conducted using four undisturbed soil columns, 0.85 m in length and 77 mm in inner diameter. Column size was selected based on the need for a large enough sample to represent macropore distribution, yet small enough to be handled easily when full of soil. During extraction of the cores, the soil

might have been slightly compacted and some cavities along the column edges might have been created. The soil was predominantly a loamy sand with an A horizon thickness of around 0.4 m. Therefore, our results are limited to this type of soil. The structure of macropores was quantified when the soil was dry. To reach dry conditions, the soil columns were placed under a set of ten light bulbs of 300 Watts each for a period of six weeks. The cores were rotated periodically to accentuate evaporation. This procedure might have created cracks and fissures that are not present when the soil is saturated. Potassium iodide was used for the tracer studies using the CAT scanner. This tracer is non-reactive and therefore, does not interact with soil particles.

## 1.6 Thesis Organization

This thesis dissertation comprises nine chapters. Chapters 1 and 2 present the general introduction and literature review. Chapter 3 focuses primarily on the development of an innovative and effective protocol using X-ray Computer Assisted Tomography (CAT) scanning for the characterization and visualization of the interconnected pore space of an agricultural soil. The CAT scans were taken with an EMI CT5005 during the summers of 1995 and 1996. This Chapter has been published in the Journal of Canadian Agricultural Engineering (Perret, J.S., S.O. Prasher, A. Kantzas and C. Langford. 1997. 3-D visualization of soil macroporosity using X-ray CAT scanning. *Can. Agr. Eng. J.*, 39(4):249-261).

Chapter 4 focuses on the quantification of a variety of soil macropore measures such as: the number of macropores per scan, soil macroporosity, surface area of each macropore, macropore's equivalent cylindrical diameter (ECD), perimeter, hydraulic radius, circularity and rectangularity. The data generated for this analysis was obtained



during the summer of 1997 using another CAT scanner (ADVENT HD200) with a better resolution and scanning time. Prior to CAT scanning the soil columns, several calibration tests were done. The CAT scanner calibration and the results of this analysis are discussed in Chapter 4. Moreover, a geostatistical analysis was performed to describe the spatial distribution and spatial continuity of soil macroporosity in one of the soil columns. These results are also presented in Chapter 4. This Chapter was published in Canadian Water Resources Journal (Perret J.S., S.O. Prasher, A. Kantzas and C. Langford. 1998. Characterization of macropore morphology in a sandy loam soil using X-ray computer assisted tomography and geostatistical analysis. *Can. Water Res. J.*, 23(2):143-165).

Chapter 5 focuses primarily on the characterization of 3-D properties of soil macropores (i.e., size, length, volume, hydraulic radius, tortuosity, inclination, interconnectivity). 3-D visualization and quantification is a powerful approach for understanding how macropore networks affect movement of water and associated chemicals. This Chapter has been submitted for publication. (Perret J.S., S.O. Prasher, A. Kantzas and C. Langford. 1998. Three-dimensional quantification of macropore networks in undisturbed soil cores. Submitted to the Journal of Agricultural Engineering Research).

In Chapter 6, the effect of preferential flow paths on water movement and non-reactive solute transport in saturated conditions is discussed. Breakthrough experiments using potassium iodide were monitored with a CAT scanner during the summers of 1996 and 1997. The methodology is discussed in Chapter 6. Efforts were made to relate the 3-D geometry of macropores to their ability to convey water and solutes. Chapter 6 also

presents a new multi-region modeling approach using X-ray CAT scanning to model macropore flow in soil under saturated conditions. Water and solute transport in the macropore domain was modeled using an analogy between macropore flow and pipe flow. The macropore domain was divided into two regions, namely the laminar and turbulent regions. Chapter 6 has been submitted for publication. (Perret J.S., S.O. Prasher, A. Kantzas and C. Langford. 1998. Development of a two-domain simulation approach using X-ray CAT scanning to model solute transport in a soil with preferential flow pathways. Submitted to the Journal of Environmental Quality).

Single Photon Emission Computer Tomography (SPECT) is an ideal tool for visualizing and quantifying tracer displacement in dynamic flow studies in a non-destructive manner. However, SPECT imaging has never been introduced to soil physics. Thus, the primary objective of the research work presented in Chapter 7 was to investigate the capabilities of SPECT scanning for visualizing preferential flow in soils. The methodology and the results of a tracer breakthrough, monitored by SPECT scanning, are presented in Chapter 7. Visualization and analysis of radioactive tracer flow patterns in 2-D, using planar imaging, and in 3-D, with the tomographic capabilities of the SPECT scanner, are also discussed in this chapter. Chapter 7 has been submitted for publication. (Perret J.S., S.O. Prasher, A. Kantzas, K. Hamilton and C. Langford. 1998. Soil-core breakthrough in intact soil columns measured by SPECT scanning. Submitted to the Soil Science Society of America Journal).

Finally, a summary and conclusions of the research project are presented in Chapter 8. Chapter 9 provides a list of recommendations for future research. A thorough list of references can be found in Chapter 10. The format of referencing follows the

guidelines of the Transactions of the ASAE. A CD-ROM can be found at the end of this thesis dissertation. This CD-ROM comprises the following items: ① the computer programs developed in this research project, ② a software, called MACROSPIN, which allows a user to visualize macropores in a soil column interactively, ③ several computer animations generated in PV-WAVE language and in 3-D STUDIO® for the visualization of soil macropores and preferential flow in soil, ④ sample data obtained by CAT and SPECT scannings for one of the soil columns, and ⑤ some pictures of the experimental setup and scanning equipment. The data collected in this project are available upon request on CD-ROM or FTP from the author or from Dr. Shiv O. Prasher (E-mail: [prasher@agreng.lan.mcgill.ca](mailto:prasher@agreng.lan.mcgill.ca)).

## CHAPTER 2

### REVIEW OF LITERATURE

---

Soil macropores enhance infiltration and serve as preferential flow paths for the transport of agricultural chemicals from soil surface to ground water. However, the mechanisms involved in water movement and chemical transport in a heterogeneous soil are not well-understood (Lal and Stewart, 1994).

This chapter comprises of eight sections. Sections 2.1, 2.2 and 2.3 deal with soil pores, soil macropores and characterization of soil macroporosity, respectively. Section 2.4 describes the basic principles of X-ray Computer Assisted Tomography (i.e., CAT scanning). Applications of CAT scanning to soil studies are explored in section 2.5. The principles and the applications of Single Photon Emission Computed Tomography (SPECT) are described in Section 2.6. Section 2.7 provides an overview of the modeling of water and solute transport in soil, and, finally, section 2.8 provides a brief summary of this chapter.

#### 2.1 Soil Pores

Soil is a very complex system. It consists of a heterogeneous mixture of solid (organic and mineral particles varying in size, shape and composition), liquid, and gaseous material. The arrangement of solid particles is called soil structure. Gaseous and liquid phases constitute the pore space. The size and arrangement of solid material

determines the shapes and sizes of pores. A pore can be defined as a void (or non-solid space) bound by solid surfaces (Dullien, 1992). Between the solid particles, arranged individually or in aggregates, there is a complex three-dimensional network of interconnected pores on which plant roots, micro-organisms and soil fauna depend for storage and movement of water, air and nutrients. Many factors contribute to the formation of this intricate soil-pore system. Knowledge of the formation and development of soil pores is important for the interpretation of complex morphology of soil structure.

### **2.1.1 Origins of soil pores**

Soil pores are formed either by physical forces or biological activity. Pores induced by physical forces are generally referred to as *physiopore*, while those formed by biological processes are called *biopores*.

#### **2.1.1.1 Physiopores**

These pores are the result of physical and chemical forces acting on the soil and are generally linear or planar in shape. They are generally formed by the shrinkage and swelling of soil, caused by drying/wetting and/or freezing/thawing cycles. Shrinking and swelling depend primarily on the moisture content of soil. These physical forces result in the formation of cracks and fissures. Once a fissure is formed, it usually reappears at the same location for a succession of shrinking and swelling cycles (Beven and Germann, 1982). Chemical weathering, cultivation techniques, and tectonic movement may also result in the formation of physiopores (Warner, 1990). These pores might contribute to water infiltration through soil. If the forces induced by water movement exceed the soil's

structural cohesiveness, erosion will occur and cause the formation of natural soil pipes. In general, these pores are less linear than cracks and fissures. Natural soil pipes are generally formed in non-cohesive soils under high hydraulic gradients.

#### 2.1.1.2 Biopores

Biopores are formed by biological processes. These pores are induced either by faunal activities or by plant roots that have decayed.

##### *Pores formed by fauna*

Biopores are generally concentrated close to the soil surface and are formed by a variety of living organisms such as arthropods (insects such as ants, springtails, mites, termites, etc.), annelids (earthworms, potworms, bristleworms, etc.), and larger burrowing animals (mice, ground squirrels, marmots, moles, gophers, prairie dogs, etc.). Figure 2.1 shows some of these organisms. Only a small number of research studies have quantified the effect of soil-living organisms on the structural properties of soil (Wood, 1989). Lack of information is partly due to the labour intensive nature of existing techniques and the insufficiency of reliable methods for quantifying the number and size



Figure 2.1: Some organisms living in soil (After Gibbons and Wilson, 1984).

of different organisms living in the soil. To date, most studies on soil organisms have identified individual species present in soil, but do not relate this information to the activity of these organisms and its impact on soil structure (Wood, 1989).

Soil organisms may be classified according to their body size (Table 2.1). Their body size is an important factor that directly affects the formation of soil pores. Most biopores induced by fauna are cylindrical in shape and may range from less than 1 mm in diameter to more than 50 mm (Beven and German, 1982).

Table 2.1: Classification of major soil organisms according to body size (After Swift et al., 1979).

Grouping	Body Width	Organisms
Microflora	< 10 $\mu\text{m}$	Bacteria, fungi
Microfauna	< 100 $\mu\text{m}$	Protozoa, nematodes
Mesofauna	100 $\mu\text{m}$ to 2 mm	Mites, springtails, termites
Macrofauna	2 mm to 20 mm	Earthworms, millepedes, slugs, ants

Some soil organisms have a greater impact on the development of pores than others. Large invertebrates, notably earthworms, ants and termites have the capacity to exert a considerable influence on soil structure.

Earthworms are found in many soils throughout temperate and tropical regions with a population ranging from less than 1 to 850 per square meter (Burgess and Raw, 1967). In temperate regions, they dominate the soil's invertebrate biomass (Curry, 1994). There are about 3000 species of earthworms. However, the lumbricidae family, which is a characteristic family of temperate regions, comprises only 10% of the total species. The formation of burrows is a distinctive feature of earthworm activity. Normally, large species, such as *Lumbricus terrestris*, which can weigh more than 5g per worm,

contribute substantially to the formation of long and continuous burrows. These earthworms usually make vertical burrows down to depths of 2 m or more (Edwards et al., 1990; Ehlers, 1975). Burrows are formed by worms eating their way through soil and pushing through cracks and fissures. These channels have diameters ranging from 1 to 12 mm with smooth walls cemented with mucous secretions. The burrowing species create permanent and empty channels. Earthworm species, such as *Aporrectodea longa* and *Lumbricus terrestris*, show diurnal patterns of activity. During their active period, these large burrowing species use these burrows to reach the surface and feed on dead organic material. The smaller and shallow-working species tend to travel primarily in the horizontal direction, opening the soil at one point and filling it as they progress.

Termites and ants are quite important in tropical and sub-tropical regions, performing a role similar to that of earthworms of temperate regions (Wood, 1989). Galleries produced by termite activities generally radiate in all directions. They are particularly numerous up to a depth of 0.9 m but can be found to a depth of 3 m (Burgess and Raw, 1967). Ants also modify soil structure by constructing nests and galleries, but their influence is usually less apparent than that of termites (Curry, 1994).

#### *Pores formed by plant roots*

Roots that have decayed generally form pores that are tubular in shape, but their presence decreases rapidly with depth. The number, arrangement and orientation of such pores depend on the age and species of the plant, as well as the soil's resistance to growth of the rooting system. Some sizes of pores induced by roots of common plants are presented in Table 2.2.



**Table 2.2:** Dimensions of pores formed by plant roots (After Hamblin, 1985).

Type of roots	Average pore diameter
Tap roots of dicotyledons	10,000 $\mu\text{m}$ to 300 $\mu\text{m}$
Nodal roots of cereals	10,000 $\mu\text{m}$ to 500 $\mu\text{m}$
Seminal roots of cereals	1000 $\mu\text{m}$ to 100 $\mu\text{m}$
Lateral roots of cereals	100 $\mu\text{m}$ to 50 $\mu\text{m}$
1 <sup>st</sup> and 2 <sup>nd</sup> order laterals of cereals	50 $\mu\text{m}$ to 20 $\mu\text{m}$
Root hairs	10 $\mu\text{m}$ to 5 $\mu\text{m}$

### 2.1.2 Classification of pores

Soil pores range from 0.003  $\mu\text{m}$  between clay particles to fissures and channels of several centimetres in diameter. Often, soil scientists describe pore size using the term equivalent cylindrical diameter (ECD). The ECD is derived from the pore size distribution of soil. The distribution of pore space, according to pore size, is computed from the soil moisture retention curve where the ECD is related to the capillary rise equation:

$$h = \frac{2\sigma \cos \omega}{\rho g r} \quad (2.1)$$

where  $h$  is the hydrostatic suction (m) or capillary rise,  $\sigma$  is the surface tension ( $\text{kg/s}^2$ ),  $\omega$  is the contact angle of water (degree),  $\rho$  is the density of water ( $\text{kg/m}^3$ ),  $g$  is the acceleration due to gravity ( $\text{m/s}^2$ ) and  $r$  is the equivalent cylindrical radius of the pore (m). The ECD of a pore can be obtained from the equivalent cylindrical radius. The pore size distribution is derived by determining the change in water content of a soil sample,

which can be expressed as a percentage of total pore space, between two pressure heads. Pressure heads are used in Equation 2.1 to determine the range of ECDs ( $d_1$  and  $d_2$ ) for the given percentage of total pore space. In other words, the volume of water withdrawn by increasing the pressure head represents the volume of pores having an ECD between  $d_1$  and  $d_2$ . This approach involves an analogy between macroscopic retention characteristics of soil and behavior of capillary tubes.

Hillel (1982) suggested that it was possible to divide the pore-size distribution of soil into two distinguishable ranges of pores referred to as *macropores* and *micropores*. He defined macropores as inter-aggregate cavities and micropores as intraggregate capillaries. The demarcation between these two terms is often arbitrary and ambiguous (Dullien, 1979; Hillel, 1982; Skopp, 1981). It would be useful to have a general agreement on pore terminology. However, there is little or no consensus for the definition and terminology used for classification of pores in terms of its ECD. There has been a large number of classification schemes based on the ECD and several contradicting definitions can be found in soil science literature (Table 2.3).

**Table 2.3:** Different classifications of pores based on their Equivalent Cylindrical Diameter.

Terminology	ECD	Reference
Micropore Mesopore Macropore	Less than 30 $\mu\text{m}$ 30 $\mu\text{m}$ to 100 $\mu\text{m}$ greater than 100 $\mu\text{m}$	Jongerius (1957)
Micropore Macropore	Less than 30 $\mu\text{m}$ Greater than 30 $\mu\text{m}$	Marshall (1959)
Micropore Very Fine pore Fine pore Medium pore Coarse pore	Less than 75 $\mu\text{m}$ 75 $\mu\text{m}$ to 1000 $\mu\text{m}$ 1000 $\mu\text{m}$ to 2000 $\mu\text{m}$ 2000 $\mu\text{m}$ to 5000 $\mu\text{m}$ greater than 5000 $\mu\text{m}$	Johnson et al. (1960)
Cryptovoid Ultramicrovoid Microvoid	Less than 0.1 $\mu\text{m}$ Less than 5 $\mu\text{m}$ 5 $\mu\text{m}$ to 30 $\mu\text{m}$	Brewer (1964)

Mesovoid	30 $\mu\text{m}$ to 75 $\mu\text{m}$	
Macrovoid	greater than 75 $\mu\text{m}$	
Very fine pore	Less than 2 $\mu\text{m}$	
Fine pore	2 $\mu\text{m}$ to 20 $\mu\text{m}$	Russel (1973)
Medium pore	20 $\mu\text{m}$ to 200 $\mu\text{m}$	
Coarse pore	greater than 200 $\mu\text{m}$	
Micropore	less than 0.3 $\mu\text{m}$	
Minipore	0.3 $\mu\text{m}$ to 30 $\mu\text{m}$	McIntyre (1974)
Macropore	30 $\mu\text{m}$ to 300 $\mu\text{m}$	
Super pore	greater than 300 $\mu\text{m}$	
Bonding pore	less than 0.005 $\mu\text{m}$	
Residual pore	less than 0.5 $\mu\text{m}$	
Storage pore	0.5 $\mu\text{m}$ to 50 $\mu\text{m}$	Greenland (1977)
Transmission pore	50 $\mu\text{m}$ to 500 $\mu\text{m}$	
Fissure	greater than 500 $\mu\text{m}$	
Macropore	greater than 1000 $\mu\text{m}$	Bouma et al. (1977)
Macropore	greater than 60 $\mu\text{m}$	Bullock and Thomansson (1979)
Macrofissure	200 $\mu\text{m}$ to 2000 $\mu\text{m}$	
Enlarged Macrofissure	2000 $\mu\text{m}$ to 10000 $\mu\text{m}$	Reeves et al. (1980)
Macropore	greater than 3000 $\mu\text{m}$	Beven (1981)
Micropore	less than 10 $\mu\text{m}$	
Mesopore	10 $\mu\text{m}$ to 1000 $\mu\text{m}$	Luxmoore (1981)
Macropore	greater than 1000 $\mu\text{m}$	
Macropore	greater than 1000 $\mu\text{m}$	Luxmoore et al. (1990)

Even with the above definitions, the ambiguity between macropores and micropores remains. The fact that these terms are not uniformly defined and used by the research community may suggest that this scheme, which attempts to set a physical limit on pore size, has major limitations.

As mentioned earlier, the equivalent cylindrical pore diameter is inferred from the capillary potential. The analogy between the macroscopic retention characteristic of pores and the behaviour of water in a capillary tube may not apply to cracks and big macropores (Skopp, 1981). In other words, by considering pores to be cylindrical and by assuming that soil-water characteristics of a pore follow the model of capillary tubes,

estimation of the equivalent cylindrical diameter may result in a fallacious description of soil porosity (Bouma, 1981). Moreover, this scheme fails to take into account essential parameters such as continuity and tortuosity of pores which are often considered more important than their size (Beven, 1981; Bouma, 1981; Logsdon et al., 1993; Skopp, 1981).

Another scheme for the classification of soil porosity was proposed by Skopp (1981) based on pore function. He suggested the following definitions:

**Macroporosity:** *“designates the pore space which provides preferential paths of flow so that mixing and transfer between pores and remaining pores is limited. Macropores may consist of interaggregate pore space, shrink swell cracks, root channels, or fauna tunnels.”*

**Matrix porosity :** *“designates that pore space which transmits water and solute at a rate slow enough to result in extensive mixing and relatively rapid transfer of molecules between different pores.”*

These two definitions describe the flow processes occurring in soil and emphasize the importance of pore structure on flow dynamics. Bouma (1981) supported these definitions by writing: " ... *I would be in favor of characterizing soils in a dynamic manner in terms of transport characteristics.*" Beven and German (1982), in their comprehensive article on water flow in soil macropores, presented a similar opinion and wrote : " *We wish to make quite clear that in using the word macropore, we are implying structures that permit the type of non-equilibrium channelling flow, whatever their size.*" Other terms such as preferential flow path or macrochannel have appeared in soil science literature with the intention of emphasising flow processes. However, once again, this scheme of classification has some disadvantages; there is still no standardized method available to measure flow in pores (Warner, 1990). Moreover, the channelling function

of a preferential flow path for a given initial and boundary condition depends on a variety of parameters and phenomena such as the initial water content, hysteresis, and temporal changes of pores due to physical or biological processes. Therefore, this approach is restricted to cases where these parameters can be well defined.

Warner (1990) pointed out that the classification of pores should include their size, shape and continuity at different depths. This holds the advantage of considering the entire soil profile. Since the geometry and distribution of pores are described as functions of depth, parameters such as tortuosity, continuity, and pore expansion-contraction can finally be quantified. From a morphological point of view, and by considering the entire soil profile, this approach is quite satisfying.

**Concluding remarks on soil pores:** Soil pores can be classified according to their mode of formation. They are either biologically induced (*biopores*) or formed by physical forces acting on the soil (*physiopores*). Large invertebrates, notably earthworms, ants and termites, have a considerable influence on soil structure. To date, most studies on soil organisms have not related the population and activity of these organisms to the structure of interconnected pore space in soil.

Soil scientists generally describe pore size using the term of equivalent cylindrical diameter (ECD). However, there is little or no consensus for the definition and terminology used for the classification of pores in terms of its ECD. Some soil scientists would be in favour of describing pore structure based on flow dynamics. However, no standardized method is available to measure the channelling flow in pores. Another approach used to classify pores is to characterize their morphology at different depths in order to describe systematically the porosity of the entire soil profile. This method offers

great potential for the characterization of three-dimensional parameters, such as pore tortuosity or continuity.

## **2.2 Soil Macropores**

A major category of soil pores is known as soil macropores. In this section, the term macropore is defined and the impact of soil macropores on water and solute movement, root penetration and soil aeration are reviewed.

### **2.2.1 Definition of macropore**

By strict definition, macropore means large pore. However, large is a relative term and this lack of clarity has led to several conflicting definitions. Section 2.1.2 clearly illustrates the lack of universal consensus on what is a large soil pore. The definition of macropore must be addressed on the bases of size and its ability to convey water and solute. This research study will follow the definition proposed by Luxmoore et al. (1990):

*“ The term macropore includes all pores in a profile that are (generally) drained at field capacity, with the latter being 1 mm or more in equivalent diameter. ”*

### **2.2.2 Impacts of soil macropores**

Once macropores have been defined, it is helpful to fully understand the impacts of soil macropores in order to evaluate their importance in hydrologic processes and soil activity. This section reviews the influence of soil macropores on different hydrologic processes and presents briefly the impacts of macropores on the growth of plant roots and soil aeration.

### 2.2.2.1 Impact on water flow and solutes transport

The effects of macropores on the transport of water and solutes through soil can be quite significant and is now well documented (Beven and Germann, 1982; Bouma, 1981; Bouma, 1990; Chen et al., 1993; Dipietro and Lafolie, 1991; Hamblin, 1985; Li and Ghodrati, 1994; Logsdon, 1995; McCoy et al., 1994; Moore et al., 1986; Quinsenberry et al., 1994; Singh and Kanwar, 1991; Timlin et al., 1994; Trojan and Linden, 1992; White, 1985). While the subject matter is not new and has been studied for many decades, a coherent theory of water and chemical movement in macroporous soils is needed.

There has long been speculation that big and continuous pores may be an important factor affecting percolation of water through soil. The idea that these voids may contribute to the movement of water dates back at least to Schumacher (1864) who wrote:

*“ The permeability of a soil during infiltration is mainly controlled by big pores, in which the water is not held under the influence of capillary forces.” (Quoted by Beven and Germann, 1982)*

Comparable ideas were also suggested by Hursh (1944) who reported that:

*“ ...in considering flow through upper soil horizons, the formulas of soil mechanics do not apply. Here porosity is not a factor of individual soil particle size but rather of the structure determined by soil aggregates which form three-dimensional lattice patterns. This structure is permeated throughout by biological channels which in themselves also function as hydraulic pathways. A single dead-root channel, worm-hole or insect burrow may govern both the draining of water and escape of air...” (Quoted by*

*Beven and Germann, 1982)*

However, it is only since the early 1980's, with growing concerns about pollution of surface and ground waters from agricultural chemicals, that macropores have been the subject of extensive research. Field and laboratory research now suggest that the standard equations predicting water and solute transport are inadequate to simulate flow through a well structured soil (Van Genuchten, 1990). The arrival of water and associated solutes at some point of interest (outlet of a drainage system, ground water or the bottom of a soil column), sooner than predicted by available theories of water and chemical movement through soil, has caused great concern. It has led to the reevaluation of our understanding of the percolation process through natural soils containing macropores (Lal and Stewart, 1994).

Thomas and Phillips (1979) are among the first researchers to have reviewed the overall impact of flow through macropores. In their comprehensive article, they have demonstrated that water flow through macropores results in:

- ① a significant and rapid water movement through the soil,
- ② non-Darcian flow,
- ③ bypass of the soil matrix, and
- ④ contamination of drainage and ground waters.

The contributions of soil macropores to water flow in soil presented by Thomas and Phillips (1979) are now well accepted by soil scientists. Each of these contributions is reviewed below.

① Significant and rapid water movement through soil: Although soil macropores comprise a small percentage of total porosity (1% to 5%), they can have a profound effect



on the rate of infiltration and redistribution of water into soil (White, 1985). The presence of macropores provides an opportunity for water and associated chemicals to move preferentially through the vadose zone. This hydrologic phenomenon is known as macropore flow. Watson and Luxmoore (1986) quantified water flow in a forested soil and found that macropore flow contributed to 73% of water movement in a saturated soil. In similar conditions, Wilson and Luxmoore (1988) reported that 85% of water ponding at the surface of a forested soil moved through soil macropores. Roth et al. (1991) studied solute transport through a layered and structured soil in Switzerland and found that macropore movement accounted for about 56% of the total water flow. Using a double-ringed infiltrometer in a corn field, Dunn and Phillips (1991a) noted that pores greater than 0.21 mm in equivalent diameter contributed to 83 % of total water flux. These experimental evidences clearly show that macropores are highly effective in transmitting water through soil.

Due to low frictional and capillary forces present in big soil pores, water flow is usually much faster through macropores than through soil matrix (Beven, 1981; Huffman and Monke, 1989; Warner, 1990). For instance, Aley (1977) estimated that water entering soil macropores contributes five times as much to groundwater recharge than does water through soil matrix. In field conditions, Bouma et al. (1982) pointed out that steady state ponded infiltration rates could be as high as 6.7 ml/s for continuous macropores. Steenhuis et al. (1986) reported that water movement from soil surface to drainage tile lines is more than two orders of magnitude faster than would be predicted by Darcy's law. Using bromide leaching studies on twenty undisturbed soil columns, Ren et al. (1996) found that the median solute velocities were 20 to 311 % faster than

corresponding piston flow velocities. Under these experimental evidences, it is clear that water can move rapidly through soil due to the presence of soil macropores.

② Non-Darcian flow in soil containing macropores: Macropore flow differs from flow through a homogeneous soil matrix where water moves uniformly, following a downward piston- like movement as shown in Figure 2.2.a. Water penetration into a homogeneous soil system takes place through small pores created by the arrangement of individual grains or soil particles. This type of flow is usually referred to as matrix flow or piston flow. In this case, Darcy's law can be used to describe the flow as the wetting front moves uniformly through the soil matrix. However, when macropores are present, water flow may be dominated by penetration through macropores (Figure 2.2.b). Water movement in soil follows the path of least resistance and as a result, flow will occur principally through large pores where the capillary and frictional forces are almost negligible. Darcy's law relies on proportionality between the gradient and

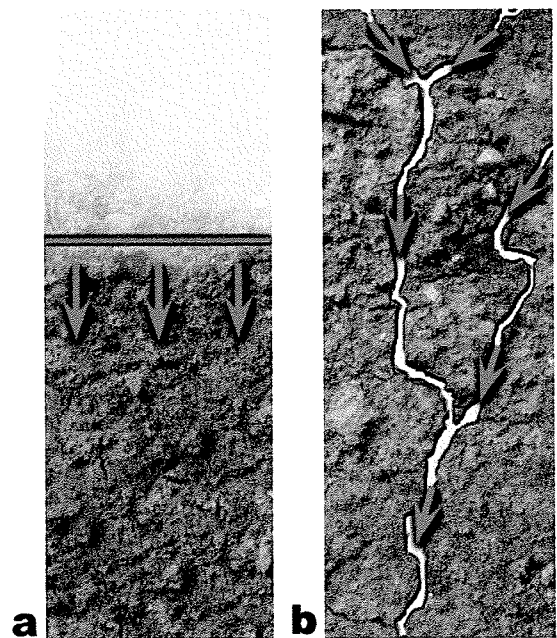


Figure 2.2: Illustration of flow through (a) a homogenous soil and (b) a soil containing macropores.

flux. However, in a well-structured soil, the hydraulic gradient in continuous macropores might be different from that of the surrounding matrix. This leads to the breakdown of traditional Darcian concepts of water flow through soil (Beven and Germann, 1982; Beven, 1981; Huffman and Monke, 1989; McCoy et al., 1994; White, 1985).

③ Bypass of the soil matrix: Bypass flow is the process of rapidly-moving water “bypassing” (flow through macropores) more slowly-moving water (matrix flow) (McCoy et al., 1994). Because macropores occupy only a small fraction of total soil volume, water and dissolved or suspended chemicals may bypass the majority of the soil matrix (Roseberg and McCoy, 1992). This process results in rapid movement of water and associated chemicals, even in unsaturated conditions (Bouma, 1990). In other words, “bypass flow” may occur when a macropore and/or the soil surrounding it is not entirely water filled. This process generally takes place as free water films, moving vertically along the pore surface (Beven and Germann, 1981), or as water packets, separated by air filled space (Bouma, 1991). In saturated conditions, water filled macropores have faster flow rates than smaller pores and solution in macropores bypasses solution in soil matrix, with little or no mixing. Thus, deep penetration of water through soil may occur in a short period of time, with a solute concentration remaining as high as the initial concentration. Obviously, this process leads to greater contamination of drainage and ground waters.

④ Contamination of drainage and ground waters: As mentioned earlier, macropore flow results in rapid movement of water and solutes through the soil profile. Short travel time may not allow contaminants, such as pesticides, to be adsorbed on and into the soil particles where they are broken down by chemical and biological actions. Consequently, any solute in the water will be quickly delivered to the drains or groundwater aquifers without being degraded. This consequence has major implications for groundwater quality.

#### 2.2.2.2 Impact of macropores on root penetration

Root distribution in the soil profile helps determine the plant's ability to absorb water and nutrients (Atkinson, 1991). As roots grow, they move into pores sufficient in size to accommodate them. Plant roots growing in a soil without large pores or fissures elongate by exerting considerable pressure on soil particles in order to displace them. The obstruction, caused by tight arrangement of soil particles, significantly slows down the advancing of root tips (Harley and Russell, 1979). However, physical obstruction is greatly reduced in soils containing macropores and as a result, root growth is encouraged (Bennie, 1991). According to Sutton (1991), the size of pore openings is more important for plant growth than the overall soil porosity. Although existing pores constrain penetration of roots, they provide favorable conditions for root growth. Several studies have shown that the presence of continuous macropores in soil significantly benefits root growth (Bennie, 1991).

#### 2.2.2.3 Impact of macropores on soil aeration

One of the most important factors influencing soil fertility, besides water and nutrient content, is soil aeration (Hillel, 1980; Glinski and Stepniewski, 1985). Roots and soil micro-organisms require that soil be aerated at a certain rate so as to prevent a deficiency of oxygen and an excess of carbon dioxide in the root zone. Insufficient aeration resulting from waterlogging, poor drainage or soil compaction inhibit crop growth (Hillel, 1980). The large soil pores determine the paths available for gas exchange between soil and atmosphere (Sutton, 1991).

**Concluding remarks on soil macropores:** For this study, we will refer to the term macropore as pores in the soil profile (generally drained at field capacity) having an

equivalent diameter greater or equal to 1 mm. Although recognition of preferential flow through soil is not new, it is only recently that attention has been focused on this phenomenon because of the possible consequences for rapid leaching of fertilizers, pesticides, particulate waste materials, and other contaminants into drainage water and underground aquifers. This phenomenon cannot be adequately described by theories conforming to Darcian principles of water flow through soil. Soil macroporosity is an essential soil characteristic which not only influences the rate of water movement and chemical transport through soil, but also plays a critical role in soil aeration and penetration of rooting systems.

### **2.3 Macroporosity: Physical Characterization**

To assess the impact of macropores on the flow and transport properties of soils, macropores must be characterized. In this section, different approaches used for the characterization of soil macropores are reviewed.

The unique property that differentiates a porous medium from other solid bodies is its complex pore structure (Dullien, 1992). A porous medium can be represented as a three-dimensional network of interconnected capillary channels, referred to as pores. In a porous medium such as soil, pores have a non-uniform structure and their geometry is often extremely difficult to characterize (Bouma, 1981; Dullien, 1992; Grevers and de Jong, 1994; Peyton et al., 1994a; Logsdon et al., 1990; Phogat and Aylmore, 1989; Roseberg and McCoy, 1992; Shepard, 1993; Warner, 1990). Attempting to describe the complexity of the pore structure of a porous media such as soil, G. Matheron (1970) wrote:

*“ Mis en face de la réalité d'un milieu poreux, l'esprit peut s'effrayer  
d'abord de la tâche à entreprendre ”*

Matheron is among the many researchers who agree that the study of pore structure of a porous media is not an easy one. Although the analysis of porous media has a long history, especially in connection with the oil recovery from underground reservoirs, it is only in the past fifteen years that this analysis has been extended to include structural properties of pores (Sahimi, 1993). The fact that pore structure is inseparable from soil's physical behavior is now well accepted by the research community. However, much discussion has been generated as to the description and classification of pore structures in soil.

There are an increasing number of research publications that have reported on the various means of characterizing soil macropores. They can be regrouped into two general approaches: indirect and direct approaches.

### **2.3.1 Indirect approaches**

The indirect approaches attempt to determine the influence of macropores by measuring flow characteristics under varying conditions (Warner et al., 1989). Several indirect methods have been developed to obtain macropore parameters. Everts and Kanwar (1993), Timlin et al. (1994), Logsdon et al. (1993), Dunn and Phillips (1991a), Dunn and Phillips (1991b), Perroux and White (1988), and Watson and Luxmoore (1986) have used tension infiltrometers to characterize the apparent conductivity and continuity of soil macropores. Tension-infiltrometers (also known as disc permeameters) offer a practical mean to obtain information on soil infiltration characteristics. Perroux and

White (1988) give a detailed description of the theory and design of a tension-infiltrometer. From the characteristics of infiltration, it is possible to qualitatively describe soil macroporosity. More precisely, by taking measurements at several soil-moisture tensions, it is theoretically possible to describe the distribution of macropores using the capillary-rise equation (see section 2.1.2- Equation 2.1). Based on the same principle, Fish and Koppi (1994), and Roseberg and McCoy (1992) evaluated soil macroporosity with air permeability techniques. This method has been used in attempts to describe soil porosity using an air pressure differential across an undisturbed soil sample or directly into the field. Roseberg and McCoy (1990) presented details on the design and operation of the air permeameter using soil samples. Prapaharan et al. (1991) and Griffiths et al. (1991) have used a different technique, known as mercury intrusion porosimetry, to characterize the size distribution of soil voids. However, the tension-infiltrometer, air permeameter and mercury intrusion porosimetry techniques have major limitations. Only a small area, at a depth relatively close to the soil surface or on top of the excavated horizon, can be characterized using tension infiltrometers or air permeameters. Moreover, measurements and distribution of soil macroporosity using permeameters remain insufficient to calculate the ECDs of macropores as a function of their geometry (Dunn and Phillips, 1991b). In other words, pore-size-distribution could be the same for many combinations of different macropore geometries, tortuosities, and lengths and thus, soil macropore structure cannot be quantified.

Another indirect approach for characterizing macropore continuity and macropore flow involves the use of breakthrough curves (BTCs) with non-reactive tracers such as bromide or chloride. Non-reactive tracers are used because they are not adsorbed by the

soil particles. This approach has been used in numerous soil studies to describe flow mechanisms through soil macropores (Ahuja et al., 1995; Anderson and Bouma, 1977; Jabro et al., 1994; Li and Ghodrati, 1994; Ma and Selim, 1994; Munyankusi et al., 1994; Quisenberry et al., 1994; Shipitalo and Edwards, 1996; Trojan and Linden, 1992). Tracing techniques can provide data that can be used to analyze heterogeneous flow patterns. The percolating solution containing non-reactive solute, moves through the soil and the effluent concentration can be monitored as a function of time (or percentage of the total soil pore volume) to obtain a measure of the range of flow velocities within the soil.

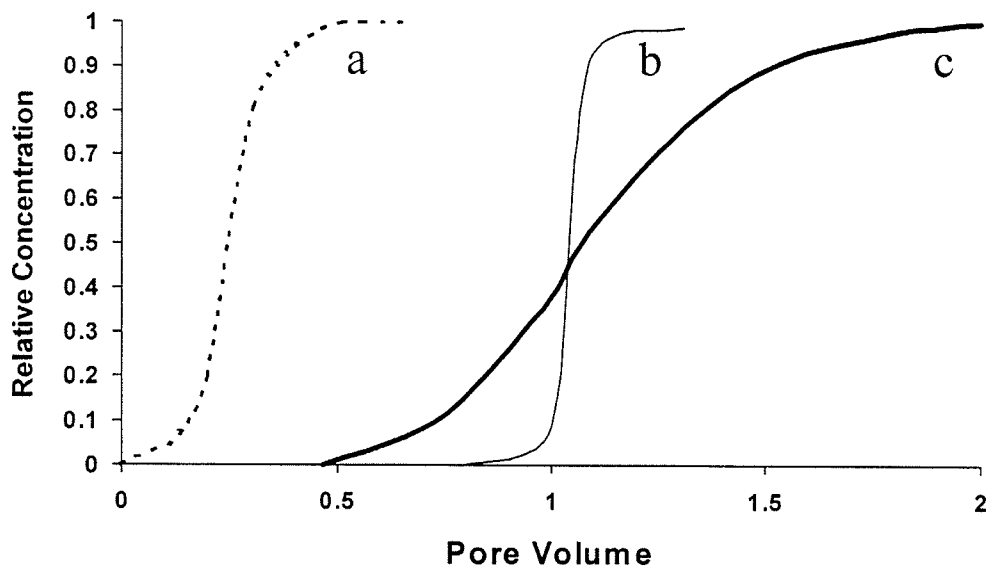


Figure 2.3: Schematic diagram showing the breakthrough curves of three types of soil (a) flow in a macroporous soil, (b) piston-type flow in a homogeneous soil, and (c) flow in a heterogeneous pore system (After Bouma, 1991).

In a well-structured soil containing macropores, solution will move rapidly and as a result, the tracer can soon be found in the effluent (Figure 2.3a). If maximum and minimum flow velocities through soil are close to the average flow velocity, percolation



of the solution will follow a piston type of movement (Figure 2.3b). The breakthrough will be much more progressive in a soil having a well graded pore system (Figure 2.3c). Therefore, flow regimes and soil structure can be characterized physically with the shape of BTCs. However, this indirect approach provides only qualitative information about soil porosity.

### **2.3.2 Direct approaches**

Quantitative analysis of macroporosity is normally obtained by direct methods. Two general approaches can be used for direct analysis of soil macropores; one is destructive (morphometric techniques), and the other is non-destructive and is achieved by emerging new technologies, such as X-ray or  $\gamma$ -ray Computer Assisted Tomography (CAT scanning) or Magnetic Resonance Imaging (MRI) techniques.

Many morphometric techniques are available to measure soil (macro)pore-size distributions. These destructive techniques are based on filling the pores of the soil either with a liquid that hardens after some time or by a dye that stains the preferential flow paths. Epoxy resin (Koppi and McBratney, 1991; Moran and McBratney, 1992; Moran et al., 1989), polyester resins (Singh et al., 1991), and paraffin (Vermeul et al., 1993) have been used for this purpose. After impregnation and hardening of the liquid, the soil sample is sectioned with a mechanical saw and polished to obtain a smooth finish. The operation is followed by digitization of the soil section and image analysis to depict soil macroporosity and to characterize its morphology. Other researchers, such as Andreini and Steenhuis (1988), Booltink and Bouma (1991), Logsdon (1995), Logsdon et al. (1990), Trojan and Linden (1992), and Wu et al. (1993) have characterized flow patterns along macropores using dye tracers such as methylene blue or lissamine yellow.

Unfortunately, there are a number of difficulties associated with these direct and destructive approaches. The greatest problem is that most impregnating agents have a low viscosity and are not miscible with water. As a result, they do not infiltrate all of soil macropores, especially in moist conditions. Moreover, preparation of soil samples and image analysis of soil pore-space patterns demand very meticulous handling in order to preserve soil structure and require considerable time for execution. Finally, these two direct approaches have the common disadvantage of destroying the soil sample's structure before it can be determined whether the dye or impregnating agent has been fully absorbed by soil macropores. This limits their application, as they cannot be repeatedly applied to studies such as water and solute movement through soil, water content changes, and other time-related work.

Until recently, no experimental technique was available for direct and non-destructive *in-situ* characterization of soil macropores. However, with the application of Computer Assisted Tomography (CAT) to soil-plant-water studies, a relatively new and exciting method is now available for non-destructive imaging of porous media such as soil. Scanning methods offer considerable potential for reliable and non-invasive *in-situ* quantification of macropores occurring in agricultural soils.

CAT scanning has rarely been exploited for systematic studies in soils, in part because most of these expensive installations are dedicated to clinical applications. Computed tomography has been developed for specific use in the medical field involving the human body. Its design and operating parameters have been optimized for soft tissues. Consequently, the first investigators of this technique had to adapt this complex and expensive technology to new conditions in order to determine its feasibility for

objects other than the human body.

In the early 1980s, CAT scan technology started to be used in non-medical fields and its great potential for non-destructive analyses was immediately recognized. In one of the first studies involving soil science, Petrovic et al. (1982) showed that CAT scanning was a promising tool for rapid determination of soil bulk density. They found that the mean bulk density in a soil core was linearly related to the core's mean X-ray attenuation coefficient. A year later, Hainsworth and Aylmore (1983) conducted experiments to examine the spatial changes in soil water content using CAT. They reported that computer assisted tomography was successful in monitoring the changes in soil water content and wrote: "*CAT scanning presents an extremely exciting possibility for studies of soil-plant water relations*". Crestana et al. (1985) used CAT to observe the change in X-ray attenuation coefficient with time as a wetting front passed through a homogeneous soil core. They demonstrated the ability of scanners to detect water movement in soil and concluded that CAT scanning was opening new possibilities for non-destructive measurements of spatial and dynamic water contents. They have also developed a miniscanner for field analysis (Crestana et al., 1986). Using small homogenized soil cores, Anderson et al. (1988) showed that the relationship between volume fraction of solids in cores and mean X-ray attenuation was linear and found the CAT approach to be a powerful tool for soil research. Jenssen and Heyerdahl (1988) applied CAT scanning to the study of packing arrangement and density of soil columns in experiments concerning water transport and wastewater purification. They stated that CAT scanning "*offers fascinating possibilities in the field of soil science*". The above studies clearly indicate that CAT scanning is a valuable tool for investigating soil-water

processes. Other investigators such as Phogat and Aylmore (1989) have also demonstrated its use in determining soil water content and bulk density. However, all of these early studies were performed using small cores that had been uniformly packed with sieved and homogenized soils. Therefore, these studies did not evaluate soil structures in their native field conditions.

Warner and Nieber (1988), Grevers et al. (1989), and Warner et al. (1989) are among the first researchers to have used CAT techniques to characterize the spatial distribution of soil macropores of undisturbed soil cores. The feasibility of CAT scanning for macropore characterization was assessed by physically sectioning the soil column along the scan plane in order to compare features of scan images with the physical section of the core. After comparison, Warner et al. (1989) reported that *“the CT scan process is a promising non-destructive method for the characterization of macropores in soil”*. Grevers et al. (1989) also found that results of the CAT scan images compared well with features observed in sections of the soil columns. However, the scans were examined and interpreted visually. Warner et al. (1989) pointed out the need to develop a comprehensive algorithm to automate the interpretation of images produced by the CAT scanner.

Following the pioneering work of Grevers et al. (1989) and Warner et al. (1989), several researchers examined CAT scanning as a method to characterize soil macropores in intact soil cores. Table 2.4 provides an annotated reference list of the research teams and publications pertaining to the application of CAT scanning to describe soil macroporosity in undisturbed soil columns.

**Table 2.4:** Studies using CAT scanning for the evaluation of pore structure of intact soil cores.

Research Institution	References	Summary
Dept. of Agr. Eng. / Dept. of Radiology University of Minnesota, USA.	Warner and Nieber (1988) Warner et al. (1989) Warner (1990)	Macroporosity in undisturbed soil columns was evaluated using computer assisted tomography.
Saskatchewan Institute of Pedology, University of Saskatchewan, CANADA.	Grevers et al. (1989) Grevers and de Jong (1994)	Soil macropore system and a compacted layer of soil were analyzed using CAT scanning and geostatistical techniques using cores of 200 mm i.d. x 160 mm.
Dept. of Agronomy & Dept. of Civil Eng. University of Missouri, USA.	Anderson et al. (1990,1992) Peyton et al. (1992,1994a,1994b) Zeng et al. (1996)	Undisturbed soil cores (76 mm i.d. x 76 mm) were scanned for evaluation structural characteristics in soils. Techniques for determination of size/location of macropores and pore water velocities description were investigated. Tracing techniques and Fractal analysis were evaluated.
Dept. of Horticulture, Dept. of Agronomy, Dept. of Human Oncology, and Dept. of Radiology, University of Wisconsin, USA.	Hanson et al. (1991)	Using 3-D visualization, the potential of visualizing pore geometry with computer assisted tomography was demonstrated.
Oklahoma State University, USA.	Brown et al. (1994)	Small-scale density variations in intact soil cores (50.8 mm i.d. x 25.4 mm) were measured and quantified using a $\gamma$ -ray tomography scanner.
Biol. And Agr. Eng. Dept., Dept. of Crop and Soil Science, and the Institute of Ecology, University of Georgia, USA.	Tollner et al. (1995)	A theory for non-destructive determination of conductivity in soil cores (150 mm i.d. x 350 mm) in terms of the Poiseuille-Carman equation was evaluated.
School of Engineering (University of Guelph) & Imaging Research laboratory (Robarts Research Institute), CANADA.	Asare et al. (1995)	A CAT scanner was used to estimate overall macroporosity of six soil columns (90 mm i.d. x 200 mm).
Dept. of Agr. And Bio. Eng., McGill University & Tomographic and Porous Media Laboratory, University of Calgary, CANADA.	Perret et al. (1996a,1996b, 1997)	Quantification of macroporosity in large intact soil cores (77 mm i.d. x 850 mm) was done. In addition, computer algorithms in the PV-WAVE language were developed to visualize and quantify the three-dimensional and interconnected pore space of soil columns.

On the basis of previous published research on CAT scanning of soil columns, it can be stated that very accurate and repeatable characterization of soil macroporosity can be achieved in a non-destructive manner as opposed to resin impregnation and physical

slicing of soil. Yet, CAT scanning has not been used to its full potential for the quantification of soil macropores and investigation of preferential flow processes. Imagery capabilities of most CAT scanners used in soil studies have been limited to two-dimensional serial scans. Very little work has been done to characterize the macroporosity of intact soil cores in terms of its three-dimensional parameters. Tollner et al (1995) pointed out the need for additional research to investigate reliable approaches to compute tortuosity and connectivity of soil macropores. Imaging in three-dimensions and quantification of three-dimensional parameters of soil macroporosity is critical to the accurate correlation of soil pore structure with preferential flow phenomena, and much additional work is needed in this area (Hanson et al., 1991).

Similarly, the use of Magnetic Resonance Imaging (MRI) has generated interest due to its capability of providing detailed non-destructive images of water. Although this imaging technique has almost been used exclusively for diagnostic purposes on human beings, a few researchers have attempted to apply it to an inorganic medium, such as soil. For instance, Bottomley et al. (1986) and Rogers and Bottomley (1987) have used a 1.5-tesla medical research MRI to study plant root systems and root growth in soil. Their results suggest that MRI can be an effective non-invasive tool for studying plant roots *in situ*. Amin et al. (1993) performed experiments on real soil blocks to assess the feasibility of MRI for mapping the spatial distribution of water. They reported that the presence of paramagnetic elements, such as iron, even at very low concentrations, creates great complications for MRI. Similarly, Rogers and Bottomley (1987) found that roots and water-filled pores of about 1 mm diameter were undetectable by MRI in soils with ferromagnetic particle content greater than 4 % by weight. Therefore, to date, MRI

applications in soil science have been quite limited due to major difficulties associated with image distortions created by paramagnetic elements.

**Concluding remarks on characterization of soil macroporosity:** The characterization of soil macropores can be accomplished by two approaches: indirect and direct. Indirect approaches attempt to determine the influence of macropores by measuring flow characteristics under varying conditions. Measurements of soil macroporosity are obtained with tension-infiltrimeters or the use of breakthrough curves (BTCs). However, indirect approaches provide only qualitative information about soil porosity. Moreover, results obtained with these techniques remain insufficient when calculating the ECDs of macropores as a function of their geometry. Quantitative analysis of macroporosity provides a more comprehensive and systematic approach and is normally obtained by direct methods. Two general approaches can be used for direct analysis of soil macropores; one is destructive (morphometric techniques), the second approach is non-destructive and is achieved by emerging new technologies, such as X-ray or  $\gamma$ -ray computer assisted tomography (CAT scanning) or Magnetic Resonance Imaging (MRI) techniques. The morphometric techniques have the disadvantage of destroying the structure of the soil sample. With recent application of Computer Assisted Tomography (CAT) to soil-plant-water studies, a relatively new and exciting method is now available for non-destructive imaging of macropores and macropore flow. CAT scanning has not been used to its full potential for the characterization of macropores and preferential flow. Very little work has been done to quantify tortuosity and connectivity of macropores. Three-dimensional characterization of soil macroporosity is essential for accurately correlating soil pore structure with preferential flow phenomena. Much additional work

is needed in this area. On the other hand, MRI appears limited for the quantification of soil macropores.

## **2.4 X-ray Computer Assisted Tomography**

X-ray Computer assisted tomography was first introduced in 1971 by G. Hounsfield, an engineer of EMI limited (Electronics Music Industries, Ltd.) in UK. The introduction of X-ray Computer Assisted Tomography initiated a revolution in medical imaging. CAT scanners enabled dramatic advances in medical diagnosis, providing a non-invasive and non-destructive means to examine internal structures of the human body. For his work, G. Hounsfield and his collaborator M. Cormack received the 1979 Nobel Prize for Medicine. X-ray CAT techniques not only provided a revolutionary tool for the medical profession but also led to recent applications in industrial and scientific fields. For example, Davis et al. (1986) demonstrated its application to industrial problems, such as non-destructive analysis of timber poles, rock samples for oil recovery, concrete pillars, plastics, electronic components, etc..

This section is divided into three parts. The first part reviews the principle of X-ray interactions with matter, while the second presents the theory of X-ray attenuation. Finally, the last section details the principles of X-ray CAT scanning in order to provide a basis for their application to materials such as soil and to understand the capabilities of a CAT scanner to quantify soil macropores.

### **2.4.1 X-ray interaction with matter**

In 1895, W. Roentgen discovered that when electrons are accelerated in a vacuum tube and collide on a metal target, fluorescent minerals glow some distance away from



the tube. Roentgen attributed this effect to a new type of radiation. He named it X-ray after the algebraic symbol X, meaning unknown quantity. X-rays are electromagnetic radiation ranging in wavelength from about 10 nm to 0.001 nm. Further investigation into the nature of X-rays indicates that there are five basic mechanisms by which X-rays interact at various structural levels of the atom. The shorter the X-ray wavelength, the greater its energy and penetrating power. Longer wavelengths, near the ultraviolet-ray band of the electromagnetic spectrum, are known as soft X-rays. The shorter wavelengths, closer to and overlapping the gamma-ray range, are called hard X-rays. Table 5 shows the mechanisms of interactions between X-ray and matter, as well as the different atomic levels which are affected by X-ray radiation. Low energy level X-rays interact with the whole atom (classical scattering), whereas high energy X-rays interact with the nucleus of the atom (photodisintegration).

**Table 2.5:** Types of interactions of X-rays with matter.

Mode of interaction	Structural level of the atom interacting with the X-ray
Classical scattering	Target atom
Photoelectric effect	Inner shell of electrons
Compton effect	Outer shell of electrons
Pair production	Nucleus
Photodisintegration	Nucleus

Two of these modes of interaction are of particular importance to radiology and computed tomography: the Compton effect and the photoelectric effect (Morgan 1983). The Compton effect (named after Arthur Compton who discovered this mechanism and in turn, received a Nobel Prize in Physics in 1927) occurs between high energy X-rays and the outer-shell electrons (Figure 2.4a). It results in two changes: ionization of the target atom, and reduction of photon energy. In their normal state, atoms are electrically

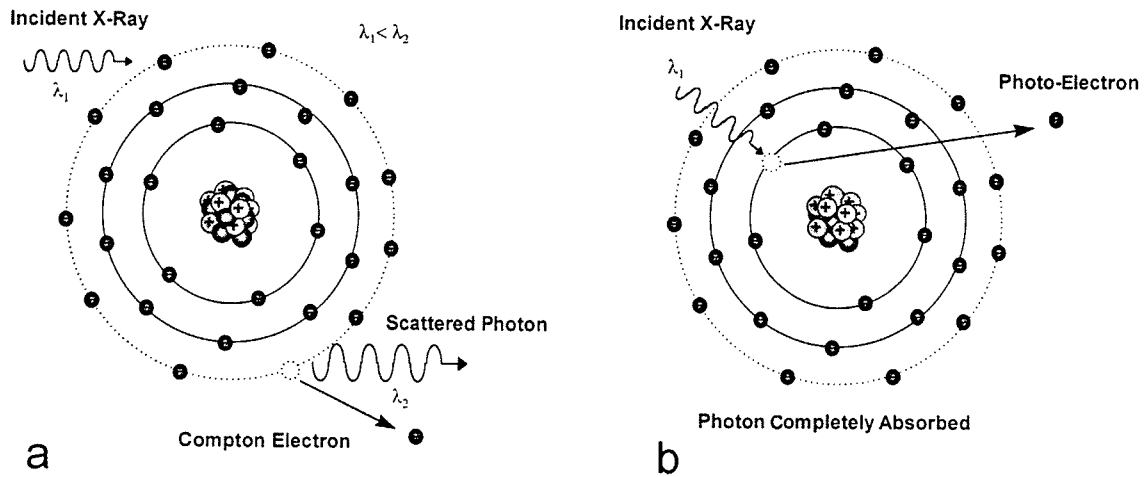


Figure 2.4: Interaction of X-rays with matter in the diagnostic X-ray energy range.  $\lambda_1$  and  $\lambda_2$  represent the wave length of the incident and scattered radiations, respectively (After Mazziotta and Gilman, 1992).

neutral. However, with the Compton effect, the incident X-ray interacts with an outer-shell electron, and ejects it from the atom. The ejected electron, called recoil electron or Compton electron, causes ionization of the atom. Surrounding atoms quickly reabsorb the Compton electron. The incident photon, having delivered some of its energy to the electron, leaves the atom with a longer wavelength. Thus, the Compton effect results in a difference between the incident X-ray's energy level and that of the scattered photon. This difference creates a "contrast" due primarily to the inspected material's electron density (Warner, 1990).

The second type of interaction is known as the photoelectric effect. The photoelectric effect occurs when the incident X-ray is totally absorbed during the ionization of an electron. In other words, the incident photon disappears and one of the k-shell electrons is rejected from the atom (Figure 2.4b). This phenomenon occurs primarily with low-energy X-rays. If the incident photon carries more energy than is necessary to eject the electron, it will transfer its residual energy in the form of kinetic

energy. Ionization of the inner shell of electrons is an unnatural state that is immediately corrected by an outer shell electron dropping into the vacancy. This electron transfer is accompanied by the emission of an X-ray called secondary radiation. This radiation gives an indication of the effective atomic number of the absorbing atom.

The difference in intensity between the incident and transmitted X-rays is related to the X-ray's attenuation along the ray path within the object under examination (Stewart, 1992). The amount of attenuation is linearly related to the irradiated object's bulk density when the energy level of the X-rays is in the Compton range. When energy levels fall within the photoelectric range, attenuation can be used to evaluate the effective atomic number of the materials being irradiated (Kantzas, 1990).

#### **2.4.2 Theory of X-ray attenuation**

Attenuation of the X-rays occurs because the object under radiation absorbs (partially or totally) the photon of the incident radiation. This results in a decreased transmitted radiation. Formation of a radiographic image is based on the spatial variation of the X-ray attenuation which results in a contrast in the detected radiation. The physical quantity that describes the attenuation by matter is called the linear attenuation coefficient ( $\mu$ ).

The intensity of an X-ray beam, measured after propagating through a sample of known thickness, can be described by Beer's law:

$$I = I_0 \exp(-\mu D) \quad (2.2)$$

where  $I$  is the transmitted intensity (eV) and  $I_0$  the incident intensity of the radiation (eV),  $D$  is the sample thickness (m) and  $\mu$  is the linear attenuation coefficient ( $m^{-1}$ ). Equation (2.2) assumes that the material being irradiated is homogeneous over distance  $D$ . Figure 2.5 illustrates various scenarios including the situation where the object under inspection has a variable linear attenuation coefficient (Fig. 2.5c. heterogeneous materials).

For real objects, such as a soil sample, the attenuation coefficient takes the form of an integral over the distance of the ray path. The ray projection can be written as:

$$\ln(I_0 / I) = \int_0^D \mu(x) dx \quad (2.3)$$

The linear attenuation coefficient depends on the bulk density (electron density) of the material, its atomic number, as well as the energy of the incident X-ray beam (Kantzas, 1990). In mathematical terms this relationship can be approximated as:

$$\mu = \rho \left[ \alpha + \beta \frac{Z^{3.8}}{E^{3.2}} \right] \quad (2.4)$$

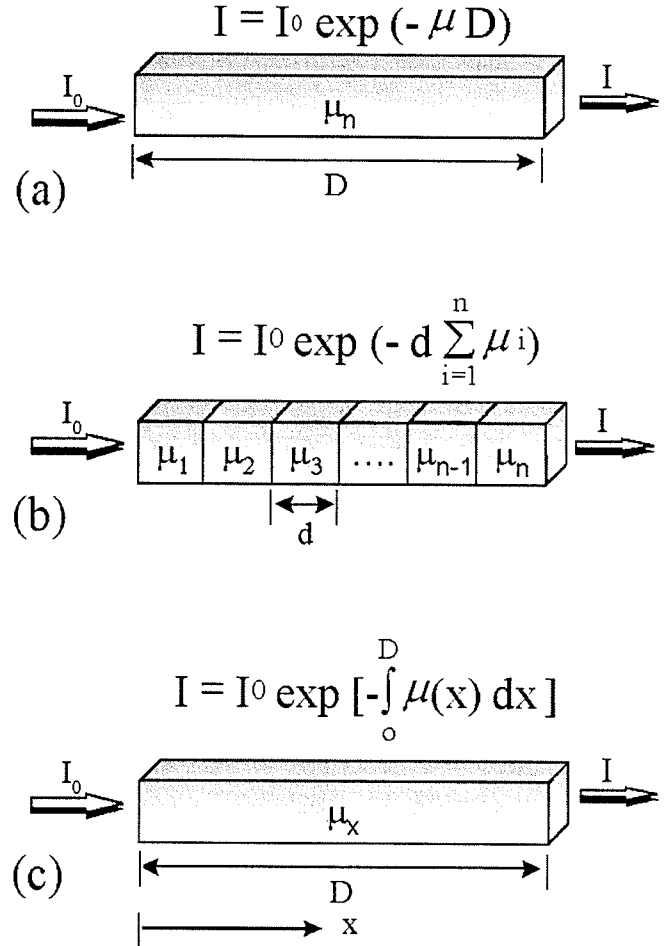


Figure 2.5: Schematic representation of the X-ray attenuation of (a) homogeneous material, (b) heterogeneous material composed of discrete units, (c) heterogeneous material with a variable attenuation coefficient over distance  $x$  (After Greenberg et al., 1983).

where  $\rho$  is the bulk density ( $\text{kg/m}^3$ ),  $\alpha$  is the Klein-Nishina coefficient ( $\text{m}^2/\text{kg}$ ), and  $\beta$  is a constant ( $\approx 9.8 \times 10^{-24} \text{ m}^2 \cdot \text{eV}^{3.2}/\text{kg}$ ),  $Z_n$  is the atomic number,  $E$  is the energy of the incident energy beam (eV). Depending on the energy level of incident radiation, the attenuation coefficient describes either the Compton or the photoelectric effect. At low energies (less than 100 keV), the photoelectric effect dominates, leading to the description of material composition; at higher energies (up to 150 keV), the Compton effect controls interaction with matter and as a result, density images can be created (Stewart, 1992).

A single ray projection cannot provide much information about the distribution of X-ray attenuation coefficients of an object at any given point along the ray path (Aylmore, 1993). The aim of CAT scan technology is to reveal the distribution of attenuation coefficients.

### 2.4.3 Principles of assisted tomography

The word *tomography* is derived from two Greek words: *tomos*, which means

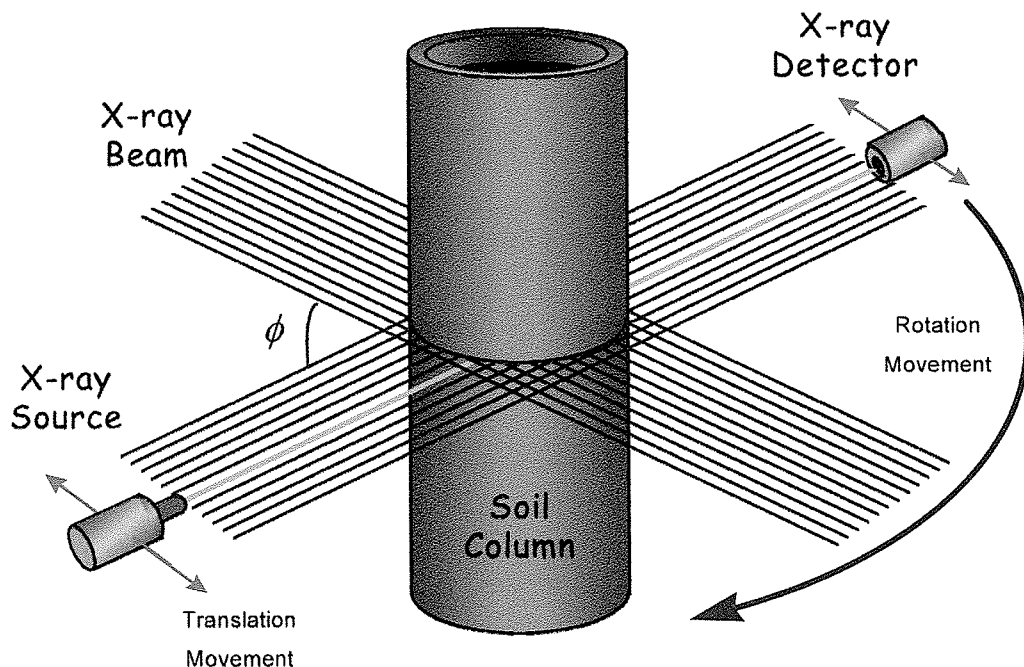


Figure 2.6: Principle of a translation-rotation CAT Scanner.

slice or section and *graphy* meaning to display or to write. A computed tomographic image displays a cross-section of the scanned object. The image is generated from multiple views of the section in a given plane (Figure 2.6). More precisely, during the CAT scan procedure, an X-ray source and a series of detectors move in synchrony around the sample to obtain a set of one-dimensional projections of X-ray attenuation at various angles (Kantzas, 1990). Using the large number of ray projections, a two-dimensional image can be reconstructed. This image displays the spatial distribution of linear attenuation coefficient for a specific slice of the object.

In the first stage of the CAT scan using a translation-rotation scanner, the X-ray source and detector follow linear motion so as to generate a set of parallel X-ray projections. At each incremental position during the translation, the X-ray tube pulses X-rays through the object. The detector (located on the opposite side of the gantry) measures the resultant strength of the X-ray. Once the set of parallel X-rays' attenuation has been recorded, the whole gantry rotates a specific angle ( $\phi$ ), and the translational movement starts again. This operation is repeated for several rotational positions.

For image reconstruction, a Cartesian co-ordinate system is used to describe transmitted radiation at any point in the slice.

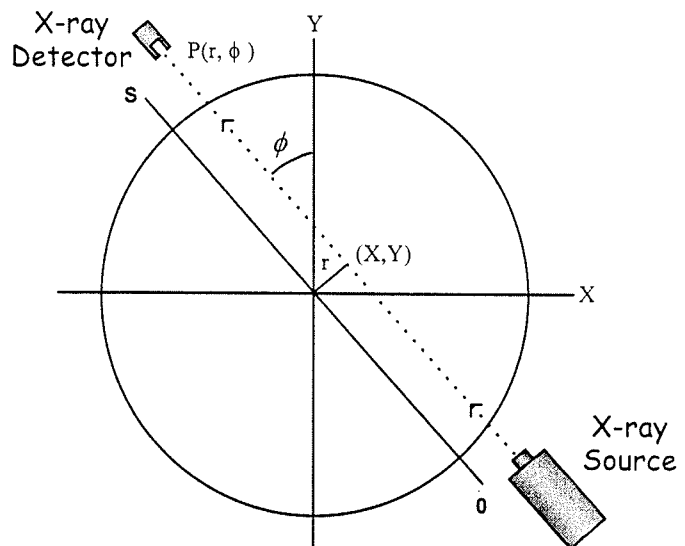


Figure 2.7: Illustration of the coordinate system for the calculation of X-ray attenuation at a given point.

Figure 2.7 is a schematic illustration of the co-ordinate system during this translation-rotation motion.

Each X-ray beam during the translation-rotation of the gantry can be designated by a specific angle ( $\phi$ ) with the Y-axis and a given distance ( $r$ ) from the origin. In addition to the (X,Y) co-ordinate system, another axis (S) parallel to the X-ray beam is used to represent the distance from the X-ray source. S varies between 0 (X-ray source) and s (detector). The transmitted X-ray intensity along a particular path ( $r, \phi$ ) is denoted by:

$$I_{(r, \phi)} = I_0 \exp \left[ - \int_0^s \mu(x, y) ds \right] \quad (2.5)$$

Equation (2.5) can be written in term of the projection value (P) of the ray path ( $r, \phi$ ) as :

$$P_{(r, \phi)} = \ln \left( \frac{I_0}{I_{(r, \phi)}} \right) = \int_0^s \mu(x, y) ds \quad (2.6)$$

Equation (2.6) is the fundamental equation of computer assisted tomography (Kantzas, 1990). With a sufficient number of projection values,  $\mu(x, y)$  can be calculated. This aspect of the CAT scan process is known as numerical reconstruction.

Three methods of numerical reconstruction have been developed to generate the two-dimensional distribution of attenuation coefficients, given that a sufficiently large set of linear integrals has been obtained. These methods are the back-projection method, iterative reconstruction, and filtered back-projection. The filtered-back projection method is commonly used and considered most accurate (Aylmore, 1993). The precise methodology by which a cross-sectional image is generated is beyond the scope of this section. For more information, the reader is referred to Kantzas (1990).

The result of numerical reconstruction is a two-dimensional matrix composed of picture elements (pixels). Each pixel corresponds to the attenuation of a small volume element called voxel (Figure 2.8).

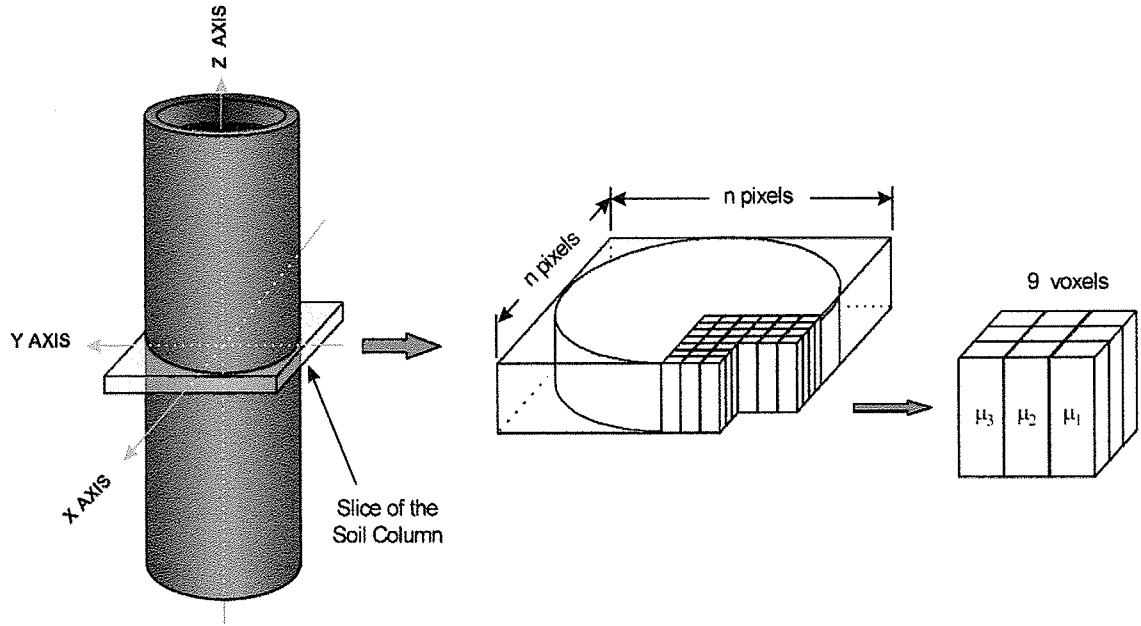


Figure 2.8: Schematic illustration of the CAT scan terminology (After Wellington and Vinegar, 1987).

After the CAT scanner has reconstructed the image, the pixel values are converted into an internationally standardized number, known as CTn (Computed Tomography number), usually expressed as follows (Haaga et al., 1994):

$$CT_n = k \frac{(\mu - \mu_w)}{\mu_w} \quad (2.7)$$

where  $\mu_w$  is the linear attenuation coefficient of water ( $\text{m}^{-1}$ ),  $\mu$  is the attenuation coefficient of the pixel in question ( $\text{m}^{-1}$ ), and CTn is the CT number, measured in Hounsfield units (HU). Although the original EMI CAT scanner used a value of 500 for  $k$ , most current scanners use a value of 1000 HU. CTn units (HU) are named in honor of



Godfrey Hounsfield who invented the first CAT Scanner. The HU scale is linear and HU for water is obviously 0 (i.e., Equation 2.7). The scale generally runs between -1000 HU and +1000 HU. A negative CTn implies that density is below that of water. Petrovic et al. (1982) reported that the CTn for a fine sandy loam soil ranged from 450 to 800 HU.

The end result of the CAT scan process is a two-dimensional array of pixels in HU, which can be displayed as an image on the system monitor or stored on magnetic tape for subsequent analysis.

## **2.5 Application of CAT Scanning to Soil Studies**

CAT scanning has become an attractive and promising tool for soil studies. Recent advances in X-ray computer assisted tomography have allowed the development of methods for rapid non-destructive analysis of soil cores. For more than a decade, several research efforts in the field of soil science have been conducted using CAT scanning. The majority of these studies has demonstrated the remarkable potential of this new technique and have shown the tremendous use of CAT images for qualitative analysis of soil properties. In addition to visual and qualitative inspection of CAT images, scanned object properties can be quantified with appropriate processing and calculations. Some properties that have been measured using CAT include: bulk density, porosity, macroporosity, water content and solute concentration. A comprehensive review of research studies on the determination of soil properties using CAT scanning has been presented in section 2.3.2.

In this section, we will review different measurements that can be obtained by the manipulation and processing of data generated with CAT scanners. It is divided into four sub-sections. The first sub-section deals with the theory behind the conversion of CT

numbers into physical properties. Bulk density and porosity mapping are reviewed in the next two sub-sections, and the last sub-section presents the analysis of tracer displacement using a CAT scanner.

### 2.5.1 Conversion of CAT scan data to physical properties

CAT images provide a discrete representation of the scanned material's X-ray attenuation. Although expressed in HU, a CT number (CTn) is a dimensionless quantity. In order to correlate the CTn to specific physical properties, one must establish the relationship between the linear X-ray attenuation and the physical parameter of interest (Kantzas, 1991). As mentioned earlier, CTn values or X-ray attenuation coefficients can be related to the electron density (bulk density) and atomic number of the material, as dictated by Equation (2.4) (Section 2.4.2):

$$\mu = \rho \left[ \alpha + \beta \frac{Z_n^{3.8}}{E^{3.2}} \right] \quad (2.4)$$

where  $\mu$  is the linear attenuation coefficient ( $\text{m}^{-1}$ ),  $\rho$  the bulk density of the material ( $\text{kg}/\text{m}^3$ ),  $\alpha$  is the Klein-Nishina coefficient ( $\text{m}^2/\text{kg}$ ), and  $\beta$  is a constant ( $\approx 9.8 \times 10^{-24} \text{ m}^2 \cdot \text{eV}^{3.2}/\text{kg}$ ),  $Z_n$  is the atomic number of the material, and  $E$  is the energy of the incident X-ray beam (eV). The first term of Equation (2.4) represents the Compton effect (X-ray energies above 100 keV), and the second term accounts for the photoelectric effect (X-ray energies below 100 keV). Based on the mode of X-ray interaction with matter, linear X-ray attenuation will reveal the scanned object's bulk density or atomic number. In other words, if the CAT scanner is operating at an X-ray energy level greater than 100 keV, distribution of linear attenuation coefficients can be related to the material's density. Below 100 keV, the CAT scan image can be used to characterize the material's

composition.

### 2.5.2 Bulk density mapping

The first reported attempt to measure spatial distribution of soil bulk density using a commercial X-ray CAT scanner was done by Petrovic et al. (1982). They showed that the bulk density of soil samples packed over a range of 1.2 to 1.6 g/cm<sup>3</sup> was linearly correlated to the X-ray attenuation coefficient. A few years later, a number of workers (Hainsworth and Aylmore, 1983; Crestana et al., 1986; Anderson et al., 1988; Warner, 1990; Aylmore, 1993) also demonstrated that CTns are linearly related to soil's bulk density. Therefore, by plotting CTns versus the bulk density of reference materials, one can easily derive a calibration line that relates bulk density to the material's X-ray attenuation coefficient. If a linear relationship holds, then the bulk density of each individual pixel can be calculated as:

$$\rho = \frac{\text{CTn} - b}{m} \quad (2.8)$$

where  $\rho$  is the bulk density of the material (kg/m<sup>3</sup>), CTn is the CT number in HU,  $b$  is the y intercept and  $m$  the slope of the calibration line. Using simple linear regression, it is possible to derive a linear function that relates raw CAT scan data to the object's bulk density; and to convert raw data into two-dimensional matrices of bulk density.

### 2.5.3 Porosity mapping

The term porosity generally refers to the volume fraction of the pore system of a porous medium (Hillel, 1982). Determination of soil's total porosity provides a simple and qualitative way to characterize the soil pore system. Determination of core porosity

has been one of the common applications of CAT scanning in petroleum engineering and is of great interest for soil science.

In practice, it is impossible to obtain an infinite number of X-ray projections; the image is reconstructed from a finite number of voxels, which could contain a mixture of solids, liquids and gases. Thus, the linear attenuation coefficient of a voxel is a combination of the linear attenuation coefficients of its content. In porous media, this relationship can be written mathematically as:

$$\mu_{(\text{voxel})} = \phi \mu_{(\text{gas} + \text{liquid})} + (1 - \phi) \mu_{(\text{solid})} \quad (2.9)$$

where  $\mu_{(\text{voxel})}$ ,  $\mu_{(\text{gas}+\text{liquid})}$ , and  $\mu_{(\text{solid})}$  are the linear attenuation coefficients of the voxel, of the fluids, and of the solids, respectively, and  $\phi$  is the voxel's porosity ( $\text{mm}^3/\text{mm}^3$ ). This equation can be expressed in terms of the CTn of the solids and fluids as:

$$CTn_{(\text{voxel})} = \phi CTn_{(\text{fluid})} + (1 - \phi) CTn_{(\text{solid})} \quad (2.10)$$

where  $CTn_{(\text{voxel})}$ ,  $CTn_{(\text{fluid})}$ , and  $CTn_{(\text{solid})}$  are the CT numbers of the voxel, of the fluids, and of the solids, respectively. Porosity can therefore be expressed as:

$$\phi = \frac{CTn_{(\text{solid})} - CTn_{(\text{voxel})}}{CTn_{(\text{solid})} - CTn_{(\text{fluid})}} \quad (2.11)$$

Since the CT numbers are linearly related to bulk density, Equation (2.11) can be extended to:

$$\phi = \frac{(m\rho_{(\text{solid})} + b) - (m\rho_{(\text{voxel})} + b)}{(m\rho_{(\text{solid})} + b) - (m\rho_{(\text{fluid})} + b)} = \frac{\rho_{(\text{solid})} - \rho_{(\text{voxel})}}{\rho_{(\text{solid})} - \rho_{(\text{fluid})}} \quad (2.12)$$

where  $\rho_{(\text{voxel})}$  is the bulk density of the voxel,  $\rho_{(\text{fluid})}$ , the bulk density of the fluids, and  $\rho_{(\text{solid})}$ , the grain density (also known as particle density).  $b$  is the y intercept and  $m$  is the

slope of the linear calibration curve relating CT numbers to bulk density.  $\rho_{(\text{voxel})}$  is obtained by converting the voxel's CT number to its bulk density value using the calibration curve. Thus, when the particle density of the solid is known and when the soil core is dry ( $\rho_{(\text{fluid})} = \rho_{(\text{air})} \approx 0$ ), the sample's porosity can easily be determined.

#### **2.5.4 Tracer analysis and real-time scanning**

Solute transport through a soil column is generally determined with a breakthrough experiment. X-ray CAT scanning can be used rapidly and non-destructively to quantify the volume concentration inside a soil core during breakthrough experiments. To the best of our knowledge, only a group of researchers at the University of Missouri (Peyton et al. 1994a; Heinze, 1994; Wigger, 1991) have used this innovative technique to measure velocity distributions in a small undisturbed soil core (76.2 mm x 76.2 mm). Using potassium iodide (KI) as the tracer solution in breakthrough experiments, they measured the average volume concentration at regular time intervals by scanning the downstream face of the core. They found this approach to be useful for analyzing breakthroughs at a cross-section in the soil column. Whereas these researchers made measurements at a single depth in a small soil core, this approach can be applied to monitor solute breakthrough at various depths in a large soil column. This novel approach offers tremendous potential in the study of preferential flow.

### **2.6 Single Photon Emission Computed Tomography**

Single photon emission computed tomography (SPECT) is a medical specialty which is unique in that it documents organ function, in contrast to X-ray CAT scanning which is based upon anatomy. In SPECT imaging, very small amounts of radioactive

material, or radiopharmaceuticals, are used to diagnose diseases. Radiopharmaceuticals are substances that are attracted to specific organs, bones, or tissues. When radiopharmaceuticals are introduced into the body, they produce emissions. A special type of camera is used to transform these emissions into images and data which provide information about the area of the body being imaged. An estimated 10 to 12 million SPECT diagnostic procedures are performed each year in the U.S (SNM, 1998). However, although SPECT scanning is commonly used in hospitals for diagnostic purposes, it has rarely been applied to engineering and has never been introduced into soil physics.

In this section, basic principles pertaining to SPECT imaging are presented in order to explain the capabilities of a gamma camera to visualize and characterize preferential flow phenomenon in soils.

### **2.6.1 Introduction to single photon emission computed tomography**

As mentioned above, SPECT is based on detecting nuclear radiation emitted from the body or an object in which a radiopharmaceutical has been introduced. It has a fundamental difference from X-ray CAT scanning in the sense that X-ray CAT scanning generates transmission images whereas SPECT scanning produces emission images (Palmer et al., 1992). In other words, during X-ray CAT scanning, an external X-ray beam passes through the patient or the object and the X-ray attenuation is recorded on the opposite side. However, during SPECT scanning, the source of radiation is coming from inside the object and is recorded externally. Because the emission sources (injected radionuclides) are inside the body cavity, this task is far more difficult than for X-ray CAT scanning, where the source position and strength (outside the body) are known at all

times. SPECT scanning can be seen as a complementary approach to CAT imaging as it allows visualization of parts of organs and their physiological functions that are not usually seen by normal X rays. X-ray CAT is primarily designed for visualization of the structure of an object or patient's anatomy, whereas, with the use of radiopharmaceuticals, SPECT imaging provides a powerful technique to inspect specific physiological functions.

### **2.6.2 Radiopharmaceuticals**

SPECT scanning involves the detection of gamma rays emitted from radioactive atoms, called radionuclides, such as Technetium-99m and Thallium-201. As long as the photons emanating from the radionuclide have sufficient energy to escape from the body or the object of interest in significant numbers, images can be generated that depict the spatial distribution of the radiopharmaceutical. Most radiopharmaceuticals consist of two parts: a radioactive label (i.e., radionuclides) and a molecule whose physical or chemical properties define the location on which the radiopharmaceutical will be adsorbed (Palmer et al., 1992). One or more atoms in the molecular structure of the radiopharmaceutical is therefore unstable. This instability results in emission of alpha, beta and gamma particles (Early and Sodee, 1995). Most common radiopharmaceuticals have short half-lives measured in hours or days. For instance, Technetium-99m (Tc-99m) has a half-life of 6.02 hours (Hamilton et al., 1997). Tc-99m is by far the most important radionuclide in current medical practice (Palmer et al., 1992). Technetium is often used in the form of sodium pertechnetate,  $\text{Na}^{99\text{m}}\text{TcO}_4^-$ . The pertechnetate ion is similar to iodide in its size and charge and is commonly used in dynamic flow studies in the human body for

acquiring rapid sequential images. Moreover, the ionic form of Tc-99m requires no special preparation.

### 2.6.3 Basic principles and instrumentation

As mentioned above, a special type of camera, a gamma or scintillation camera, is used to transform these emissions into images and data which provide information about the area in which the radioactive tracer is present. The gamma camera of the TIPM laboratory in Calgary is presented in Figure 2.9.

The gamma rays emitted by radionuclides interact with matter in two important ways (Jaszczak, 1988). The first involves scattering of the gamma ray off electrons in the atoms and molecules. This scattering process is

called Compton scattering. Some Compton scattered photons are deflected outside the scintillation camera's field of view and are lost to the detection process (Floyd et al., 1984). The second interaction consists of a photon being absorbed by an atom in the body with an associated jump in energy level (or release) of an electron in the same atom. This process is called the photoelectric effect and is described in Section 2.4.2.

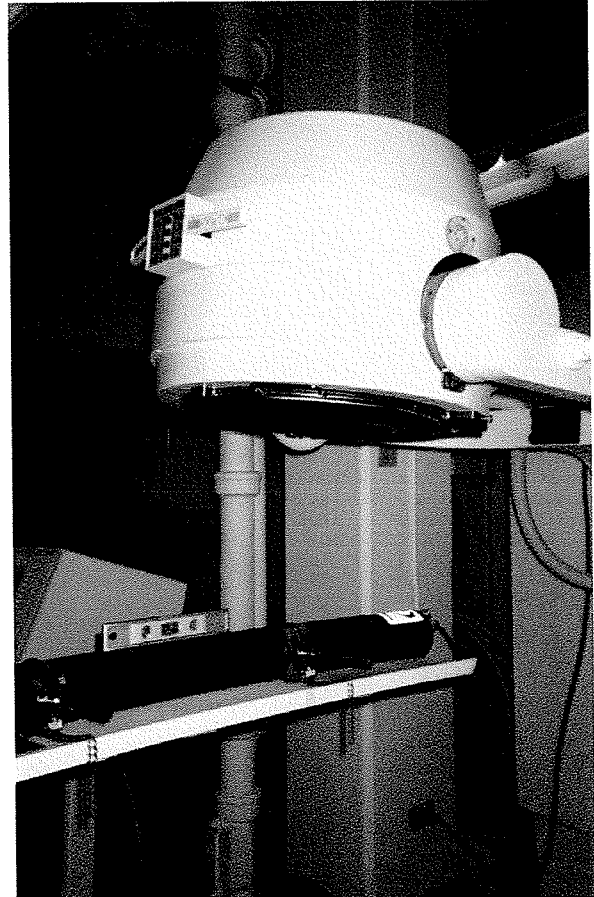


Figure 2.9: Siemens Orbitor Gamma Camera at the TIPM laboratory in Calgary (Alberta)



Single photon emission computed tomography requires collimation of gamma rays emitted by the radiopharmaceutical. The purpose of collimation is to mechanically confine the direction of the incident photons and to localize the site of the emitting source (Cho et al., 1993). Collimation has the greatest effect on determining SPECT system spatial resolution and sensitivity. Sensitivity of a SPECT scanner relates to how many photons per second are detected and spatial resolution relates to the size of each picture element. The collimator contains thousands of square, round or hexagonal parallel channels through which gamma rays are allowed to pass. A Gamma camera equipped with a collimator is called an Anger camera, after its inventor H. Anger. Most Anger scintillation cameras have spatial resolutions of 4 to 9 mm at the surface of a high-resolution, parallel hole collimator (Palmer et al., 1992). Collimators generally improve resolution by excluding scatter. Collimators for SPECT imaging are typically made of lead.

Gamma rays, traveling along a path that coincides with one of the collimator channels, will pass through the collimator unabsorbed and interact with a large sodium iodide (NaI) crystal creating light. These light photons are then guided toward photocathodes of an array of photomultiplier (light sensitive) tubes, where they are converted into electrons, multiplied and finally, converted into an electrical signal (Cho et al., 1993). In other words, behind the crystals, a grid of photomultiplier tubes collect the light for processing. The principle components of a scintillation camera are shown in Figure 2.10.

The brightness of each flash is proportional to the amount of energy deposited in the crystal, which is proportional to the energy of the incident photon. Thus, both the

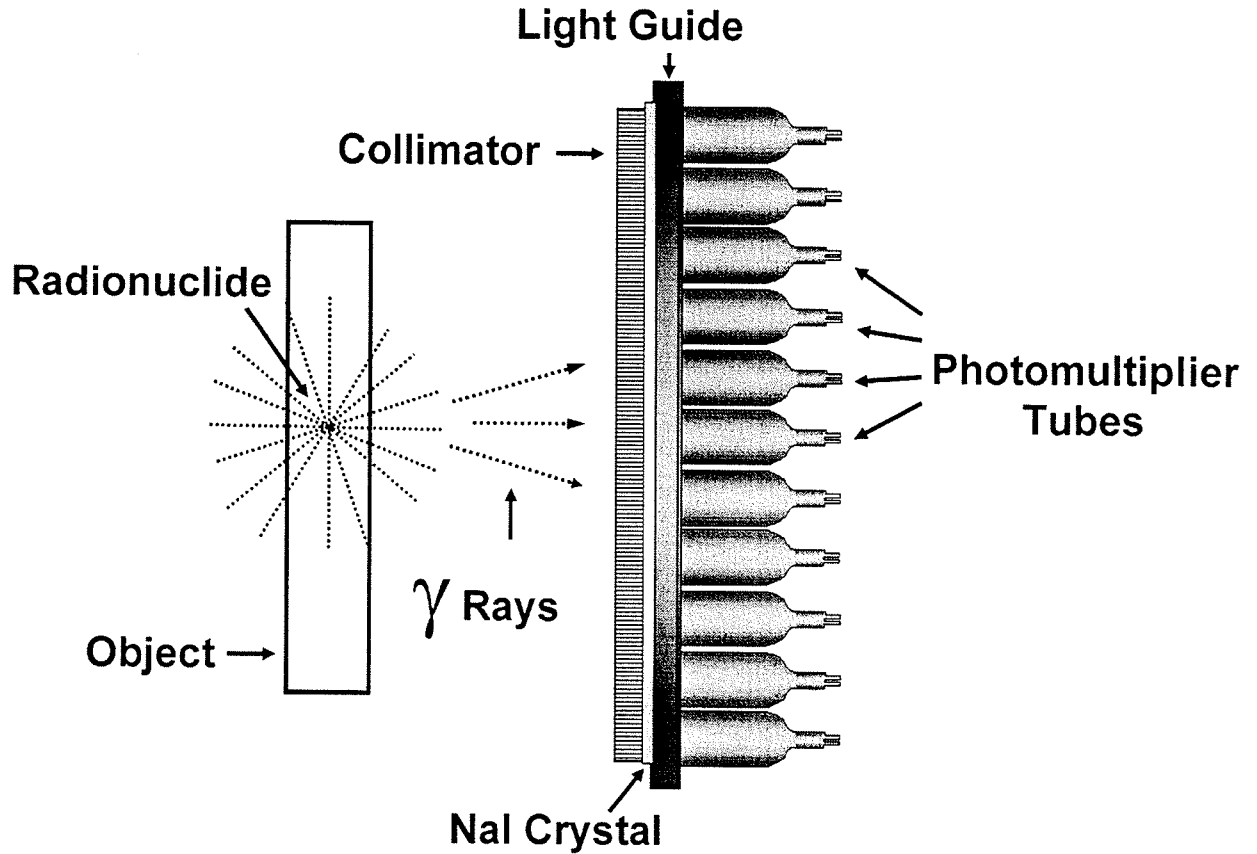


Figure 2.10: Basic principles and components of a gamma camera

number and energy of incident photons can be recorded. Moreover, the collimator attached to the NaI crystal and position logic circuits relate the position of each scintillation to the x, y coordinates of a two-dimensional projection image. The electrical pulse generated by each of the photomultiplier tubes is then discriminated to retain only the pulse that lies within a prescribed energy window. This task is achieved by pulse-height analyzer circuits. A retained pulse is known as a count.

Similarly to CAT scanning, the count rates can be stored in computer memory in a matrix of pixels. The numeric value of each pixel represents the counts recorded at that particular location. The size of each pixel is typically much greater than that of X-ray

CAT scanning and ranges from 2 to 9 mm (Palmer et al., 1992). It should be mentioned, however, that this resolution is dependent on the size of the scintillation camera and the collimator. Once in digital form in memory, the images can be displayed with various contrast and brightness, or stored for further and more detailed analysis. The images can be evaluated to define temporal and spatial changes in the concentration of radionuclides. This dynamic investigation of sequential images is similar to the analysis of time-lapse photography. This allows the detection of functional changes occurring over minutes to hours that may be difficult to investigate in static images. As a result, sequential images provide a powerful approach to visualize and quantify tracer displacement in dynamic flow studies in a non-destructive manner.

## **2.6.4 Image acquisition and processing**

“Single Photon Emission” refers to the uniform and isotropic emission of photons in all directions during the decay of radionuclides. These emissions can be recorded either as planar projection images or in a tomographic fashion.

### **2.6.4.1 Planar imaging**

Planar single photon images are a pictorial representation of the radioactive decay that emanates from within the patient or the object of interest. More precisely, it is a two-dimensional representation of a three-dimensional object. It depicts the three-dimensional distribution of radiopharmaceutical onto a planar two-dimensional surface producing a projection image. This type of imaging was developed by Hal Anger in the late 1950s (Cho et al., 1993). A planar single photon image is very similar to a standard radiograph, however, the photons do not pass through the object but are emitted from

within the object. Moreover, typical scintillation cameras have a temporal resolution of about 1.5 to 3 microseconds (Palmer et al., 1992). Therefore, planar imaging can be used in dynamic studies in which changes in the distribution of radiation can be observed. However, in order to register enough radioactive counts to generate a planar single photon image, it is standard to acquire the  $\gamma$ -rays during 0.5 to 1 second.

#### 2.6.4.2 Tomographic imaging

The first SPECT device was the MARK IV developed by D.E. Kuhl and R.Q. Edwards in the early 1960s. However, it was not until the introduction of X-ray CAT scanning in the mid 1970s that clinical SPECT scanners were developed allowing qualitative and quantitative image analysis for medical use (Cho et al., 1993).

Tomographic single photon images are acquired by detecting the radioactive decay activity from different angles around the object. This is accomplished by rotating the

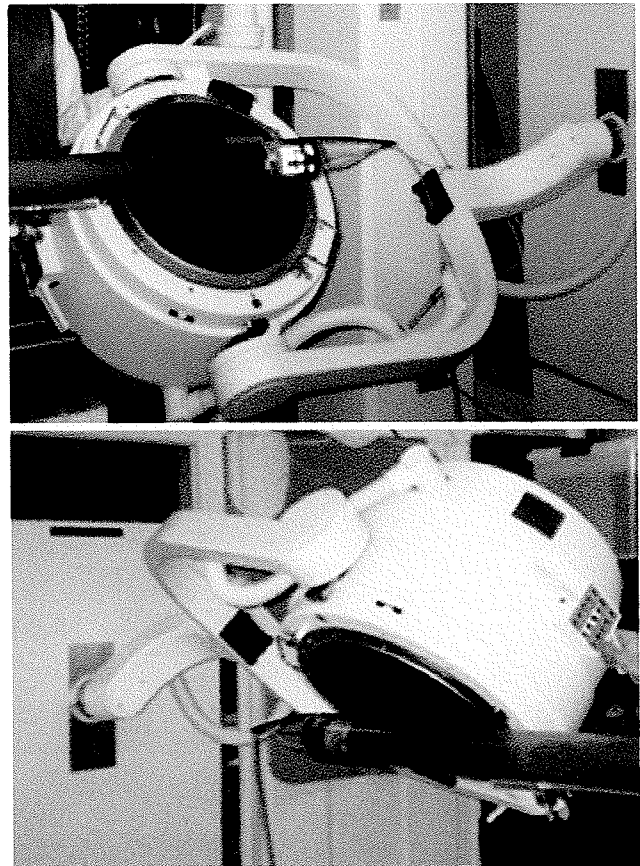


Figure 2.11: Rotation of the gamma camera around a column of soil

camera head around the object and recording data from multiple projections. In order to achieve this, the scintillation camera is mounted onto a gantry designed to allow the

camera head to orbit around the object as shown in Figure 2.11. The data are then stored in a computer and reconstructed in a manner analogous to X-ray CAT scanning (Section 2.4.3). As a matter of fact, there are no significant differences between X-ray computed tomography and nuclear emission computed tomography (Palmer et al., 1992). As the camera rotates, it records the spatial distribution of the radioactive decay within the volume of the object. In other words, during SPECT scanning, multiple planar single photon images are acquired. More precisely, the scintillation camera rotates around the object of interest, stopping at selected intervals and generating images at each view. These images are then stored in a computer until the entire object has been viewed from multiple angles. A series of cross-sectional images or matrices of the object are then generated using a filtered back-projection reconstruction algorithm. It should be mentioned, however, that the spatial resolution of SPECT is usually worse than that of planar images. In most applications, the camera head is rotated entirely around the patient or the object to reconstruct a cross-section. For typical studies, the time required for data collection, as the camera head rotates entirely around the patient, is usually about 10 to 20 minutes (Cho et al., 1993).

### **2.6.5 Application of SPECT scanning**

SPECT scanning is widely used in medical diagnosis, more specifically in a field known as nuclear medicine. As mentioned earlier, 10 to 12 million nuclear medicine imaging and therapeutic procedures are performed each year in the US alone. Today, nearly all cardiac patients in developed countries receive a SPECT scan to detect artery disease or a damaged heart. Investigation of liver, kidneys, thyroid gland and many other organs are similarly leading applications of SPECT (Coleman et al., 1986). It is used

routinely to help diagnose restriction of blood flow to parts of the brain, cancer, stroke, lung disease and many other physiological abnormalities.

Scintillation camera technology has been introduced to the industrial field since the mid 1980s. For instance, photon emission imaging has been used to perform visual and radiometric scans of nuclear facilities. Sedaghat et al. (1988) developed a technique, using a gamma camera, to characterize cross flow in a two sub-channel nuclear fuel assembly. Gamma camera technology has also been adapted to conduct contamination surveys inside buildings connected with nuclear production (Chesnokov et al., 1997; Mottershead and Orr, 1996).

The gamma camera has brought a new dimension to disciplines such as particle tracking and flow analysis in mixing reactor vessels. Castellana and Dudley (1984) were among the first researchers to visualize particle motion in fluid-solid systems using a gamma camera. With a similar approach, Lin et al. (1985) measured the solid motion of radioactive particles, in gas fluidized beds, with a series of photomultiplier tubes. Still today, radioactive particle tracking offers great potential for measurement of recirculating phase velocities in gas-fluidized beds and bubble columns (Hamilton et al., 1997). Scintillation cameras have also been used in determining the hydrodynamics and radial distributions of velocity in vertical riser reactors and mixing reactor vessels (Castellana et al., 1984; Berker and Tulig, 1986; Legoupil et al., 1997). The potential of SPECT scanning for imaging a gas-flow fluidization test rig and fluid flow in a gasification unit is discussed by Jonkers et al. (1990). Other applications to the field of engineering include measurements of liquid film thickness on the surface of a rotating disk

(Castellana and Hsu, 1984) and analysis of radioactive ball trajectories within the charge of a rotary grinding mill (Powell and Nurick, 1996).

Nuclear technology has also been utilized in oil recovery fields to visualize dynamic oil displacement in porous media. For instance, Huang and Gryte (1988) used a gamma camera to observe immiscible displacement of oil in thin slabs of a porous medium saturated with water. In their study, Technitium-99m was used as a tracer for the water phase. The authors showed that photon emission imaging provides a powerful approach to determining local fluid saturations in quantitative terms. Using nuclear imaging techniques, Lien et al. (1988) studied one-dimensional saturation distributions in 0.75 m long sandstone cores at reservoir pressures and temperatures. Information on one-dimensional fluid saturation distributions was obtained by labeling fluid phases with nuclear tracers and detecting radiation with a gamma camera. They reported that the apparatus fulfilled its objective: imaging displacement processes at reservoir conditions. Charlier et al. (1995) applied  $\gamma$ -ray absorption techniques in order to determine permeability of oil during a tertiary gas gravity drainage experiment. Using this technique, they were able to visualize fluid saturation distribution in the core as a function of the injected gas' volume.

Although the power of non-invasive and *in situ* SPECT scanning has been demonstrated for dynamic industrial processes, and for oil recovery, this technique has never been applied to soil studies nor to the visualization and characterization of preferential flow phenomenon. This approach opens new avenues, both in 2-D and in 3-D, for tracer studies in porous media, such as soil.

## **2.7 Modeling of Water and Solute Transport**

Extensive research has been conducted to determine the functional relationship between pore geometry and saturated water flow in heterogeneous soil. However, this problem has not been easy to resolve (Huffman and Monke, 1989). In this section, we will briefly review various modeling approaches that have been used to simulate flow and solute transport in soils. This review is by no means exhaustive; rather, the emphasis here is on the problems associated with macropore flow.

Different methods have been developed to characterize and model water and solutes fluxes in soil. These approaches can be divided into two main categories (Steenhuis et al., 1990). The first approach relies on the use of stochastic models whereas the second is phenomenological, based on deterministic approaches. Phenomenological approaches are more common and therefore, will be discussed in more details.

### **2.7.1 Stochastic approaches**

The spatial variability of the soil structure is so complex that some researchers have suggested that stochastic modeling would be appropriate (Grochulska and Klavivko, 1994). Rather than describing the complex mechanisms of chemical movement in soil, they have proposed to use a transfer function based on the probability density function of the solute travel time. Beven and Young (1988) suggested that the transfer functions could be estimated from the fluxes from a volume of medium through the use of time series analyses. Although this approach is attractive in principle, it is site specific and requires extensive measurements at any new site (Bouma, 1991). Moreover, Steenhuis et al. (1990) pointed out that these stochastic models are often extremely complex and do not guarantee validity for locations and processes for which they have not been



calibrated.

## 2.7.2 Phenomenological approaches

In phenomenological models, solute transport in soil is explained by a deterministic or a mathematical interpretation. The deterministic model is then solved using either analytical or numerical techniques. This section is divided into 3 sub-sections. The first sub-section introduces the standard convection dispersion models used in simulating solute transport, while the second sub-section deals with the potential of multi-region modeling. Finally, the last sub-section presents an alternate model to consider flow through macropores.

### 2.7.2.1 Classical approach: convection dispersion models

Most of these types of models use Richard's equation for water movement and convection dispersion models with various types of sorption sites and chemical and physical non-equilibrium mechanisms for chemical transport. The classical convection dispersion equation (CDE) can be written as:

$$R \frac{\partial C}{\partial t} = D_c \frac{\partial^2 C}{\partial z^2} - V \frac{\partial C}{\partial z} \quad (2.13)$$

where  $C$  is the solute concentration ( $\text{g/mm}^3$ ),  $t$  is the time (s),  $D_c$  is the coefficient of hydrodynamic dispersion ( $\text{mm}^2/\text{s}$ ),  $z$  is the vertical position along the flow path (mm),  $V$  the average velocity (mm/s) and  $R$  is a retardation factor (dimensionless). Equation 2.13 assumes linear equilibrium adsorption and transport in one-dimension. If there are no interactions between soil particles and solute,  $R$  is 1.0. Many management and research

models are based on the CDE approach, such as PRZM-2 (Carsel et al., 1995), PESTFADE (Clemente et al., 1993), LEACHM (Hutson and Wagenet, 1989), MOUSE (Steenhuis et al., 1987), DRAINMOD-N (Breve, 1994). However, Kumar and Kanwar (1997), Hornberg et al. (1990) and Steenhuis et al. (1990) pointed out that these models lack the capability of simulating solutes in drainage waters. For instance, many column and field studies of solute transport in soil showed substantial deviation between measured effluent concentration and those calculated using the CDE approach (Hutson and Wagenet, 1995). Inaccurate predictions are attributed to a lack or inadequate consideration of macropore flow (Smith et al., 1991). One method to improve the CDE approach is to divide the flow in soil into several regions.

#### 2.7.2.2 Multi-region modeling

Ma and Selim (1997) discussed the potential offered by multiregion modeling. They pointed out that this approach is one of the research areas in the forefront of soil physics and hydrology disciplines. This approach is based on simplification of the flow region into different domains, such as mobile water versus immobile water, transient flow versus steady flow, and laminar flow versus turbulent flow. For instance, one simplification is to divide the flow field into the following domains: the macropore flow domain where rapid transport may occur preferentially and micropore flow domain where solute transport is occurring in the surrounding matrix at a much slower rate (Figure 2-12).

Van Genuchten and Wierenga (1976) were among the first researchers to have proposed a dual-porosity model with the concept of mobile-immobile water. Since then, solute transport using a two-region approach has been considered by a number of

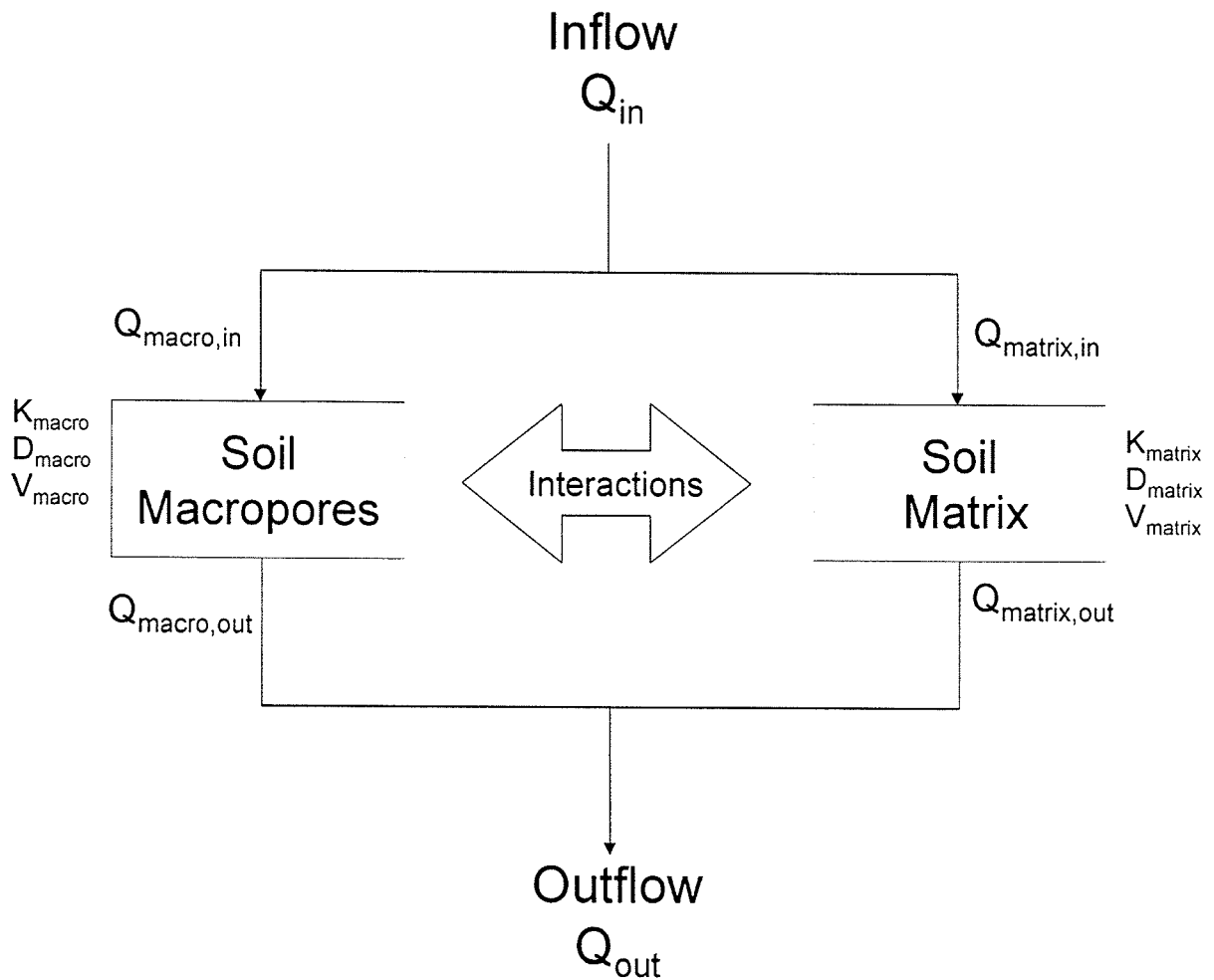


Figure 2.12: Schematic representation of the two-flow domain system where  $Q$  represents flow rate,  $K$  the soil's conductivity,  $D$  the coefficient of hydrodynamic dispersion,  $V$  the average velocity in the respective flow domains.

investigators (Ma and Selim, 1997; Hutson and Wagenet 1995; Chen and Wagenet, 1992; Steenhuis et al., 1990; Germann et al., 1984; Nielsen et al., 1986). Although dual-porosity models based on the CDE offer insights into the mechanisms that have an important bearing on preferential flow, they are not easily applied to describe observations in large intact soil cores or from field blocks where the nature of the flow pathways is essentially indeterminate (Hornberg et al., 1990). The criteria of demarcation between flow domains

are not well understood. As a result, the input parameters are rather arbitrarily defined and difficult to determine (Steenhuis et al., 1990; Hutson and Wagenet 1995).

Knowledge of soil macropore structure, along with a suitable technique for measurement of flow characteristics of water and associated solutes through soil, provide a solution to establish a demarcation between flow domains. The use of CAT fulfils these requirements. CAT scanning offers great potential to quantify soil macropore structure in great detail and to monitor the breakthrough of water through soil. With this information, the macropore flow domain and matrix flow domain can be isolated accurately. Once the flow domains have been identified, one can proceed with the formulation of the models and the initial and boundary conditions to be used for each flow region.

The Richard's equation and the CDE are commonly used to describe water flow and solute transport in homogeneous soils and as a result, modeling of vertical flow and chemical movement in the matrix domain is not difficult (Chen and Wagenet, 1992). The challenge is to describe flow through the macropore domain.

#### 2.7.2.3 Pipe flow in the macropore domain

As mentioned above, water flow in the macropore domain is often not described properly by the conventional Richard's equation (Hutson and Wagenet, 1995; Wagenet and Germann, 1989; Germann, 1990). Channelling behaviour of macropore suggests that pipe flow is an appropriate descriptor of flow in the macropore domain (Chen and Wagenet, 1992). As a matter of fact, soil macropores form conduits like pipes, but their complex tortuosity, their continuities/discontinuities, their variable sizes, etc., create an obstacle to the application of the theory of pipe flow. At a conceptual level, however, the analogy is possible. Transport of water through a macropore network can be considered

as a function of the transmitting properties of the macropore network. The Poiseuille model can be used to represent pores as capillary tubes (or pipes) (Kantzas and Chatzis, 1988). Assuming that the flow of water is laminar and that the macropore is smooth and circular, the water flux through the pore can be estimated by the Poiseuille equation, given as:

$$Q_{\text{pore}} = \frac{\pi \left(\frac{d}{2}\right)^4 \rho g}{8 \eta} \times \frac{\Delta H}{L_e} \quad (2.14)$$

where  $Q_{\text{pore}}$  is the rate of volume flow through the pore ( $\text{m}^3/\text{s}$ ),  $d$  is the effective diameter of the pore (m),  $\rho$  is the density of water ( $\text{kg}/\text{m}^3$ ),  $g$  is the gravitational acceleration ( $\text{m}/\text{s}^2$ ),  $\eta$  is the dynamic viscosity ( $\text{kg}/\text{m}\cdot\text{s}$ ),  $\Delta H$  is the pressure head (m) and  $L_e$ , the effective length of the pore (m). Poiseuille equation has been used in numerous studies on macropore flow. For instance, Chen and Wagenet (1992) mentioned that, by applying the Poiseuille's law, Germann and Beven (1981) were able to find that only a small change of macroporosity resulted in flow velocities, ranging from 0.03 to 40 m/s. Radulovich et al. (1989) developed a method for characterizing macropore size distribution based on the Poiseuille equation and on water breakthrough curves in a saturated steady-state flow condition. Dunn and Phillips (1991b) used Poiseuille law to evaluate the flow characteristics in simulated non-uniform macropore systems during saturated conditions. Their artificial macropores consisted of several straight-walled glass tubes of three different inside diameters, ranging from 0.94 mm to 5.08 mm. They found that Poiseuille law described well the flow dynamics in artificial macropores. Ahuja et al. (1993)

developed a model and studied characteristics of preferential flow using the Poiseuille equation. They concluded that: *"further experimental studies on the nature and geometry of macropores and the nature and dynamics of flow in them are certainly needed"*.

McCoy et al. (1994), Lal and Stewart (1994), Chen and Wagenet (1992), Bouma (1991), Ma and Selim (1997) pointed out that despite the efforts to describe preferential movement of solutes along macropores in quantitative terms, it is still not possible to quantitatively predict water and chemical movement in soils containing macropores.

## **2.8 Concluding Remarks**

In this chapter, the origins of soil pores, their classification and the soil macropore definition have been presented. Various impacts of soil macroporosity have also been discussed. Soil macropores play a determining role in water movement and chemical transport. The effects of macropores on rapid transport of water and solutes through the soil and consequences for rapid leaching of fertilizers, pesticides, particulate waste materials, and other contaminants into drainage water and ground aquifers is now well documented. However, our understanding of the mechanisms of water movement in soil is still limited due to a lack of quantitative measurements of soil macroporosity.

Various methods of characterizing soil macroporosity have been reviewed with an emphasis on the promises offered by Computer Assisted Tomography (CAT) scanning. X-ray CAT scanning offers considerable potential for reliable and non-destructive *in-situ* characterization of macropores occurring in agricultural soils and for real-time examination of flow mechanisms through soil. Most soil studies involving CAT scanning have been limited to the analysis of two-dimensional serial scans. Yet, CAT

scanning has not been used to investigate preferential flow processes in large intact soil cores.

To accurately correlate soil pore structure with preferential flow phenomena, it is essential to quantify three-dimensional parameters, such as the tortuosity of macropores. Additional research is needed to develop reliable approaches for computing tortuosity and connectivity of soil macropores and to relate these parameters to the preferential flow process.

Single Photon Emission Computer Tomography (SPECT) is based on the detection of nuclear radiation injected into an object and is mainly used for inspection of specific physiological functions in the human body. It provides a powerful tool to image and characterize temporal and spatial changes of radionuclide concentrations. Although SPECT imaging has been commonly used in hospitals, it has rarely been applied to engineering and never been introduced to a discipline such as soil physics. SPECT scanning brings a new dimension to 2-D and 3-D dynamic tracer studies involving visualization and quantification of flow in a porous media such as soil.

Considerable research efforts have been made to model water and solute fluxes in soil. The modeling approaches can be classified into two types of models, stochastic and phenomenological. Stochastic models are based on a mass transfer function which relies on a probability density function of the solute travel time. Although this approach has advantages in that it does not require a description of the soil structure, it is found to be often complex and site and process specific. As a result, stochastic models lack guarantee of validity. On the other hand, phenomenological or deterministic models employ a truly mechanistic approach. Most of these models are based on Richard's

equation and convection-dispersion equation. Although these models have been successfully used for simplified systems, their usefulness and applicability become questionable in “real” soil, where the structure is complex and heterogeneous. A multi-region modeling approach has been developed to divide the flow domains into regions in which flow dynamics are more or less uniform. This approach holds promise for simulating solute transport under non-equilibrium conditions. However, at this stage, the demarcation between the flow domains is arbitrarily defined. CAT scanning provides an ideal tool to determine and isolate these flow domains.



## PREFACE TO CHAPTER 3

Soil macropores have been recognized as an important component of the soil structure which directly contribute to preferential water flow and chemical transport through the soil and into ground waters. The importance of macropores in many soil-water processes has motivated many researchers to describe their sizes and shapes. Several approaches were developed to characterize macroporosity. These approaches are briefly described in this chapter. However, efforts to describe macropores in quantitative terms have not yet resulted in a comprehensive theoretical framework that allows a complete representation of their geometry. This is partly due to the fact that macropores are very difficult to visualize and characterize bearing in mind that the macropore networks are complex three-dimensional structures and that soil is opaque.

Computer Assisted Tomography (CAT) offers considerable potential for reliable and non-destructive *in-situ* characterization of macropores occurring in agricultural soils. Several researchers have used CAT techniques for characterizing spatial distribution of soil macropores of undisturbed soil cores. However, there is still a need to develop comprehensive algorithms to visualize macropore in 3-D and to automate the analysis and interpretation of macropore geometry directly from CAT scan data.

Chapter 3 focuses primarily on the development of an innovative and effective protocol using X-ray Computer Assisted Tomography (CAT) scanning for the characterization and visualization of the interconnected pore space of an agricultural soil. The CAT scans were taken with an EMI CT5005 during the summers of 1995 and 1996.

The voxels generated with this CAT scanner had a resolution of 0.75 mm x 0.75 mm x 2.0 mm. Several computer programs were developed in the PV-WAVE programming language for the analysis and visualization of soil macropores in three-dimensions. These programs have been included in attached CD-ROM. This Chapter has been published in the Journal of Canadian Agricultural Engineering (Perret, J.S., S.O. Prasher, A. Kantzas and C. Langford. 1997. 3-D visualization of soil macroporosity using X-ray CAT scanning. *Can. Agr. Eng. J.*, 39(4):249-261). For the sake of completeness, some material in this chapter is repeated from the previous chapter so that this paper can stand on its own. The candidate was responsible for designing and conducting the research experiments, developing computer codes for the visualization and analysis of data and preparation of this paper. Dr. Shiv O. Prasher, professor at the Agricultural and Biosystems Engineering Department of McGill University, contributed in all aspects of this research project. He provided the necessary funds and assistance for this research, including the supervisory guidance and revision of this manuscript before its submission for publication. Dr. A. Kantzas, Director of the Tomographic Imaging and Porous Media (TIPM) Laboratory in Calgary, Alberta, and associate professor at the University of Calgary's Department of Chemical and Petroleum Engineering, provided access to CAT scanning facilities of the TIPM laboratory. Dr. Kantzas also made invaluable suggestions during CAT scanning. Dr. C. Langford, University of Calgary's vice-president research and professor at the Department of Chemistry, was the principal investigator for the NSERC Collaborative Project Grant.

## CHAPTER 3

### 3-D VISUALIZATION OF SOIL MACROPOROSITY USING X-RAY CAT SCANNING

---

#### 3.1 Abstract

Computer Assisted Tomography (CAT) offers considerable potential for reliable and non- destructive *in-situ* characterization of macropores occurring in agricultural soils. Several researchers have used CAT techniques for characterizing spatial distribution of soil macropores of undisturbed soil cores. However there is still a need to develop comprehensive algorithms to automate the analysis and interpretation of macropore geometry directly from CAT scan data.

Four undisturbed soil columns (800 mm long x 77 mm diameter) were extracted from a loamy sand field in Central Canada, and scanned for the visualization and characterization of their interconnecting macropore structure. A total of 240 scans of 3-mm depth were taken for each column. After conversion of the raw CAT scan data into density matrices, two- and three-dimensional soil density reconstructions were generated. With the elaboration of numerous computer programs in the PV-WAVE language, this analysis gives a detailed representation of the spatial variations of the macropore structure and heterogeneity of the soil.

### 3.2 Résumé

La technique de CAT scanning (Computer Assisted Tomography) offre une opportunité unique pour la caractérisation des chemins d'écoulement préférentiel présents dans les sols agricoles. Cette approche permet de visualiser et d'étudier les macropores du sol de façon fiable et non destructive, et ainsi, de mieux comprendre le mouvement rapide de l'eau et des composés chimiques à travers le sol. Il est essentiel de quantifier ce phénomène hydrologique afin d'acquérir une meilleure compréhension de l'impact de ce phénomène sur la contamination des eaux souterraines. Le nombre de macropore par unité de surface, leur diamètre, leur orientation, leur circularité, ainsi que leur tortuosité influencent directement le phénomène de flot préférentiel et pourtant, ces paramètres ne sont pas pris en considération dans la plupart des modèles mathématiques utilisés pour la prédiction du transport de l'eau et des composés chimiques dans le sol. Dans cet article, nous présentons ces différents paramètres tel qu'évalués à l'aide de rayon X en utilisant un scanner modèle EMI CT5005. Plusieurs colonnes de sol (0.8 m x 77 mm de diamètre) ont été prélevées intactes dans un champ du centre du Canada. Un total de 240 sections de 3 mm d'épaisseur ont été scannées permettant ainsi la visualisation et l'analyse de la structure des macropores de chaque colonne. Après transformation des données brutes générées par le CAT scanner en matrices représentant la densité volumétrique du sol, la porosité de chaque colonne a été redéfinie en deux et trois dimensions. Cette analyse permet de représenter en détail la variation spatiale des chemins d'écoulement préférentiel ainsi que les hétérogénéités du sol.

### 3.3 Introduction

A number of investigators have established that the presence of macropores results in rapid movement of water and associated solute through the soil profiles (Beven and Germann, 1982). Since flow through macropores is much faster than through the soil matrix, travel time for water and dissolved chemicals is directly affected by the number of macropores per unit area and also their continuity. Short travel time may not allow contaminants, such as pesticides, to be adsorbed on and into the soil surfaces and broken down by chemical and biological action. To obtain a better understanding of these soil-water processes, the characterization of the macropores (ie: areal distribution, size, shape, continuity, etc.) is essential.

Several researchers have used indirect approaches, such as the use of breakthrough curves or tension infiltrometers to study macroporosity. However, indirect approaches only provide qualitative information about soil porosity. Quantitative analysis of macroporosity provides a more comprehensive and systematic approach and is normally obtained by direct methods. Koppi and McBratney (1991), Moran and McBratney (1992), Singh et al. (1991), and Vermeul et al. (1993) used an impregnation and sectioning technique, by intruding paraffin or epoxy resin into the soil profile and sectioning the soil sample with a mechanical saw. Other researchers such as Booltink and Bouma (1991), Logsdon (1995), Trojan and Linden (1992), and Wu et al. (1993) characterized flow patterns along macropores using dye tracers such as methylene blue. These two direct approaches have the common disadvantage, i.e, the destruction of the soil sample before verifying that the dye, the paraffin or the resin has been fully impregnated throughout the macropore structures of the soil profile.

In the early 1980s, CAT scan technology started to be used in non-medical fields and its great potential for non-destructive analyses was immediately recognized. In one of the first studies involving soil science, Petrovic et al. (1982) showed that CAT scanning was a promising tool for rapid determination of soil bulk density. They found that the mean bulk density in a soil core was linearly related to the core's mean X-ray attenuation coefficient. A year later, Hainsworth and Aylmore (1983) conducted experiments to examine the spatial changes in soil water content using CAT. They reported that computer assisted tomography was successful in monitoring the changes in soil water content and wrote: "*CAT scanning presents an extremely exciting possibility for studies of soil-plant water relations*". Crestana et al. (1985) used CAT to observe the changes in X-ray attenuation coefficient with time as a wetting front passed through a homogeneous soil core. They demonstrated the ability of scanners to detect water movement in soil and concluded that CAT scanning was opening new possibilities for non-destructive measurement of spatial and dynamic water contents. They also developed a CT miniscanner for field analysis (Crestana, 1986). Using small homogenized soil cores, Anderson et al. (1988) showed that the relationship between volume fraction of solids in cores and mean X-ray attenuation was linear and found the CAT approach to be a powerful tool for soil research. Jenssen and Heyerdaghl (1988) applied CAT scanning to study the packing arrangement and density of soil columns, used in experiments concerning water transport and wastewater purification. They stated that CAT scanning "*offers fascinating possibilities in the field of soil science*".

The above studies clearly indicate that CAT scanning is a valuable tool for investigating soil-water processes. Other investigators, such as Phogat and Aylmore

(1989), have also demonstrated its potential for measuring of soil water content and bulk density.

However, all of these early studies were performed using small cores that had been uniformly packed with sieved and homogenized soils. Therefore, these studies did not evaluate soil structures in their native field conditions.

Warner et al. (1989) were among the first researchers to use CAT techniques for characterizing the spatial distribution of soil macropores of undisturbed soil cores. The feasibility of CAT scanning for macropore characterization was assessed by physically sectioning the soil column along the scan plane in order to compare features of scan images with the physical section of the core. Warner et al. (1989) reported that "*the CT scan process is a promising non-destructive method for the characterization of macropores in soil*". However, the scans were examined and interpreted visually. They pointed out the need to develop a comprehensive algorithm to automate the interpretation of images produced by the CAT scanner. Moreover, the distance between consecutive scans in their study varied from 10 to 50 mm, leaving a big gap of "unexplored" soil. These gaps can cause a major problem in the interpretation of the results since continuity and tortuosity of macropores cannot be assessed.

Grevers et al. (1989) also investigated soil macropore system by comparing images from CAT scanning with images obtained by physically sectioning the soil core. They found that the results of the CAT scan images compared well with features observed in the sections of the soil columns. In their study, the length of the soil cores was limited to 160 mm. Thus, their investigation was limited to a small region of the vadose zone.

Following the pioneering work of Grevers et al. (1989) and Warner et al. (1989),

several researchers examined, in greater detail, the use of CAT scanning for characterization of soil macropores in intact soil cores. Table 3.1 provides an annotated reference list of the research work on CAT scanning for describing soil macroporosity in undisturbed soil columns.

**Table 3.1:** Studies using CAT scanning for the evaluation of pore structure of intact soil cores.

Research Institution	Summary	Limitations	References
Dept. of Agr. Eng. / Dept. of Radiology University of Minnesota, USA.	Macropores were detected with CAT scanning. By sectioning the soil core, the validity of CAT scanning was also verified. The number and size of macropores were approximately the same below a depth of 50 mm.	<ul style="list-style-type: none"> <li>- Visual interpretation of scan images</li> <li>- Distance between scans varying from 10 to 50 mm</li> <li>- No consideration were given to the geometry and three-dimensional parameters of macropores</li> </ul>	Warner et al. (1989)
Saskatchewan Institute of Pedology, University of Saskatchewan, CANADA.	The soil macropore system and a compacted soil layer were analyzed using CAT scanning. The validity of CAT scanning was verified with impregnating techniques. A soil macroporosity of 15.7 % was measured. The average area of a single macropore was found to be 20.4 mm <sup>2</sup> .	<ul style="list-style-type: none"> <li>- Small soil cores (160 mm in length)</li> <li>- Analysis of macropores performed on grey-scale images (not directly from the CAT scan raw data)</li> <li>- No consideration was given to the geometry and three-dimensional characterization of macropores</li> </ul>	Grevers et al. (1989) Grevers and de Jong (1994)
Dept. of Agronomy & Dept. of Civil Eng. University of Missouri, USA.	Undisturbed soil cores (76 mm diameter x 76 mm long) were scanned for evaluating the structural characteristics of soils (bulk density). Bulk density correlated well with the size and location of artificial macropores.	<ul style="list-style-type: none"> <li>- Very small soil cores</li> <li>- No consideration was given to the geometry and three-dimensional parameters of macropores</li> </ul>	Anderson et al. (1990) Peyton et al. (1992)
Dept. of Horticulture, Dept. of Agronomy, Dept. of Human Oncology, and Dept. of Radiology, University of Wisconsin, USA.	Macropore structures were reconstructed and visualized in 3-D from CAT scan data.	<ul style="list-style-type: none"> <li>- This study neither quantified nor characterized the 2-D or 3-D geometry of macropores.</li> </ul>	Hanson et al. (1991)
Biol. And Agr. Eng. Dept., Dept. of Crop and Soil Science, and the	A theory for non-destructive determination of conductivity in soil cores (150 mm diameter x 350 mm long) in terms of the Poiseuille-	<ul style="list-style-type: none"> <li>- Small soil</li> <li>- 50 mm distance between scans</li> </ul>	Tollner et al. (1995)



Institute of Ecology,  
University of  
Georgia, USA.

Carman equation was evaluated. It  
was found that the number of  
macropores decreases with depth

- No consideration was given  
to the three-dimensional  
parameters of macropores

School of  
Engineering  
(University of  
Guelph) & Imaging  
Research  
laboratory (Robarts  
Research Institute),  
CANADA.

A CAT scanner was used to  
estimate the overall macroporosity  
of six soil columns. They reported a  
decrease in macroporosity with  
depth and found a greater variability  
closer to the surface.

- Small soil cores, 90 mm diameter x  
200 mm long  
- Distance between scans was 20 mm  
- No consideration was given to  
geometrical characterization and  
three-dimensional parameters of soil  
macropores

Asare et al. (1995)

---

Up to now, the application of CAT scanning has offered a very accurate and repeatable way to bypass the resin impregnation and other physical slicing operations in the standard optical approach to pore characterization analysis. However, CAT has not been used to its full potential for the quantification of soil macropores and investigation of preferential flow processes. In most studies, the sizes of undisturbed soil cores were too small and the distances between consecutive scans were too large to generate accurate and complete characterization of soil macropores.

Some recent studies, like Asare et al. (1995), used CAT scanning to investigate soil macropores. However, their study is limited to the variations of macroporosity in the A and B horizons. Their relatively small soil columns (200 mm long x 90 mm in diameter) were scanned every 20 mm, leaving a big gap of unknown information between two consecutive scans. Moreover, no consideration was given to the number of macropores, their size, position and geometry. In addition, three-dimensional parameters, such as tortuosity, connectivity, etc. were not quantified.

Imaging capabilities of most CAT scanners used in soil studies have been limited to two-dimensional serial scans. Very little work has been done to characterize the macroporosity of intact soil cores in terms of their three-dimensional parameters. Tollner

et al. (1995) pointed out the need for additional research to investigate reliable approaches for computing tortuosity and connectivity of soil macropores. Imaging in three-dimensions and quantification of three-dimensional parameters of soil macroporosity is critical in order to accurately correlate soil pore structure with preferential flow phenomena, and much additional work is needed in this area (Hanson et al., 1991).

The present research is currently investigating and modeling macroporosity and preferential flow processes in four large undisturbed soil columns (800 mm x 77 mm), using computer assisted tomography with an X-ray based scanner. In this study, each soil column was scanned in 240 positions, leaving no gap of information between two consecutive scans. Computer programs were developed in the PV-WAVE language for systematic quantification and visualization of soil macroporosity directly from CAT scan data. Some of these computer algorithms are presented in this paper. The visualization part of this work enabled us to generate 3-D views of the structure of macropores to an unprecedented level.

### **3.4 Materials and Methods**

#### **3.4.1 Soil columns**

In July 1995, four undisturbed soil columns of 800 mm in length and 77 mm in diameter were taken from a field site at the Macdonald Campus of McGill University in Ste-Anne-de-Bellevue, Quebec. The land slope was less than one percent. The columns were extracted from an uncultivated field border that had been covered for many years with a combination of quack grass (*Elytrigia repens*), white clover (*Trifolium repens*) and wild oat (*Avena fatua*). Periodic mowing during the summer was the only cultural

practice. The soil cores were obtained by driving a polyvinyl chloride (PVC) pipe into the soil with a backhoe. The lower end of the PVC pipe was shaped to a thin cutting edge in order to reduce the compaction inside the column and to facilitate the insertion of the pipes into the soil. After the extraction of the columns, the cutting edge was removed, allowing the end of the PVC pipe to be sealed with a PVC cap. The soil columns were

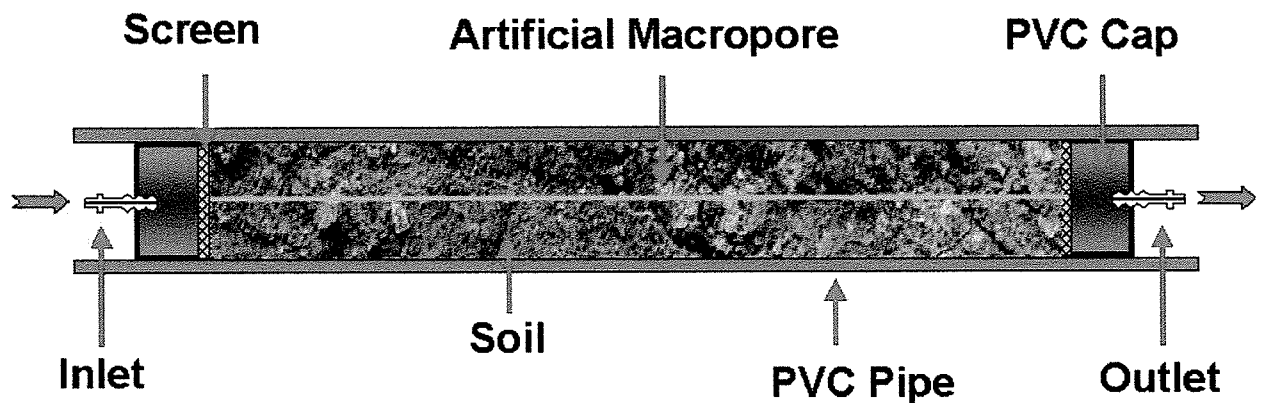


Figure 3.1: Schematic illustration of the design of the soil column with the artificial macropore.

extracted during a period when the soil moisture was near field capacity. Between the time of excavation and the time of scanning, the cores were free to drain through a small outlet located at the bottom of the PVC pipes. Change in moisture content due to evaporation was minimal, since both ends of the columns were sealed to prevent any soil loss during transportation. One of the soil columns was drilled from top to bottom to verify the ability of the CAT scanner to portray the size and the location of a known pore. This artificial macropore consisted of a polyethylene tube of 1 mm in inner diameter. (Figure 3.1).

The soil belongs to the Chicot series. The Chicot soils are developed from sandy

materials over a calcareous till, and as a result they are generally well drained (Lajoie and Baril, 1954). They usually contain a high percentage of fine sandy loam.

The soil properties of the soil profile were determined by taking small samples from five locations at the field plot. The soil of this site was predominantly a loamy sand with an A horizon thickness of around 0.4 m. A summary of the results of soil analysis is presented in Table 3.2.

**Table 3.2:** Selected properties of a Chicot soil under a combination of quack grass (*Elytrigia repens* (L.) Nevski.), white clover (*Trifolium repens* L.) and wild oat (*Avena fatua* L.).

Depth (m)	Bulk Density (Mg/m <sup>3</sup> )	$\rho_g^1$ (Mg/m <sup>3</sup> )	$\omega^2$ (%)	Clay (%)	Silt (%)	Sand (%)	OM <sup>3</sup>	CEC <sup>4</sup>	pH	Description
0.0-0.15	1.36	2.51	23.9	6	12	82	3.96	9.66	6.32	Dark brown with fine crumb structures – slightly firm
0.15-0.30	1.27	2.52	24.7	5.5	12.5	82				
0.30-0.45	1.30	2.59	24.2	7	9	84				
0.45-0.60	1.30	2.60	21.5	5	8	87	1.20	8.01	6.01	Brown to yellowish brown – compact layer with occasional rocks presence of earthworm channels
0.60-0.75	1.46	2.64	11.8	8	8	84				
0.75-0.90	1.64	2.59	14.2	14.5	8.5	77				

- 1 Mineral grain density
- 2 Gravimetric water content at field capacity
- 3 Organic matter content (g/g)
- 4 Cation Exchange Capacity (cmol/kg)

For determination of soil bulk density, percentage of clay, silt and sand and gravimetric water content, the reader is referred to Mehuys (1995). For determination of particle density and chemical analysis of soil, an X-ray spectrometer was used following the method given by Jones (1982). The determination of organic matter was achieved by following the methodology given by Nelson and Sommers (1982). For cation exchange capacity and pH, the reader is referred to Hendershot et al. (1993a) and Hendershot et al.

(1993b).

### 3.4.2 Computer tomography process

Each of the four columns was scanned separately using an EMI CT5005 full body scanner. In turn, each column was carefully placed horizontally in the CT unit so that the X-ray beam would intersect the soil column perpendicularly to its longitudinal axis (Figure 3.2). During the computer tomography process, an X-ray source and an array of detectors rotate in synchrony around the column. A multiple set of data is generated from a number of views around a section of the core. More precisely, during a scan with the EMI CT5005, the scanning assembly rotates by

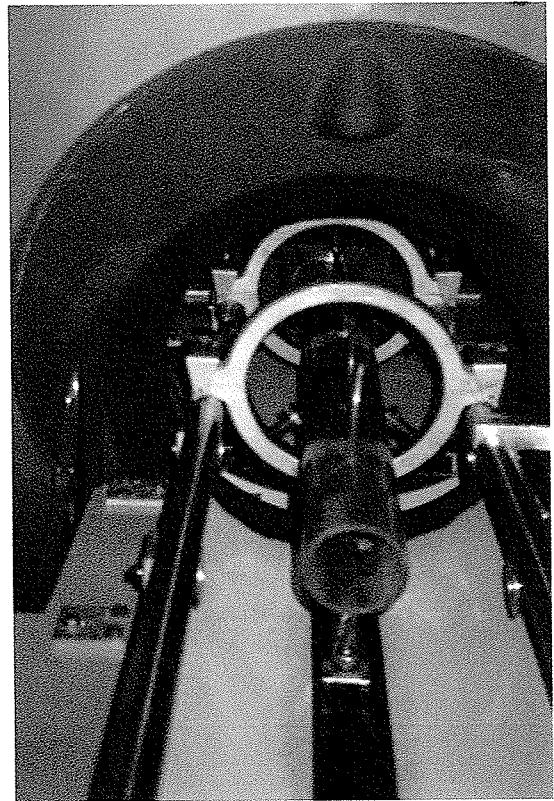


Figure 3.2: Position of the soil core in the CAT scanner.

incremental steps of ten degrees around the core. This sequential rotation is repeated for 180 degrees to collect sufficient data to reconstruct a single slice. The X-ray attenuations obtained from the different angular positions are combined to generate the cells or pixels (picture element) of a 320x320 element matrix. Each individual pixel represents a specific CTn value (Computer Tomography number) or a specific X-ray attenuation coefficient normalized with respect to water. The CTns constitute the standard output of a CAT scanner (CAT scan raw data) and are usually expressed in Hounsfield Units (HU).

In this study, the CAT scan system parameters were set to 140 peak kV and 28 mA. A total of 240 sections or scans were obtained for each column in order to leave no gap between two consecutive scans. For each scan, the volume element size, often referred to as a voxel, was 0.75 by 0.75 by 3.0 mm.

### **3.4.3 Matrix conversion and selection of region of interest**

Each scan was recorded on a magnetic tape and transferred to a UNIX workstation and to a Pentium 133 MHz PC for further data manipulation. Although expressed in HU, a CTn value is a dimensionless quantity. The CTn for water is roughly 0 and -420 for air. The CTn values or X-ray attenuation coefficients are a function of the electron density (bulk density) and atomic number of the material. It has been previously demonstrated that the CTns are linearly related to the bulk density of the soil (Anderson et al., 1988). The soil columns were mounted inside a core holder assembly made of a hollow Plexiglas annulus partitioned into four chambers filled with two liquids. Water and mineral oil were used as reference materials. By plotting CTns versus the bulk density of reference materials and using a simple linear regression, one can easily derive a calibration curve that relates bulk density to the X-ray attenuation coefficient of the scanned material. A FORTRAN program (Convert.f) was developed to compute the calibration line of each scan. Once the linear calibration equations have been established, a computer algorithm transforms CTn arrays into matrices of bulk density. Part of the algorithm also allows the computation of porosity distribution of the soil. When the minerals constituting the soil particles have been identified, the porosity of each individual pixel may be estimated with the following equation (Kantzas, 1990) :

$$\phi = \frac{\rho_g - \rho_b}{\rho_g - \rho_f} \quad (3.1)$$

where  $\phi$  represents the porosity of the volume element,  $\rho_g$  is the grain density (density of the mineral making up the solid portion of the soil matrix),  $\rho_b$  is the bulk density, and  $\rho_f$  is the fluid density. The fluid density in this case is the density of air.

An additional algorithm has been added to the program for selection of the region of interest (ROI). Only part of the 320x320 matrix is actually used to investigate soil macroporosity. The resulting matrix requires only 96 kilobytes of disk space and is composed of an array of 115 by 115 elements.

#### **3.4.4 Selection of programming language**

Presumably, any high level programming language, such as FORTRAN, could have been used for post-processing and manipulation of the two-dimensional matrices. FORTRAN is considered to be a scientific language and is useful for applications where numerous computations are required. Unfortunately, the imaging capabilities of FORTRAN are poor. Therefore, PV-WAVE, a language with imaging capabilities and suited for both UNIX and PC environments, was chosen. The PV-WAVE language is a comprehensive programming environment that integrates state-of-the-art numerical and graphical analyses. This programming language is widely used for analyzing and visualizing technical data in many fields, such as medical imaging, remote sensing and engineering. PV-WAVE is an ideal tool for working with arrays, such as CAT scan data, because of its array-oriented operators and its ability to display and process data in the ASCII and Binary I/O format.

### 3.4.5 Visualization of soil macroporosity

Visual inspection of bulk density and porosity matrices is an important step towards the understanding and analysis of the complex macropore structure. In this section, various ways of visualizing soil macropores are presented.

An interactive algorithm (Jofran.pro) has been developed in PV-WAVE for comprehensive inspections of the bulk density and porosity matrices and creation of cross-sectional images. In order to generate images, the program converts the ASCII matrices into the BINARY format. Each pixel value is scaled to a range of 0-255 to form the image. In this context, an image is a two-dimensional array of pixels for which each

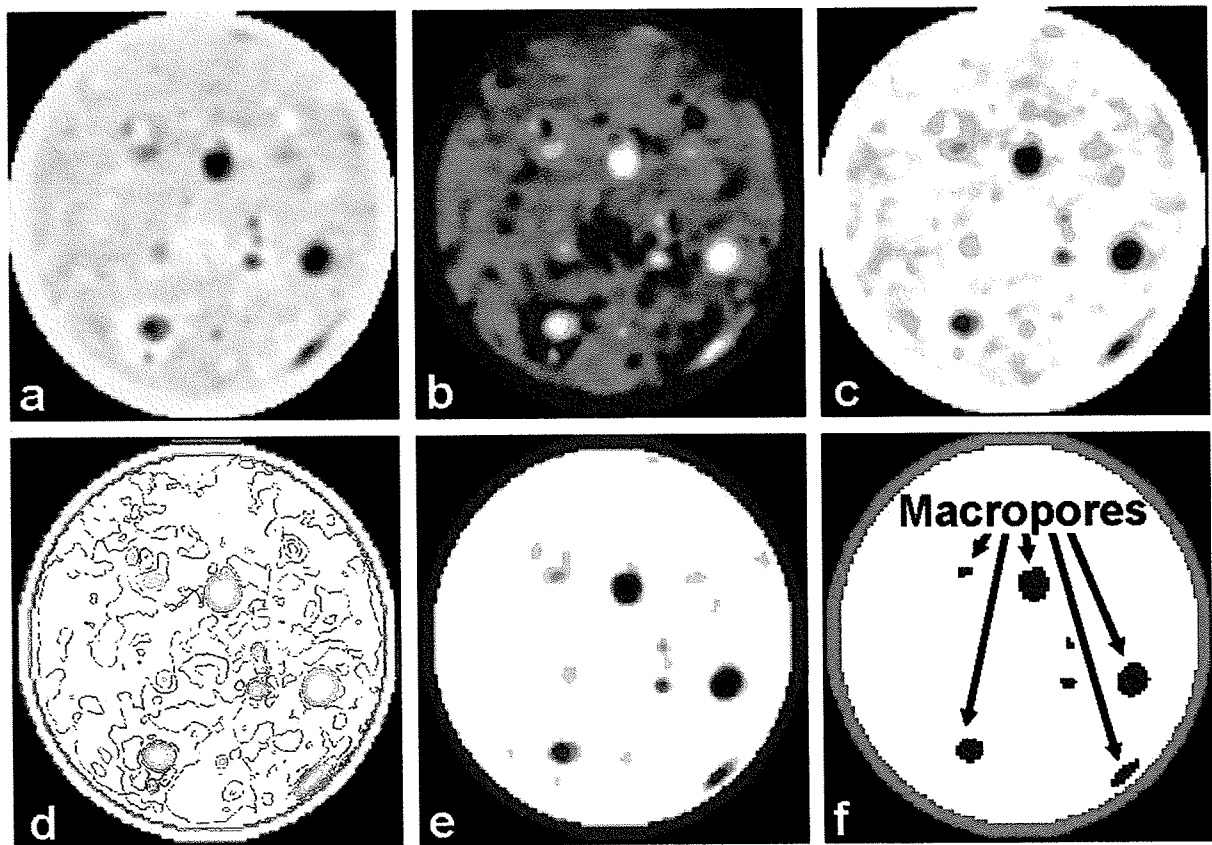


Figure 3.3: Cross-sectional images; (a), (b) and (c) contrast enhancement using different color tables, (d) contour map, (e) partial threshold and (f) total threshold of the soil macropores.



element is attributed to a color depending on its value. This program was specially designed to allow:

- ① Selection of different color tables for contrast enhancement,
- ② Continuous mapping,
- ③ Contour mapping,
- ④ ROI examination (with the determination of summary statistics),
- ⑤ Estimation of feature coordinates, and
- ⑥ GUI (graphical-user-interface) threshold to isolate soil macropores.

To enhance or mask portions of the image, a binary threshold was used for better detection of soil macropores. Jofran.pro was used extensively for the visualization of cross-sectional images and the examination of shape, size, and distribution of macropores. Some of these cross-sectional images are presented in Figure 3.3.

Longitudinal views are useful for visualizing the distribution of the low and high density areas along the length of the soil column. To generate longitudinal views, we have developed a program in PV-WAVE called Longi\_mak.pro. This program stacks up 240 sections, one on top of the other, and “cuts” through a vertical plane to extract a vertical cross-sectional slice from the three-dimensional block of data. The position of the plane that bisects the volume of data is determined using a fixed pixel depth. For each column, 115 longitudinal images can be generated in the x-direction and in the y-direction. Figure 3.4 displays longitudinal views of the four soil columns using a pixel depth in the x-direction of 50 (middle of the columns).

In hospitals, three-dimensional imagery has recently been possible with the aid of powerful stereotactic radiosurgery computer programs (Hanson et al., 1991). However,

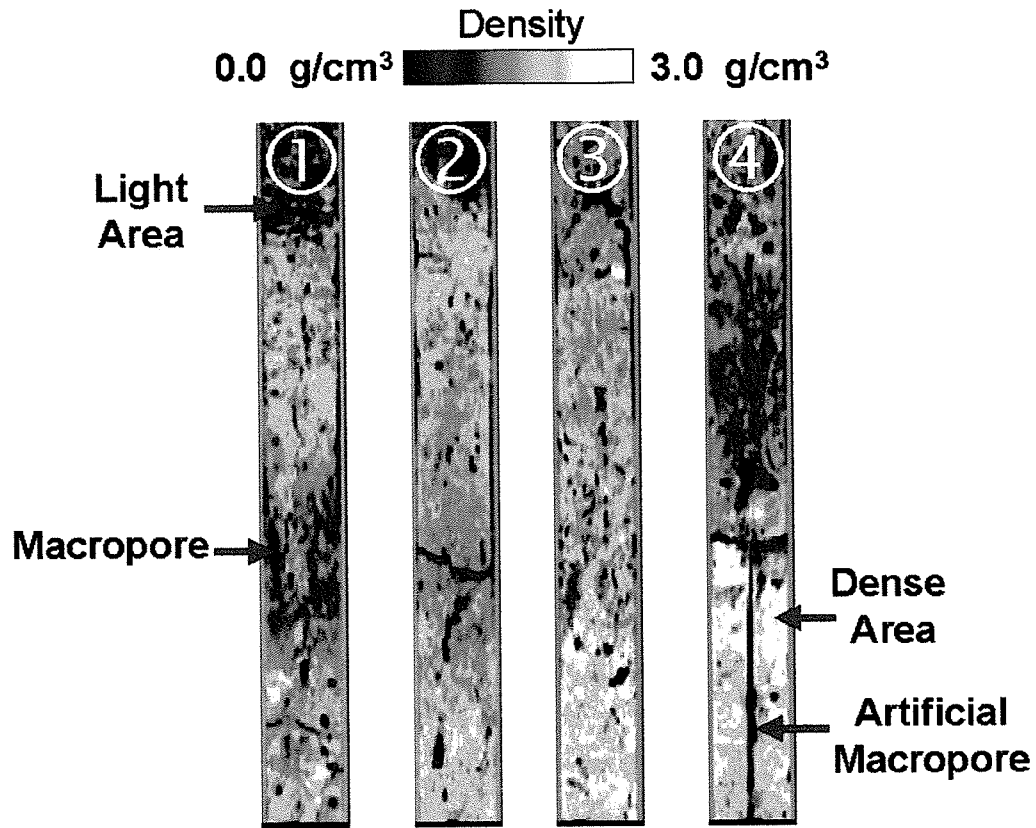


Figure 3.4: Longitudinal views of the four soil columns.

these softwares are very expensive and not offered on typical medical scanners (Aylmore, 1993).

Since 3-D imaging is critical to accurate correlation of soil pore structure and space with flow processes occurring in the soil, we decided to develop our own three-dimensional reconstructive methodology.

Three programs in PV-WAVE were developed to generate three-dimensional models of the macropores entirely based on the CAT scan data. These three algorithms permit a three-dimensional image to be reconstructed from multiple contiguous scans. The first program (Make3D.pro) isolates macropores in the 2-D matrices, rescales the values of each pixel to a range of 0-255 and combines them into a 3-D ASCII array.

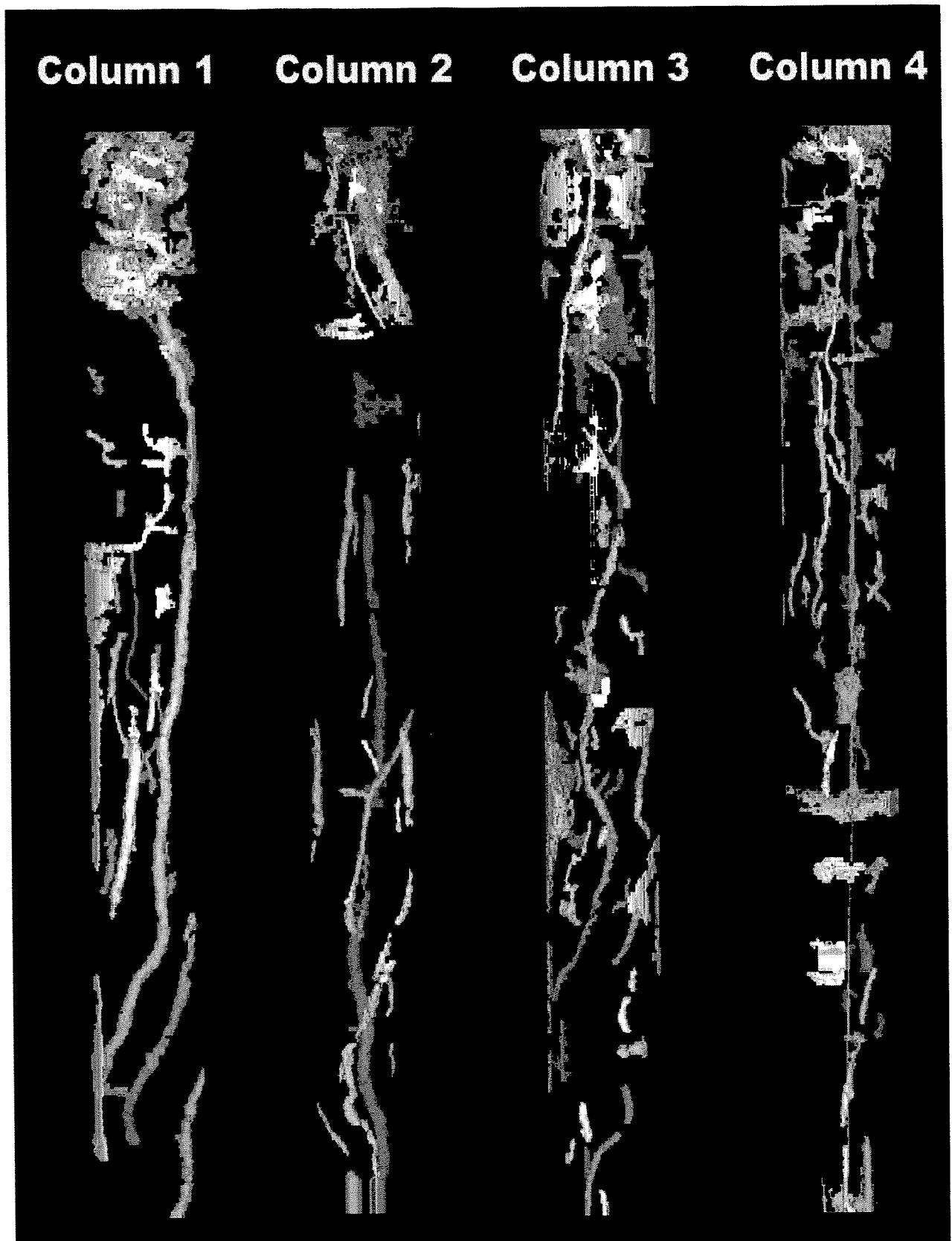


Figure 3.5: Three-dimensional reconstruction of soil macropores of the four soil columns. The artificial macropore can be observed in column 4.

The second program (Conv\_binary.pro) converts the 3-D ASCII array into Binary I/O format. The Binary I/O format is the simplest and most efficient form of I/O. Images and large data sets are usually stored and manipulated using Binary I/O in order to minimize the processing load on the machine. The third program (Rview.pro) produces a list of vertices and polygons that describes the three-dimensional surface of macropores. Each voxel is visited to find polygons formed by the macropores. The polygons are then combined and rendered to reconstruct an exact three-dimensional representation of the interconnected network of soil pores and cavities. The reconstructed image allows the visualization of soil macropores as never seen before (Figure 3.5). Several macropores are displayed as vertical descending structures. It should be noted that the artificial macropore in column 4 is clearly visible.

#### **3.4.6 Quantification of soil macroporosity**

The quantification of soil macropores seeks to identify inherent macropore characteristics such as their number, size and geometry. These characteristics are used to describe macropores or the attributes of macropores prior to the subsequent task of classification and modeling. A program (Macro.pro) was written to recognize, extract and quantify the features of interest (i.e., the macropores) for each of the two-dimensional arrays. This comprehensive program provides a variety of measures of soil macropores, such as the number of macropores per scan, the surface area of each macropore, the equivalent cylindrical diameters, the perimeter, the circularity and the rectangularity. The size of the macropores is usually described in terms of its surface area ( $A_{\text{cross-section}}$ ) and its perimeter ( $P$ ). A more intuitive indicator of macropore size is the equivalent cylindrical diameter ( $d_{\text{eq}}$ ) of the pore. It is usually derived from the surface area as:

$$d_{eq} = \sqrt{\frac{4A_{\text{cross-section}}}{\pi}} \quad (3.2)$$

The shape of the macropore is generally characterized by computing its circularity ( $C_{\text{circ}}$ ) and rectangularity ( $R_{\text{rec}}$ ). The circularity is defined as the ratio of the perimeter of the macropore over the circumference of a circle having a diameter equal to the equivalent diameter of the macropore (Perret et al., 1996a). It can be written as:

$$C_{\text{circ}} = \frac{P}{d_{eq}\pi} \quad (3.3)$$

Since the circumference is the smallest closed line that embraces a two-dimensional figure, circularity can never be less than one. Circularity equal to one implies that the macropore is circular. A circularity much greater than one indicates that the macropore is elliptical. Rectangularity is given by the area of the macropore divided by the area of a bounding box formed around the macropore ( $A_{\text{box}}$ ) (Tollner et al., 1995) and is written in mathematical terms

as follows:

$$R_{\text{rec}} = \frac{A_{\text{cross-section}}}{A_{\text{box}}} \quad (3.4)$$

The rectangularity can never exceed one. Rectangularity close to one implies that the macropore tends to be rectangular in shape.

For each column, the algorithm examines more than

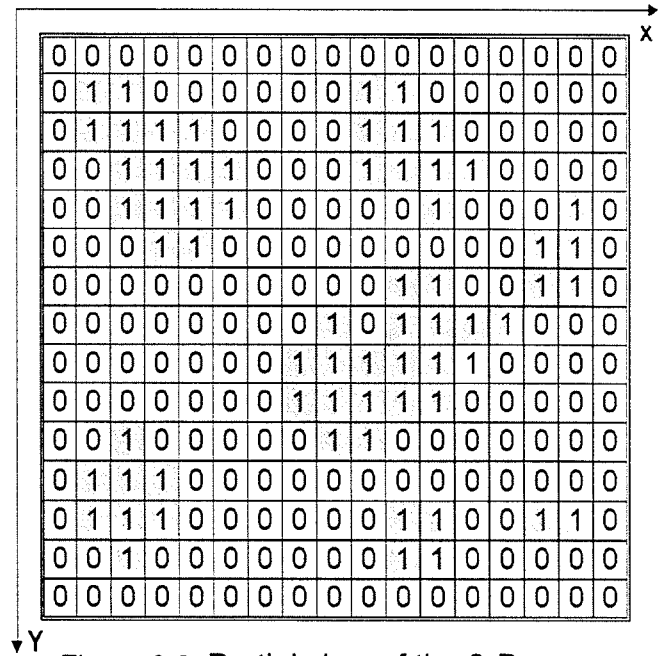


Figure 3.6: Partial view of the 2-D array after segmentation.

310,000 data points in order to characterize the macroporosity. The first task accomplished by Macro.pro is to partition the two-dimensional array into regions of 1 for the pores and 0 for the soil matrix. The pores contain either water or air (i.e., density lower than 1). Thus, by applying a threshold on all the pixels in the bulk density matrices having a value lower than one, the pore can be isolated (Figure 3.6). This process is called segmentation.

Once the two-dimensional matrices have been transformed into 0 and 1 elements,

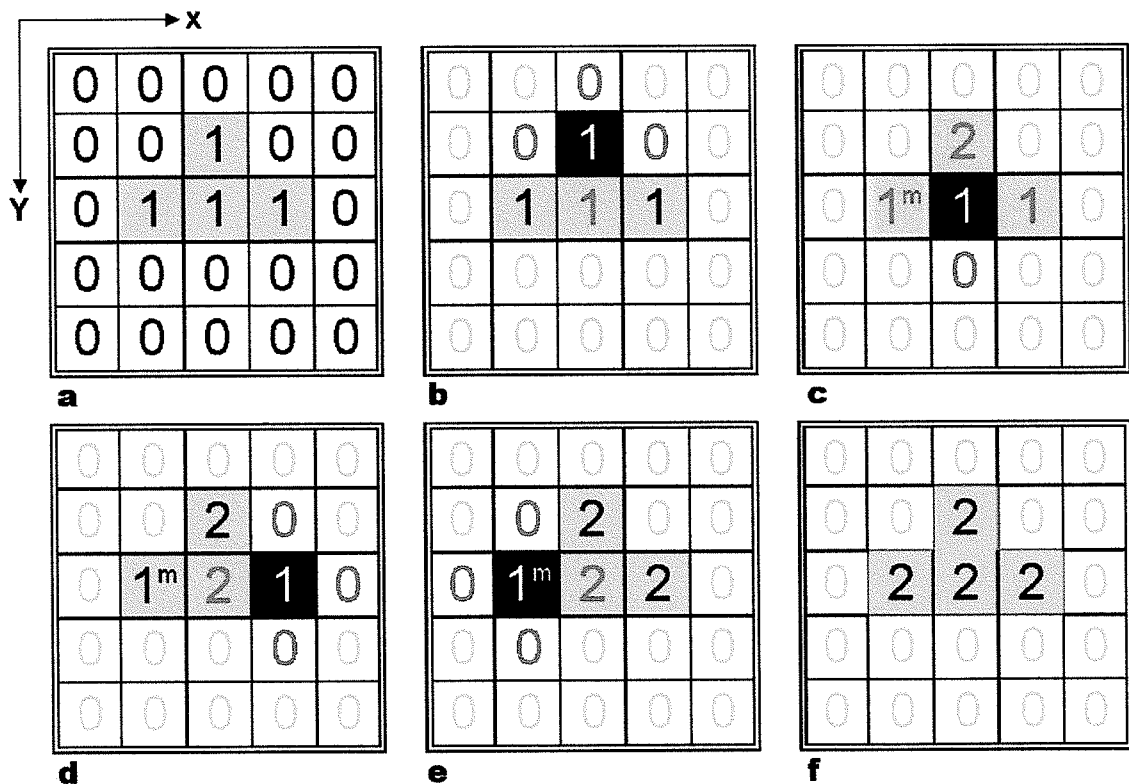


Figure 3.7: Illustration of the clustering algorithm. (a) Initial matrix. (b) The first pixel is located and the four nearest neighbors are checked for values of 1. (c) The visited pixel changed to a value different than 1 (2 in this case) and the investigation moves to the neighbor having a value of 1 (if two or more neighbors have a value of 1, the algorithm puts them in "memory"). The four new neighbors are evaluated. Two neighboring pixels have a value of 1, therefore, one of them is put in memory (denoted by 1<sup>m</sup>). (d) The previous pixel is changed to 2 so that the algorithm will ignore it. None of the four neighboring pixels has a value of 1, thus, the algorithm moves to the pixel in memory. (e) A value 2 is substituted in the previous pixels and the new neighbors are investigated. None have a value of 1 and no pixel in memory can be recalled. (f) The evaluation of this pore is completed.

the algorithm must recognize each individual pore, registered as a set of contiguous 1. Two matrix elements having a value of 1 are said to be part of the same pore if they are sharing a common side. In other words, to be part of the same pore, a pixel needs to have a value of 1 and to be located in one of the four nearest neighbour locations of the other pixel. In a single pass of the two-dimensional array, our algorithm recognizes and regroups pixels belonging to the same pore. This part of the program is referred to as the clustering algorithm (Figure 3.7).

A sub-routine in the clustering algorithm assesses the number of pixels, perimeter and rectangularity of the pore. Some of the pores are too small to be classified in the macropore category. If the equivalent diameter of the pore is less than 1 mm, then the pore is removed from the two-dimensional matrix by resetting each of its pixels to 0. This simple process is called filtering. After filtering, all macropore attributes are computed. Macro.pro can be used either for one section or for the 240 sections of a soil column. All macropore attributes are stored in an ASCII file for further analysis on a worksheet.

### **3.5 Results and Discussion**

Variations in bulk density and total porosity were investigated as the first basic properties of the soil. As noted earlier, the density matrix is based on the X-ray attenuation coefficient of each voxel of the scan. Each voxel contains a mixture of solid particles (mineral grains, organic matter), air and water. Therefore, the X-ray attenuation coefficient and hence the bulk density matrix is affected by the water content of the soil at the time of scanning. In other words, the density matrices represent the wet bulk density of the soil. It was assumed that the soil columns were at field capacity during the

CAT scan process. Gravimetric moisture content of the soil, at field capacity, was estimated at 20.2 %. With gravimetric moisture content known, the dry bulk density was evaluated as:

$$\rho_{b.dry} = \frac{\rho_{b.wet}}{1 + \omega} \quad (3.5)$$

where  $\rho_{b.dry}$  ,  $\rho_{b.wet}$  denote the dry and wet bulk density of the soil and  $\omega$  designates gravimetric moisture content. With this formula, the dry bulk density was calculated and averaged for every section of the soil columns. In addition, the total porosity of the soil was evaluated by:

$$\phi = 1 - \frac{\rho_{b.dry}}{\rho_g} \quad (3.6)$$

where  $\phi$  represents the total porosity of the soil and  $\rho_g$  is the mineral grain density. The mineral grain density, also known as the soil particle density, was estimated by X-ray Fluorescence with a PW240 spectrometer. It was measured at six depths and was averaged for the soil profile at 2.58 Mg/m<sup>3</sup>. Figure 3.8 shows the variations of the dry bulk density and the total porosity with respect to depth, for every soil column.

The bulk density of the soil ranges from approximately 1.2 to 1.89 Mg/m<sup>3</sup> while, the minimal and maximal values for total porosity are 27.5 and 53.7 percent, respectively. The field site, from which the soil columns were extracted, is used as a passageway for machinery during the summer activities. Marshall and Holmes (1988) mentioned that bulk density of a sandy loam soil which has been compacted by regular traffic, could



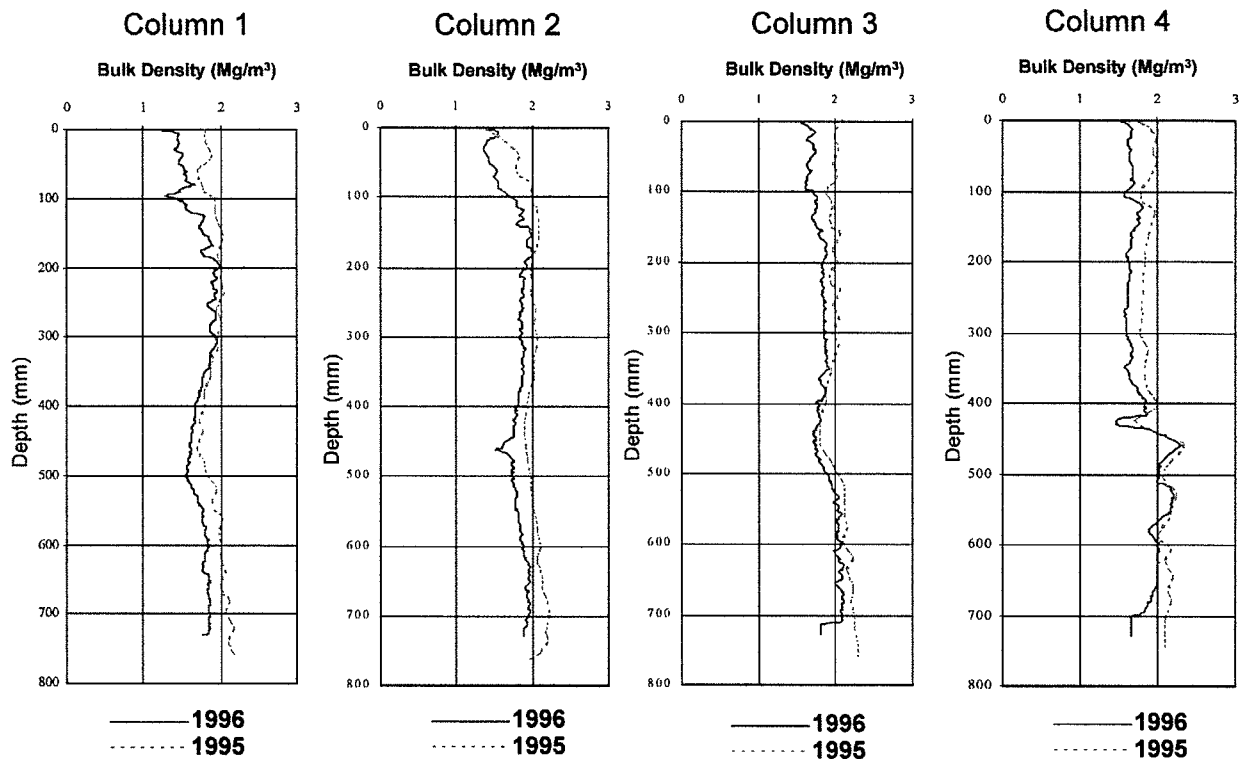


Figure 3.8: Dry bulk density changes with depth of the soil profile.

reach  $1.90 \text{ Mg/m}^3$  with porosity values around 28.0 percent. Thus, results presented in Figure 3.8 appropriately describe soil conditions observed on the field site. The density tends to increase with depth. This observation may be attributed to an increase in compaction of the soil particles and a decrease in the organic matter content with respect to distance from soil surface.

Spatial resolution of the image, as determined by the scanner and the reconstruction algorithm, is 0.75 mm. If the boundary of a pore falls in the middle of a pixel, the scanner will generate a CTn value that is an average of the attenuation of the soil matrix and air. The possibility that a pore of approximately 0.75 by 0.75 mm coincides with a pixel is very small. Thus, a pore must be significantly larger than 0.75 mm to enable detection and accurate identification. Pores greater than 1.0 mm in

diameter could be easily identified and characterized. This category of pore was defined as macropores by Luxmoore et al. (1990). However, it should be mentioned that the geometry of soil pores is rarely circular and, therefore, the concept of diameter is no longer adequate. Consequently, the term equivalent cylindrical diameter is used to describe the size of non-circular/circular pores. For every section of the soil columns, the number of pores having an equivalent cylindrical diameter greater or equal to 1 mm (macropores) was evaluated.

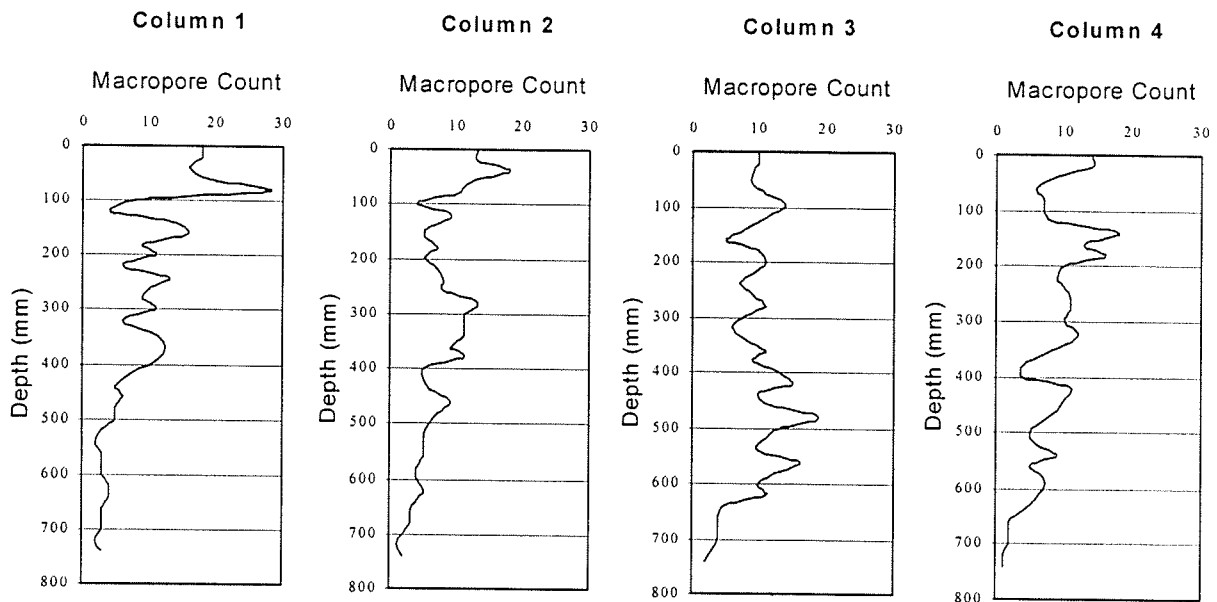


Figure 3.9: Number of macropores with respect to depth.

The results are shown in Figure 3.9. In general, the number of macropores decreases with depth. The decrease in number of macropores is due to a decrease in biological activity. The number of macropores close to the soil surface may be affected by plant roots and species of oligochaetes (earthworms, potworms, bristleworms, etc.) that are not present deeper in the profile. Since a high biological activity will result in

formation of more macropores, one might expect that macroporosity decreases with depth. However, in column 3, this trend is not as obvious as it is for the other columns. During transportation, the soil from the middle of column 3 was accidentally loosened. This incident provides a reliable explanation for the jumbled macropore count observed for this column.

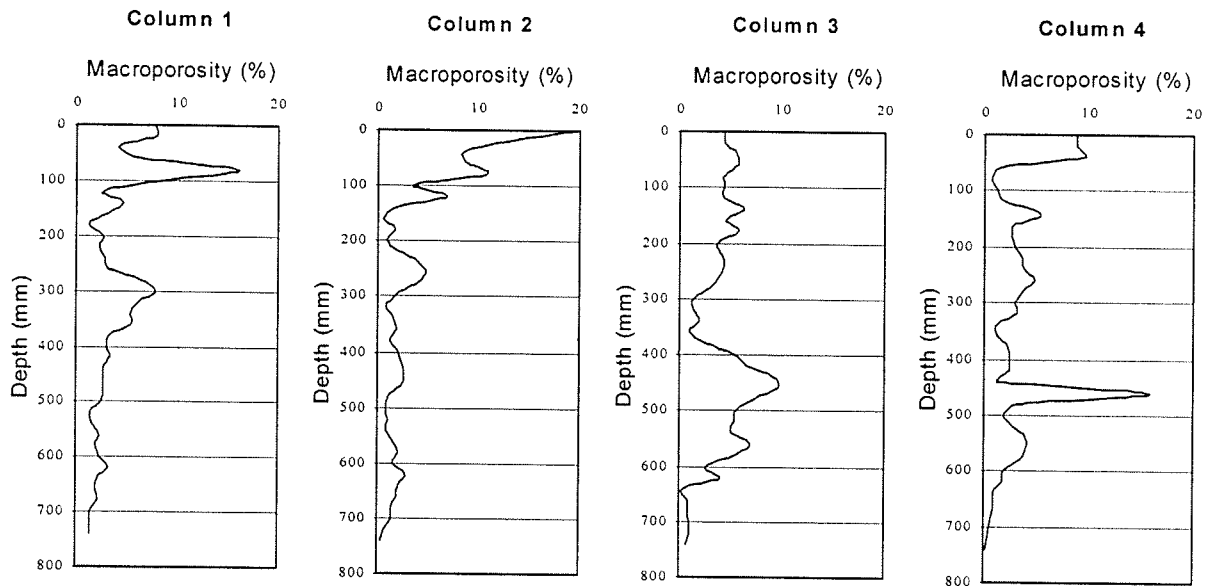


Figure 3.10: Areal distribution of soil macropores with respect to depth.

The areal distribution of the soil macropores was also investigated by dividing the sum of all the pixels, belonging to the soil macropores, by the total number of pixels of the section. In other words, the areal distribution of the soil macropores, sometimes referred to as macroporosity, is given by the ratio of the surface area occupied by macropores over the total surface of the section.

The areal distribution was evaluated for every depth and is presented in Figure 3.10. Since the biological activity close to the soil surface is more intense, one should

anticipate a lower macroporosity deeper into the soil profile. As expected, macroporosity decreases with depth.

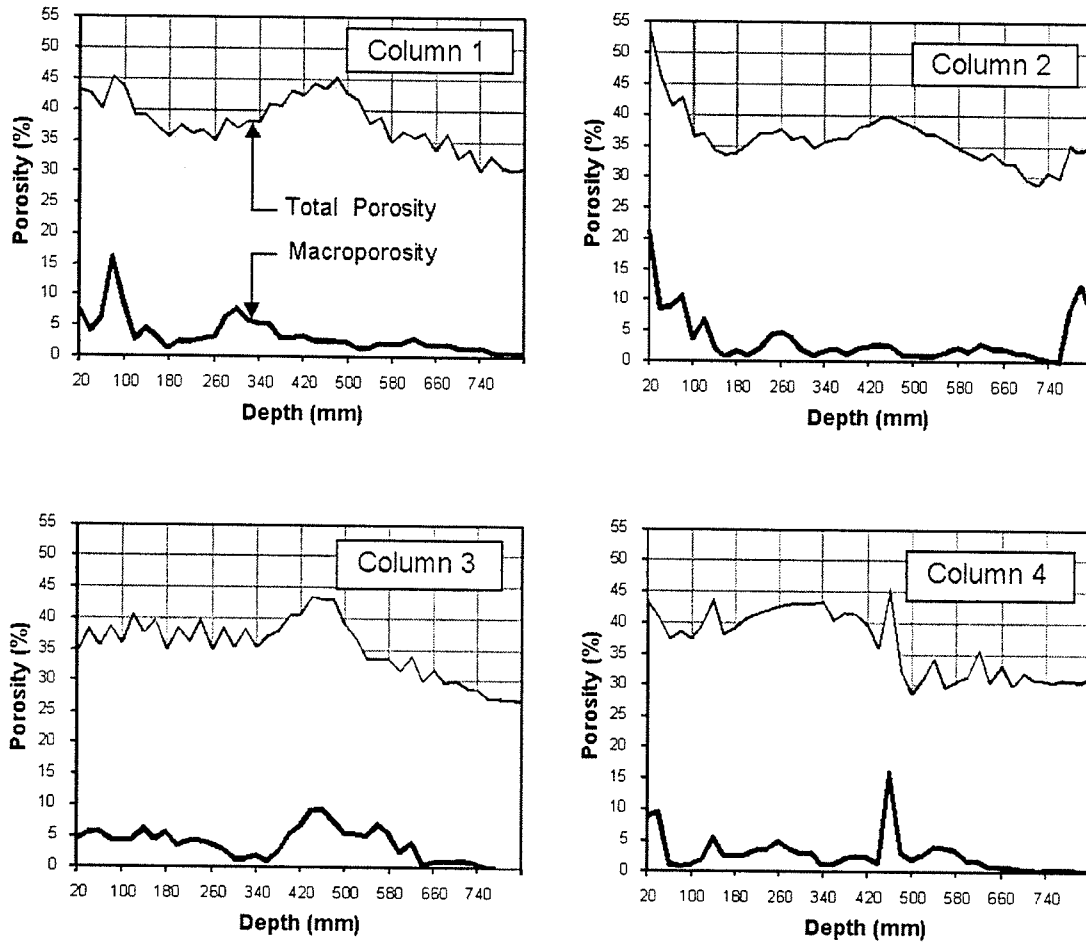


Figure 3.11: Relative contribution of soil macroporosity with respect to depth.

A comparison of the total porosity to the macroporosity of the soil indicates the relative contribution of the soil macropores to the porosity of the porous medium (Figure 3.11). Figure 3.11 shows similar trends for the total porosity and for the macroporosity of the soil columns. Although macroporosity represents a minor portion of the soil porosity, it clearly affects the behaviour of the total porosity of the soil. White (1985) reported that soil macropores comprise a small percentage of the total porosity (1% to

5%). Edwards et al. (1990) observed macroporosity having a range from 0.4 % to 3.8%. However, these figures were estimated with infiltration techniques and thus, some dead-ended macropores which do not participate to water flux were not considered.

CAT scanning provides a more systematic approach for estimating macroporosity as all soil cavities are taken into consideration. Thus, higher values of macroporosity are obtained using CAT scanning. Asare et al. (1995), for instance, have reported values of macroporosity ranging from 13.8 to 36.1%. Therefore, the results obtained in our study seem to be reasonable.

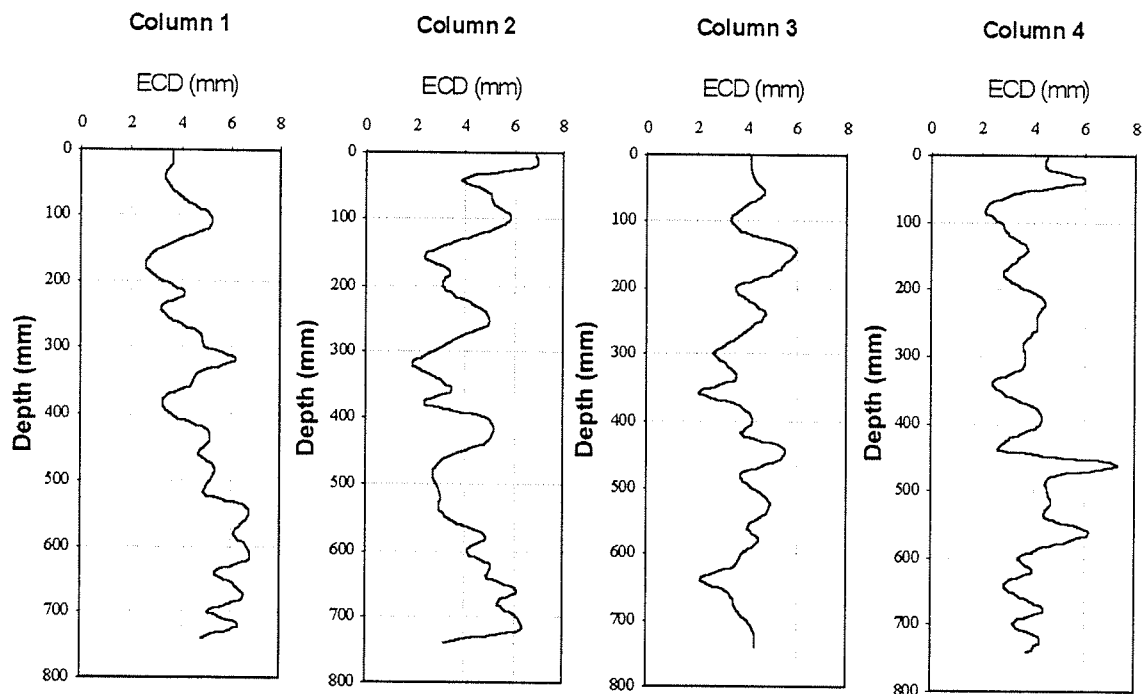


Figure 3.12: - Average equivalent diameter of the soil macropores with respect to depth.

As mentioned earlier, the size of the macropores may be inferred from their equivalent diameter. The average equivalent diameter was computed for each section of soil in order to investigate the changes in size of macropores with respect to depth. The

results are presented in Figure 3.12. The assumption is that the size of biopores changes with depth, however, it is difficult to recognize a trend or a pattern in the fluctuations of the equivalent diameter. The presence of roots and arthropods, such as ants or beetles, close to the soil surface could have led to two distinct regions in the soil profile. However, the size of the macropores does not seem to be affected by depth. The geometry of a macropore may be investigated by estimating its circularity and rectangularity. Circularity is defined as the ratio of the perimeter of the macropore over the circumference of a circle having a diameter equal to the equivalent diameter of the macropore. Since the circumference is the smallest closed line that embraces a two-dimensional figure, the circularity can never be lower than one. A circularity equal to one implies that the macropore is circular. A circularity much greater than one indicates

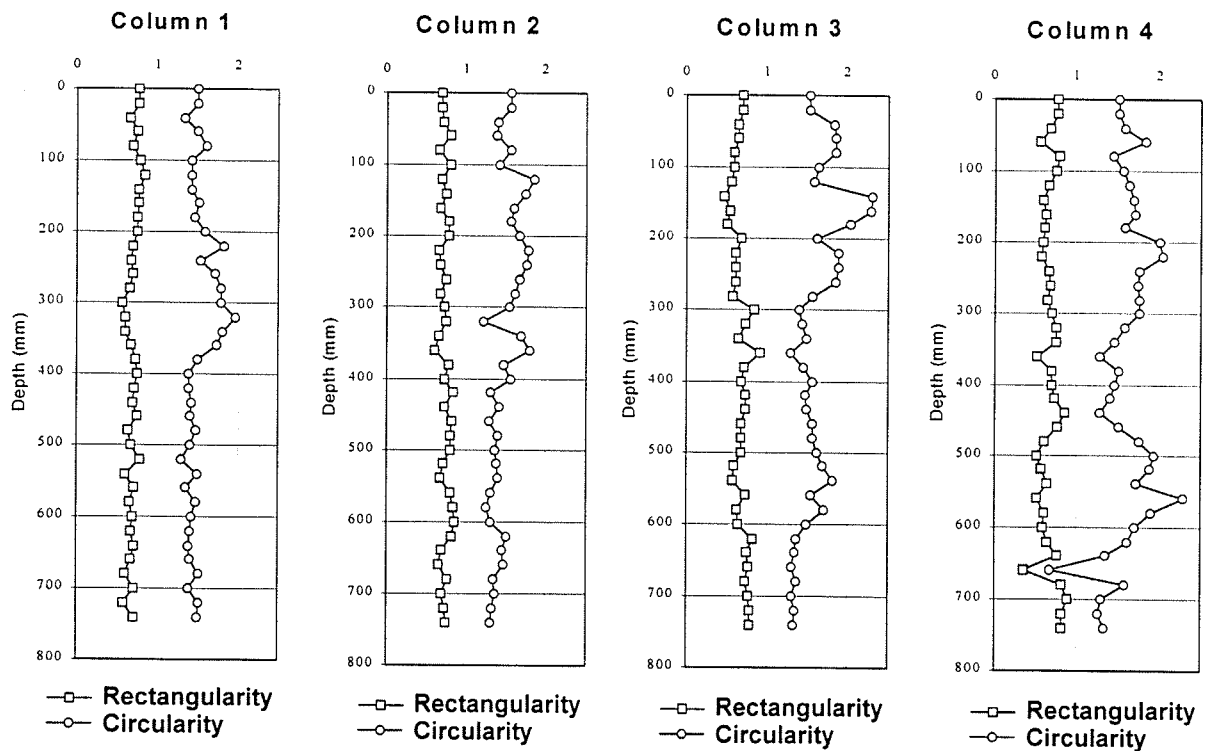


Figure 3.13: Average circularity and rectangularity of soil macropores with respect to depth.

that the macropore is elliptical. Rectangularity is given by the area of the macropore divided by the area of a bounding box formed around the macropore. The rectangularity can never exceed one. A rectangularity close to one implies that the macropore tends to be rectangular in shape.

The average circularity and rectangularity were calculated for every section of the soil column in order to examine the changes in geometry of the soil macropores with respect to depth (Figure 3.13). The geometry of the soil macropores seems to be independent of the distance from the soil surface. Although the circularity and the rectangularity fluctuate, there is no clear evidence of a tendency to increase or decrease with depth. It should be noted, however, that the rectangularity oscillates around 0.70. This means that the geometry of the macropores tends to occupy a rectangular surface at approximately seventy percent.

Although macropores are less numerous deeper into the soil profile, they tend to have the same size and geometry. This implies that the origin or mode of formation of macropores is approximately the same throughout the soil profile. In temperate regions, earthworms dominate the soil's invertebrate biomass (Curry, 1994). The formation of burrows is a distinctive feature of earthworm activity. Normally, large species, such as *Lumbricus terrestris*, which can weigh more than 5 g per worm, contribute substantially to the formation of long and continuous burrows. This species of earthworms has been observed in the soil columns used in this study. These earthworms usually make vertical burrows down to depths of 2 m or more (Edwards et al., 1990; Ehlers, 1975). These channels have a diameter ranging from 1 to 12 mm with smooth walls cemented with mucous secretions. The burrowing species create permanent and empty channels, which

tends to run vertically. Since these types of macropore are present both close to the soil surface and deeper into the soil profile and therefore, one might expect that, on average, the equivalent diameter, circularity and rectangularity do not decrease nor increase with depth in a soil column of 0.72 m in length.

### **3.6 Summary and Conclusions**

The integration of computer programming in the PV-WAVE language, hardware and medical imaging devices in soil studies gives the ability to investigate the interconnected pore space of large undisturbed soil columns to an unprecedented level. With the development of computer programs in PV-WAVE, the analysis of soil macropores was performed directly on CAT scan data. Pores larger or equal to 1.0 mm in equivalent diameter may be readily detected, visualized and quantified. The data generated by the CAT scan process was manipulated in order to accentuate different features of the soil. Soil macropores were isolated by thresholding certain values of the density matrices. This approach was utilized for each section of the soil columns in order to evaluate: the number of macropores, the surface area, the equivalent diameter, the circularity and the rectangularity of each individual macropore. Both the amount and surface area occupied by soil macropores decrease with depth. It was also observed that the size of the macropores is not affected by the distance from the soil surface. Moreover, the geometry of the macropores is apparently not a function of the distance from the soil surface.

3-D imaging is critical in order to accurately correlate soil pore structure and space with flow processes occurring in soil. Programs in PV-WAVE were developed to



visualize the complex three-dimensional network of interconnected pore space. These 3-D reconstructions are unique.

Additional research is needed, particularly with respect to the continuity and tortuosity of the macropore. In the near future, geostatistics and fractal analysis will be used to complete the quantification of the soil macropores.

## PREFACE TO CHAPTER 4

The CAT scanning procedure and computer programs developed for the characterization and visualization of soil macropores using the EMI CT5005 scanner were presented and discussed in Chapter 3. In the summer of 1997, a second CAT scanner was used to improve the pixel resolution and scanning time. This allowed us to perform the macropore analysis at a resolution of 195  $\mu\text{m}$  by 195 $\mu\text{m}$ . Prior to CAT scanning the soil columns, several calibration tests were done to determine the relation between the CT numbers and the physical properties of various samples. Calibration of the CAT scanner is briefly discussed in this Chapter.

Chapter 4 focuses principally on the quantification of a variety of soil macropore measures such as: number of macropores per scan, soil macroporosity, surface area of each macropore, macropore's equivalent cylindrical diameter (ECD), perimeter, hydraulic radius, circularity and rectangularity. A geostatistical analysis was also performed to describe the spatial distribution and spatial continuity of soil macroporosity of one the soil column. The results of this analysis are presented herein. The computer programs developed in PV-WAVE for this study are included in the attached CD-ROM.

This Chapter was published in Canadian Water Resources Journal (Perret J.S., S.O. Prasher, A. Kantzas and C. Langford. 1998. Characterization of macropore morphology in a sandy loam soil using X-ray computer assisted tomography and geostatistical analysis. *Can. Water Res. J.*, 23(2):143-165). For the sake of completeness, some material in this chapter is repeated from previous chapters so that this paper can

stand on its own. The candidate was responsible for designing and conducting the research experiments, developing computer codes for the visualization and analysis of data and preparation of this manuscript. Dr. Shiv O. Prasher, professor at the Agricultural and Biosystems Engineering Department of McGill University, contributed in all aspects of this research project. He provided the necessary funds and assistance for this research, including supervisory guidance and revision of this paper before submission for publication. Dr. A. Kantzas, Director of the Tomographic Imaging and Porous Media (TIPM) Laboratory in Calgary, Alberta, and associate professor at the University of Calgary's Department of Chemical and Petroleum Engineering, provided access to CAT scanning facilities of the TIPM laboratory. Dr. Kantzas also made invaluable suggestions during CAT scanning. Dr. C. Langford, University of Calgary's vice-president research and professor at the Department of Chemistry, was the principal investigator for the NSERC Collaborative Project Grant.

## CHAPTER 4

# CHARACTERIZATION OF MACROPORE MORPHOLOGY IN A SANDY LOAM SOIL USING X-RAY COMPUTER ASSISTED TOMOGRAPHY AND GEOSTATISTICAL ANALYSIS

---

### 4.1 Abstract

Our understanding of the factors affecting leaching of chemicals such as pesticides and fertilizers into soils is limited, in part, due to a lack of adequate non-destructive measurements of soil pore size distribution. The recent application of X-ray Computer Assisted Tomography scanning to non-medical fields such as soil physics has allowed the development of a new and non-destructive technique with considerable potential for quantification of soil and water processes. This study was undertaken to develop an innovative protocol for the characterization and visualization of soil macropores. This paper focuses primarily on the characterization of macropore morphology in large undisturbed soil columns using a 4<sup>th</sup> generation X-ray CAT scanner. The objective of this study was to assess, in quantitative terms, variations in the morphology of macropores as a function of depth. In order to evaluate these variations, the number of macropores, soil macroporosity, macropore size, hydraulic radius, and circularity have been computed and are presented in this paper. Moreover, aspects of geostatistics which

have been used to describe the spatial distribution and spatial continuity of soil macroporosity are also presented. Pores larger or equal to 1.0 mm in equivalent diameter were readily detected. It was found that the average macroporosity of the four soil columns fluctuated between 2.1 and 3.8 %. Moreover, macroporosity was found to decrease significantly with depth. Similarly, the number of macropores decreased by 0.7 % to 2.5 % over the entire depth of the soil columns. It was also found that the macropore-size distributions exhibited a peak for all soil columns and at all depths for macropores having an equivalent cylindrical diameter ranging from 2 mm to 4 mm. The number of macropores falling into this category decreased with depth. From the hydraulic radius distributions, it was inferred that about 20 % of macropore throats have a diameter of 1.6 mm. Moreover, it was noted that the relative percentage of circular macropores increased with depth. Semi-variograms showed spatial dependency for most soil sections up to 22 pixels (i.e., 17 mm).

## 4.2 Résumé

Notre compréhension des facteurs affectant l'infiltration de composés chimiques tels que les pesticides et les engrais dans le sol est limitée par le manque de techniques non-destructrices pour mesurer la distribution des pores du sol. L'application récente de la technique de CAT scanning dans des domaines non-médicaux, tel que la physique du sol, a permis le développement d'une nouvelle approche pour la quantification des phénomènes d'écoulement dans le sol. Cette étude a été entreprise pour développer un protocole innovateur visant à caractériser et visualiser les macropores du sol. Plus précisément, cet article présente une approche pour caractériser la morphologie des macropores dans 4 grandes carottes de sol avec un CAT scanner de la 4ème génération.

L'objectif de cette étude est d'étudier les variations de la morphologie des macropores en fonction de la profondeur. Pour évaluer ces variations, la macroporosité du sol, le nombre de macropores, leurs tailles, leurs rayons hydrauliques, et leurs circularités ont été calculés. De plus, des techniques de géostatistique utilisées pour décrire la distribution spatiale de la macroporosité du sol, sont aussi présentées. Les pores plus grands que 1.0 mm de diamètre, (c.-à-d., les macropores), furent détectés sans problème. Les résultats indiquent que le macroporosité moyenne des quatres colonnes de sol fluctue entre 2.1 et 3.8%. De plus, le macroporosité diminue avec la profondeur. De la même façon, il a été trouvé que le nombre de macropores diminuait de 0.7% à 2.5% pour l'ensemble des colonnes de sol. Il a aussi été découvert que les distributions de la taille des macropores présentent un sommet pour toutes les colonnes de sol et à toute profondeur pour les macropores qui ont un diamètre cylindrique de 2 à 4 mm. Le nombre de macropores tombant dans cette catégorie diminue avec la profondeur. Après avoir étudié la distribution des rayons hydrauliques des macropores, il a été conclu qu'environ 20% des gorges des macropores ont un diamètre de 1.6 mm. De plus, il a été noté que le pourcentage relatif de macropores circulaires augmentait avec la profondeur. La distribution et la continuité spatiale des macropores du sol, estimées par analyse géostatistique, a montré que la dépendance spatiale pour la plupart des sections du sol s'étendait jusqu'à 22 pixels (c.-à-d., 17 mm).

## 4.3 Introduction

### 4.3.1 Soil macropore

By strict definition, macropore means large pore. However, large is a relative term and this lack of clarity has led to several conflicting definitions. However, in this research study, the definition proposed by Luxmoore et al. (1990), where “ *the term macropore includes all pores in a profile that are (generally) drained at field capacity, with the latter being 1 mm or more in equivalent diameter* ”, was followed.

It is now accepted that water percolation can be greatly accentuated by the presence of macropores in the soil (Bouma, 1981; Chen et al., 1993; Dipietro and Lafolie, 1991; Li and Ghodrati, 1994; Logsdon, 1995; Moore et al., 1986; Quinsberry et al., 1994; Singh et al., 1991; Timlin et al., 1994; Trojan and Linden, 1992). Soil heterogeneity is often attributed to non-uniform aggregate size distribution, which in turn determines a non-uniform pore size distribution. Soil pore connectivity and size play a determining role in water and solute flow characteristics (Ma and Selim, 1997). Intuitively, large and continuous pores facilitate water transport. As a result, the presence of preferential flow paths (macropores) results in rapid movement of water and associated solutes through soil profiles. It plays a very important role in the transport of nutrients and agricultural chemicals from surface to sub-soil and eventually, to ground water and drainage effluent that feed streams. Rapid flow has a major impact on drainage and groundwater quality since it may not allow contaminants, such as pesticides, to be adsorbed on and into the soil particles and broken down by chemical and biological actions.

Knowledge of soil structure, along with a suitable technique for measurement of flow characteristics of water and associated solutes through soil, is essential to understanding the mechanisms of preferential flow. In a porous medium such as soil, pores have a non-uniform structure and their geometry is often extremely complicated to characterize (Bouma, 1981; Dullien, 1992; Grevers and de Jong, 1994; Peyton et al., 1994a; Logsdon et al., 1990; Phogat and Aylmore, 1989; Roseberg and McCoy, 1992; Shepard, 1993; Warner, 1990).

#### **4.3.2 Characterization of macroporosity in soil**

There are an increasing number of research projects reported in recent literature that propose various means of characterizing soil macropores. Two general approaches for the analysis of macropores can be found in literature, namely, indirect and direct approaches.

Indirect approaches attempt to determine the influence of macropores by measuring flow characteristics under varying conditions (Warner et al., 1989). Several indirect methods have been developed to obtain macropore parameters. Everts and Kanwar (1993), Timlin et al. (1994), Logsdon et al. (1993), Dunn and Phillips (1991a.), Dunn and Phillips (1991b.), Perroux and White (1988), and Watson and Luxmoore (1986) have used tension infiltrometers to characterize the apparent conductivity and continuity of soil macropores. Macropore continuity and macropore flow can also be assessed by breakthrough curves (BTCs) with non-reactive tracers such as bromide, chloride and tritiated water. This approach has been used in numerous soil studies to describe flow mechanisms through soil macropores (Ahuja et al., 1995; Anderson and Bouma, 1977; Jabro et al., 1994; Li and Ghodrati, 1994; Ma and Selim, 1994; Munyankusi et al., 1994;



Quisenberry et al., 1994; Shipitalo and Edwards, 1996; Trojan and Linden, 1992). In a well-structured soil, solution will move rapidly and as a result, the tracer can soon be found in the effluent. Therefore, flow regimes and soil structure can be characterized from the shape of BTCs. However, indirect approaches have a major limitation, as they can provide only qualitative information about soil macroporosity.

Quantitative analysis of macroporosity provides a more comprehensive and systematic approach and is normally obtained by direct methods. Two general approaches can be used for direct analysis of soil macropores; one is destructive (morphometric techniques), and the other is non-destructive and is achieved by emerging new technologies, such as X-ray or g-ray Computer Assisted Tomography (CAT scanning).

Many morphometric techniques are available to measure soil (macro)pore-size distributions. These destructive techniques are based on filling the pores of the soil either with a liquid that hardens after some time or with a dye that stains the preferential flow paths. Epoxy resin (Koppi and McBratney, 1991; Moran and McBratney, 1992; Moran et al., 1989), polyester resins (Singh et al., 1991), and paraffin (Vermeul et al., 1993) have been used for this purpose. After impregnation and hardening of the liquid, the soil sample is sectioned with a mechanical saw and polished to obtain a smooth finish. The operation is followed by digitization of the soil section and image analysis to depict soil macroporosity and to characterize its morphology. Other researchers, such as Andreini and Steenhuis (1988), Booltink and Bouma (1991), Logsdon (1995), Logsdon et al. (1990), Trojan and Linden (1992), and Wu et al. (1993) have characterized flow patterns along macropores using dye tracers such as methylene blue or lissamine yellow. Unfortunately, a number of difficulties and problems are associated with these direct and

destructive approaches. The greatest problem is that most impregnating agents have a low viscosity and are not miscible with water. As a result, they do not infiltrate into all of soil macropores, especially in moist conditions. Moreover, preparation of soil samples and image analysis of soil pore-space patterns demand very meticulous handling in order to preserve soil structure and require considerable time for execution. Finally, these two direct approaches have the common disadvantage of destroying the soil sample's structure before verifying that the dye or impregnating agent has been fully absorbed by soil macropores. This limits their application, as they cannot be repeatedly applied to studies involving time such as water and solute movement through soil, water content changes, etc.

With the application of Computer Assisted Tomography (CAT) to soil-plant-water studies, a relatively new and exciting method is now available for non-destructive imaging of porous media such as soil. Several researchers such as, Warner et al. (1989), Grevers et al. (1989), Grevers and de Jong (1994), Anderson et al. (1990), Peyton et al. (1992), Hanson et al. (1991), Tollner et al. (1995), Asare et al. (1995) have recognized the great potential offered by CAT scanning for characterizing of soil macroporosity. However, CAT scanning has not been used to its full potential for the quantification of soil macropores and investigation of preferential flow processes. In most studies, the sizes of undisturbed soil cores were too small and the distances between consecutive scans were too large to generate accurate and complete characterization of soil macropores (Perret et al., 1997).

This paper focuses primarily on the characterization of macropore morphology in large undisturbed soil columns using a 4<sup>th</sup> generation X-ray CAT scanner. The objective

of this study is to assess, in quantitative terms, variations in the morphology of macropores as function of depth. In order to evaluate these variations, the number of macropores, soil macroporosity, macropore size, hydraulic radius, and circularity have been computed and are presented in this paper. Moreover, aspects of geostatistics, which have been used to describe the spatial distribution and spatial continuity of soil macroporosity, are also presented.

## **4.4 Materials and Methods**

### **4.4.1 Columns extraction and soil properties**

Four undisturbed soil columns, 0.85 m in length and 77 mm in diameter, were extracted from an uncultivated field border, located at the Macdonald Campus of McGill University in Ste-Anne-de-Bellevue, Quebec. The hydraulic bucket of a backhoe was used to drive polyvinyl chloride (PVC) pipes in small increments of about 80 mm. The objective was to obtain soil cores that were disturbed as little as possible in order to obtain samples representative of natural conditions.

Column size was selected based on the need for a large enough sample to represent macropore distribution, yet small enough to be handled easily when full of soil. PVC was chosen for the cores because it has a relatively low X-ray attenuation coefficient. The soil had been covered for many years with a combination of quack grass (*Elytrigia repens* (L.) Nevski.), white clover (*Trifolium repens* L.) and wild oat (*Avena fatua* L.). The soil belongs to the Chicot series and is predominantly a sandy loam with an A horizon thickness of around 0.4 m. Details of the soil characteristics are presented in Table 4.1.

**Table 4.1:** Selected properties of a Chicot soil under a combination of quack grass (*Elytrigia repens* (L.) Nevski.), white clover (*Trifolium repens* L.) and wild oat (*Avena fatua* L.).

Depth (m)	Bulk Density (Mg/m <sup>3</sup> )	$\rho_g^1$ (Mg/m <sup>3</sup> )	$\omega^2$ (%)	Clay (%)	Silt (%)	Sand (%)	OM <sup>3</sup>	CEC <sup>4</sup>	pH	Description
0.0-0.15	1.36	2.51	23.9	6	12	82	3.96	9.66	6.32	Dark brown with fine crumb structures – slightly firm
0.15-0.30	1.27	2.52	24.7	5.5	12.5	82				
0.30-0.45	1.30	2.59	24.2	7	9	84				
0.45-0.60	1.30	2.60	21.5	5	8	87	1.20	8.01	6.01	Brown to yellowish brown – compact layer with occasional rocks presence of earthworm channels
0.60-0.75	1.46	2.64	11.8	8	8	84				
0.75-0.90	1.64	2.59	14.2	14.5	8.5	77				

- 1 Mineral grain density
- 2 Gravimetric water content at field capacity
- 3 Organic matter content(g/g)
- 4 Cation Exchange Capacity (cmol/kg)

#### 4.4.2 Soil column preparation

The soil columns were scanned under dry and saturated conditions. To reach dry conditions, the soil columns were placed under a set of ten light bulbs of 300 watts each for a period of six weeks. The cores were rotated periodically to accelerate evaporation. Both ends of the four soil columns were open to the atmosphere so that moisture could evaporate.

One of the soil columns was drilled from top to bottom to verify the ability of the CAT scanner to portray the size and the location of a known pore. This artificial macropore consisted of a polyethylene tube of 1 mm in inner diameter. PVC caps were

installed in order to create an empty space at the end of the column. The purpose of this space was to allow water and tracers to penetrate uniformly through the column cross-section. To prevent the soil from collapsing, a plastic screen was placed on both ends of the soil column.

#### **4.4.3 CAT scanning**

A modified medical ADVENT HD200 whole body CAT scanner was used for this study at the TIPM laboratory, Calgary. Computed Tomography (CT) or Computer Assisted Tomography (CAT) is a method of diagnostic imaging used for viewing non-destructive, cross-sectional “slices” of the human body or an object. This scanner incorporates a fourth generation scan geometry, fast scan times (up to 2 s/scan) and high pixel resolution (up to 195  $\mu\text{m}$  by 195  $\mu\text{m}$ ). In most CAT scanners, the actual collection of patient data occurs in the gantry where the patient lays horizontally. However, the ADVENT HD200 was modified to allow vertical scanning. For that purpose, the CAT scanner gantry was rotated by an angle of 90° and positioned on a metal frame designed to hold the whole gantry horizontally.

During CAT scanning, each column was placed vertically in the scanner unit so that the X-ray beam intersected the soil column perpendicularly to its longitudinal axis. A bubble level indicator was used to ensure that the soil column was vertical. The longitudinal axis of the core was positioned at the center of the CT gantry. During the computer tomography process, the X-ray tube generates the X-ray beam and rotates around the soil column. A pre-collimator modulates the thickness of the X-ray beam. For the present study, the collimator was set to a thickness of 2 mm. The transmission and detection of this thin and rotating X-ray beam through the soil column results in the

collection of a large number of attenuation measurements taken at discrete angles. For this purpose, an array of 720 detectors is located within the gantry. Once collected, this data is mathematically reconstructed to generate a 512x512 matrix. To produce a mean X-ray energy beam in the Compton energy range, the CAT scan system parameters were adjusted to

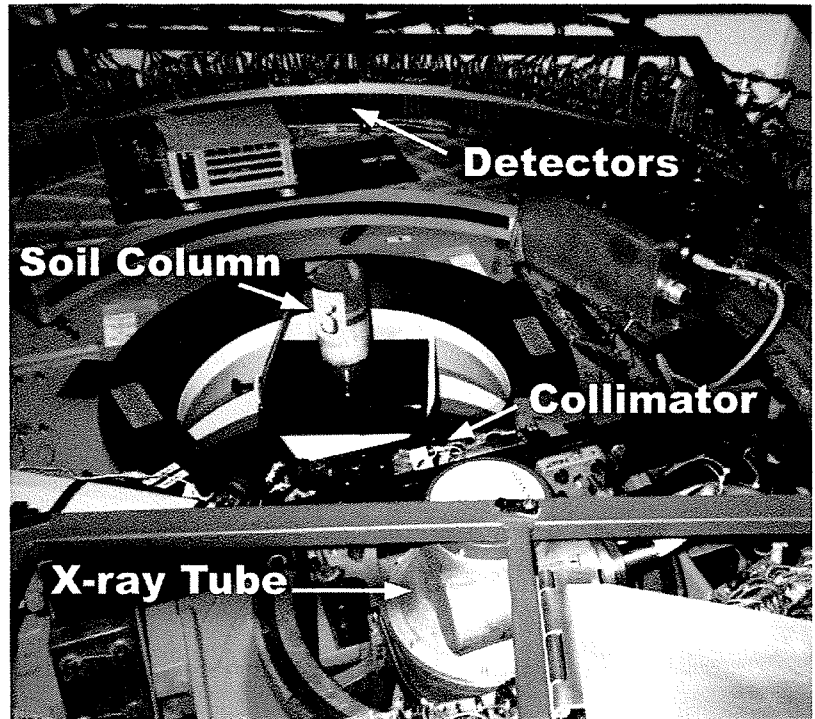


Figure 4.1: Open view of the gantry of the X-ray CAT scanner (ADVENT HD200 whole body CAT scanner - TIPM laboratory, Calgary).

120 peak kV and 50 mA. Figure 4.1 shows an open view of the gantry of the CAT scanner.

The position of the core was set mechanically for each scan with a digital indexing ruler having a precision of  $\pm 0.001$  mm. A total of 360 sections or scans was obtained for each column, leaving no space between two consecutive scans.

#### 4.4.4 Calibration and data conversion

CT numbers are the standard output of a CAT scanner and are usually expressed in HU's (Hounsfield Units) which are dimensionless. A series of calibration tests was performed to determine the relation between the CT numbers and the physical properties of various samples. More precisely, a large numbers of liquids and solids were tested to

establish the linear relationship between CT number and bulk density at 120 peak kV and 50 mA. A calibration curve was obtained using a simple regression algorithm (Figure 4.2).

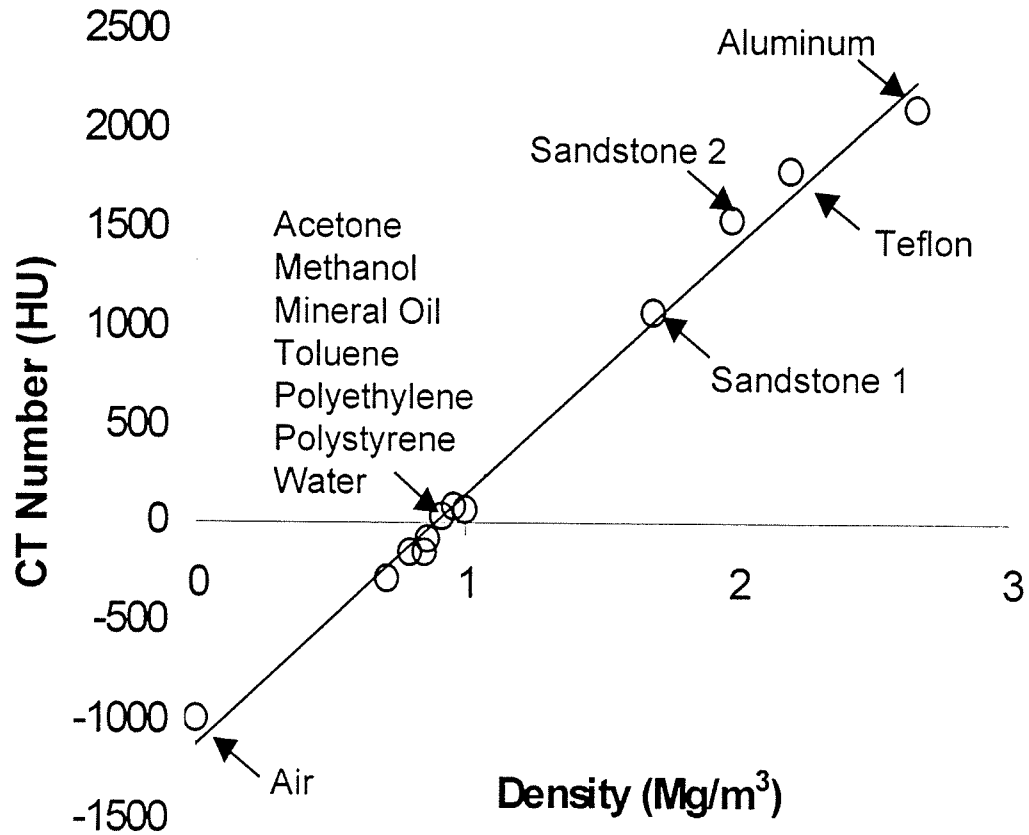


Figure 4.2: Results of calibration tests performed at 120 kV and 50 mA to determine the relation between the CT numbers and density of various samples.

Pixels from each scan were recorded on a magnetic tape, transferred to a SUN4 workstation under the UNIX operating system and converted to a bulk density value. A FORTRAN program was developed to compute the calibration line of each scan. Once the linear calibration equations were established, a computer algorithm transformed CAT scan arrays into matrices of bulk density. Part of the algorithm also allowed for

computation of the soil section's porosity distribution on a voxel basis. The remaining analysis was done using the PV-WAVE language on a Pentium II 300 MHz PC equipped with 128 Mb of RAM.

#### 4.4.5 Image generation and visualization of soil macropores

PV-WAVE is a comprehensive programming environment that integrates state-of-the-art numerical and graphical analyses. PV-WAVE is an ideal tool for working with arrays such as our CAT scan data, because of its array-oriented operators and its ability to display and process data in the ASCII and Binary I/O format.

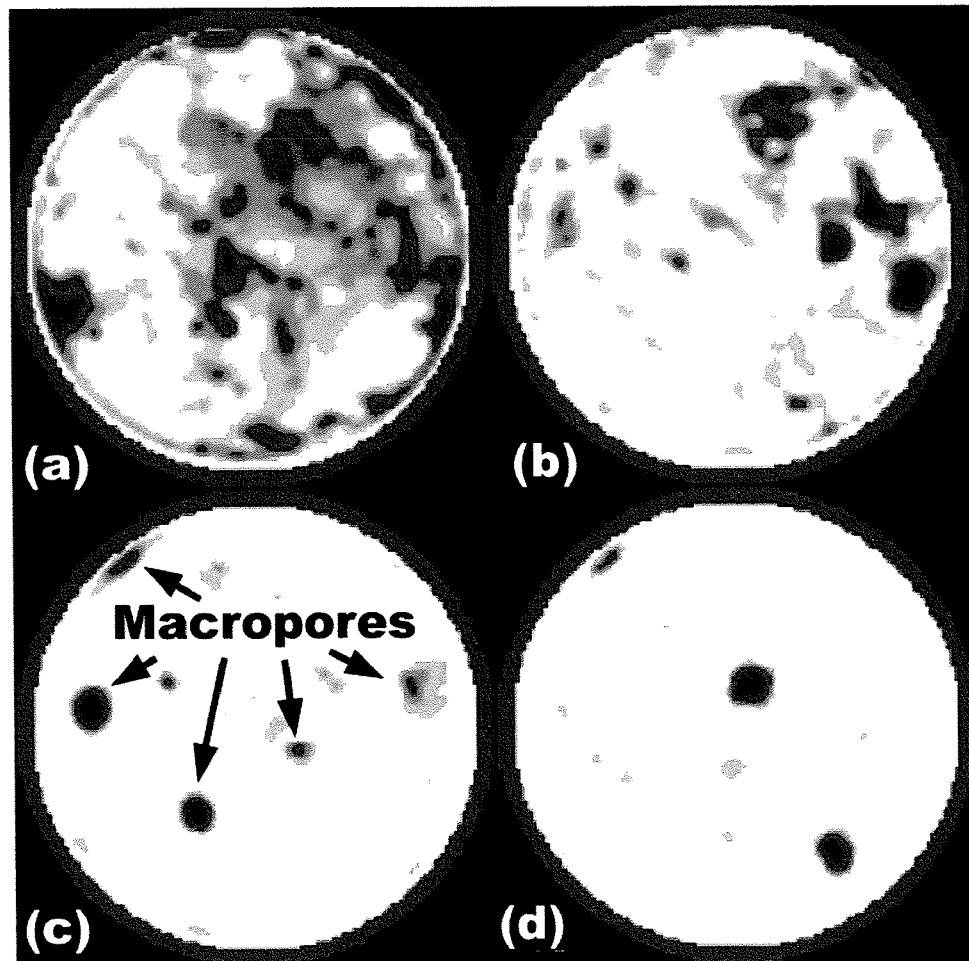


Figure 4.3: Visualization of cross-sectional images generated by "Jofran.pro". These cross-sectional images belong to Column 1 and were scanned at (a) 2 mm, (b) 50 mm, (c) 400 mm and (d) 600 mm.



Visual inspection of bulk density and porosity matrices is an important step towards the understanding and analysis of the macropore's complex structure. An interactive algorithm (Jofran.pro) was developed in PV-WAVE for comprehensive inspections of the bulk density and porosity matrices and for the creation of cross-sectional images. The program converts ASCII matrices into BINARY format in order to generate images. Each pixel value is scaled to a range of 0-255 to form the image. In this context, an image is a two-dimensional array of pixels for which each element is attributed to a color depending on its value. A binary threshold was used for better detection of soil macropores to enhance or mask portions of the image. The computer program was used extensively to produce cross-sectional images and examine shape, size, and macropore distribution. Some cross-sectional images of Column 1 scanned at different depths are presented in Figure 4.3.

Longitudinal images are useful in visualizing low and high-density area distributions along the soil column length. A program in PV-WAVE, called Longi\_mak.pro, was developed to generate longitudinal views. This program stacks up 360 sections, one on top of the other, and "cuts" through a vertical plane to extract a vertical cross-sectional slice from the three-dimensional block of data. The position of the plane that bisects the volume of data is determined using a fixed pixel depth. 512 longitudinal images can be generated in the x-direction and in the y-direction for each column.

In hospitals, three-dimensional imagery has recently been possible with the aid of powerful stereotactic radiosurgery computer programs (Hanson et al., 1991). However, these softwares are very expensive and not offered on typical medical scanners (Aylmore,

1993). No software package was available at the TIPM laboratory for three-dimensional visualization of CAT scan data. Since 3-D imaging is critical to the accurate correlation of soil pore structure and space with flow processes occurring in the soil, we decided to develop our own three-dimensional reconstructive methodology.

Three programs in PV-WAVE were developed to permit a three-dimensional image to be reconstructed from multiple contiguous scans. The first program (Make3D.pro) isolates macropores in 2-D matrices, scales the values of each pixel to a range of 0-255 and combines them into a 3-D ASCII array. The second program (Conv\_binary.pro) converts the 3-D ASCII array into binary I/O format. The binary I/O format is the simplest and most efficient form of I/O. Images and large data sets are usually stored and manipulated using binary I/O in order to minimize the machine's processing load. The third program (Rview.pro) produces a list of vertices



Figure 4.4: Three-dimensional reconstruction of the interconnected network of soil pores and cavities of Column 1. A computer program called "Rview.pro" generated this reconstructed image.

and polygons that describes the macropore's three-dimensional surface. Each voxel is visited to find polygons formed by the macropores. The polygons are then combined and rendered to reconstruct an exact three-dimensional representation of the interconnected network of soil pores and cavities. The reconstructed image allows for the visualization of soil macropores as never observed before. Figure 4.4 shows a 2D projection of the three-dimensional reconstruction of Column 1.

#### **4.4.6 Characterization of soil macroporosity**

Quantification of soil macropores seeks to identify inherent macropore characteristics such as their number, size and geometry. These characteristics are used to describe macropores or the attributes of macropores prior to the subsequent task of classification and modeling. A program (Macjo97.pro) was written to recognize, extract and quantify soil macropores for each of the two-dimensional arrays. This comprehensive algorithm provides a variety of soil macropore measures such as: number of macropores per scan, soil macroporosity, surface area of each macropore, macropore's equivalent cylindrical diameter (ECD), perimeter, hydraulic radius, circularity and rectangularity.

Pore size is usually determined experimentally by measuring pressure imposed by the pore structure on fluid retention/penetration. For instance, it can be computed from the soil moisture retention curve where the ECD is related to water potential by means of the capillary rise equation. This approach involves an analogy between macroscopic retention characteristics of soil and behavior of capillary tubes. However, the analogy between the macroscopic retention characteristic of pores and the behaviour of water in a capillary tube may not apply to cracks and big macropores (Skopp, 1981). In other

words, by considering pores to be cylindrical and by assuming that soil-water characteristics of a pore follow the model of capillary tubes, estimation of the equivalent diameter may result in a fallacious description of soil porosity (Bouma, 1981). Using matrices generated by the CAT scanner, macropore size is described in terms of its surface area considering all pixels ( $195\ \mu\text{m} \times 195\ \mu\text{m}$ ) belonging to the macropore domain. A more intuitive indicator of macropore size is the equivalent cylindrical diameter (ECD) which can be derived from the surface area it occupies. In other words, it represents the diameter of a circle that covers the same surface area than the actual pore. Evidently, in a porous medium such as soil, the macropore size or ECD will be heterogeneous. To reveal the distribution of macropores according to their size at different depth, each soil column was divided into six sections of 120 mm each. The macropore-size distribution was then evaluated in each of these sections.

Macropores are not regularly shaped. The neck of the pore is an important feature of pore geometry, which directly controls percolation rates. A neck (also known as pore throat) is defined as the local minimum in pore space size (Kwiecien et al., 1990). The pore throat is located where the minimum mean radius of curvature of a gas/liquid interface is observed. This corresponds to the location of maximum capillary pressure. Maximum capillary pressure within a macropore is very difficult to measure. However, the hydraulic radius is a good approximation of the mean radius of curvature (Kwiecien, 1987; Dullien, 1992). The hydraulic radius of the pore can be simply computed by the ratio of the cross-sectional area to the perimeter of the macropore. The hydraulic radius has been evaluated since it is a good indication of the pore neck position and of the pore expansion/contraction.

The shape of the macropore was characterized by computing its circularity and rectangularity. We have slightly modified the definition of circularity given by Perret et al. (1997) as we are now calculating circularity as the ratio of the circumference of a circle having a diameter equal to the macropore's equivalent diameter to macropore perimeter. Since the circumference is the smallest closed line that embraces a two-dimensional figure, circularity can never be greater than one. Circularity equal to one implies that the macropore is circular. A circularity less than 0.5 indicates that the macropore is elongated. Rectangularity is given by the macropore's area divided by the area of a bounding box formed around the macropore (Tollner et al., 1995). The rectangularity can never exceed one. Rectangularity close to one implies that the macropore tends to be rectangular in shape.

As mentioned above, a program called Macjo97.pro was developed to quantify soil macroporosity. For each column, the algorithm examines more than 94,000,000 voxels in order to characterize the macroporosity. The first task, accomplished by Macjo97.pro, is to partition the two-dimensional sections into regions of 1 for the pores and 0 for the soil matrix. The pores contain either water or air (i.e., density lower than 1). Thus, by applying a threshold on all pixels in the bulk density matrices having a value lower than one, the pore can be isolated. This process is called segmentation. Once the two-dimensional matrices have been transformed into 0 and 1 elements, the algorithm must recognize each individual pore, registered as a set of contiguous 1's. Two matrix elements having a value of 1 are said to be part of the same pore if they are sharing a common side. In other words, to be part of the same pore, a pixel needs to have a value of 1 and must be located in one of the four nearest neighbouring locations of the other pixel.

In a single pass of the two-dimensional array, the algorithm recognizes and regroups pixels belonging to the same pore. This part of the program is referred to as the clustering algorithm. Some of the pores are too small to be classified in the macropore category. If the equivalent diameter of the pore is less than 1 mm, then the pore is removed from the two-dimensional matrix by resetting each of its pixels to 0. This simple process is called filtering. After filtering, all macropore attributes are computed. The program can be used either for one section or for the 360 sections of a soil column. All macropore attributes were stored in an ASCII file for further analysis on a worksheet.

#### 4.4.7 Geostatistical analysis

Classical statistics ignores the presence of spatial correlation (Mallants et al., 1995). On the other hand, geostatistics calculates spatial correlations between observations made at neighbouring locations. This implies that within a given range of spatial dependence, soil properties such as macroporosity, can be described as a function of their spatial correlation. Semi-variance describes this spatial correlation. Dutilleul and Legendre (1993) pointed out that analysis of semi-variance was a great tool for the quantification of spatial heterogeneity and the examination of spatial data. Semi-variance,  $\gamma(h)$ , as presented by Journel and Huijbregts (1978), is estimated as follows:

$$\gamma(h) = \frac{\sum_{i=1}^n [Z(x_i) - Z(x_i + h)]^2}{2n} \quad (4.1)$$

where  $n$  is the number pairs of observation separated by lag distance  $h$ , and  $Z(x_1), Z(x_2), Z(x_3), \dots, Z(x_n)$  are data values measured at locations  $x_1, x_2, x_3, \dots, x_n$ . The

semi-variance  $\gamma(h)$  is generally plotted against lag distance  $h$ . This graphical representation is called the semi-variogram (Figure 4.5).

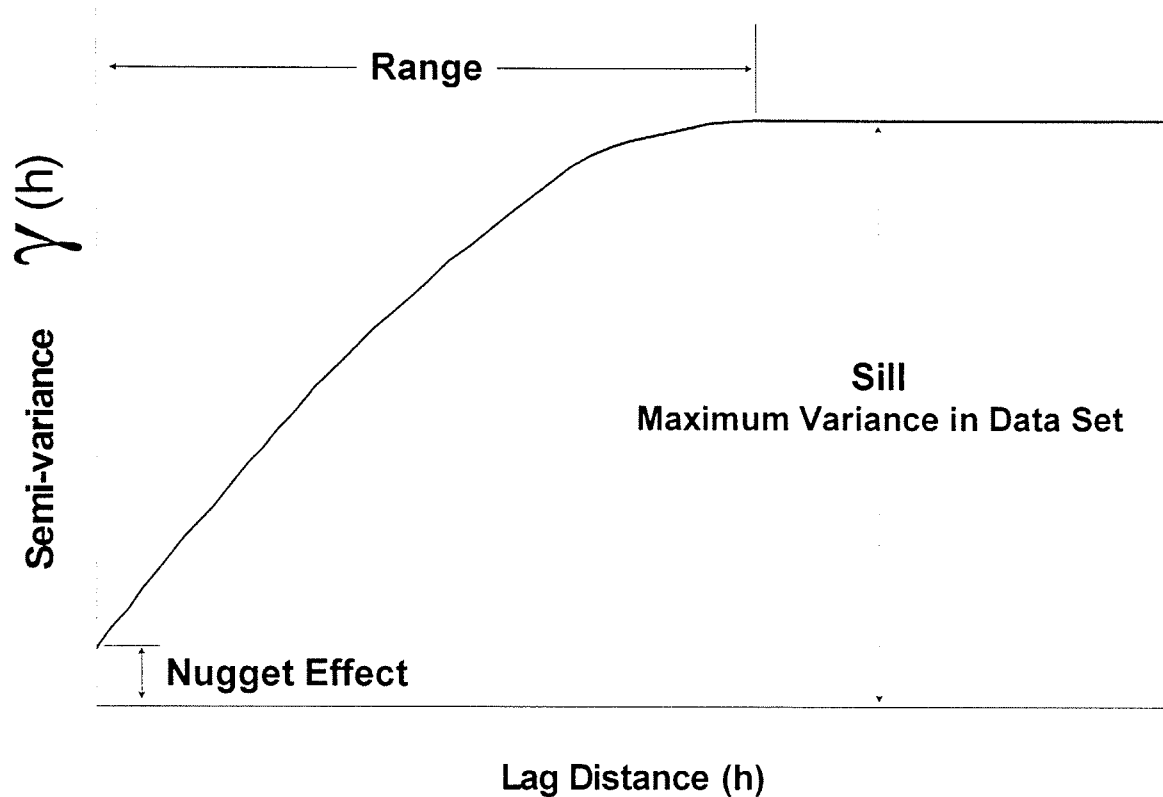


Figure 4.5: Idealized semi-variogram.

Estimation of the variogram from sample data is critical to a geostatistical study. The lag distance at which semi-variance becomes more or less constant is known as range of the semi-variogram. Sample data separated by lag distances smaller than the range are spatially correlated. When the lag distance approaches a value greater than the range, sample data are independent of one another. In other words, range indicates the degree of spatial continuity (Grevers and de Jong, 1994). The sill approximates sample variance

for stationary data. The nugget effect indicates significant variability over distances less than the minimum sampling interval. The semi-variogram shape is indicative of the variable  $Z(x)$ 's spatial behavior (Journel and Huijbrets, 1978).

Spatial distribution of soil macropores should be reflected in the semi-variogram of two-dimensional matrices obtained with the CAT scanner. Geo-EAS (Geostatistical Environmental Assessment Software), developed by Englund and Sparks (1992), is a robust geostatistics package that performs two-dimensional geostatistical analyses of spatially distributed data. Analysis of semi-variograms calculated from bulk density matrices should allow the evaluation of the degree of spatial continuity of soil macropores in serial sections of soil columns. GEO-EAS was used for calculation of semi-variograms of Column 1 at every 30 mm interval. The data files read by GEO-EAS are simple ASCII text files and cannot contain more than 1000 data points. However, each bulk density matrix contains 262,144 data points. Two computer programs to resize the original array to a matrix containing 1000 elements (Rscalejo.pro) and to generate the

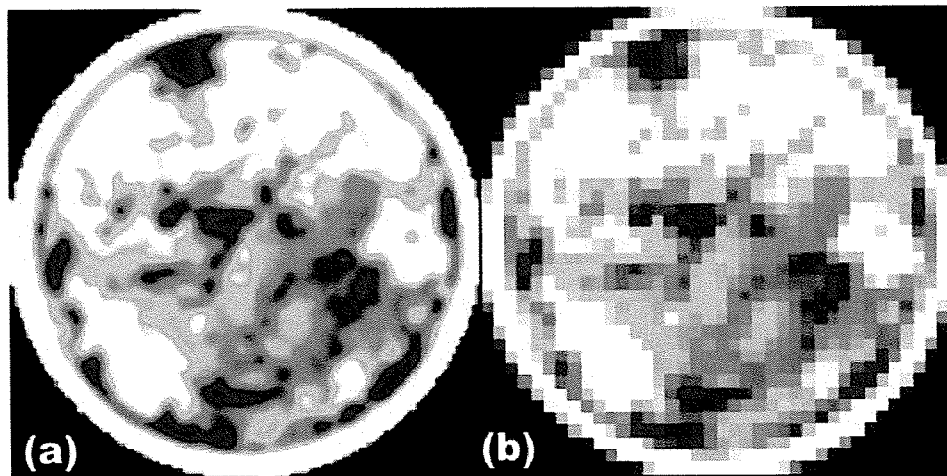


Figure 4.6: (a) Original bulk density matrix (262,144 elements);  
(b) resized matrix containing only 961 data points.



input data files for GEO-EAS in the proper format (Geo\_outjo.pro) were written in PV-WAVE. Figure 4.6 shows an original bulk density array and its resized version.

## 4.5 Results and Discussion

### 4.5.1 Changes in macroporosity and number of macropores with depth

Soil macroporosity was evaluated for each of the 360 sections by dividing the sum of all pixels belonging to soil macropores by the total number of pixels. In other words, macroporosity was calculated by computing the percentage of surface area

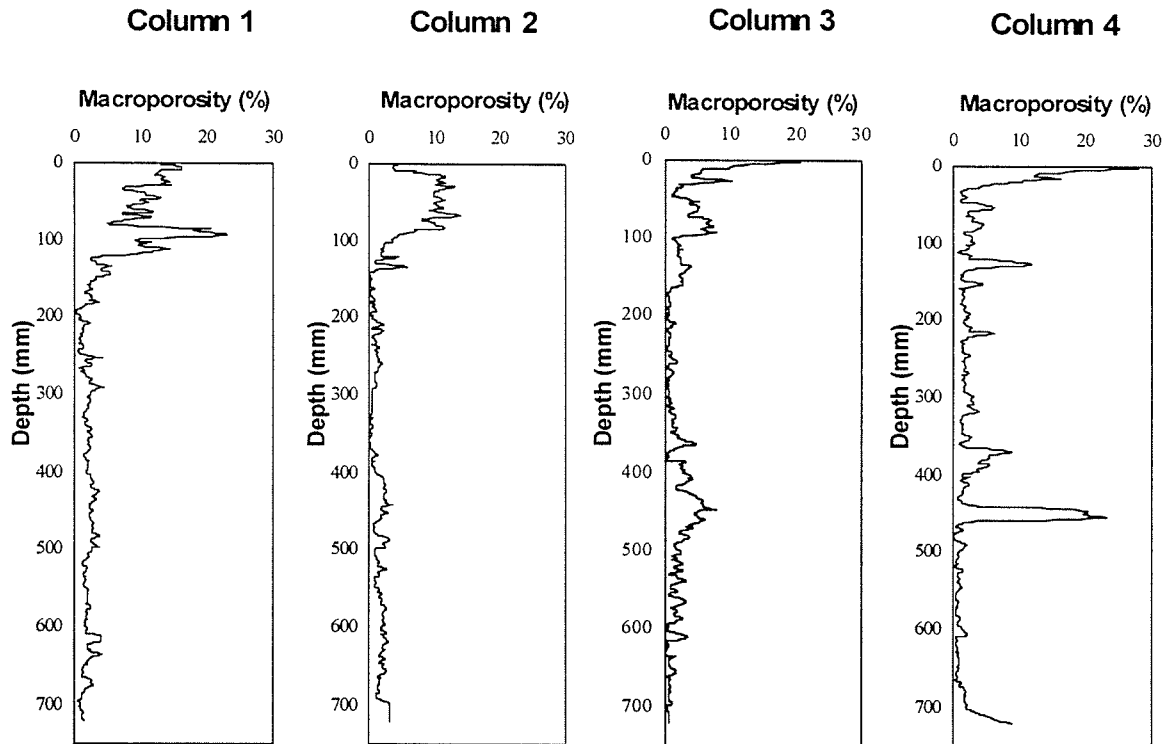


Figure 4.7: Macroporosity variations of the four soil columns with respect to depth.

occupied by soil macropores for every section. Results are shown in Figure 4.7. The average macroporosity for the four soil columns fluctuates between 2.1 to 3.8 %. These results are in accordance with those of Edwards et al. (1990), who reported macroporosity ranging from 0.4 % to 3.8%. In order to describe trend of macroporosity changes versus depth, SAS 6.12 was used. After performing an ANOVA, it was decided to transform macroporosity data with a logarithmic transformation in order to reduce the coefficient of variability. The trends were then analysed using the PROC REG procedure with a linear model. A T-test was performed to evaluate the degree of significance of the slope of linear model for the four soil columns. Column 1, 2 and 4 revealed a significant decrease of macroporosity over the entire depth of the soil columns with T-test values of the order of 0.0001. Although Column 3 also displayed a decreasing trend, it was not statistically significant. Overall, these results show a significant decrease of soil macroporosity with depth. These results can be easily explained since biological activity (i.e., fauna and plant roots) and effect of climatic variations (i.e., wetting/drying, freezing/thawing cycles) result in a greater macroporosity close to the soil surface.

The number of pores having an equivalent diameter greater or equal to 1 mm (macropores) was evaluated. The results are shown in Figure 4.8.

In general, the number of macropores tends to decrease with depth. However, in column 3, this trend is not as obvious as it is for the other columns. During transportation, soil from the middle of column 3 may have accidentally been loosened. This incident provides a reliable explanation for the jumbled macropore count observed for this column. Similarly to the approach followed with macroporosity data, a logarithmic transformation was applied on macropore count to analyse trends and to

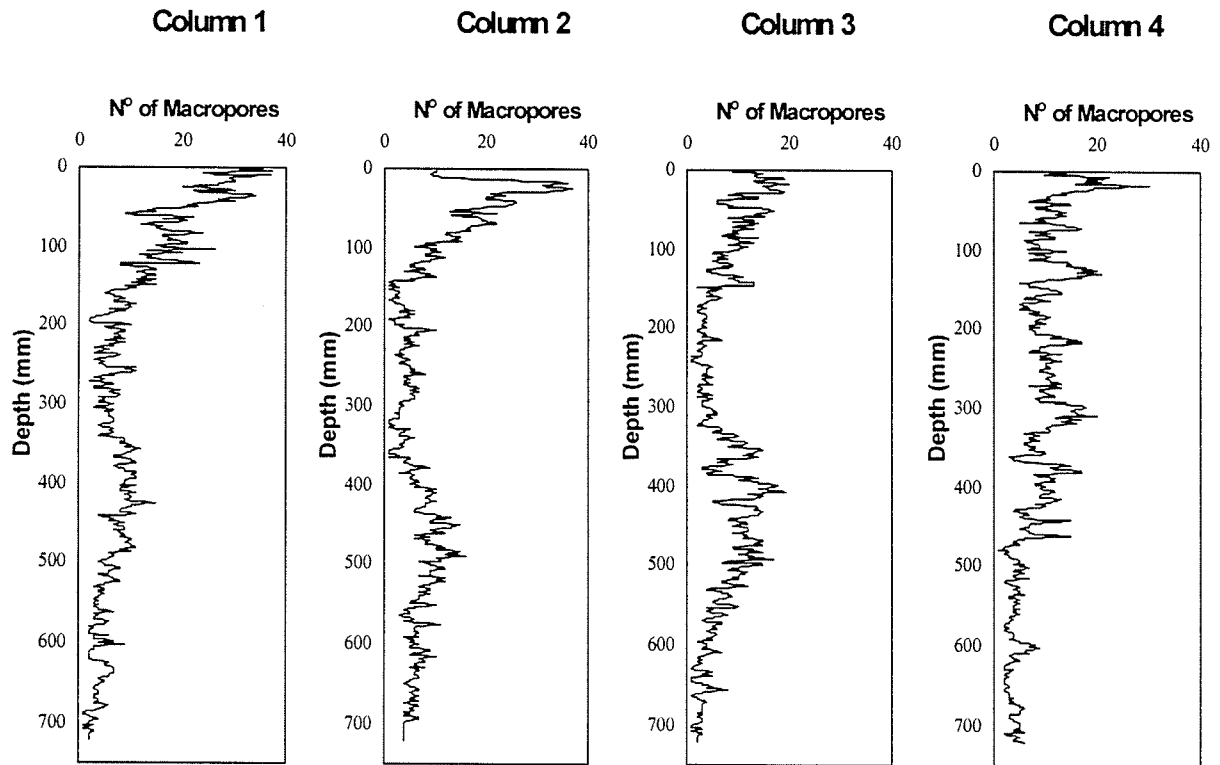


Figure 4.8: Results of the macropore count for the four soil columns.

evaluate the degree of significance of the slope of a linear model fitted to the transformed data. As expected, the decreasing trend was significant for all columns with T-test values of 0.0001. The decrease in number of macropores in the four soil columns ranges from 0.7 % to 2.5%. However, in all of the four columns, the number of macropores tends to decrease more substantially in the top 200 mm of the soil profile. Therefore, the changes in number of macropores with respect to depth were analysed separately in the top 200 mm and the remaining section of the soil columns. The results indicated that, for Column 1 and 2, the number of macropores were decreasing by 12.9 and 12.7 %, respectively, in the top 200 mm whereas Column 3 and 4 showed a decrease of 6,3 and 3.8 % in this portion of the soil profile. From 200 to 720 mm, the macropore count in Column 1, 2 and

3 was not significantly increasing nor decreasing with an average of 1400 macropores per square metre. Burges and Raw, (1967) pointed out that the number of earthworms per square meter could range up to 850 specimens in temperate regions. Knowing that earthworms are not the only vector of macropore formation and that earthworms can create more than one burrow, this figure seems appropriate.

#### **4.5.2 Macropore-size distribution with respect to depth**

As pointed out above, the macropore-size distribution has been evaluated in 6 different sections of 120 mm each. Results are expressed in percentage of the total number of macropores falling in a particular size range. Macropore-size distributions obtained for each section of the four soil columns are shown in Figure 4.9. It can be observed that in all soil columns and for all sections, the distribution curves exhibit a peak for macropores with an ECD ranging from 2 mm to 4 mm. It can also be seen that for Column 1,2 and 4, the number of macropores falling in that size range decreases with depth. In Column 3, the distribution of number of macropores ranging from 2 mm to 4 mm is relatively higher from depth 240 mm to 600 mm than in the other columns. This can again be explained by the fact that soil from the middle of Column 3 may have accidentally been loosened during transportation. In Column 1, the distribution curves from depth 240 mm to 720 mm show a clear peak around macropore size of 8 mm. This indicates that for this portion of the soil profile, we should encounter macropores with an ECD of approximately 8 mm. This was verified by inspection of the porosity matrices with the computer program Jofran.pro. Some of these macropores can be seen in Figure 4.3a and 4.3c.

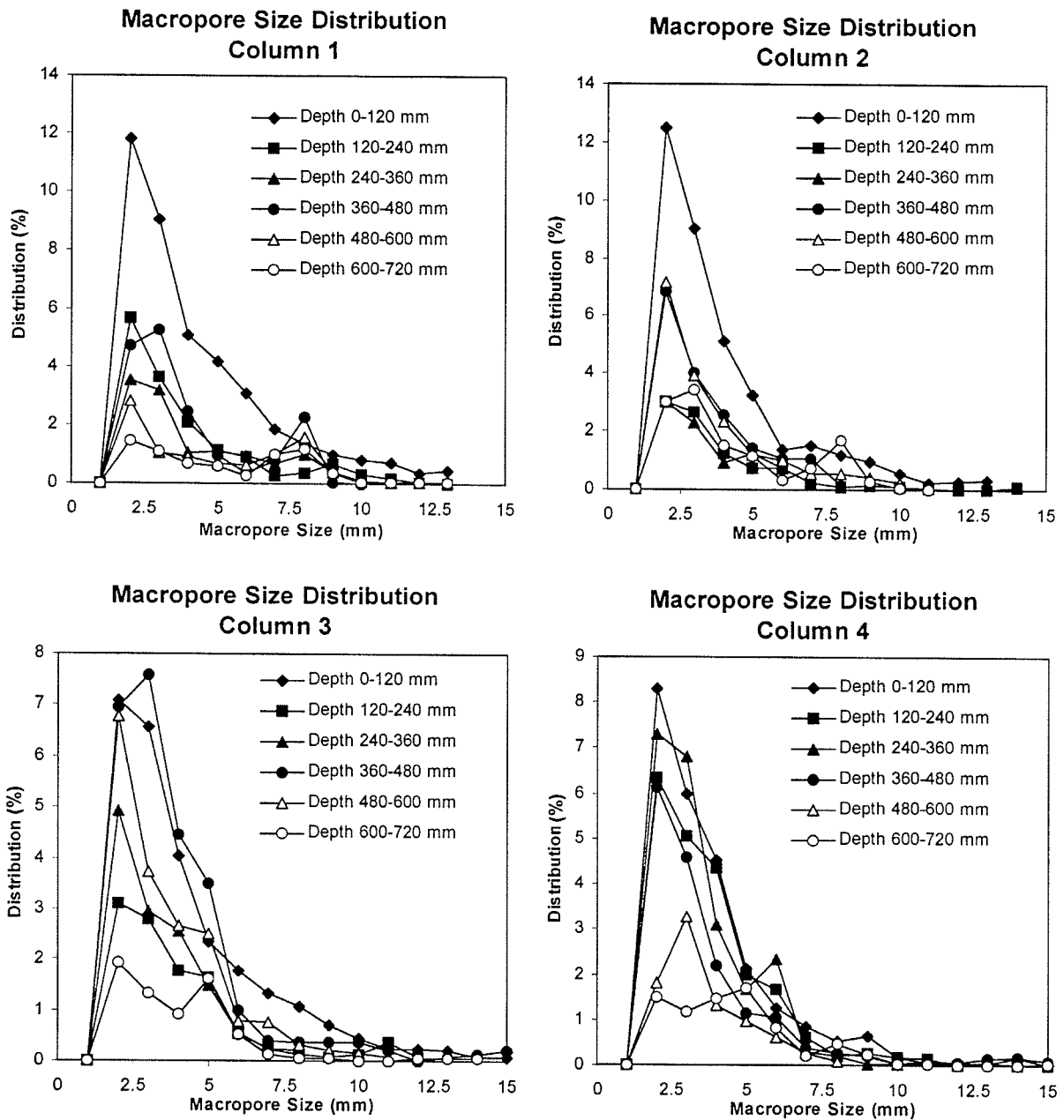


Figure 4.9: Macropore-size distributions of four soil columns obtained for different sections of the soil profile.

Macropore area-size distributions were also investigated for the four soil columns by multiplying the number of macropores falling in a particular size range by their average equivalent cylindrical diameter. This transformation permits to depict the

contribution of each macropore-size to the overall macroporosity of the soil columns. These results are presented for Column 1 in Figure 4.10.

By comparing the macropore-size distribution of Column 1 (Figure 4.9) with these results, it can be seen that the area-size distributions give a better description of the contribution of large

macropores. The peaks observed for macropores with an ECD around 8 mm in Column 1 (Figure 4.9) are not contributing significantly to macropore-size distribution. However, this category of macropores have a great effect on the area-size distribution and thus, on macroporosity.

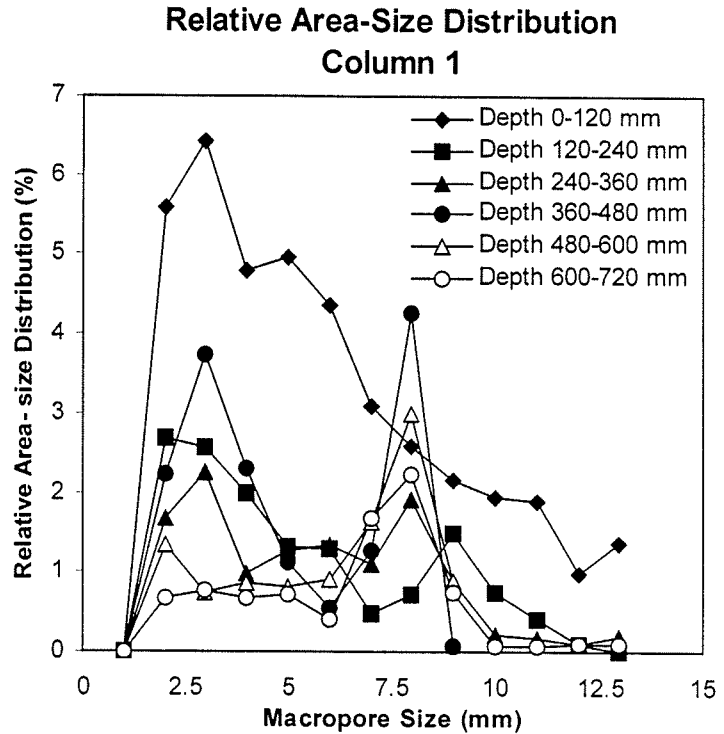


Figure 4.10: Relative area-size distributions of macropores for one of the four soil columns.

#### 4.5.3 Hydraulic radius and circularity of soil macropores

As mentioned above, the hydraulic radius is a good indication of the necks or throat of macropores. It is an important geometrical parameter since macropore throats directly control percolation rates in the macropore domain. The greater the hydraulic radius, the greater the capacity of an open macropore to convey water and associated chemicals. Similarly to the approach followed to investigate macropore-size distribution,

the hydraulic radius were evaluated in six different sections of 120 mm each. Hydraulic radius distributions obtained for each section and for the four soil columns are shown in Figure 4.11.

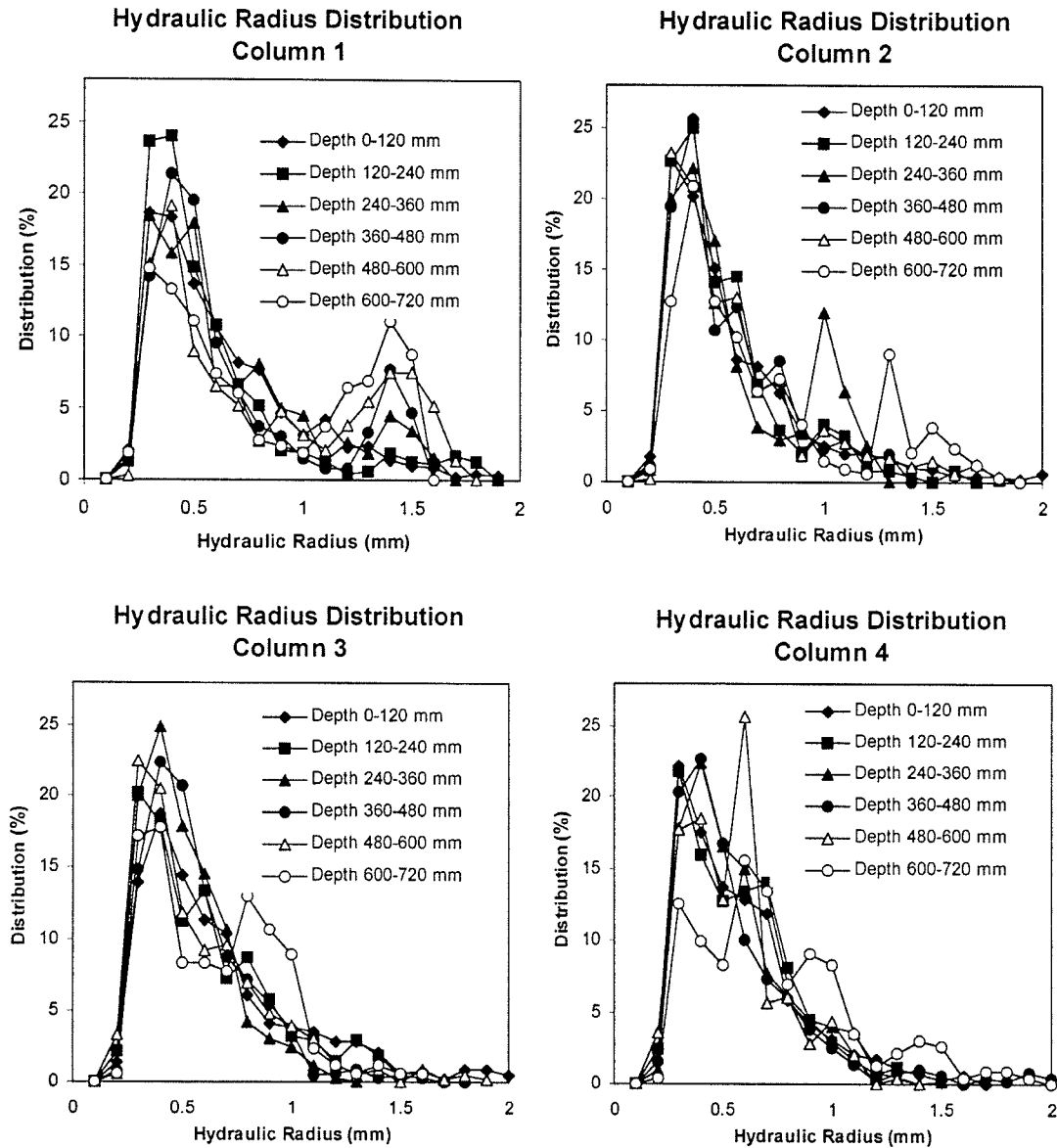


Figure 4.11: Hydraulic radius distributions obtained for different sections of the soil profile.

In all soil columns and for all sections, it can be observed that the distribution curves exhibit a peak for hydraulic radius of the order of 0.4 mm and that they are not

depth-dependent. For circular macropores, the diameter can be calculated as the hydraulic radius multiplied by four. Assuming that most macropores are circular in shape, this implies that about 20 % of macropore throats have a diameter of approximately 1.6 mm. From the hydraulic radius distributions of Column 1, we can observe the presence of peaks for hydraulic radius of about 1.4 mm. As pointed out earlier, a large hydraulic radius gives an indication of the macropore ability to convey water. This was verified for Column 1 with a series of saturated hydraulic conductivity measurements performed at various water heads. It was mentioned earlier that one of the soil columns was drilled from top to bottom in order to insert a polyethylene tube of 2.4 mm in outer diameter. Since this “artificial macropore” is circular and has a constant diameter, its presence should be reflected in the hydraulic radius distributions at a hydraulic radius of 0.6 mm. This artificial macropore was installed in Column 4. By comparing hydraulic radius distributions, we can observe a secondary peak at hydraulic radius of 0.6 mm in the results obtained for Column 4. This secondary peak depicts the artificial macropore.

Circularity distributions were evaluated in six different sections of 120 mm each in order to examine the changes in soil macropore geometry with respect to depth. Results are presented in Figure 4.12. In all columns, the distributions peak at circularity values of approximately 0.8. This implies that in the soil selected for this study, the macropores are quite circular in shape. Moreover, we can observe that the peaks increase with depth. In other words, the relative percentage of circular macropores increases with depth, or inversely, the percentage of elongated macropores decreases with depth. Elongated macropores are generally the result of physical forces acting on the soil. They



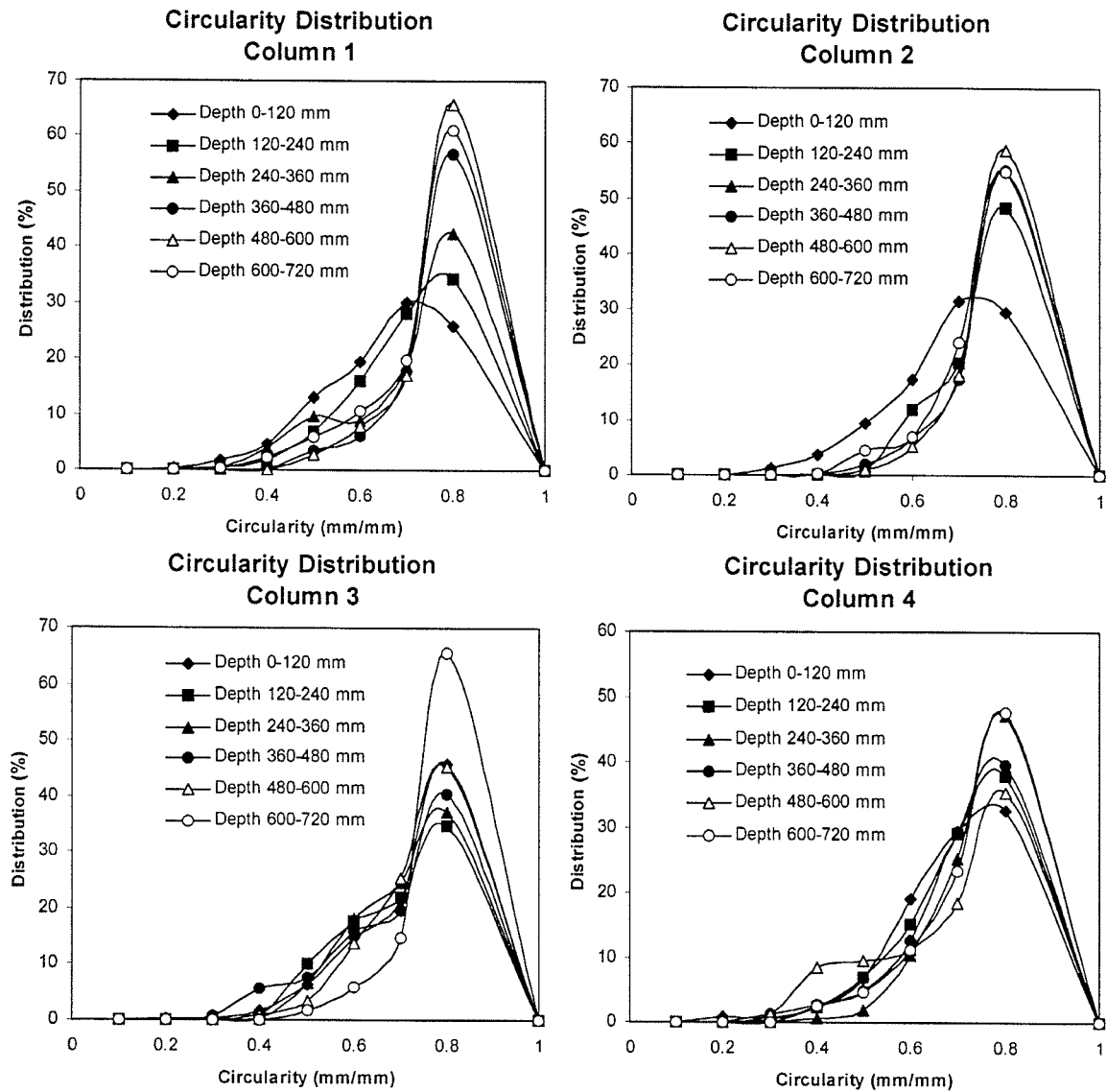


Figure 4.12: Circularity distribution of four soil columns obtained for different sections of the soil profile.

are generally formed by the shrinkage and swelling of soil, caused by drying/wetting and/or freezing/thawing cycles. These physical forces result in the formation of cracks and fissures. Since this type of macropores is formed close to the soil surface, it appears normal that deeper in the soil profile, the percentage of elongated macropores decreases.

Another indication of the presence of elongated or less circular macropores close to the soil surface is revealed by the degree of peakedness of the circularity distributions.

For instance, in Column 1, circularity distributions in regions close to soil surface are flatter than deeper in the soil profile. To evaluate the relative peakedness or flatness of the circularity distributions, the kurtosis was calculated. The kurtosis was found to increase for deeper sections of the soil profile. Therefore, the shape of macropore is less diversified deeper into the soil profile.

#### 4.5.4 Results of the geostatistical analysis

Results of the geostatistical analysis of density are presented in Table 4.2. In most cases, semi-variogram shapes resembled the spherical model. As mentioned earlier, the semi-variogram's shape is indicative of the variable's spatial behavior. This type of model is known to show good continuity of the variable (Grevers and de Jong, 1994).

**Table 4.2:** Summary of the geostatistical analysis for Column 1 based on bulk density matrices generated by X-ray CAT scanning.

Depth	Nugget effect	Sill	Range ( <i>pixels</i> )	Model
3	0.000	0.180	22.5	Spherical
33	0.000	0.150	17.1	Spherical
63	0.000	0.115	27	Exponential
93	0.000	0.065	15	Exponential
123	0.000	0.055	22.5	Spherical
153	0.000	0.068	36	Spherical
183	0.000	0.047	39	Spherical
213	0.000	0.045	10.5	Spherical
243	0.005	0.034	36	Spherical
273	0.005	0.018	24	Spherical
303	0.012	0.044	24	Spherical
333	0.013	0.043	15	Spherical
363	0.005	0.031	24	Spherical
393	0.002	0.013	39	Spherical
423	0.004	0.011	30	Spherical
453	0.000	0.010	21	Spherical
483	0.001	0.008	12	Spherical
513	0.003	0.023	21	Spherical

573	0.000	0.040	12	Spherical
603	0.000	0.070	18	Spherical
633	0.000	0.098	15	Spherical
663	0.075	0.120	18	Spherical

It should be noted that the nugget effect is almost negligible. This indicates that there is no significant variability over distances less than the resolution of the bulk density matrices. Although the resolution of the bulk density matrices was reduced to matrices containing 1000 elements, it does not appear to be a limiting factor in evaluating the spatial correlation of bulk density since the nugget effect is almost negligible. The sill is decreasing with depth. Since the sill approximates sample variance, this indicates that the spatial variability of CAT scan data decreases with depth. This is presumably attributable to higher biological activity close to the soil surface. The semi-variogram's range denotes the degree of spatial continuity. Since range oscillates around 22 pixels, two elements in the bulk density matrices are spatially correlated up to a distance of about 17 mm.

## 4.6 Summary and Conclusions

This study was undertaken to develop an innovative protocol for the characterization and visualization of soil macropores. X-ray computed tomography has been a useful technique in estimating soil macroporosity of undisturbed soil columns. The ability of CAT scanning to visualize soil pore structure offers considerable potential for reliable characterization of soil macropores. Pores larger or equal to 1.0 mm in equivalent diameter were readily detected. This approach was utilized for each section of the soil column in order to evaluate: number of macropores, surface area, equivalent diameter, and circularity and rectangularity of each individual macropore. From these

preliminary results, some interesting observations may be made. It was found that the average macroporosity of the four soil columns was fluctuating between 2.1 and 3.8 %. Moreover, macroporosity was found to decrease significantly with depth. Similarly, the number of macropores was decreasing by 0.7 % to 2.5 % over the entire depth of the soil columns. It was also observed that the soil profile exhibited two distinct regions. The first region (0 to 200 mm) showed a rapid decrease in number of macropores (i.e., from 3.8 to 12.9 %) whereas in the second region, 200 to 720 mm, the number of macropores was not changing significantly with depth with a average macropore count of 1400 per square meter. Moreover, it was found that the macropore-size distributions exhibited a peak for all soil columns and at all depth for macropores having an equivalent cylindrical diameter ranging from 2 mm to 4 mm. The number of macropores falling in this category was decreasing with depth. From the hydraulic radius distribution, it was inferred that about 20 % of macropore throats have a diameter of 1.6 mm. Moreover, it was noted that the relative percentage of circular macropores was increasing with depth. The spatial continuity of pixels in serial sections of one soil column was studied using geostatistical analysis. Semi-variograms showed spatial dependency for most soil sections up to 22 pixels (i.e., 17 mm). This limit on spatial dependence indicates the degree of spatial continuity. Moreover, geostatistical analysis indicates greater spatial variability of serial sections in the top soil.

The three-dimensional arrangement of network of soil macropores partly controls the rate of water and solute movement through soil. In the near future, macropore continuity, inclination, three-dimensional hydraulic radius, macropore expansion/contraction, and tortuosity of macropore networks will be analysed using

three-dimensional reconstruction techniques. These results, combined to the results presented in this paper, will be used to determine and quantify the effect of macroporosity on saturated hydraulic conductivity.

## PREFACE TO CHAPTER 5

Transport phenomena in a porous medium are strongly dependent on its three-dimensional pore structure. However, very little work has been done to characterize the macroporosity of intact soil cores in terms of its three-dimensional parameters.

3-D visualization and quantification is a powerful approach for understanding how macropore networks affect movement of water and associated chemicals, especially for preferential flow studies where these relationships have not yet been fully established. Once the 3-D geometry of soil preferential flow paths is known, it can serve as a starting point for computer simulations of water movement in a natural soil profile.

Chapter 5 focuses primarily on the characterization of 3-D properties of soil macropores. More precisely, the objective of the study presented herein was to determine quantitatively the 3-D soil macropore parameters (i.e., size, length, volume, hydraulic radius, tortuosity, inclination, interconnectivity) of several undisturbed soil columns through a three-dimensional reconstruction. The results of this work show promise for future studies in the area of soil macropore quantification. The computer programs developed for this study are included in the attached CD-ROM. This Chapter has been submitted for publication. For the sake of completeness, some material in this chapter is repeated from previous chapters so that this paper can stand on its own. (Perret J.S., S.O. Prasher, A. Kantzas and C. Langford. 1998. Three-dimensional quantification of macropore networks in undisturbed soil cores. Submitted to the Journal of Agricultural Engineering Research). The candidate was responsible for designing and conducting the

research experiments, developing computer codes for the visualization and analysis of data and preparation of this paper. Dr. Shiv O. Prasher, professor at the Agricultural and Biosystems Engineering Department of McGill University, contributed in all aspects of this research project. He provided the necessary funds and assistance for this research, including supervisory guidance and revision of this manuscript before submission for publication. Dr. A. Kantzas, Director of the Tomographic Imaging and Porous Media (TIPM) Laboratory in Calgary, Alberta, and associate professor at the University of Calgary's Department of Chemical and Petroleum Engineering, provided access to CAT scanning facilities of the TIPM laboratory. Dr. Kantzas also made invaluable suggestions during CAT scanning. Dr. C. Langford, University of Calgary's vice-president research and professor at the Department of Chemistry, was the principal investigator for the NSERC Collaborative Project Grant.

## CHAPTER 5

# THREE-DIMENSIONAL QUANTIFICATION OF MACROPORE NETWORKS IN UNDISTURBED SOIL CORES

---

### 5.1 Abstract

The role of macropores in soil and water processes has motivated many researchers to describe their sizes and shapes. Several approaches have been developed to characterize macroporosity, such as the use of tension infiltrometers, breakthrough curve techniques, image-analysis of sections of soils and even X-ray CAT scanning. Until now, efforts to describe macropores in quantitative terms have been concentrated on their 2-D geometry. The objective of this study is to quantify, in a non-destructive manner, 3-D properties of soil macropores in four large (800 mm x 77 mm diameter) undisturbed soil columns taken from a field site at the Macdonald Campus of McGill University in Ste-Anne-de-Bellevue, Quebec. The main characteristics of the geometry and topology of macropore networks were determined using X-ray CAT scanning and three-dimensional reconstruction techniques. Our results suggest that the numerical density of macropores varies between 13,421 to 23,562 networks per cubic meter of the sandy loam soil. It was found that the majority of the macropore networks had a length of 40 mm, a volume of  $60 \text{ mm}^3$  and a wall area of  $175 \text{ mm}^2$ . It was found that the greater the length



of networks, the greater the hydraulic radius. The inclination of the networks ranged from vertical to an angle of about 55 degrees from vertical. The overall tendency of the distributions of the inclination of networks suggested that the smaller the inclination, the greater the number of macropores. Results for tortuosity indicated that most macropore networks had a three-dimensional tortuous length 15% greater than the distance between its extremities. More than 60% of the networks were made up of 4 branches. For Column 1, it was found that 82% of the networks had zero connectivity.

## **5.2 Introduction**

Soil structure consists of a three-dimensional network of pores. Large pores play an important role in allowing roots, gas and water to penetrate into the soil. The higher the macropores density, the more the soil is exploitable by plant roots (Scott et al., 1988a). Similarly, the more continuous the macropores, the more freely gases interchange with the atmosphere. Continuous macropores also have a direct effect on water infiltration and solute transport in soil.

According to Sutton (1991), the size of pore openings is more important for plant growth than is the overall soil porosity. Although existing pores constrain penetration of roots, they provide favorable conditions for root growth. Several studies have shown that the presence of continuous macropores in soil significantly benefits root growth (Bennie, 1991). One of the most important factors influencing soil fertility, besides water and nutrient content, is soil aeration (Hillel, 1980; Glinski and Stepniewski, 1985). Large soil pores are the paths available for gas exchange between soil and atmosphere (Sutton, 1991). In natural soils, water movement follows paths of least resistance (i.e., preferential flow paths). Intuitively, large and continuous pores facilitate water transport.

It is now well known that the size and connectiveness of soil pores play a determining role in flow characteristics of water and transport of solutes through soil (Ma and Selim, 1997). Jury and Flühler (1992) stated that: “ *fluid transport through well defined structural voids is not predictable unless the distributions of the voids, aperture sizes and shapes, depths of penetration, and interconnectivity are known*”.

The importance of macropores in many soil-plants-roots processes has motivated many researchers to describe their sizes and shapes. Several approaches have been developed to characterize macroporosity. Among them are tension infiltrometers (Everts and Kanwar, 1993; Timlin et al., 1994; Logsdon et al., 1993), breakthrough curve techniques (Ahuja et al., 1995; Jabro et al., 1994; Li and Ghodrati, 1994; Ma and Selim, 1994) and image-analysis of sections of soils (Koppi and McBratney, 1991; Moran and McBratney, 1992; Singh et al., 1991; Vermeul et al., 1993). Warner et al. (1989), Grevers et al. (1989), Anderson et al. (1990), Hanson et al. (1991), Tollner et al. (1995), Asare et al. (1995) and Heijs et al. (1996) have also recognized the great potential offered by CAT scanning for characterizing soil macroporosity.

However, efforts to describe macropores in quantitative terms have not yet resulted in a comprehensive theoretical framework that allows a complete representation of their geometry. This is partly due to the fact that macropores are very difficult to observe and characterize bearing in mind that the macropore networks are complex three-dimensional structures and that soil is opaque. Up to now, most of the work done on the quantification of soil macropores was concentrating on their two-dimensional geometry. A few researchers such as Hanson et al. (1991), Heijs et al. (1996) and Perret et al. (1997) have used reconstructive imagery, allowing 3-D visualization of the macropore space, but

have not quantified soil macroporosity in three-dimensions.

### **5.3 Need for 3-D Analysis**

Transport phenomena in a porous medium are strongly dependent on its three-dimensional pore structure (Chatzis and Dullien, 1977). Kwiecien (1987) stressed that models for the prediction of dynamic properties of real porous media must be based on the three-dimensional pore geometry. 3-D visualization and quantification is a powerful approach for understanding how macropore networks affect movement of water and associated chemicals, especially for preferential flow studies where these relationships have not yet been fully established. Once the 3-D geometry of soil preferential flow paths is known, it can serve as a starting point for computer simulations of water movement in a natural soil profile. Therefore, one of the first tasks to undertake in order to understand the relationship between geometry of the pore space and flow field is to determine the 3-D pore space.

Very little work has been done to characterize the macroporosity of intact soil cores in terms of its three-dimensional parameters. Tollner et al. (1995) pointed out the need for additional research to investigate reliable approaches for computing tortuosity and connectivity of soil macropores. Imaging in three-dimensions and quantification of three-dimensional parameters of soil macroporosity are critical in order to accurately correlate soil pore structure with preferential flow phenomena, and much additional work is needed in this area (Hanson et al., 1991).

The present investigation is a study of the 3-D properties of soil macropores. The main characteristics of a porous media that affect fluid flow are: porosity, numerical density, pore shape (size, length, volume, hydraulic radius, tortuosity) and pore

interconnectivity or genus per unit volume (Constantinides and Payatakes, 1989). Therefore, the objective of this study is to determine quantitatively the above parameters of soil macropores in four undisturbed soil columns through a three-dimensional reconstruction from two-dimensional matrices generated by a X-ray CAT scanner. The results of this work show promise for future studies in the area of soil macropore quantification.

## **5.4 Terminology**

As mentioned above, the objective of this work is to determine the properties of 3-D macropore networks through reconstruction of CAT scan matrices by computer. Various standard geometrical parameters are meaningful to quantify the structure of 3-D macropore networks, such as their relative position, length, volume, specific wall area and orientation. Such parameters are explicit and do not need to be defined. However, several terms that are used to describe soil structure and their 3-D attributes are fuzzier and need to be clarified. Some of these terms are defined below:

### **5.4.1 Macropore**

At first, the definition of macropore may seem simple. However, as we come to consider the complexity of a macropore, its definition may become hazy and ambiguous. By strict definition, macropore implies a large pore. However, large is a relative term and this lack of clarity has led to several conflicting definitions.

It would be useful to have a general agreement on pore terminology. However, up to now, there is little or no consensus for the definition and terminology used for classification of pores in general. There has been a large number of classification

schemes based on the equivalent cylindrical diameter (ECD) and several contradicting definitions can be found in soil literature (Table 5.1).

**Table 5.1:** Different classifications of pores based on their Equivalent Cylindrical Diameter.

Terminology	ECD	Reference
Micropore	Less than 30 $\mu\text{m}$	Jongerius (1957)
Mesopore	30 $\mu\text{m}$ to 100 $\mu\text{m}$	
Macropore	greater than 100 $\mu\text{m}$	
Micropore	Less than 30 $\mu\text{m}$	Marshall (1959)
Macropore	Greater than 30 $\mu\text{m}$	
Micropore	Less than 75 $\mu\text{m}$	Johnson et al. (1960)
Very Fine pore	75 $\mu\text{m}$ to 1000 $\mu\text{m}$	
Fine pore	1000 $\mu\text{m}$ to 2000 $\mu\text{m}$	
Medium pore	2000 $\mu\text{m}$ to 5000 $\mu\text{m}$	
Coarse pore	greater than 5000 $\mu\text{m}$	
Cryptovoid	Less than 0.1 $\mu\text{m}$	Brewer (1964)
Ultramicrovoid	Less than 5 $\mu\text{m}$	
Microvoid	5 $\mu\text{m}$ to 30 $\mu\text{m}$	
Mesovoid	30 $\mu\text{m}$ to 75 $\mu\text{m}$	
Macovoid	greater than 75 $\mu\text{m}$	
Very fine pore	Less than 2 $\mu\text{m}$	Russel (1973)
Fine pore	2 $\mu\text{m}$ to 20 $\mu\text{m}$	
Medium pore	20 $\mu\text{m}$ to 200 $\mu\text{m}$	
Coarse pore	greater than 200 $\mu\text{m}$	
Micropore	Less than 0.3 $\mu\text{m}$	McIntyre (1974)
Minipore	0.3 $\mu\text{m}$ to 30 $\mu\text{m}$	
Macropore	30 $\mu\text{m}$ to 300 $\mu\text{m}$	
Super pore	greater than 300 $\mu\text{m}$	
Bonding pore	Less than 0.005 $\mu\text{m}$	Greenland (1977)
Residual pore	Less than 0.5 $\mu\text{m}$	
Storage pore	0.5 $\mu\text{m}$ to 50 $\mu\text{m}$	
Transmission pore	50 $\mu\text{m}$ to 500 $\mu\text{m}$	
Fissure	greater than 500 $\mu\text{m}$	

Macropore	Greater than 1000 $\mu\text{m}$	Bouma et al. (1977)
Macropore	Greater than 60 $\mu\text{m}$	Bullock and Thomansson. (1979)
Macrofissure	200 $\mu\text{m}$ to 2000 $\mu\text{m}$	Reeves et al. (1980)
Enlarged Macrofissure	2000 $\mu\text{m}$ to 10000 $\mu\text{m}$	
Macropore	Greater than 3000 $\mu\text{m}$	Beven (1981)
Micropore	Less than 10 $\mu\text{m}$	Luxmoore (1981)
Mesopore	10 $\mu\text{m}$ to 1000 $\mu\text{m}$	
Macropore	greater than 1000 $\mu\text{m}$	
Macropore	Greater than 1000 $\mu\text{m}$	Luxmoore et al. (1990)

---

These definitions fail to remove ambiguity from the delimitation between macropores and micropores. However, in this research study, the definition proposed by Luxmoore et al. (1990) was followed. They stated: “ *the term macropore includes all pores in a profile that are (generally) drained at field capacity, with the latter being 1 mm or more in equivalent diameter*”.

Up to now, definitions of macropore make no specific reference to its size nor to its shape in a three-dimensional context. The lack of information describing their shapes has led to the generality used in defining macropores (Kwiecien, 1987). Part of the goal of this study is to characterize the shapes and other three-dimensional parameters of macropore networks with the aid of computer programs in order to describe their geometry and eventually, to help clarify the definition of a soil macropore.

### 5.4.2 Macropore network

In a porous medium, a network is a set of macropores that are interconnected such that there is a passage from any part of the set to every other part (Scott et al., 1988a). Thus, the concept of macropore network implies a three-dimensional structure.

### 5.4.3 Branch

As mentioned above, a macropore network is a set of macropores that are interconnected. A branch is a portion of the macropore network connecting to the rest of the network.

### 5.4.4 Tortuosity

Tortuosity ( $\tau$ ) is one of the most meaningful three-dimensional parameters of pore structure. Carman introduced the concept of tortuosity in 1937 as the square of the ratio of the “effective average path” in the porous medium ( $L_e$ ) to the shortest distance measured along the direction of the pore ( $L$ ). Several researchers have reviewed this definition (Hillel, 1982; Marshall and Holmes, 1988; Jury et al., 1991; Sahimi, 1995) and have redefined tortuosity as:

$$\tau = \frac{L}{L_e} \quad (5.1)$$

Tortuosity is a dimensionless factor always greater than one, which expresses the degree of

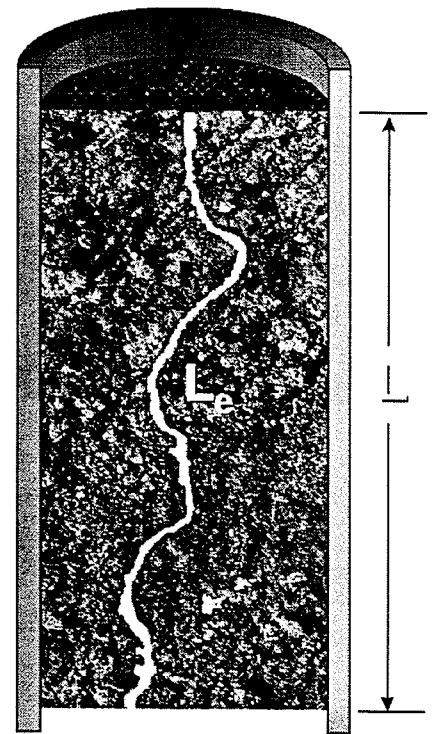


Figure 5.1: Tortuosity of a soil macropore.

complexity of the sinuous pore path (Figure 5.1). Tortuosity can easily be related to the conductivity of a porous medium since it provides an indication of increased resistance to flow due to the pore system's greater path length (Dullien, 1979). The term continuity is sometimes used to describe pore tortuosity. Richter (1987) has defined pore continuity as the reciprocal of tortuosity.

#### 5.4.5 Hydraulic radius in three-dimensions

Another relevant parameter is the hydraulic radius of the macropore network. Macropores are not regularly shaped. The neck (also known as pore throat) of a pore is an important feature of pore geometry which directly controls percolation rates. A neck is defined as the local minimum in pore space size (Kwiecien et al., 1990). The pore throat is located where the minimum mean radius of curvature of a gas/liquid interface is observed. This corresponds to the location of maximum capillary pressure. Maximum capillary pressure within a macropore is very difficult to measure. However, the hydraulic radius is a good approximation of the mean radius of curvature (Kwiecien, 1987; Dullien, 1992). The hydraulic radius ( $R_h$ ) of a pore can be simply computed as:

$$R_h = \frac{\text{Volume of Pore}}{\text{Wall Area of Pore}} \quad (5.2)$$

Necks can therefore easily be located by identifying local minima in the hydraulic radii of macropores. The reason for using the hydraulic radius as a measure of pore throat is that it is a useful measure of size in the case of irregularly shaped pores (Dullien, 1992). The hydraulic radius can provide a good indication of the pore neck position and of the pore expansion/contraction.



#### 5.4.6 Topology of macropore networks

A complete description of pore structures requires geometrical as well as topological information (Macdonald et al., 1986). Topology deals with properties of an object in a space that remain unaltered when that space is deformed. The topology of macropore networks concerns essentially the number per unit volume and the degree of connectivity of macropore networks regardless of their shape. The number of networks, defined later as numerical density, is a measure of the complexity of pore structure (Scott et al., 1988a). Topological parameters characterizing the morphology of a porous medium are the numerical density, coordination number, connectivity and genus (Dullien, 1992). Each of these terms is defined below.

##### 5.4.6.1 Numerical density of networks

The number of networks per unit volume regardless of their size or shape is the numerical density. Scott et al. (1988a) pointed out that it is very difficult to determine this quantity. Up to now, this information was roughly estimated by cutting parallel plane sections through soil. Essentially, numerical density was only accessible in two-dimensions. One of the major drawbacks of this approach is that there is not a one-to-one correspondence between the number of networks estimated in the 2-D sections and those in three-dimension (Scott et al., 1988a).

##### 5.4.6.2 Coordination number

One of the simplest concepts for characterizing pore topology is the coordination number ( $Z$ ). It is defined as the number of pore throats that meet at a given point along a pore (Sahimi, 1995). In other terms, the coordination number determines the number of

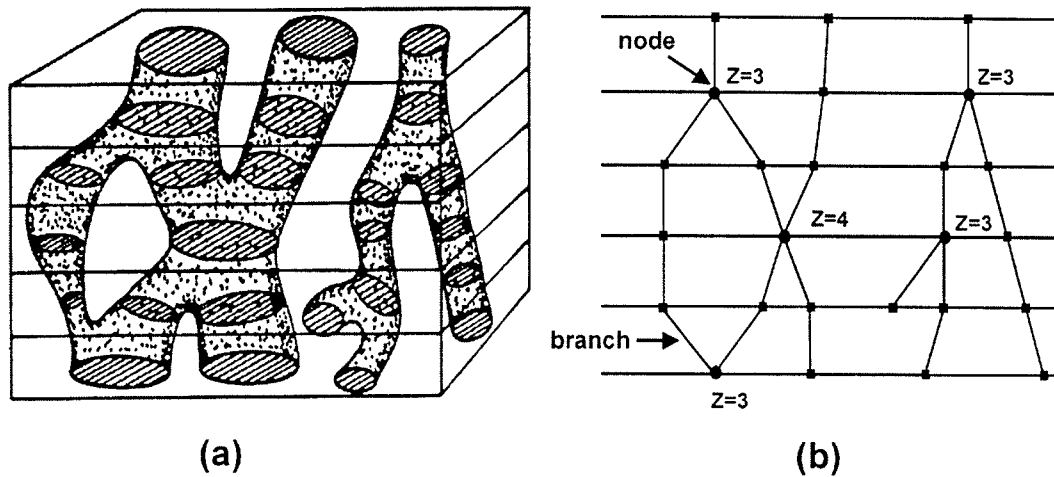


Figure 5.2: Schematic representation of (a) pore space, (b) coordination number on a branch-node-chart (After Dullien, 1992).

branches meeting at one node. Until now, the only approach to determining the coordination number has been to reconstruct a “branch-node chart” of the pore structure (Figure 5.2) from a series of parallel sections of the porous medium (Dullien, 1992).

#### 5.4.6.3 Connectivity and genus of macropore networks

The concept of connectivity ( $C_{\text{con}}$ ) can also be used to characterize the topology of a complex system such as soil macroporosity. Connectivity is a measure of the number of independent paths between two points within pore space (Macdonald et al., 1986). In other words, connectivity is the number of non-redundant loops enclosed in a specific geometrical shape. Each macropore network has a connectivity, which is a positive integer equal to the number of different closed circuits between two points in the network. If there is only one circuit then the connectivity is equal to zero. The term connectivity density is sometime used to define the connectivity per unit volume (Scott et al., 1988b). Figure 5.3 shows four different shapes to illustrate the notion of connectivity (Figure 5.3 a, b, c and d display a connectivity of 1, 1, 2 and 3, respectively).

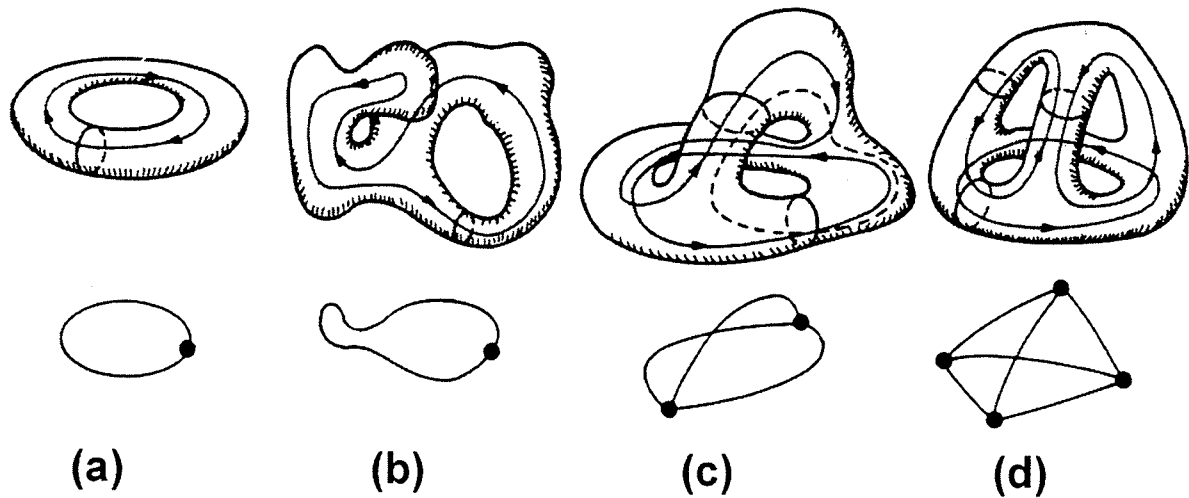


Figure 5.3: Illustration of the concept of connectivity and genus (From Macdonald et al., 1986).

The genus ( $G$ ) of a pore system is defined as the largest number of non-intersecting cuts that can be made through a shape without disconnecting any part from the rest (Dullien, 1992). A general theorem of topology states that the genus is numerically equivalent to connectivity. Macdonald et al. (1986) strongly suggested that an accurate determination of the genus would help to elaborate new and better flow models.

Although these topological concepts have been given increased attention in recent years in the field of petroleum recovery, they have not yet been used to describe the spatial characteristics of a soil macropore network. We propose to evaluate the coordination number and the connectivity/genus of soil macropores in order to describe their complex geometry.

## 5.5 Materials and Methods

### 5.5.1 Soil cores

In July 1995, four undisturbed soil columns, 800 mm in length and 77 mm in diameter, were taken from a field site at the Macdonald Campus of McGill University in Ste-Anne-de-Bellevue, Quebec. Column size was selected based on the need for a large enough sample to represent macropore distribution, yet small enough to be handled easily when full of soil. The hydraulic bucket of a backhoe was used to drive polyvinyl chloride (PVC) pipes in small increments of about 80 mm. The objective was to obtain soil cores that were disturbed as little as possible in order to obtain samples representative of natural conditions. The site had been covered for many years with a combination of quack grass (*Elytrigia repens* (L.) Nevski.), white clover (*Trifolium repens* L.) and wild oat (*Avena fatua* L.). The soil belonged to the Chicot series and was predominantly a sandy loam with an A horizon thickness of around 0.4 m. The land slope was less than one percent.

The soil columns were scanned under dry as well as saturated conditions. To reach dry conditions, the soil columns were placed under a set of ten light bulbs of 300 watts each for a period of six weeks. The cores were rotated periodically to accelerate evaporation.

A polyethylene tube of 1 mm in inner diameter was inserted in one of the soil columns to verify the ability of the CAT scanner to portray the size and the location of a known macropore.

### 5.5.2 X-ray CAT scanning

A modified medical ADVENT HD200 whole body CAT scanner was used for this study at the TIPM laboratory in Calgary, Alberta. Computed Tomography (CT) or Computer Assisted Tomography (CAT) is a method of diagnostic imaging used for non-destructive imaging of cross-sectional “slices” of the human body or an object. This scanner incorporates a fourth generation scan geometry with scan times as short as 2 s/scan and a high pixel resolution (up to 195  $\mu\text{m}$  by 195  $\mu\text{m}$ ). In most CAT scanners, the actual collection of patient data occurs in the gantry where the patient lays horizontally. However, the ADVENT HD200 was modified to allow vertical scanning. For that purpose, the CAT scanner gantry was rotated by an angle of 90° and positioned on a metal frame designed to hold the whole gantry horizontally.

During CAT scanning, each column was placed vertically in the scanner unit so that the X-ray beam intersected the soil column perpendicularly to its longitudinal axis. A bubble level indicator was used to ensure that the soil column was vertical. The longitudinal axis of the core was positioned at the center of the gantry of the scanner. During the computer tomographic process, the X-ray tube rotated around the soil column. A pre-collimator modulated the thickness of the X-ray beam. For this study, the collimator was set to a thickness of 2 mm. The transmission and detection of this thin and rotating X-ray beam through the soil column resulted in the collection of a large number of attenuation measurements taken at discrete angles. For this purpose, an array of 720 detectors was located within the gantry. Once collected, the data were mathematically reconstructed to generate a 512 x 512 matrix. To produce a mean X-ray energy beam in the Compton energy range, the CAT scan system parameters were

adjusted to 120 peak kV and 50 mA. Figure 5.4 shows a view of the rotated gantry of the CAT scanner.

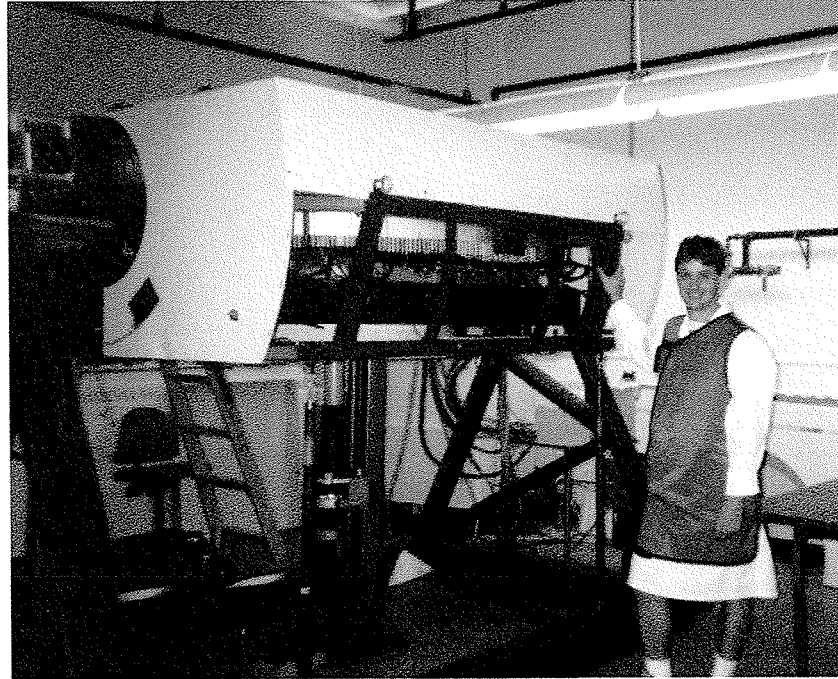


Figure 5.4: View of the rotated gantry of the Advent HD200

The position of the core was set mechanically for each scan with a digital indexing ruler having a precision of  $\pm 0.001$  mm. A total of 360 sections or scans was obtained for each column, leaving no space between two consecutive scans.

Data from each scan were recorded on a magnetic tape, transferred to a SUN4 workstation, running under the UNIX operating system, and converted to a bulk density value. A FORTRAN 77 program was developed to compute the calibration line of each scan. Once the linear calibration equations were established, a computer algorithm transformed CAT scan arrays into matrices of bulk density. Part of the algorithm also allowed for computation of the soil section's porosity distribution on a voxel (i.e., volume

element) basis. The remaining analysis was done using the PV-WAVE language on a 300 MHz Pentium II PC equipped with 128 Mb of RAM.

### **5.5.3 3-D reconstruction of macropores**

The PV-WAVE language was chosen for computer programming in this study. The PV-WAVE language is a comprehensive programming environment that integrates state-of-the-art numerical and graphical analyses. This programming language is widely used for analyzing and visualizing technical data in many fields, such as medical imaging, remote sensing and engineering. PV-WAVE is an ideal tool for working with large arrays such as our CAT scan data, because of its array-oriented operators and ability to display and process data in the ASCII and Binary I/O formats. Another reason that motivated this choice was PV-WAVE's ability to be used under both UNIX and PC environments.

Four computer programs were developed to reconstruct, visualize and quantify 3-D macropore structures in soil columns. The first program called "Filterjo.pro", thresholds the macropores in the 360 two-dimensional bulk density matrices before isolating macropore networks in three-dimensions. Each pixel can represent only two states of the dry soil columns, pore space or soil matrix. The first task accomplished by "Filterjo.pro" is to partition two-dimensional matrices into regions of 1 for pores and 0 for soil matrix. This transformation is called segmentation. The program then regroups pixels belonging to the same pore (clustering) following a set of rules described by Perret et al. (1997). A filtering subroutine is then executed. For that purpose, a criterion is used to determine if the pore belongs to the macropore domain. The criterion is based on the size of the pore. If the pore has an equivalent cylindrical diameter less than 1 mm, it is

removed from the matrix. After filtering, a median smoothing is applied on each matrix with a neighborhood of two pixels. This process is similar to smoothing with an average filter, but it does not blur edges larger than the neighborhood. Median smoothing was used since it has been found to be effective in removing noise (Visual Numerics, 1994). Each pixel in the resulting matrix is then multiplied by  $-1$ . Therefore, matrix elements have a value of 0 (i.e., soil) or  $-1$  (i.e., macropores). The resulting two-dimensional matrices are then stored in a file ready for the three-dimensional analysis.

A second computer program, called “Netjo.pro”, was developed to recognize and isolate three-dimensional macropore networks. The first step in developing this program was to establish a set of rules, which were used to determine how the macropore space in each 2-D matrix was connecting to each other in 3-D. Several different clustering criteria were used. The first algorithm was based on a “six nearest neighbour” rule in three-dimension (Figure 5.5a). With this algorithm, similar voxels (with a value of  $-1$ ) are clustered together if they are beside, above, or below one another. In other words, all clustered voxels are joined by at least one planar face. Although, this algorithm was fast, it did not cluster all voxels belonging to a network in a single pass when the 3-D structure of the network was very complex and showing a high degree of connectivity. Therefore, a second clustering algorithm was developed based on the “twenty six neighbouring” rule (Figure 5.5b). This algorithm clusters all voxels belonging to the macropore domain around the voxel of interest if they share a face, an edge or even a corner by visiting the top and bottom 2-D matrices. In other words, two voxels will be registered as part of the same group of pore volume if they have a value of  $-1$  and share a common corner. Thus, the clustering algorithm examines the twenty-six nearest neighboring voxels in



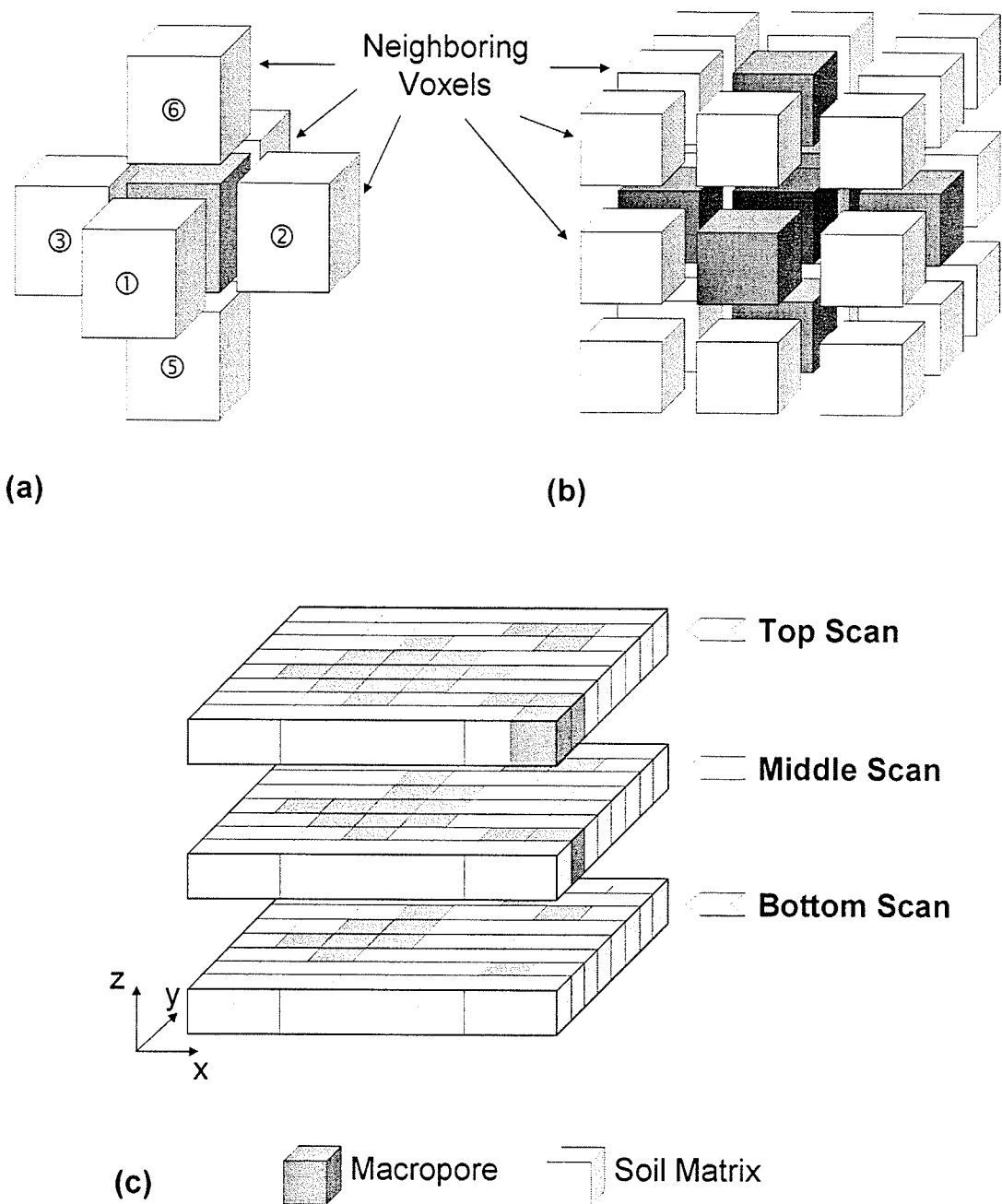


Figure 5.5: Illustration of (a) the six nearest neighboring voxels and (b) twenty six neighboring voxels; (c) Superposition of consecutive 2-D matrices for the 3-D algorithm.

three-dimensions. In order to do so, each cross-section of the soil column is analyzed by superimposing its adjacent sections (Figure 5.5c.). A 3-D filtering algorithm was incorporated in "Netjo.pro" to eliminate all networks having a length less or equal to 10 mm. These macropores were removed since it was assumed they are not contributing to preferential flow. The output of this program is a large three-dimensional matrix that contains matrix elements of 0 (i.e., soil matrix domain) and 1, 2, 3,..., n for the macropore domain where each integer represents a network. In other words, each voxel belonging to a network has an integer value. For instance, if a soil column has 45 independent macropore networks, all voxels of the last network will have a value of 45. This approach was successfully implemented in the recognition and reconstruction of macropore networks.

The third program (Rview.pro) produces a list of vertices and polygons that describes the three-dimensional surface of macropores. Each voxel is visited to find polygons formed by the macropores. The polygons are then combined and rendered to reconstruct an exact three-dimensional representation of the macropore networks. The reconstructed image allows the visualization of 3-D macropore networks (Figure 5.6).

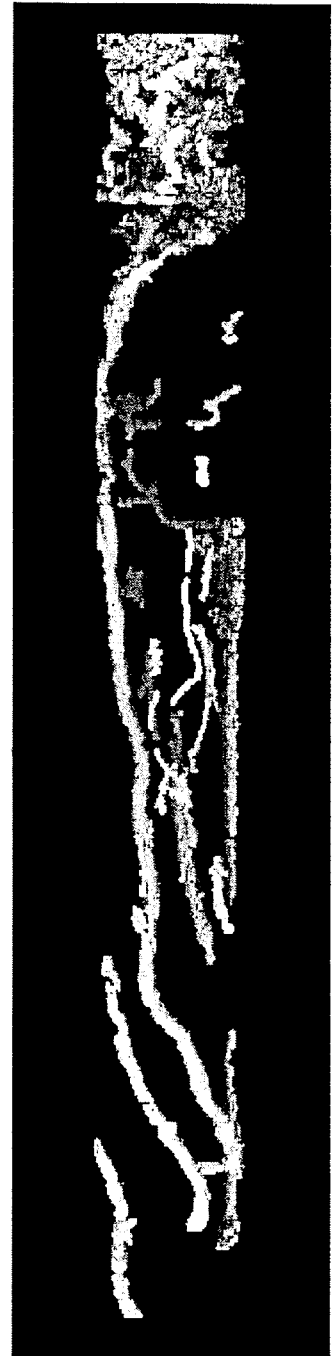


Figure 5.6: 3-D reconstruction of macropore networks in Column 1

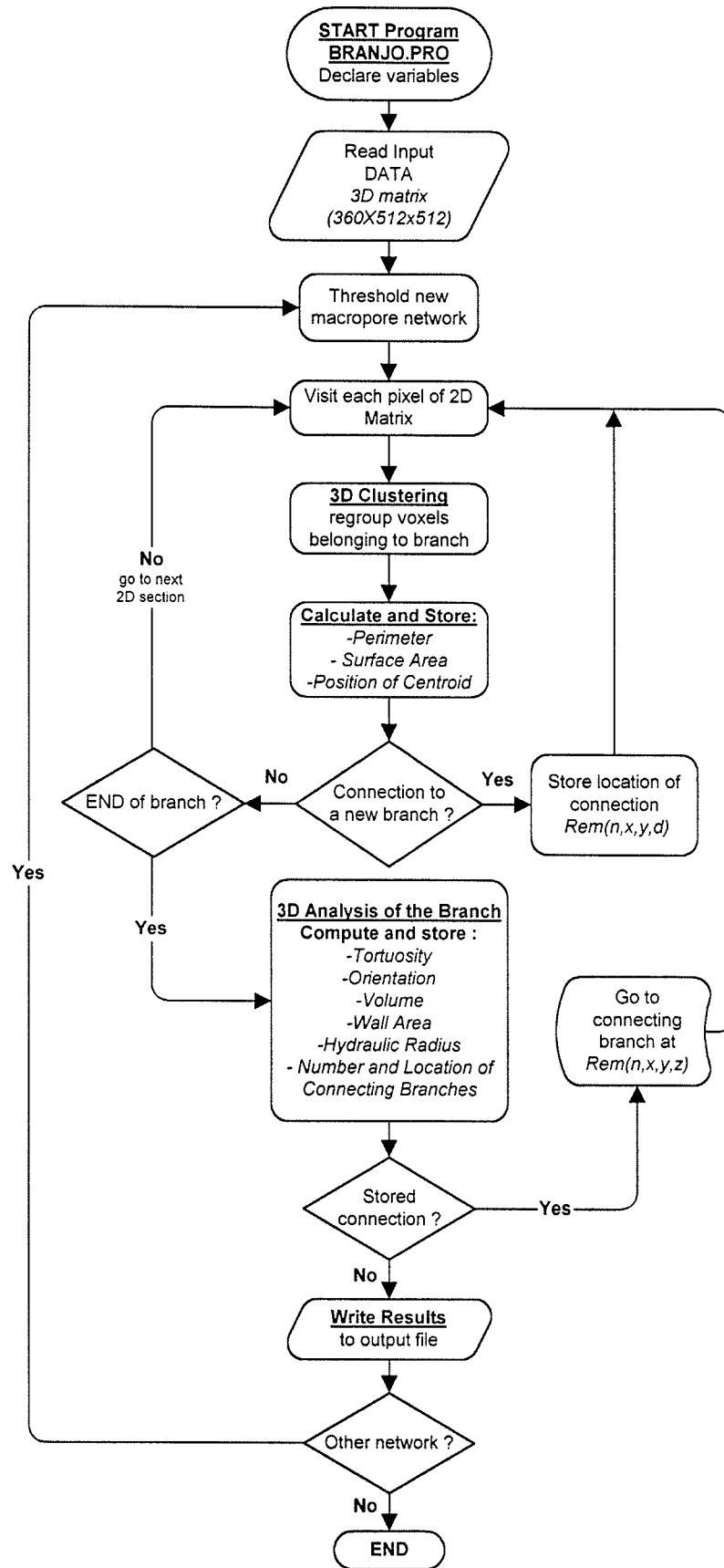


Figure 5.7: Flow diagram of the PV-WAVE program "Branjo.pro"

The last program, called “Branjo.pro”, was developed to isolate and characterize each connecting branch in a macropore network. The first task accomplished by the program is to read the three-dimensional matrix generated by “Netjo.pro”. Then, it thresholds all the voxels having a value of 1 (i.e., first macropore network). Starting at the top section of the soil column, the algorithm visits each voxel for every section until it finds a voxel belonging to Network 1. Then, using the six nearest neighbouring rule, “Branjo.pro” isolates and clusters each voxel of the first branch of the network. As the branch is being clustered, the program computes the perimeter, surface area and the centroid of the branch in each section. When the program finds a connection to a new branch, it stores the location of the connection in order to investigate properties of this new branch at a later time. Once the program has reached the end of the branch, it computes its tortuosity, orientation, length, volume, wall area, hydraulic radius and the number and location of other connecting branches. At that stage, the program moves on to the location of a stored connection (if present) and evaluates the properties of the new branch. Once all the branches of a particular network have been analyzed, results are written to an ASCII file for further analysis on a worksheet. Then, the program repeats the same process for the second macropore network and so on for Network 2 to n. A detailed flow diagram of “Branjo.pro” is given in Figure 5.7.

## 5.6 Results and Discussion

### 5.6.1 Numerical density, relative position and length of macropore networks

Figure 5.8 shows the number, vertical position and length of macropore networks found in soil columns. Each vertical bar represents a macropore network. An integer number has been assigned to each network (from left to right) in order to refer to them. For example, Network No 18 of Column 1 starts at approximately a depth of 250 mm and ends at a depth of 680 mm. The total number of networks per soil column is summarized in Table 5.2. Column 3 has the greatest number of networks (i.e., 79 networks). The numerical density was calculated from the number of networks per soil column (Table 5.2).

**Table 5.2:** Selected properties of macropore networks for each of the soil columns.

Property	Column1	Column2	Column 3	Column 4
Number of Networks	45	47	79	54
Numerical Density (networks/m <sup>3</sup> )	13,421	14,018	23,562	16,106
Macroporosity	3.8 %	2.18 %	2.59 %	2.79 %
Average Volume (mm <sup>3</sup> )	445.6	245.9	173.5	273.4
Average Tortuosity (mm/mm)	1.27 ± 0.25*	1.20 ± 0.18	1.31 ± 0.29	1.27 ± 0.25
Average Hydraulic Radius (mm)	0.14 ± 0.05	0.13 ± 0.07	0.12 ± 0.05	0.13 ± 0.04

\* Standard Deviation

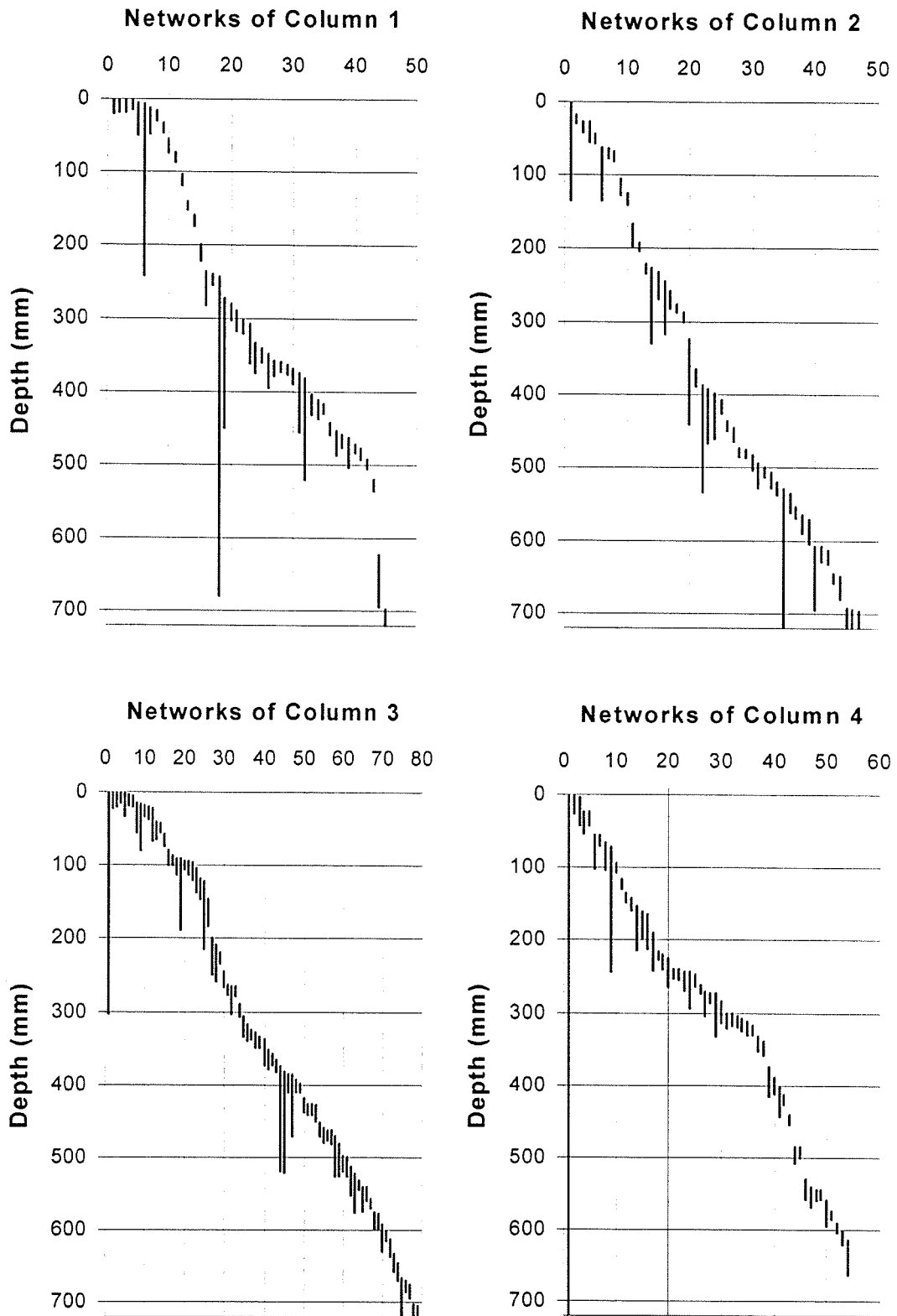


Figure 5.8: Number, relative position and vertical length of macropore networks in the four soil columns

It can be observed that the numerical density varies significantly from one soil column to the other, although they were taken from the same site with only a distance of approximately 0.5 m between them. The macroporosity was evaluated for each soil columns (Table 5.2) and is in accordance with the observations made by Edwards et al. (1990), who reported macroporosities ranging from 0.4 to 3.8 %.

One would expect that the number of macropore networks per unit volume would have a consequential effect on macroporosity. More precisely, it would make sense that soil columns with a large numerical density would have a large macroporosity and vice-versa. However, our results do not confirm this supposition nor indicate a direct relationship between numerical density and macroporosity. For instance, Column 1, which has the smallest numerical density (i.e., 13,421 macropore networks per cubic meter), has the greatest macroporosity. Column 3 with a numerical density of 23,562 networks/m<sup>3</sup> exhibits a much smaller macroporosity (i.e., 2.59%). These results can be explained by the difference in average network volume. The average network volume in Column 1 is more than 2.5 times that of Column 3. This explains the relatively high macroporosity of Column 1. Therefore, one can not use numerical density as an indication of macroporosity.

The vertical length and position of macropore networks can be evaluated in Figure 5.8. This provides a good indication of the long networks that might have a significant impact on vertical water and chemical displacement. The artificial macropore (i.e., polyethylene tubing) running through the soil in Column 4 has been readily detected and identified as Network No 1.

Figure 5.9 shows the frequency distributions of the length of the macropore networks in the four soil columns. The distributions peak at approximately 40 mm for all soil columns. This indicates that the majority of the macropore networks has a length of 40 mm. As expected, the distributions are skewed to the left showing the presence of a few long networks, especially for Columns 1 and 4.

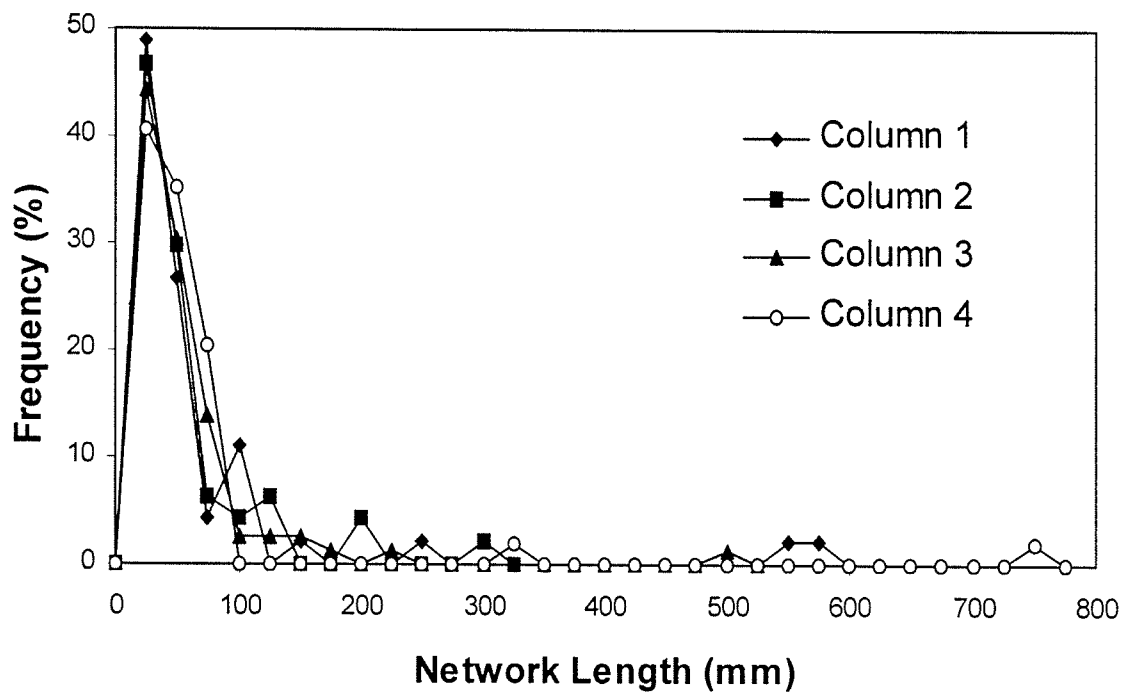


Figure 5.9: Frequency distributions of the length of macropore networks in the four soil columns.

### 5.6.2 Volume, wall area and hydraulic radius

The average network volume is presented in Table 5.2 for each column. The frequency distributions were evaluated in order to represent the tendency of volume networks in the four soil columns. Since the distributions were substantially skewed, results are displayed on a semi-log graph (Figure 5.10).



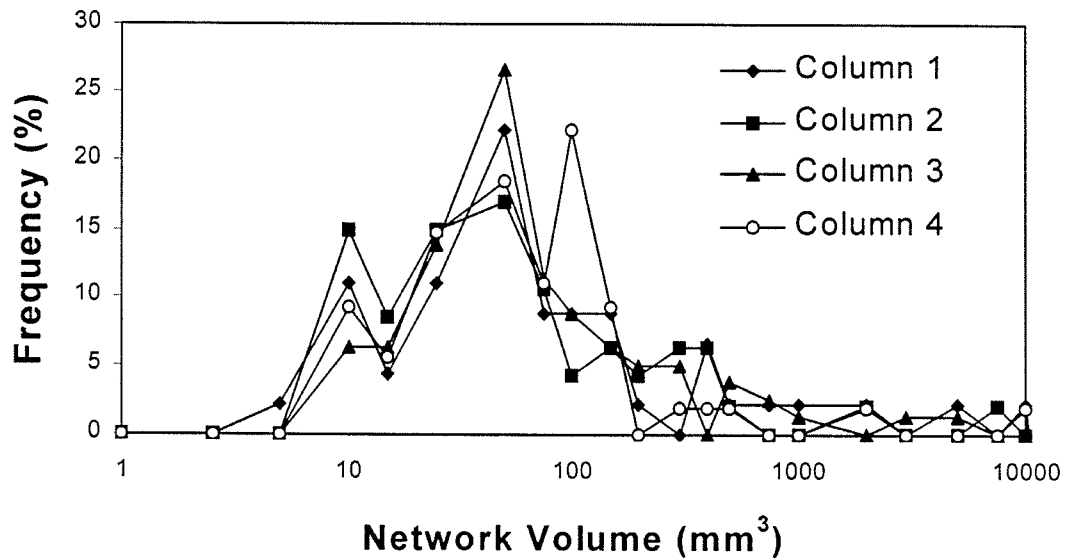


Figure 5.10: Frequency distributions of volume of macropore networks in the four soil columns.

The mode is equal to  $60 \text{ mm}^3$  and is approximately the same for the four columns. Knowing that the majority of the macropore networks have a length of 40 mm, this implies that most networks have an equivalent cylindrical diameter of approximately 1.4 mm. The network volume distributions suggest that about 2.5 % of the networks have a volume greater than  $7500 \text{ mm}^3$ . In other terms, 2.5 % of the networks have a volume equivalent to a capillary of 2.4 m by 2 mm in diameter or a spherical cavity of 24 mm in diameter.

Similarly, the distributions of the wall area of macropore networks have been evaluated (Figure 5.11). Again, results suggest the same pattern for all soil columns. The mode of the distributions is approximately  $175 \text{ mm}^2$ . A secondary peak, however, can be observed for networks having a wall area of  $1200 \text{ mm}^2$ . With the prevailing

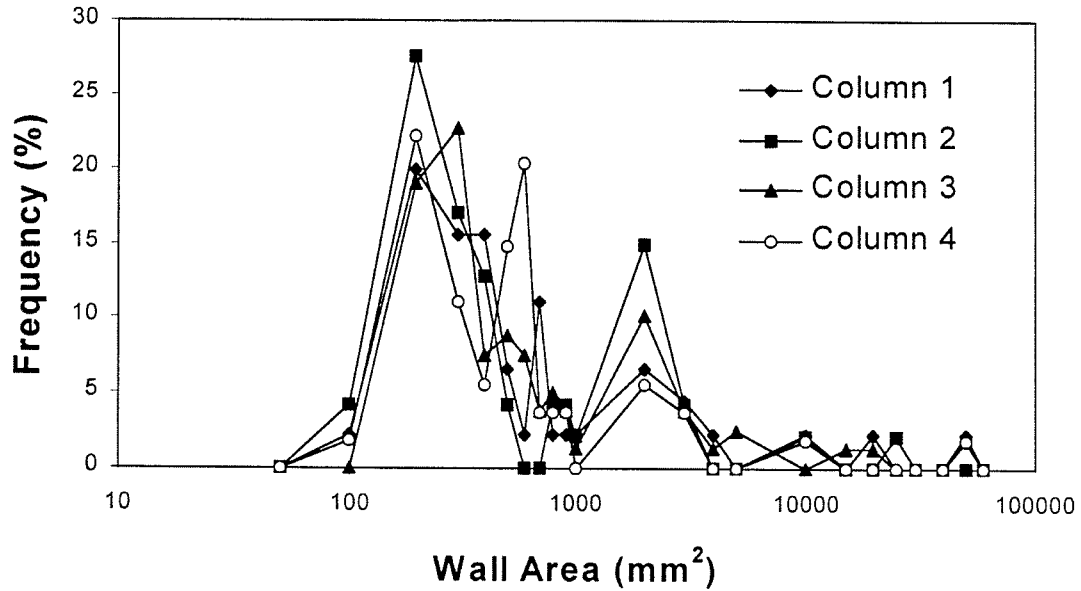


Figure 5.11: Frequency distributions of wall area of macropore networks in the four soil columns.

macropore network length of 40 mm, it implies that two sizes of networks may be found in this soil. The first category, which accounts for about 18 to 28 % of the networks, represents networks with an equivalent diameter of 1.4 mm and the second category delineates networks with an equivalent cylindrical diameter of approximately 9.5 mm.

As mentioned earlier, the hydraulic radius is a useful measure of size in the case of irregularly shaped pores. Just like tortuosity, it is a good indication of ability of the network to convey fluids. The greater the hydraulic radius, the greater is its transport capacity. The hydraulic radius of every network found in the soil columns is presented in Figure 5.12.

It can be observed that there is no apparent relationship between hydraulic radius and depth. However, longer networks have greater hydraulic radii than shorter networks.

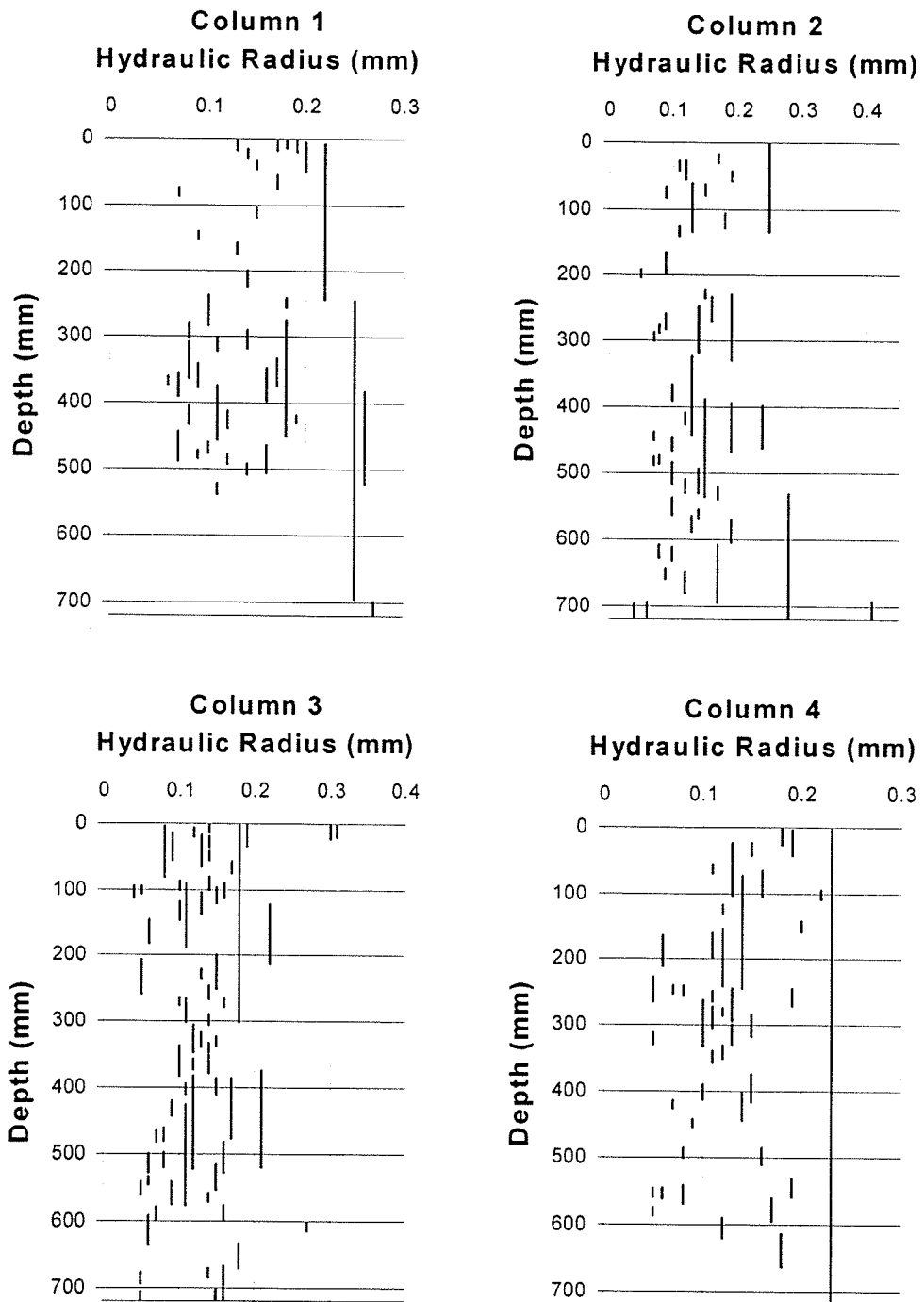


Figure 5.12: Hydraulic radius of macropore networks in the four soil columns.

For instance, the artificial macropore of Column 4 running from top to bottom of the soil has the greatest hydraulic radius of the column. Since long pores have a greater ability to

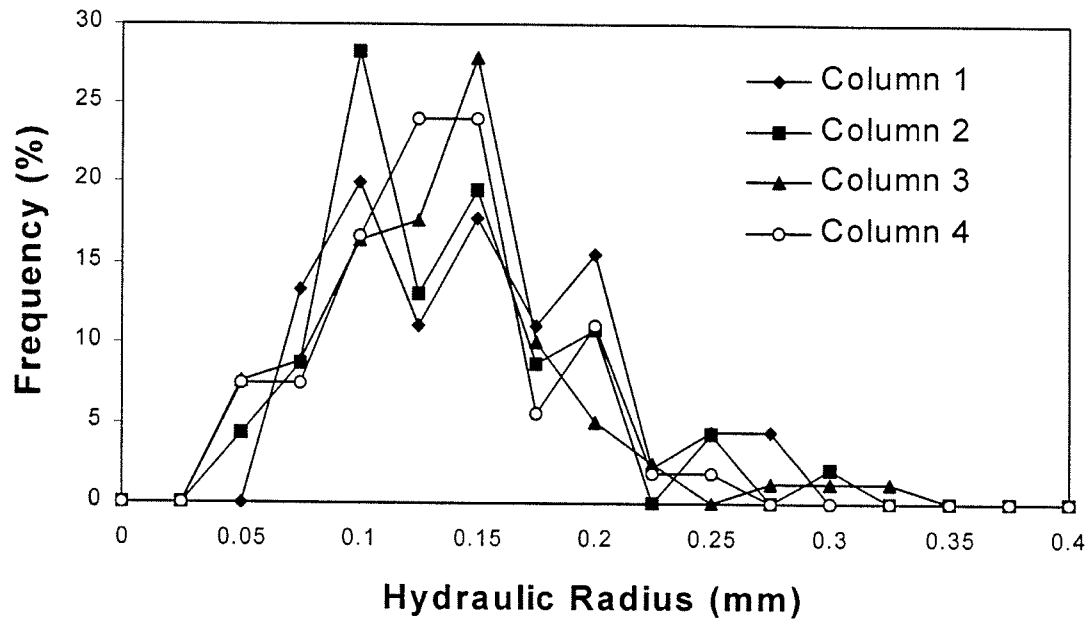


Figure 5.13: Frequency distributions of hydraulic radius of macropore networks in the four soil columns.

convey water, these results are expected. The frequency distributions of hydraulic radius were also assessed for every column and are shown in Figure 5.13.

The distributions of hydraulic radius are almost symmetrical with a mode of approximately 0.13. Here again, networks in all soil columns show a similar trend.

### 5.6.3 Inclination and tortuosity

Figure 5.14 shows the frequency distributions of the inclination of macropore networks. The inclination of networks ranges from vertical to an angle of about 55 degrees from vertical for some networks. The overall tendency suggested by the data is that the greater the inclination, the fewer are the number of macropore networks. However, the inclination fluctuates erratically and there is no evidence of a clear trend.

As mentioned above, tortuosity is a dimensionless factor always greater than one, which expresses the degree of complexity of the pore path. A macropore network with a

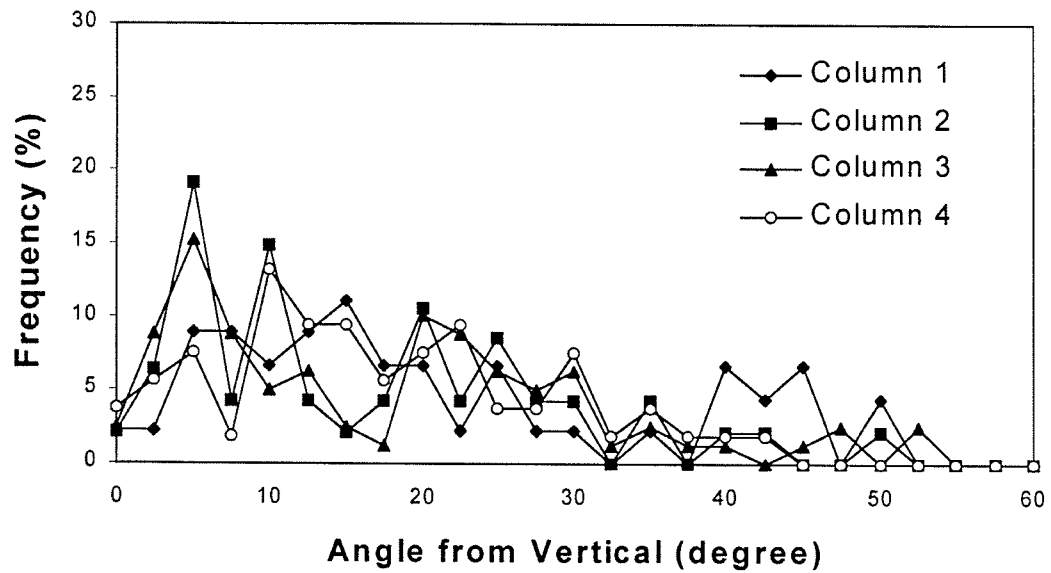


Figure 5.14: Frequency distributions of macropore network inclination.

tortuosity of one implies that the length of the effective or tortuous path of network is equal to the shortest distance measured along its direction. In other words, it indicates that the network follows a straight path. As tortuosity increases and moves away from one, the path of the macropore network becomes more tortuous.

Figure 5.15 shows the distributions of the tortuosity of macropore networks found

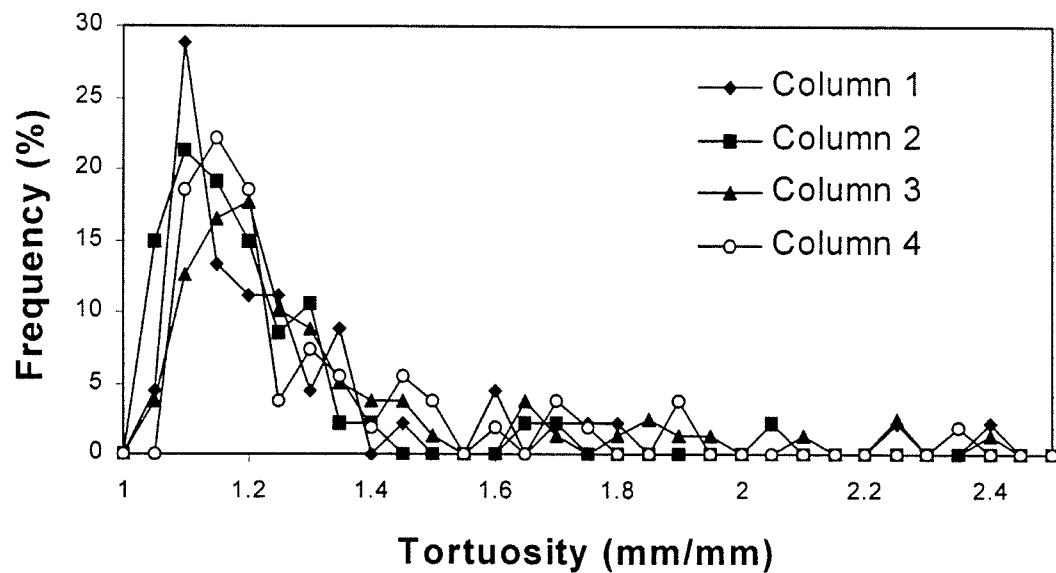


Figure 5.15: Frequency distributions of tortuosity of macropore networks.

in the four columns. The distributions are similar and skewed to the right with a mode of approximately 1.15. Most of the networks have a tortuosity in the range 1 to 1.4. Thus, the majority of the macropore networks have a three-dimensional tortuous length 15 % greater than the distance between their extremities. Some macropore networks have a tortuosity as high as 2.4.

#### 5.6.4 Number of branches, branch-node chart and connectivity

Results presented above were obtained by analyzing each network in the soil columns. As mentioned earlier, a macropore network is a set of branches that are interconnected. The parameters that have been evaluated for each network (i.e., number of networks, relative position, length, wall area, volume, hydraulic radius, orientation, and tortuosity), can be assessed in a similar fashion for each branch of every macropore networks. However, on average, the number of branches per soil column was calculated

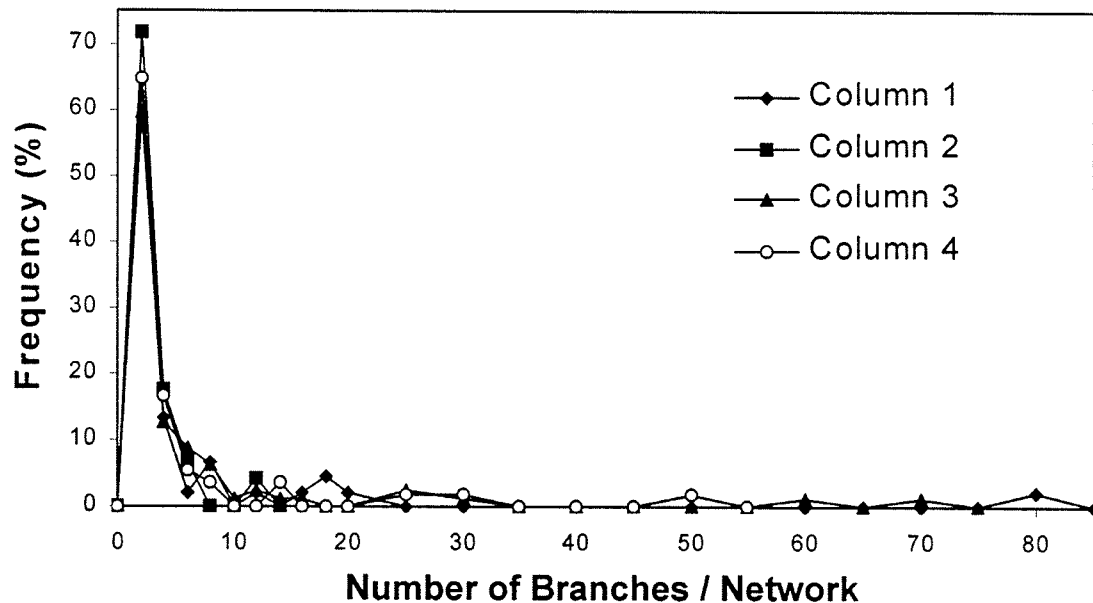


Figure 5.16: Frequency distributions of number of branches per macropore network.

to be equal to 288. To include analysis of each branch of all four soil columns in this paper will be too exhaustive. Therefore, it was decided to limit the investigation to branches of five large networks of Column 1 only.

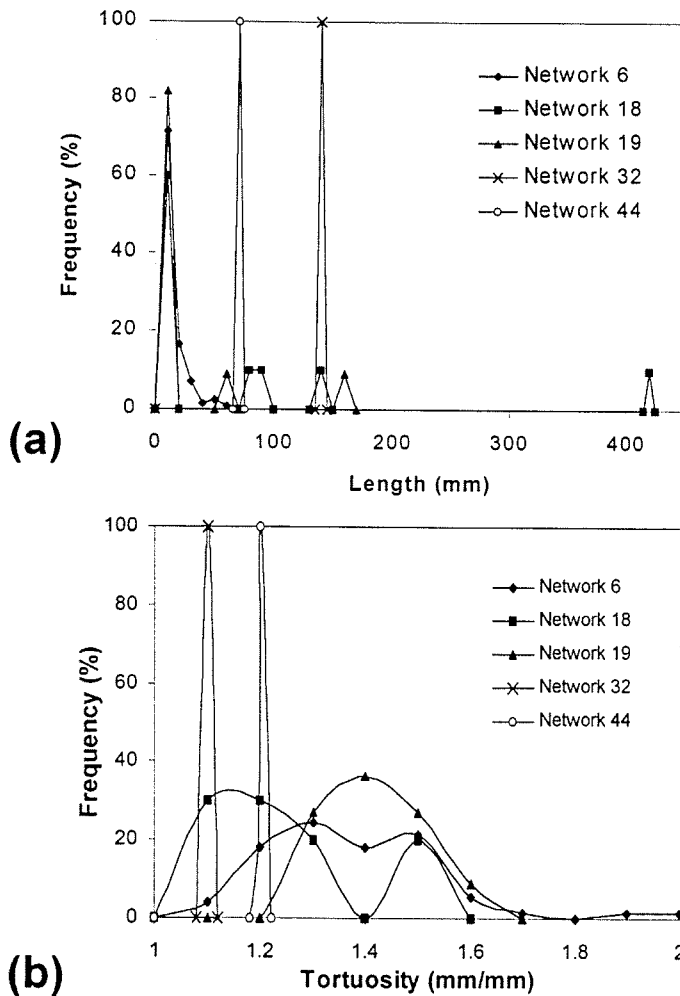


Figure 5.17: Frequency distributions of (a) length and (b) tortuosity of branches for selected Networks of Column 1.

Figure 5.16 shows the distributions of the number of branches per network for every soil column. The distributions for each column follow the same trend. The mode of the distributions suggests that most macropore networks are made up of approximately 4 branches. The distributions are skewed to the left, indicating the presence of very few networks with a large number of branches. The distributions of length of the branches of Networks 6, 18, 19, 32 and 44 in Column 1 are presented in

Figure 5.17a. Only networks which have a length greater than average were selected. As indicated in Figure 5.8, Network 6, 18, 19, 32 and 44 of Column 1 have a length greater the average macropore network. Figure 5.17a suggests that more than 60 % of the

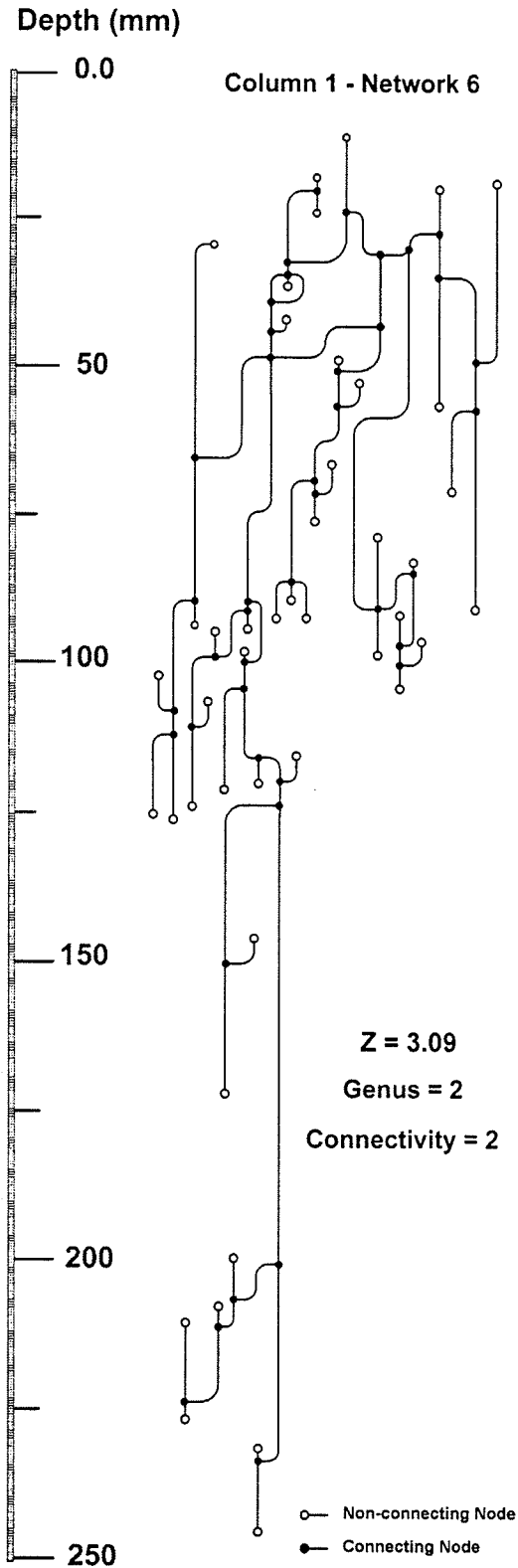


Figure 5.18: Branch-node chart for Network 6 of Column 1

branches of Network 6, 18 and 19 have a length of 10 mm. Since Network 32 and 44 have only one branch of 150 and 79 mm long, respectively, a single peak reaching 100 % in their distributions was expected.

The distributions of the tortuosity of the branches of these networks are shown in Figure 5.17b. The distributions do not suggest a trend, as tortuosity of the branches seems to vary significantly from one network to the other. Again two peaks reaching 100 % can be observed for Network 32 and 44 for the same reason discussed above.

As mentioned earlier, one of the simplest concepts for characterizing pore topology is the coordination number ( $Z$ ). It is defined as the number of branches meeting at a connecting node. In mathematical terms, the average coordination number of a network can be written as:



$$Z_{avg} = \sum_{i=1}^n Z_i f_i \quad (5.3)$$

where  $Z_i$  is the number of branches connected to a node of type  $i$  and  $f_i$  is the relative frequency of such node. A branch-node-chart was constructed for Network 6 of Column 1 to illustrate the concept of average coordination number (Figure 5.18). A branch-node chart is a representation of the three-dimensional arrangement of the pore networks in a 2-D plane. Network 6 was selected because of its high number of branches. The branch-node-chart of Network 6 gives an idea of its ability to transmit a fluid. More precisely, it indicates branches which may act as preferential flow paths and also, dead-ended set of branches which will not be part of the main channels.

A total of 42 connecting nodes can be found on Network 6. Three branches connect on 38 nodes. The remaining 4 nodes connect 4 branches. Therefore, the coordination number of Network 6 can be calculated as follows:

$$Z_{avg} = 3 \times \frac{38}{42} + 4 \times \frac{4}{42} = 3.09 \quad (5.4)$$

The average number of branches meeting at a node is 3.09. Like tortuosity, this gives an indication of increased resistance to flow due to the degree of “branchedness” of the macropore network.

The genus or connectivity of Network 6 was also evaluated. This was achieved by counting the number of non-redundant loops enclosed in Network 6. Two non-redundant

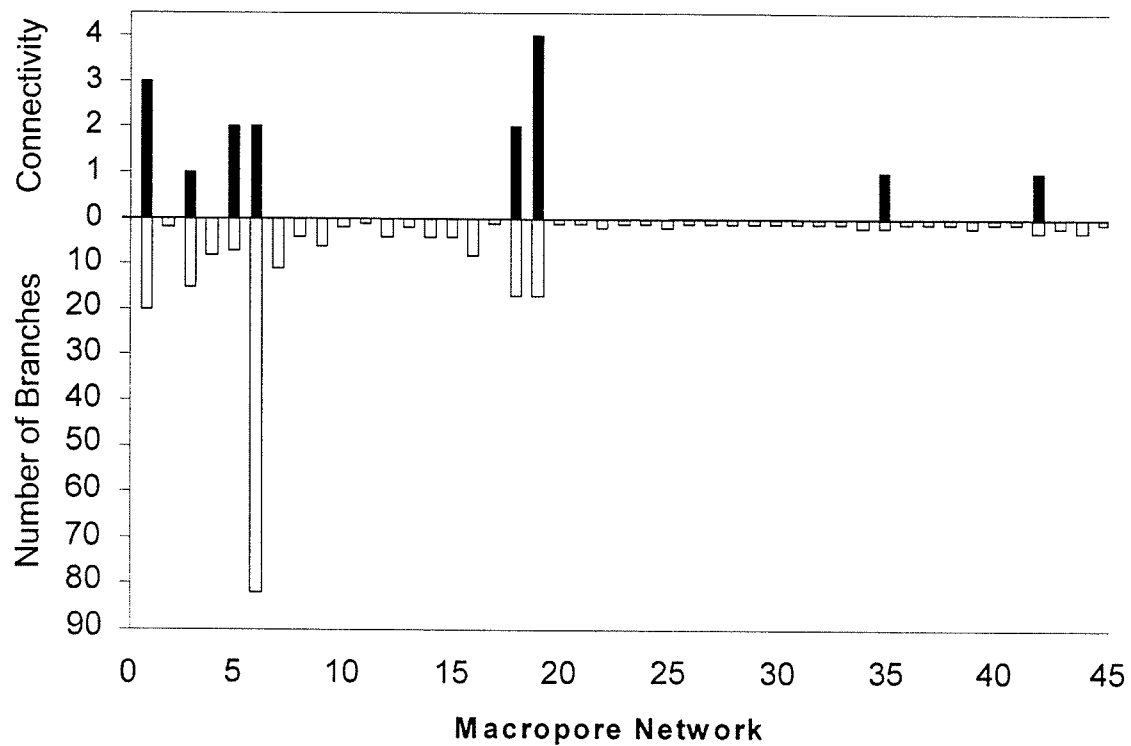


Figure 5.19: Connectivity of macropore networks and their number of branches (Column 1)

loops can be isolated in Figure 5.18. Thus, the connectivity of Network 6 is equal to 2. Similarly, the connectivity was calculated for every network of Column 1. Results are shown in Figure 5.19. The number of branches per network increases the probability of finding non-redundant loops in the three-dimensional structure of the networks. Therefore, the connectivity and the number of branches were plotted on the same graph to verify this relationship for each macropore network. However, no direct relationship can be observed in Figure 5.19. Macropore networks with one branch do not contain loops and therefore, have a connectivity equal to 0. As mentioned above, the term connectivity density is sometimes used to define the connectivity per unit volume. In the case of Column 1, the connectivity density is equal to  $4772 \text{ loops/m}^3$ .

## 5.7 Summary and Conclusions

X-ray CAT scanning has been a useful approach to threshold macroporosity of undisturbed soil columns in a non-destructive manner. The main characteristics of the geometry and topology of macropore networks were determined using three-dimensional reconstruction techniques. For that purpose, several programs were written in the PV-WAVE programming language.

Our results suggested that the numerical density varies between 13,421 to 23,562 macropore networks per cubic meter of soil. No direct relationship could be observed between numerical density and macroporosity. The position and the length of macropore networks were evaluated. The artificial network installed in one of the soil column was readily detected. It was found that the majority of the macropore networks had a length of 40 mm, a volume of  $60 \text{ mm}^3$  and a wall area of  $175 \text{ mm}^2$ . However, some macropore networks, although representing a small percentage, could reach a length of 750 mm, a volume of  $10,000 \text{ mm}^3$  and a wall area of  $50,000 \text{ mm}^2$ .

The hydraulic radius in three-dimensions was also assessed as an indication of the ability of the networks to convey water. It was found that the greater the length of networks, the greater the hydraulic radius. On average, macropore networks had a hydraulic radius of 0.13 mm.

Our results on network inclination suggest that it ranges from vertical to an angle of about 55 degrees from the vertical. The overall tendency of network inclination distributions suggests that the smaller the inclination, the greater the number of macropores.

Results for tortuosity indicated that the majority of the networks had a tortuosity between 1 and 1.4. The mode of the tortuosity distributions suggested that most macropore networks had a three-dimensional tortuous length 15% greater than the distance between its extremities. It was found that some macropore networks had a tortuosity as high as 2.4.

More than 60% of the networks are made up of 4 branches. The connectivity was assessed for Column 1. Our results for Column 1 suggested that 82% of the networks had a connectivity of zero. The connectivity density was equal to 4772 non-redundant loops per cubic meter.

As mentioned above, the three-dimensional arrangement of network of soil macropores plays a determining role in the rate of water and solute movement through soil. These results can be used to determine and quantify the effect of 3-D geometry of macropore network on solute transport through soil columns.

## **5.8 Acknowledgements**

The authors wish to thank Daniel Marentette for his help and suggestions in the technical part of this work. The authors also gratefully acknowledge the financial support provided by the Natural Sciences and Engineering Research Council of Canada (NSERC) and ESTAC (Environmental Science and Technology Alliance Canada).

## PREFACE TO CHAPTER 6

Visualization and quantification of soil macropores in two- and three-dimensions has been presented and discussed in the last three chapters. Imaging in three-dimensions and quantification of soil macroporosity's three-dimensional parameters are critical in order to accurately correlate soil pore structure with the preferential flow phenomena. In this chapter, we will concentrate on water movement and non-reactive solute transport in soil macropores of one soil column, and eventually, describing how to model macropore flow.

Considerable research efforts have been made to model water and solute fluxes in soil. Different types of modeling approaches are reviewed in this chapter. Most current models are based on the Richard's equation for water flow and the convective-dispersion equation for solute transport. Although these models have been successfully used for simplified systems, their usefulness and applicability become questionable in "real" soils, where the structure is complex and heterogeneous. A multi-region modeling approach holds promise for simulating solute transport under non-equilibrium conditions and where flow dynamics differ from one region to another (i.e., macropore domain versus micropore domain). However, till now, the demarcation between flow domains is arbitrarily defined. Thus, a reliable technique that isolates and characterizes flow domains in soils needs to be developed.

CAT scanning provides an ideal tool to determine and isolate each flow domain. Breakthrough experiments using potassium iodide were monitored with the CAT scanner during the summers of 1996 and 1997. The methodology that was used for these experiments is discussed in this chapter. Chapter 6 also presents a new multi-region modeling approach to model macropore flow in soil under saturated conditions. Efforts were made to relate the 3-D geometry of macropores to their ability to convey water and solutes. Water and solute transport in the macropore domain was modeled using an analogy between macropore flow and pipe flow. The macropore domain was divided into two regions, namely the laminar and turbulent regions. Modeling results suggest that this approach provides a reasonable approximation of the overall tendency of breakthrough in the macropore domain.

Several computer programs were developed in PV-WAVE for this study. These programs are included in the attached CD-ROM. Chapter 6 has been submitted for publication. For the sake of completeness, some material in this chapter is repeated from previous chapters so that this paper can stand on its own. (Perret J.S., S.O. Prasher, A. Kantzas and C. Langford. 1998. Development of a two-domain simulation approach using X-ray CAT scanning to model solute transport in a soil with preferential flow pathways. Submitted to the Journal of Environmental Quality).

The candidate was responsible for designing and conducting the research experiments, developing computer codes for the visualization and analysis of data and finally, preparation of the thesis. Dr. Shiv O. Prasher, professor at the Agricultural and Biosystems Engineering Department of McGill University, contributed in all aspects of this research project. He provided the necessary funds and assistance for this research,

including the supervisory guidance and the reviewing of manuscripts before their submission for publication. Dr. A. Kantzas, Director of the Tomographic Imaging and Porous Media (TIPM) Laboratory in Calgary, Alberta, and associate professor at the University of Calgary's Department of Chemical and Petroleum Engineering, provided access to CAT scanning facilities of the TIPM laboratory. Dr. Kantzas also made invaluable suggestions during CAT scanning. Dr. C. Langford, University of Calgary's vice-president research and professor at the Department of Chemistry, was the principal investigator for the NSERC Collaborative Project Grant.

## CHAPTER 6

# DEVELOPMENT OF A TWO-DOMAIN SIMULATION APPROACH USING X-RAY CAT SCANNING TO MODEL SOLUTE TRANSPORT IN A SOIL WITH PREFERENTIAL FLOW PATHWAYS

---

### 6.1 Abstract

Despite recent research efforts to determine and model the dynamics of macropore flow, it is still not possible to quantitatively predict water and chemical movement in soil containing macropores. Several researchers have pointed out the potential offered by multi-region modeling. However, the criteria used to define boundaries between flow regions have been up to now defined arbitrarily. Therefore, there is a need to develop a reliable technique to isolate and characterize flow domains in soil.

The primary objective of this study was to develop a reliable method for isolating and characterizing flow domains in a large undisturbed soil column using a CAT scanner. CAT scanning offers tremendous potential for non-destructive quantification of tracer volume concentration inside soil columns during breakthrough experiments. This approach allows for real-time examination of flow mechanisms through soil macropores at various depths along the length of soil columns. Several computer programs were



written in the PV-WAVE language to quantify the three-dimensional geometry of macropore and characterize the spatial distribution of solute at thirteen depths in the soil column. With knowledge of the macropore structure and the spatial distribution of the solute, breakthrough in the macropore and matrix flow domains was evaluated.

Very soon after the tracer application, the occurrence of macropore flow was detected. However, a fraction of the flow in macropores was relatively slow. This was due to the presence of dead-end branches or cavities which, from a geometrical point of view, belong to the macropore domain, but do not contribute to preferential flow. This raises the question of effective flow in the macropore domain and suggests that the macropore domain should be defined both in terms of the geometry of macropores and of their ability to convey tracer preferentially.

Flow in the matrix domain suggested that part of the matrix contains small pores that are connected to macropore networks. These pores contribute to a rapid tracer build up in the matrix domain. The breakthrough curves measured in the matrix domain were fitted using the convection dispersion equation (CDE) with CXTFIT 2.0. The high regression coefficients obtained suggest that the CDE model describes breakthrough in the matrix domain quite well. Solute transport in the macropore domain was modeled using the analogy between macropore flow and pipe flow. The macropore domain was divided into two regions, namely the laminar and turbulent regions. A modified version of Poiseuille's law was used to model solute breakthrough in the laminar region. For the turbulent region, a new formula was derived based on Manning's equation. The modifications were done so that these simple models would take into account the distribution density functions of macropore size and hydraulic radius. This approach

provides us with a reliable approximation of the overall breakthrough of solutes in the macropore domain.

## 6.2 Introduction

Although macropores represent a small percentage of total soil porosity (1% to 5%), they can have a profound effect on the rate of infiltration and redistribution of water into soil (White, 1985). The presence of macropores provides an opportunity for water and associated chemicals to move preferentially through the vadose zone. This phenomenon is known as preferential flow or macropore flow. Several studies clearly demonstrate the importance of the contribution of macropore flow to total flux. Watson and Luxmoore (1986) quantified water flow in a forested soil and found that macropore flow contributed to 73% of water movement in a saturated soil. In similar conditions, Wilson and Luxmoore (1988) reported that 85% of water ponded at the surface of a forested soil moved through soil macropores. Roth et al. (1991) studied solute transport through a layered and structured soil in Switzerland and found that macropore movement accounted for about 56% of the total water flow. Using a double-ring infiltrometer in a corn field, Dunn and Phillips (1991a) noted that pores greater than 0.21 mm in equivalent diameter contributed to 83 % of the total water flux.

Due to low frictional and capillary forces present in big soil pores, water flow is usually much faster through macropores than through the soil matrix (Beven, 1981; Huffman and Monke, 1989; Warner, 1990). For instance, Aley (1977) estimated that water entering soil macropores contributes five times as much to groundwater recharge than does water through soil matrix. In field conditions, Bouma et al. (1982) pointed out that steady state ponded infiltration rates could be as high as 6.7 ml/s for continuous macropores. Steenhuis et al. (1986) reported that water movement from soil surface to drainage tile lines is more than two orders of magnitude faster than would be predicted by

Darcy's law. Using bromide leaching studies on twenty undisturbed soil column, Ren et al. (1996) found that the median solute velocities were up to 311 % faster than corresponding piston flow velocities.

As suggested above, macropore flow plays a very important role in the transport of nutrients and agricultural chemicals from surface to sub-soil and eventually, to ground water and drainage effluent that feeds streams. Rapid flow has a major impact on drainage and groundwater quality since it may not allow contaminants, such as pesticides, to be adsorbed on and into the soil particles and broken down by chemical and biological actions. Consequently, any solute will be quickly delivered to the drains or groundwater aquifers without being degraded. Development of management systems based on accurate models which take soil macroporosity into account, is crucial in order to decrease the adverse impacts on water quality.

### **6.2.1 Modeling approaches**

Extensive research has been conducted to determine and model the dynamics of water and solute fluxes in macroporous soil. However, this problem has not been easy to resolve (Huffman and Monke, 1989). McCoy et al. (1994), Lal and Stewart (1994), Chen and Wagenet (1992), Bouma (1991) and Ma and Selim (1997) pointed out that despite the efforts to describe preferential movement of solutes along macropores in quantitative terms, it is still not possible to quantitatively predict water and chemical movement in soils containing macropores. Different methods have been developed to characterize and model water and solutes fluxes in soil. These approaches can be divided into two main categories (Steenhuis et al., 1990). The first approach relies on the use of stochastic models whereas the second is phenomenological or based on deterministic approaches.

Phenomenological approaches are more common and therefore, will be discussed in more details in this paper.

The spatial variability of the soil structure is so complex that some researchers have suggested that stochastic modeling would be appropriate (Grochulska and Kladvko, 1994). Rather than describing the complex mechanisms of chemical movement in soil, they have proposed to use a transfer function based on the probability density function of the solute travel time. Beven and Young (1988) suggested that the transfer functions could be estimated from the fluxes from a volume of medium through the use of time series analyses. Although this approach is attractive in principle, it is site specific and requires extensive measurements at any new site (Bouma, 1991). Moreover, Steenhuis et al. (1990) pointed out that these stochastic models are often extremely complex and lack guarantee of validity for locations and processes for which they have not been calibrated.

On the other hand, phenomenological models describe solute transport in soil in a deterministic way. The deterministic model is solved using either analytical or numerical techniques. Most of these types of models use Richard's equation for water movement and the convection dispersion equation (CDE) with various types of sorption sites and chemical and physical non-equilibrium for chemical transport. Many management and research models are based on the CDE approach, such as PRZM-2 (Carsel et al., 1995), PESTFADE (Clemente et al., 1993), LEACHM (Hutson and Wagenet, 1989), MOUSE (Steenhuis et al., 1987), DRAINMOD-N (Breve, 1994). However, Kumar and Kanwar (1997), Hornberg et al. (1990) and Steenhuis et al. (1990) pointed out that these models lack the capability of simulating solute concentrations in the subsurface drainage water. For instance, many column and field studies of solute transport in soil showed substantial

deviation between measured effluent concentration and those calculated using the CDE approach (Hutson and Wagenet, 1995). Inaccurate predictions are attributed to a lack or inadequate consideration of macropore flow (Smith et al., 1991).

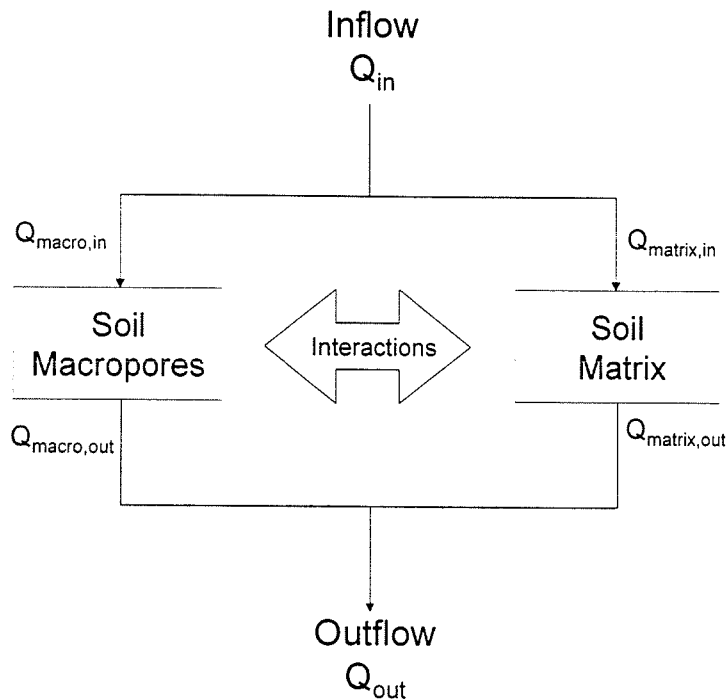


Figure 6.1: Schematic representation of the two-flow domains system;  $Q$  represents flow rate

One method to improve the CDE approach is to divide flow in soil into several regions. Ma and Selim (1997) discussed the potential offered by multi-region modeling. They pointed out that this approach is one of the research areas in the forefront of soil physics and hydrology disciplines. This method simplifies of the flow

region into different domains, such as mobile water versus immobile water, transient flow versus steady flow, and laminar flow versus turbulent flow. For instance, one simplification is to divide the flow field into the following domains: the macropore flow domain where rapid transport may occur preferentially and the micropore flow domain where solute transport is occurring in the surrounding matrix at a much slower rate (Figure 6.1).

Van Genuchten and Wierenga (1976) were among the first researchers to have

proposed a multi-region model with the concept of mobile-immobile water in soil. Since then, solute transport using a two-region approach has been considered by a number of investigators (Ma and Selim, 1997; Hutson and Wagenet 1995; Chen and Wagenet, 1992; Steenhuis et al., 1990; Germann et al., 1984; Neilsen et al., 1986). Although multi-region models based on the CDE offer insights into the mechanisms that have an important bearing on preferential flow, they are not easily applied to describe observations in large intact soil cores or from field blocks where the nature of the flow pathways is essentially indeterminate (Hornberg et al., 1990). The criteria of demarcation between flow domains are not well understood. As a result, the input parameters are rather arbitrarily defined and difficult to determine (Steenhuis et al., 1990; Hutson and Wagenet 1995). Therefore, there is a need to develop a reliable technique to isolate and characterize flow domains in soil.

This paper focuses primarily on the characterization of macropore flow in a large undisturbed soil column using a 4<sup>th</sup> generation X-ray CAT scanner. CAT scanning offers tremendous potential for non-destructive quantification of tracer volume concentration inside a soil column during breakthrough experiments. This approach allows for real-time examination of flow mechanisms through soil macropores at various depths along the length of the soil column. Thus, the objectives of this study were to develop a non-destructive approach to: (1) monitor the breakthrough of water and non-reactive solutes through soil; (2) isolate the macropore flow domain and matrix flow domain, and (3) develop a model to simulate solute transport in the macropore domain of the saturated soil column.

## 6.3 Materials and Methods

### 6.3.1 Soil column

One undisturbed soil column, 850 mm in length and 77 mm in diameter, was extracted from the border of an uncultivated field, located at the Macdonald Campus of McGill University in Ste-Anne-de-Bellevue, Quebec, Canada. The hydraulic bucket of a backhoe was used to drive a polyvinyl chloride (PVC) pipe in small increments of about 80 mm. The objective was to obtain a soil core that was disturbed as little as possible in order to obtain a sample representative of natural conditions. Column size was selected based on the need for a sample large enough to represent macropore distribution, yet small enough to be handled easily when full of soil. PVC was chosen for the cores because it has a relatively low X-ray attenuation coefficient.

The soil had been covered for many years with a combination of quack grass (*Elytrigia repens* (L.) Nevski.), white clover (*Trifolium repens* L.) and wild oat (*Avena fatua* L.). The soil belongs to the Chicot series and was predominantly a sandy loam with an A horizon thickness of around 0.4 m. For more information on the physical and chemical properties of the soil, the reader is referred to Perret et al. (1997).

PVC caps were installed in order to create an empty space at the end of the column. This space allows water and tracers to penetrate uniformly through the column cross-section. A plastic screen was placed on both ends of the soil column to prevent the soil from collapsing.



### 6.3.2 CAT scanning and macropore characterization

A medical ADVENT HD200 whole body CAT scanner was used at the TIPM (Tomographic and Porous Media) laboratory in Calgary, Alberta. Computed Tomography (CT) or Computer Assisted Tomography (CAT) is a method of diagnostic imaging used for non-destructive viewing of cross-sectional “slices” of the human body or any object. This scanner incorporates a fourth generation scan geometry with scan times as short as 2 s/scan and high pixel resolution up to 195  $\mu\text{m}$  by 195  $\mu\text{m}$ . In most CAT scanners, the actual data collection occurs in the gantry where the patient lays horizontally. However, the ADVENT HD200 was modified to allow vertical scanning. For that purpose, the CAT scanner gantry was rotated by 90° and positioned on a metal frame designed to hold the whole gantry horizontally. This unique feature allows performing experiments in which gravitational forces cannot be ignored.

A total of 360 sections or scans was obtained for each column, leaving no space between two consecutive scans. With the development of computer programs in the PV-WAVE language, the analysis of soil macropores was performed directly on CAT scan data. Macropores were readily detected, visualized and quantified. Data generated by the CAT scan process was manipulated in order to accentuate different features of the soil. Soil macropores were isolated by thresholding certain values of the density matrices. This approach was utilized for each section of the soil columns in order to evaluate: the number of macropores, the macroporosity, and various macropore parameters, such as the equivalent diameter, the hydraulic radius, the tortuosity, the circularity and the rectangularity. The spatial continuity of pixels in serial sections of one soil column was studied using geostatistical analysis. For more details on the two-dimensional

quantification of soil macropores, the reader is referred to earlier work presented by Perret et al. (1997, 1998a).

3-D reconstruction is critical in order to correlate pore structure with the flow processes occurring in soil. Programs in PV-WAVE language were developed to visualize the complex three-dimensional network of interconnected pore space (Figure 6.2a, b). The main characteristics of the geometry and topology of macropore networks were determined using three-dimensional reconstruction techniques. Results of the 3-D analysis have been presented in a previous paper (Perret et al., 1998b).

### 6.3.3 Column saturation

Entrapment of air in soil can lead to blocked pore passages. Air inside the soil columns was removed by diffusing CO<sub>2</sub> through the soil columns for a period of 24 hours.

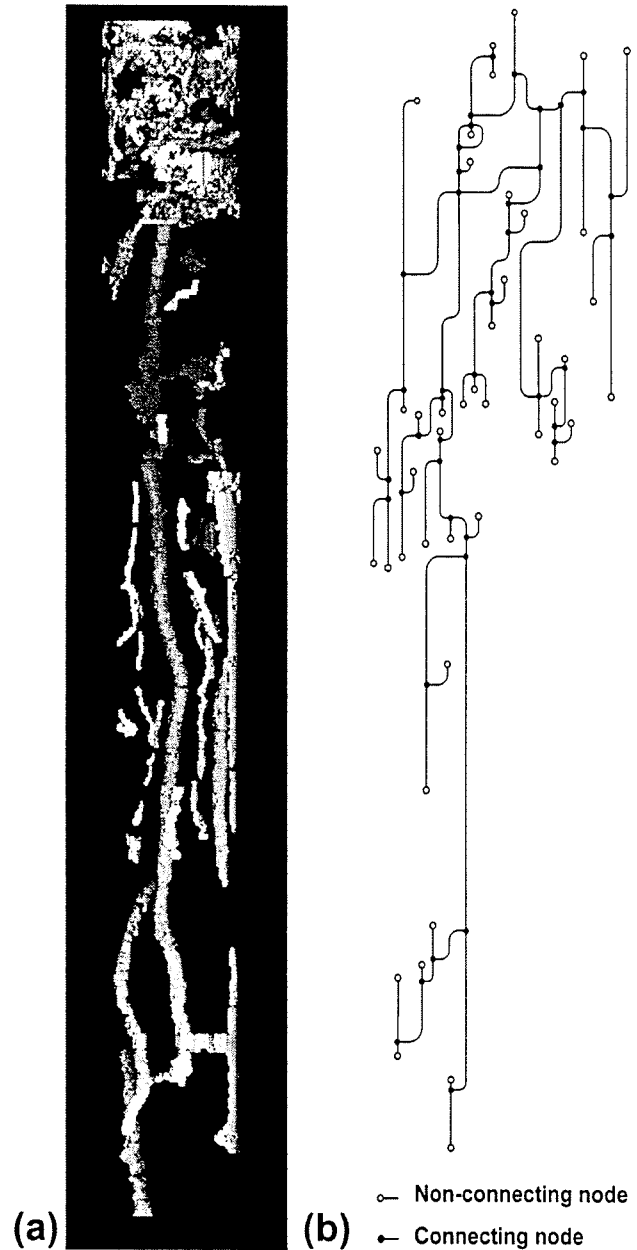


Figure 6.2: (a) 3-D view of Column 1 (b) Branch node chart of a macropore network (network 6) running from a depth of 10 to 245 mm.

Since  $\text{CO}_2$  dissolves in water, the empty spaces of the soil were easily saturated. After filling the soil cavities with  $\text{CO}_2$ , undisturbed soil cores were slowly saturated by gradually increasing the water level over a period of 3 days. Prior to core saturation, the water was de-aerated in a 25-L vessel that had been connected to a vacuum pump.

#### 6.3.4 Selection of non-reactive solute

Potassium iodide (KI) and sodium iodide (NaI) are non-sorbing tracers that have been successfully used in medical diagnosis and petroleum engineering to evaluate solute transport in the human body and in rock samples (Anderson et al., 1992; Kantzas, 1990). Therefore, both KI and NaI were tested in water solutions and in saturated soils with the CAT scanner to evaluate their ability to absorb incident X-rays. Sixteen samples were prepared at

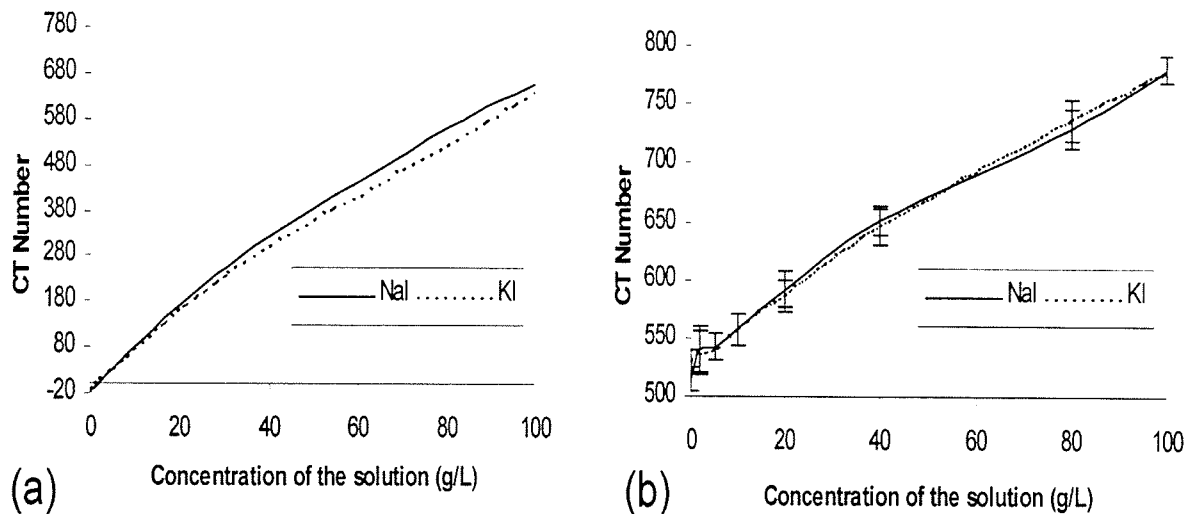


Figure 6.3: X-ray attenuation coefficient of sodium iodide and potassium iodide; (a) water solution, (b) soil saturated with the tracer solution. The error bars represent standard deviation.

concentrations of 0, 2, 5, 10, 20, 40, 80 and 100 g/L of NaI and KI in water. The same concentrations were used to saturate sixteen soil samples. These samples were then scanned to evaluate their response to X-rays. Figure 6.3 shows the average CT number of these aliquots. CT numbers are the standard output of a CAT scanner and are usually expressed in HU's (Hounsfield Units) which are dimensionless.

Figure 6.3 indicates that there is very little difference between the X-ray absorption of NaI and KI. The  $K^+$  and  $Na^+$  cations appear to have only a minor effect on the CT Number. Both NaI and KI can be used as tracers in the soil. However, since the cost of NaI is twice that of KI, the latter was selected for our experiment. As indicated in Figure 6.3, the CT number of water saturated soil is equal to 525 HU. In order to get a good signal from the tracer, its concentration should be such that it creates an increase in the CT number of at least 100 HU. The CT number obtained for soil saturated with potassium iodide at a concentration of 60g/L was equal to 675HU. A concentration of 60 g/L was therefore selected for this study.

#### **6.3.5 Breakthrough measured by X-ray CAT scanning**

The breakthrough experiment was performed on only one of the saturated soil columns. Before scanning, the soil column was placed vertically in the scanner unit and a hydraulic gradient of 0.1 m was maintained at the upstream face of the soil column to reach steady-state flow. A simple system was constructed for this purpose (Figure 6.4). A thin layer of mineral oil was maintained on top of the water to minimize gas exchange between air and de-aerated water. A digital scale was placed at the other end of the

column to collect the effluent and measure the flow rate. The flow rate was kept constant at 0.0351 L/min (i.e., 7.5 mm/min) during the entire breakthrough experiment.

The column was scanned at thirteen different depths with an interval of 50 mm between each consecutive scan. The column was scanned at these thirteen positions, before introducing the tracer, to evaluate the soil's initial state under saturated flow conditions.

The next step was to initiate the continuous application of the tracer to produce a gradual increase in concentration throughout the soil. The tracer solution in the breakthrough experiment contained 60 g/L of KI. The column was scanned at one of the thirteen positions every 45 seconds.

10 ml of effluent were sampled every 3 minutes to evaluate breakthrough in the effluent. The soil column was then flushed with de-aerated water for a period of 12 hours and scanned again to evaluate any possible changes in soil structure.

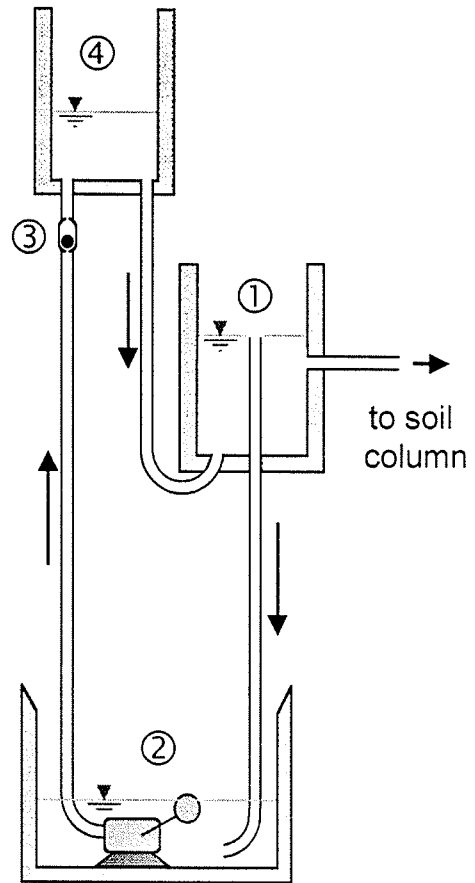


Figure 6.4: Experimental setup used to maintain a constant water head; ① Constant head apparatus, ② pump activated/ deactivated with a float, ③ one-way valve, ④ water stored at higher potential energy.

### 6.3.6 Analysis of the solute breakthrough and recognition of the flow domains

Several programs in the PV-WAVE language were developed for visualization and analysis of the breakthrough experiment. Only the region representing soil, water and tracer is of interest for the analysis of the breakthrough. Two programs were written to isolate the saturated soil column in its initial state (Inijo.pro) and during breakthrough (Tracerjo.pro). For the initial saturated conditions of the soil core, each element of the matrices represented water, soil or a mixture of the two. On the other hand, each pixel of the matrices obtained during KI breakthrough represented water, soil, tracer or a

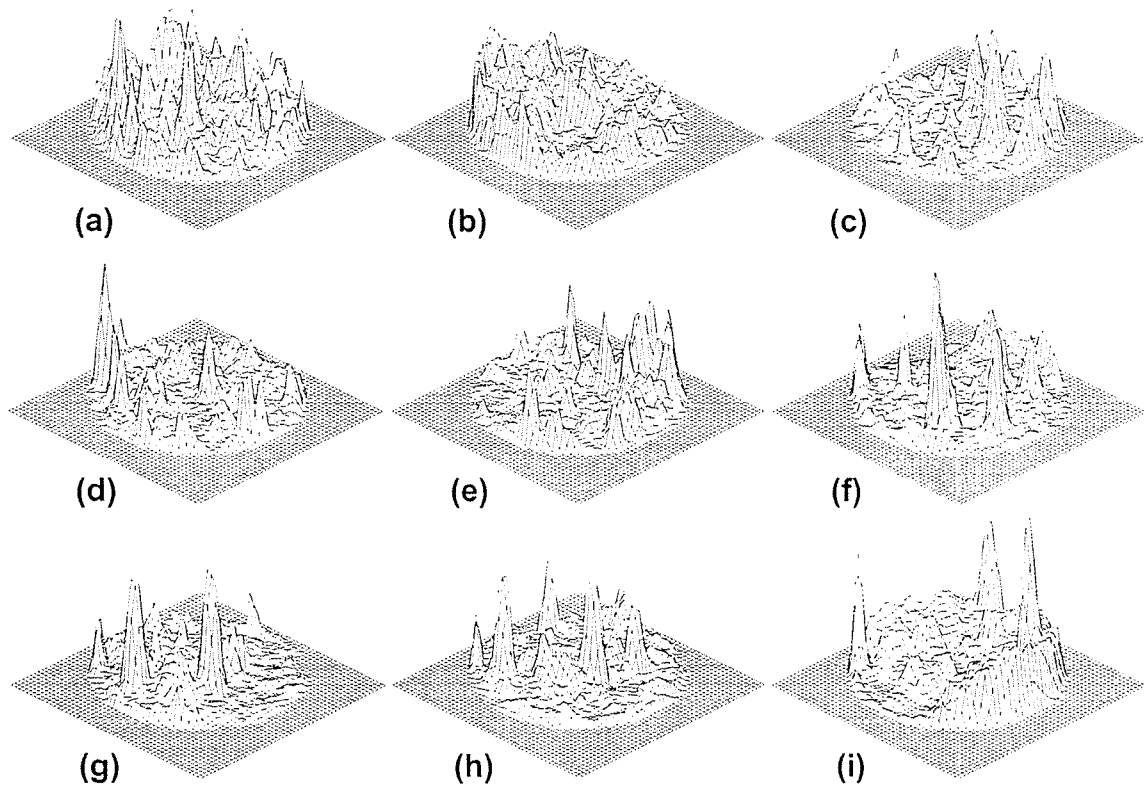


Figure 6.5: Three-dimensional representation of concentration of potassium iodide at different depths and times. (a) depth=50 mm, time=14.27 min; (b) depth=100 mm, time=14.78 min; (c) depth=150 mm, time=15.28 min; (d) depth=200 mm, time=15.83 min; (e) depth=250 mm, time=16.50 min; (f) depth=350 mm, time=20.03 min; (g) depth=450 mm, time=20.97 min; (h) depth=500 mm, time=21.67 min; (i) depth=650 mm, time=23.90 min.

combination of these three elements. Therefore, by subtracting the initial state matrices from the matrices obtained during breakthrough at respective depths, matrices representing tracer concentration were obtained. A program called Diftjo.pro was developed for this purpose. A subroutine of Diftjo.pro allowed visual inspection of the breakthrough. Visual representations of some of these matrices are shown in Figure 6.5. Each peak represents a region of high concentration and therefore indicates flow in the macropore domain.

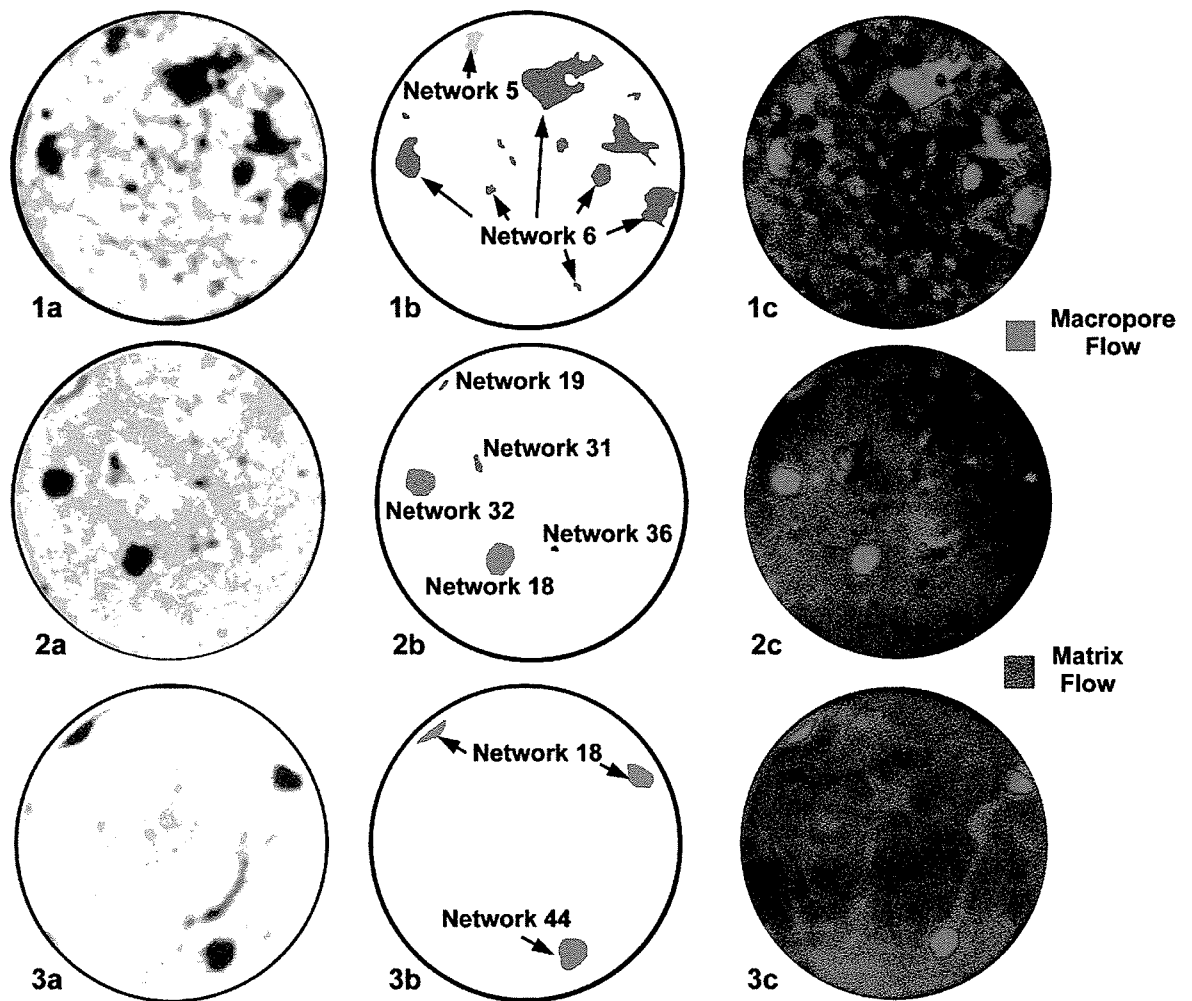


Figure 6.6: Cross-sectional views of the soil column at depth (1) 50 mm, (2), 450 mm and 650 mm; (a) dry conditions, (b) position of macropore networks and (c) tracer flux in the macropore and matrix domains

Breakthrough curves were calculated for each of the thirteen depths. A program, called BTCmjo.pro, was developed to calculate the changes with time in average concentration at every depth. As mentioned above, the 3-D structure of macropore networks in the soil column has been quantified in an earlier study (Perret et al., 1998b). By superimposing the macropore structure on the actual tracer flux at respective depths, it became possible to divide the flow domain into macropore flow and matrix flow (Figure 6.6). An algorithm in BTCmjo.pro was developed to determine solute concentrations in the macropore and matrix flow domains. For each of the thirteen depths and for a given time step, the program reads two data files, one containing the concentration values, and the other containing the position of the macropore network. For each pixel belonging to the macropore domain, it records the corresponding concentration value into an array. The program also performs the same task for the matrix domain (micropores) and creates another array of concentration values. Once the two arrays have been defined, an average concentration value is calculated for both the macropore and matrix flow domains. BTCmjo.pro also allows visualization of concentration flux in respective flow regions (Figure 6.6c). Following a similar approach, another program called BTCntjo.pro was developed to quantify the tracer breakthrough in each individual macropore network.

## **6.4 Results and Discussion**

The results and discussion is divided into four sections. The results obtained for the overall breakthrough, including both matrix and macropore domains, are presented and discussed in the first section. As mentioned above, the tracer breakthrough in the soil was divided into two flow regions. Thus, Sections 6.4.2 and 6.4.3 present the results



obtained for the breakthrough in matrix and macropore domains, respectively. Finally, the last section deals with modeling.

#### 6.4.1 Overall breakthrough

Figure 6.7 shows an early initial breakthrough in the effluent, before one pore volume has passed through the column. Czapar et al. (1992), Bouma (1991), and Singh and Kanwar (1991) pointed out that an early breakthrough in an undisturbed soil column was an indication of macropore flow. It took approximately 2.75 pore volumes for the effluent concentration to reach the inflow concentration (Figure 6.7). In case of uniform tracer flux through soil, it would imply that the entire mobile pore-water fraction of the soil (i.e., fraction of total pore water contributing to the solute transport) is completely saturated with the tracer. However, the breakthrough curves measured for every depth in the soil column indicate that

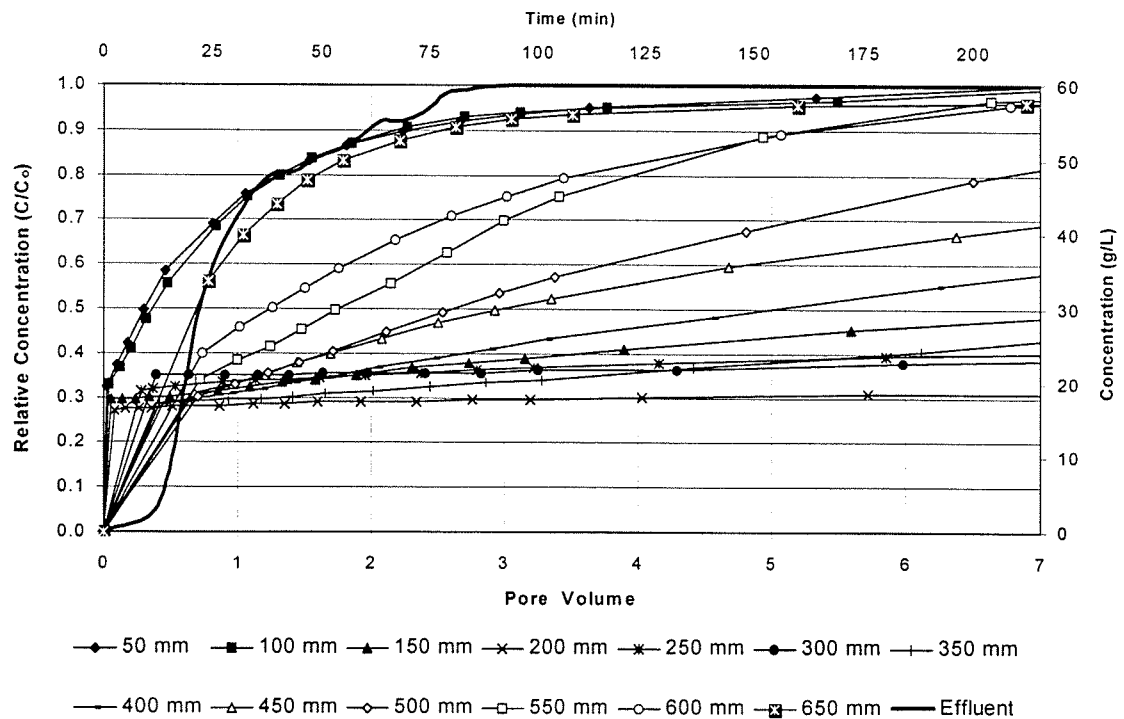


Figure 6.7: Breakthrough curves measured at thirteen depths along the soil column and in the effluent

even after 80 minutes, the concentration in the soil had not yet reached 60 g/L (i.e., inflow concentration). Therefore, the mobile pore-water fraction is not yet saturated with the tracer. These results ascertain the occurrence of macropore flow in the undisturbed soil column. Moreover, Figure 6.7 shows a quick increase at the very beginning of the breakthrough for all depth. Again, this is the result of macropore flow.

Concentration increased gradually at 50 mm and 100 mm depths. The relative concentration eventually reached 0.9 and the tracer build up became very slow. At that stage, one can assume that the soil matrix is almost saturated with the influent at 50 mm and 100 mm depths. A different shape of breakthrough curves can be observed for depths 150 to 400 mm. After a rapid increase to a relative concentration of approximately 0.3, the tracer build up was very slow. The rapid increase during the early stage of the breakthrough is due to macropore flow. Once macropores have been saturated with the inflow solution, the tracer diffuses from the macropores to the matrix flow domain. This explains the relatively slow increase in the remaining part of the breakthrough curve (BTC). This suggests that the solute front is located at a depth between 100 mm and 150 mm at the end of the breakthrough experiment. A faster rate of tracer build up can be observed for depths 450 and 650 mm. The BTCs for these depths suggest that the buildup is faster closer to the end of the soil column. This is attributed to the concentration gradient existing between these depths and the lower end of the soil column. As mentioned earlier, a space was created at the end of the soil column to permit to water to leave uniformly from the column's cross-section. This space reached the inflow concentration before the lower section of the soil core was saturated with the tracer due to macropore flow. Since the lower end of the column is at a higher

concentration, the tracer diffused upward against the direction of flow. This concentration gradient explains the high tracer build up at depth relatively close to the end of the column.

#### **6.4.2 Breakthrough in the matrix domain**

As mentioned above, the criteria of demarcation between flow domains was difficult to determine up to now. As a result, the demarcation between flow domains was arbitrarily defined. However, our approach provides means by which to monitor the breakthrough of water and non-reactive solutes through the matrix and macropore flow domains.

Results for the matrix flow domain are shown in Figure 6.8. A very fast increase in concentration can be observed for the 50 mm and 100 mm depths in the first few minutes of the breakthrough (Figure 6.8). It is followed by a more gradual tracer build up until it reaches inflow concentration. The shape of the BTCs for these depths is distinct from that of the lower depths. The explanation can be attributed to three factors. The first is the high macroporosity in the top region of the soil column (i.e., between 10 % and 20 % from 0 to 100 mm compared to less than 5 % at lower depths - see Fig. 6.2 for a visual representation of high macroporosity in this region). This high level of macroporosity contributes directly to fast diffusion in the matrix domain since it provides a greater exchange surface with the soil matrix. The second factor is the relatively short distance from the inflow concentration (i.e., top of the soil column) which creates a high concentration gradient. And the third factor is the presence of small pores that did not qualify in the macropore category but which play a significant role in breakthrough through the matrix domain. The fact that the relative concentration approaches 1 at the end of the breakthrough experiment suggests that the soil

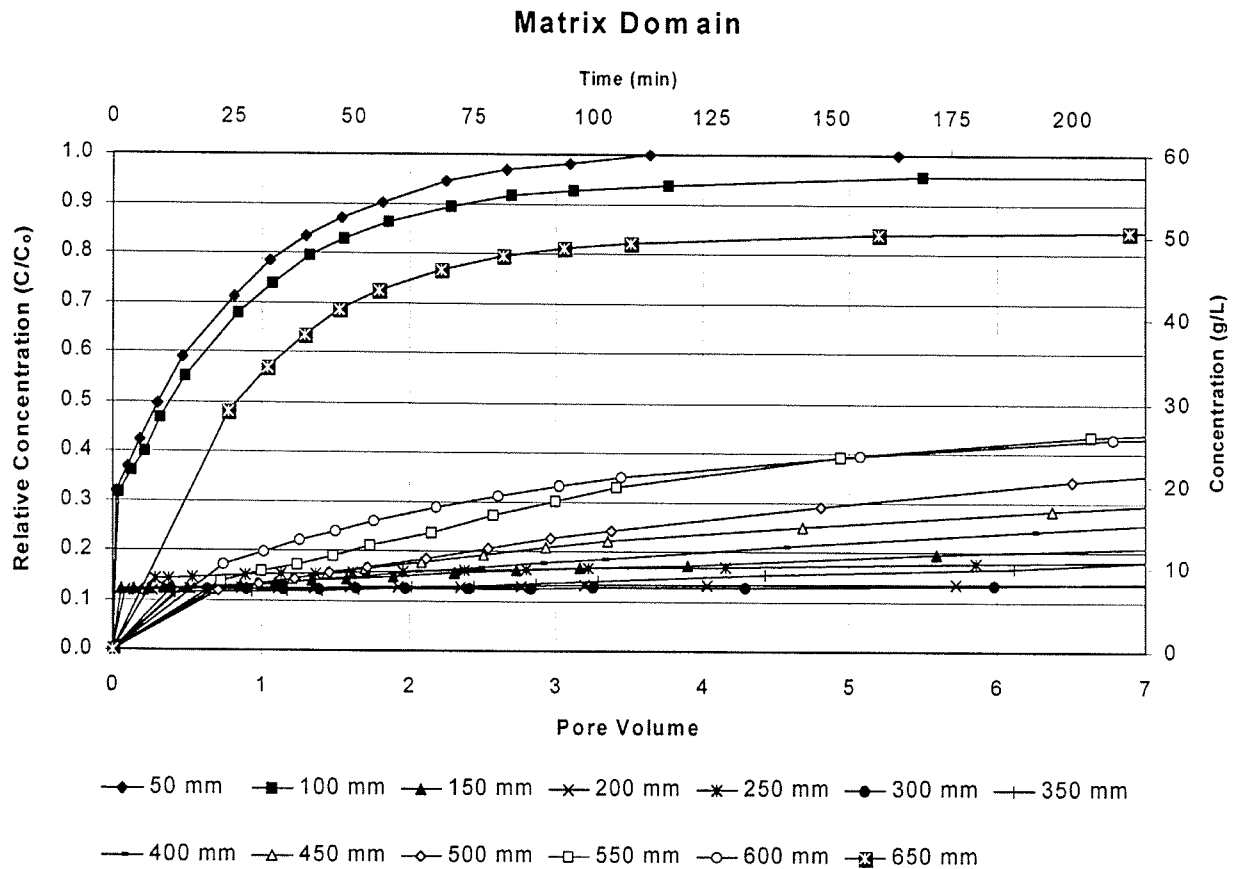


Figure 6.8: Tracer breakthrough in the matrix domain.

matrix is almost saturated with the tracer solution at depths of 50 and 100 mm. The solute front in the soil is therefore located close to a depth of 100 mm after 7 pore volumes (end of the breakthrough experiment).

A different breakthrough is observed for depths of 150 to 600 mm. The early breakthrough (i.e., before one pore volume) suggests that, (1) part of the matrix contains small pores (meso or micropores) that are connected to macropore networks and therefore contribute to a fast tracer build up, and/or (2) there is a rapid diffusion from the macropores to the matrix domain. After that initial build up, diffusion occurs at a slower rate as the radial distance from the source (i.e., macropore) gets more important. Again, as distance from the

end of the soil column decreases, the rate of tracer build up increases. This upward and counter flow diffusion in the soil matrix is quite obvious for the 650 mm depth, which is only 70 mm away from the end of the column.

### 6.4.3 Breakthrough in the macropore domain

Figure 6.9 shows the tracer breakthrough in the macropore domain. As expected, the shape of the breakthrough curves is quite different than that obtained for the matrix domain. At each scanned position, the relative concentration reaches 0.5 much before one pore volume. This strongly suggests occurrence of very rapid flow in the macropore

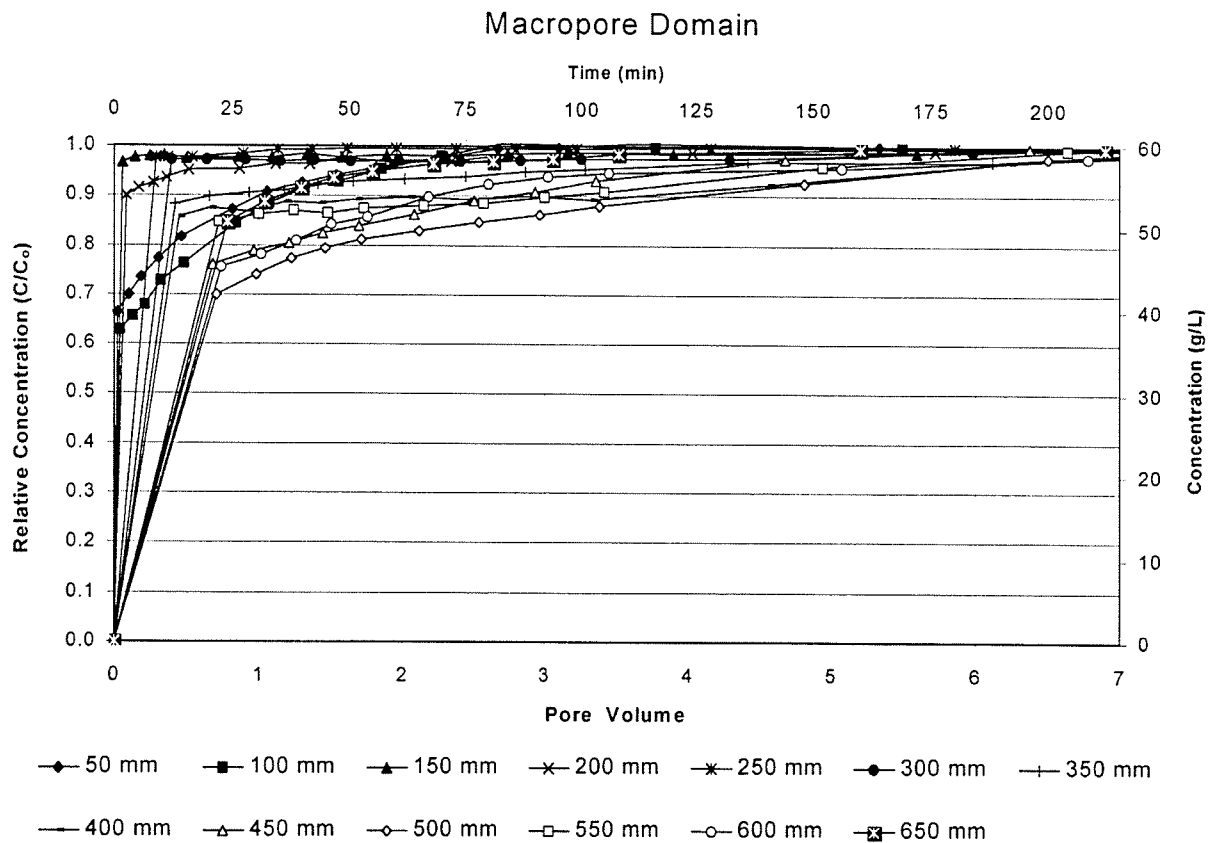


Figure 6.9: Tracer breakthrough in the macropore domain.

domain. Due to the scanning sequence which was used in order to concentrate on the top region of the soil column during the early breakthrough, some of the lower depths were scanned for the first time only 24 minutes after tracer application. Therefore, the build up rate might be even steeper for these lower depths.

The breakthrough at depths of 50 and 100 mm does not display the same characteristics as for other depths. After a rapid increase to a relative concentration of

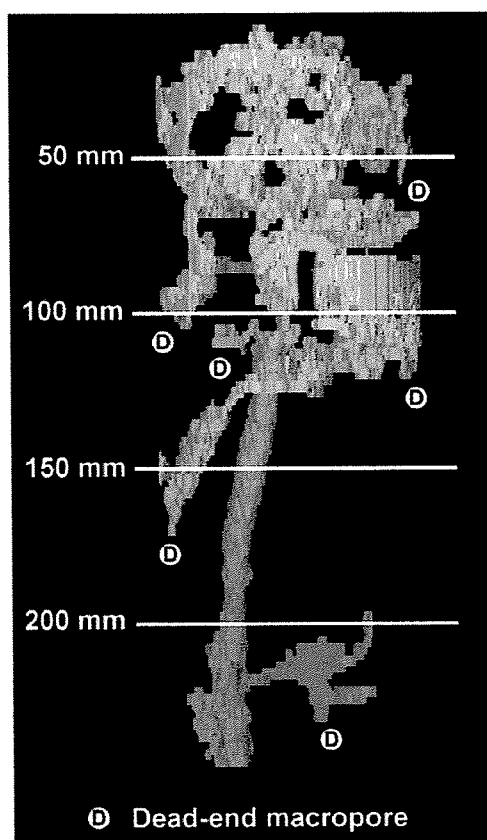


Figure 6.10: 3-D reconstruction of macropore network 6 with some of its dead-end macropores.

about 0.65, the tracer build up becomes much slower with a breakthrough typical of flow through the soil matrix. As mentioned earlier, the macroporosity at these depths is much higher than at lower depths. For instance, 13 macropores or macropore branches can be found at the 50 mm depth whereas, on average, only 4 are found at lower depths. Some of these macropores may be dead-end branches or cavities and therefore, may not contribute significantly to macropore flow. As a matter of fact, the breakthrough at the 50 mm and 100 mm depths suggests the presence of cavities and dead-end macropores. Although these cavities are part of the macropore domain from a geometrical point of view, their ability to transmit

water depends on matrix flow. Several dead-end branches were observed in one of the macropore networks branching out in this region of the soil column. Only a few of these

dead-end macropores are shown in Figure 6.10. As mentioned above, although the macroporosity at 50 and 100 mm depths is high, the breakthrough time is slower than at

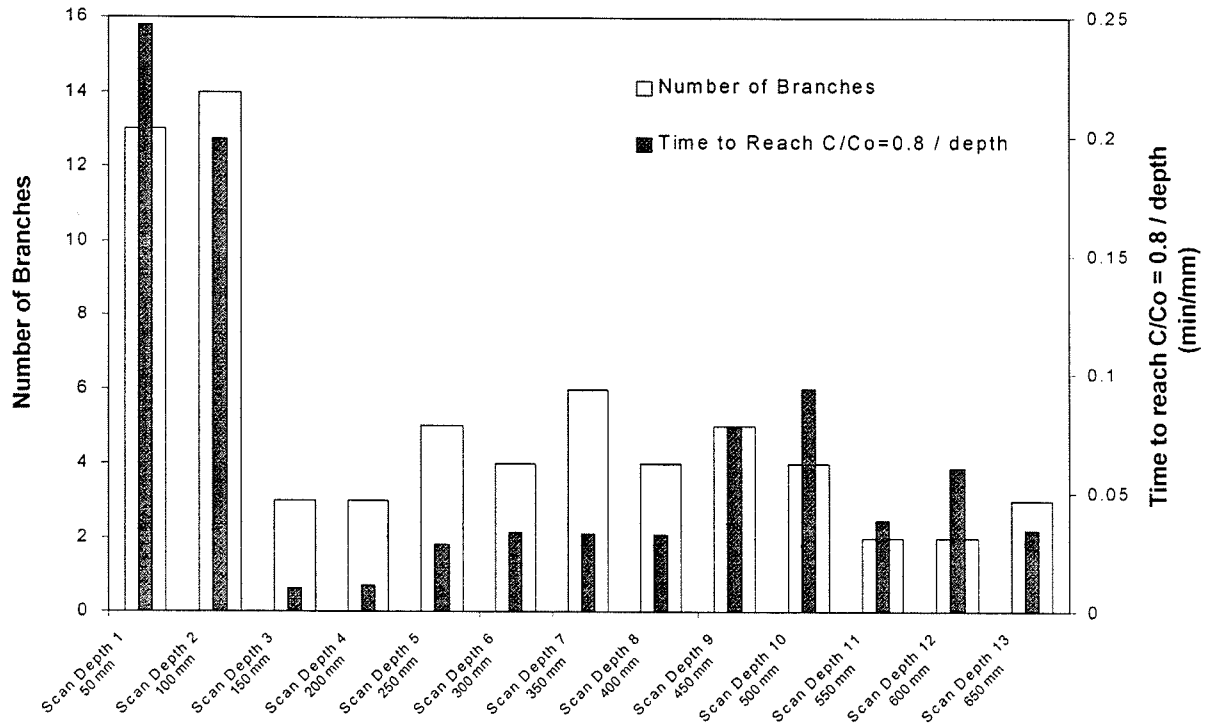


Figure 6.11: Number of macropore branches and normalized time to reach a relative concentration of 0.8 for every scanned positions

depths where the number of macropore networks or macropore branches is much lower. Thus, the question of the effective flow in the macropore domain arises. It would seem reasonable to assume that the greater the number of macropores, the faster the breakthrough. In order to investigate this relationship, the number of macropore branches and the time necessary to reach a relative concentration of 0.8 was evaluated (Figure 6.11). The time was normalized with depth. This was done to ensure that the effect of depth was taken into account. Although the 50 mm and 100 mm depths have the greatest number of macropore

branches, as shown in Figure 6.11, they seem less effective in transmitting water and tracer than the lower depths. For instance, with only 3 macropore branches, scan depths 3 and 4 reached a relative concentration of 0.8 in the least relative time. The overall trend in Figure 6.11 was verified with a relative concentration of 0.9. However, it was not evaluated for relative concentration less than 0.8 since the first concentrations recorded for 450, 500 and 600 mm depths were approximately equal to 0.75. Thus, extrapolation of relative concentrations below 0.75 would be imprecise since it would depend on the time lag between the beginning of the tracer application and the first scan taken at these depths. Our results strongly suggest that the number of macropore branches does not determine the ability of the macropore domain to be flow effective.

In this study, soil macropores were defined in terms of their geometrical characteristics under dry conditions using the definition given by Luxmoore et al. (1990):

*“ The term macropore includes all pores in a profile that are (generally) drained at field capacity, with the latter being 1 mm or more in equivalent diameter.”*

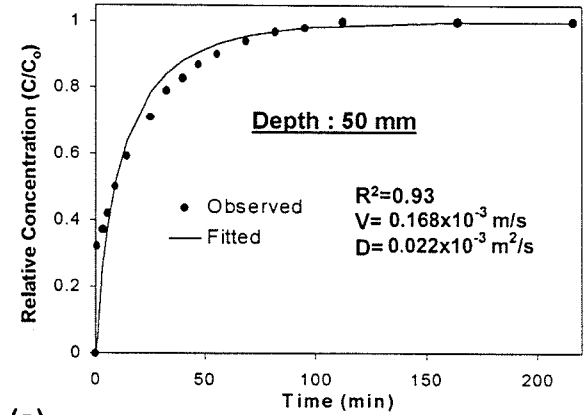
From a morphological point of view, this definition is satisfying. However, this definition has limitations when considering ability to convey water, solutes or even gases. Skopp (1981) proposed a definition of macroporosity based on its function where macroporosity: *“(...) designates the pore space which provides preferential paths of flow so that mixing and transfer between pores and remaining pores is limited. Macropores may consist of interaggregate pore space, shrink swell cracks, root channels, or fauna tunnels”*. Although this definition describes the flow processes occurring in soil and emphasizes the importance of pore structure on flow dynamics, it does not answer the question of how to isolate macropore domain. With the approach presented in this paper,



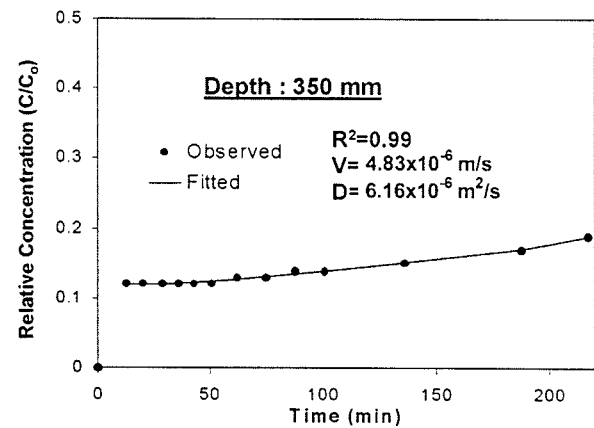
it could be possible to isolate the macropore domain by considering (1) the size of pores and (2) their ability to convey tracer by setting a pre-defined concentration threshold which depicts macropore flow in these pores. This approach will be investigated in future research.

#### 6.4.4 Modeling

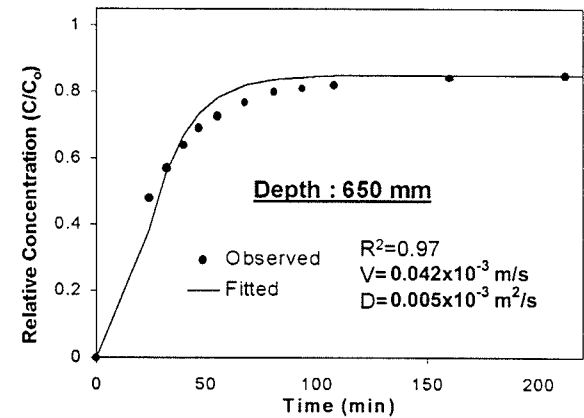
Figure 6.12 shows measured and simulated breakthrough curves in the matrix domain. The simulated breakthrough curves were obtained with the convective-dispersive model using the non-linear least square program, CXTFIT 2.0 (Toride et al., 1995). The convective term of the model describes the apparent pore-water velocity,  $V$ , which averages numerous local flow velocities (Li and Ghodrati, 1995). The dispersive term,  $D$ , is an overall dispersion coefficient used to



(a)



(b)



(c)

Figure 6.12: Observed and fitted breakthrough curves in the matrix flow domain for selected depths.  $R^2$  is the coefficient of determination of the regression between observed versus simulated values;  $V$  is the average pore-water velocity and  $D$  is the hydrodynamic dispersion coefficient.

characterize the effects of diffusion and hydrodynamic dispersion. High values of  $D$  indicate a great degree of hydrodynamic dispersion. In some cases, a retardation factor is used to describe the interactions between solute and soil. For this study, the retardation factor was fixed as 1.0 since the tracer used was non-reactive.

It seems that the CDE model described the BTCs at different depths quite well, reflected by high regression coefficients (Figure 6.12). However, the values of  $V$  and  $D$  used to fit the observed BTCs vary substantially for each depth. The pore-water velocity at the 350 mm depth, for instance, is almost two orders of magnitude lower than that at the 650 mm depth. This can be explained by the fact that pore-water velocity at the 350 mm depth was estimated without taking into account the early tracer build up (first 10 min of the breakthrough) in order to obtain a satisfying fit of the observed data. The early tracer build up indicates the presence of small pores connected to the main macropore networks. This strongly suggests that the matrix domain should be divided into two sub-domains, namely the mesopore and the micropore domain. The mesopore would account for the early tracer build up through pores smaller than macropores. CDE assumes that the entire water in the soil profile participates uniformly to solute transport. However, this assumption does not hold when considering one flow region in the matrix domain. By sub-dividing the matrix flow domain into two regions, the flux in each region will become more uniform and thus, this should lead to more accurate estimation of  $V$  and  $D$ .

The capabilities of CXTFIT model, based on the CDE, were tested to describe solute transport in the macropore domain. However, results showed a very poor fit of the rapid tracer build up in macropores. Thus, it was decided to use a different approach.

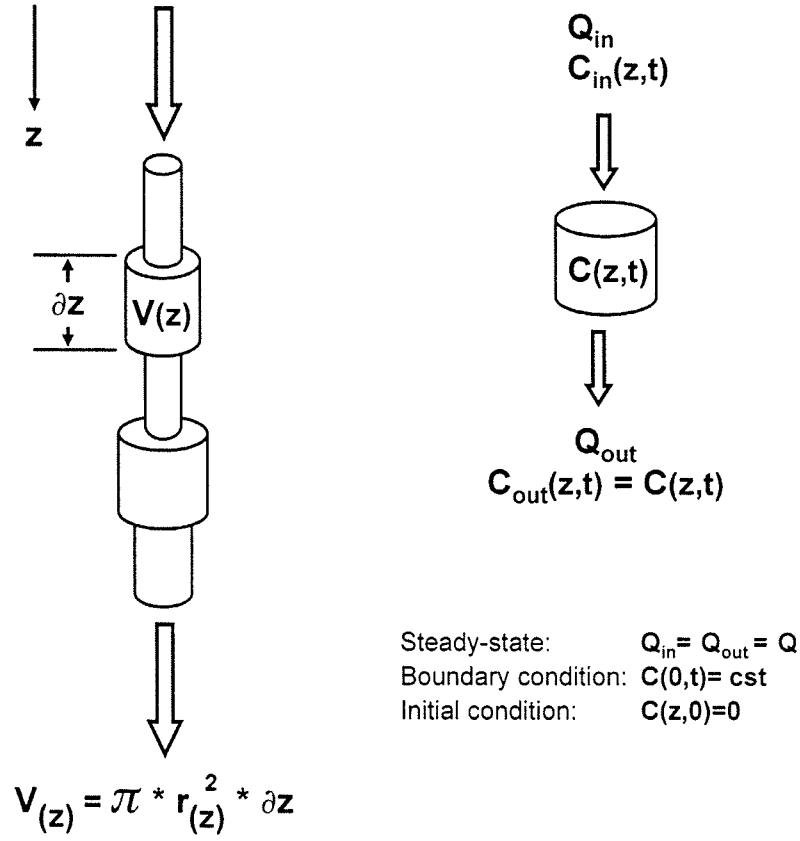


Figure 6.13: Schematic representation of macropores using the analogy with tubular reservoirs.

Solute displacement in macropores was modeled using the analogy between macropore networks and a series of small tubular reservoirs (Figure 6.13). Each reservoir has a volume  $V(z)$  equal to the scan thickness (i.e., 2 mm) multiplied by the average cross-sectional area of macropores at depth  $z$ . The incoming concentration,  $C_{in}$ , is equal to the concentration of the upper reservoir. The changes in concentration in each reservoir can be expressed as a simple first order homogeneous differential equation:

$$\frac{dC(z,t)}{dt} = \frac{[C_{in}(z,t) - C(z,t)]Q(z)}{V(z)} \quad (6.1)$$

where  $z$  is the depth [L],  $t$  is time [T],  $C(z,x)$  is the concentration of the reservoir [M/L<sup>3</sup>],  $C_{in}(z,t)$  is the incoming concentration [M/L<sup>3</sup>],  $Q(z)$  is the flow rate [L<sup>3</sup>/T] and  $V$  is the

volume of the reservoir [ $L^3$ ]. By multiplying Equation (6.1) with the integrating factor (i.e.,  $e^{Q(z)t/V(z)}$ ), we obtain the following differential equation:

$$\frac{d}{dt} \left( e^{\frac{Q(z)t}{V(z)}} C_{(z,t)} \right) = e^{\frac{Q(z)t}{V(z)}} \frac{[C_{in}(z,t)]Q(z)}{V(z)} \quad (6.2)$$

Integrating both sides from  $t=0$  to  $t=t$  and applying the initial condition  $C_{(z,0)}=0$ , we obtain:

$$C_{(z,t)} = C_{in}(z,t) \left( 1 - e^{-\frac{Q(z)t}{V(z)}} \right) \quad (6.3)$$

To simulate solute transport in the macropore domain using Equation (6.3), the boundary condition, as well as the flow rate,  $Q(z)$ , and the volume of each tubular reservoir,  $V(z)$ , need to be known. The boundary condition can be formulated for our breakthrough experiment as:  $C(0,t)=60$  g/L. Assuming that water flow is laminar and that the macropore is smooth and circular, the water flux through the pore can be estimated by the Poiseuille equation given as:

$$Q = \frac{\pi r^4 g}{8 \nu_k} \times \frac{\Delta H}{\Delta L} \quad (6.4)$$

where  $Q$  is the rate of volume flow through the pore ( $m^3/s$ ),  $r$  is the effective radius of the pore (m),  $g$  is the acceleration due to gravity ( $9.81 \text{ m/s}^2$ ),  $\nu_k$  is the kinematic viscosity

( $1.01 \times 10^{-6} \text{ m}^2/\text{s}$  for water at  $20^\circ \text{C}$ ),  $\Delta H$  is the pressure head (m) and  $L$  is the length of the pore(m). Ahuja et al. (1993) developed a model and studied characteristics of preferential flow using Poiseuille's law. They concluded that: *"further experimental studies on the nature and geometry of macropores and the nature and dynamics of flow in them are certainly needed"*. With the CAT scanning approach, the geometry of macropores was characterized in a very detailed manner. Therefore, we suggest a few modifications to Equation (6.4) in order to take into account the overall tortuosity and the distribution of macropore size at every depth:

$$Q_{\text{macropore-laminar}}(z) = \frac{\pi g}{8 \nu_k} \times \frac{\Delta H}{\tau \Delta L} \int_{r_{\min}}^{r_{\text{critical}}} f_s(r, z) [r(z)]^4 dr \quad (6.5)$$

where  $Q_{\text{macropore-laminar}}$  is the flow rate in the laminar region of macropore domain at depth  $z$ ,  $\tau L$  is the effective length of the macropores where  $\tau$  is the overall tortuosity,  $f_s(r, z)$  is the distribution density function of macropore sizes at depth  $z$ , and  $r(z)$  is the radius of the macropores at depth  $z$ . The pressure head is applied over entire length of macropores. Thus, the average macropore length was computed by multiply the column length with tortuosity in Equation (6.4). This results in a lower hydraulic gradient which accounts for losses induced by tortuosity. Moreover, instead of using an average macropore radius in Equation (6.3), it was decided to integrate the macropore size distribution to take into account the different macropore sizes.

As mentioned above, Poiseuille's law assumes that flow is laminar. However, flow in large macropores may be turbulent. In order to describe the flow regimes in the

macropore domain, we propose to divide it into two flow region: laminar and turbulent. The Reynolds number is commonly used to determine the flow regime. In a flow inside a rough-walled pipe, it is found that the transition between laminar and turbulent flow occurs at a Reynolds number of approximately 2000 (Potter et al., 1997). This quantity, often called critical Reynolds number ( $Re_{critical}$ ), is given as:

$$Re_{critical} = \frac{\mathcal{V} 2 r_{critical}}{\nu_k} \approx 2000 \quad (6.6)$$

where  $\mathcal{V}$  is the velocity (m/s),  $r_{critical}$  is the radius of the pore (m) at which the transition occurs. Since the flow velocity is equal to flow rate divided by area, Equation (6.6) can be modified as:

$$r_{critical} = \frac{1000 \nu_k A}{Q} \quad (6.7)$$

Combining Equation (6.4) and (6.7), we obtain:

$$r_{critical} = \sqrt[3]{\frac{8000 \nu_k^2 \Delta L}{g \Delta H}} \quad (6.8)$$

Given that the hydraulic gradient was maintained at 0.1 m during the breakthrough experiment and that the column length was 0.72 m,  $r_{critical}$  was found to be 1.82 mm from Equation (6.8). Therefore, we assumed that water flow in macropores greater than 3.63 mm in diameter was turbulent.

Chen and Wagenet (1992) suggested that average macropore flow velocities under turbulent condition could be approximated with Manning's formula:

$$v = \frac{R_{\text{hydraulic}}^{\frac{2}{3}} S^{\frac{1}{2}}}{\eta_r} \quad (6.9)$$

where  $v$  is the velocity (m/s),  $R_{\text{hydraulic}}$  is the hydraulic radius (m) (i.e., ratio of the cross-sectional water area of the conduit over the wetted perimeter),  $S$  is the slope of the energy line (m/m), and  $\eta_r$  is the roughness coefficient. The slope of the energy line is simply  $\Delta H / \Delta L$ , and the flow rate can be computed by multiplying the velocity by the area. Thus, Equation (6.8) can be rewritten in term of the flow rate as:

$$Q = \frac{\pi r^2}{\eta_r} \times \sqrt{\frac{\Delta H}{\Delta L}} \times R_{\text{hydraulic}}^{\frac{2}{3}} \quad (6.10)$$

The flow rate in the turbulent regions of the macropore domain can be estimated using Equation (6.10). However, it was decided to incorporate the distribution of macropore size, the distribution of hydraulic radius and macropore tortuosity in Equation (6.10) to get a better representation of the macropore geometry. Using the same rationale as in Equation (6.5), the following Equation was obtained:

$$Q_{\text{macropore-turbulent}}(z) = \frac{\pi}{\eta} \times \sqrt{\frac{\Delta H}{\tau \Delta L}} \times \left[ \int_{r_{\text{critical}}}^{r_{\text{max}}} f_s(r, z) [r(z)]^2 dr \right] \left[ \int_{r_{\text{critical}}}^{r_{\text{max}}} f_r(r, z) [R_{\text{hydraulic}}(r, z)]^{\frac{2}{3}} dr \right] \quad (6.11)$$

where  $Q_{\text{macropore-turbulent}}$  is the flow rate in the laminar region of macropore domain at depth  $z$ ,  $f_r(r,z)$  is the distribution density function of macropore hydraulic radii at depth  $z$ , and  $R(r,z)$  is the hydraulic radius of macropore size  $r$  at depth  $z$ . Finally, Equations (6.5) and (6.11) can be combined to approximate the water flux in the macropore domain at depth  $z$ :

$$Q(z)_{\text{macropore}} = Q(z)_{\text{macropore-laminar}} + Q(z)_{\text{macropore-turbulent}} \quad (6.12)$$

Several macropores properties are necessary to solve Equations (6.3) and (6.12) and simulate solute transport in the macropore domain of the soil. In practice, the distribution density function of macropore size,  $f_s(r,z)$ , and hydraulic radii,  $f_r(r,z)$ , at a given depth  $z$ , the overall tortuosity  $\tau$ , the macropore size  $r(z)$  and hydraulic radius  $R(r,z)$ , and the volume of each tubular reservoir  $V(z)$  at depth  $z$  are very difficult to obtain. However, all these parameters can be quantified using 2-D and 3-D reconstruction of macropores from CAT scan data and are presented in Perret et al. (1998a, 1998b). Chen and Wagenet (1992) pointed out that it reasonable to assume that  $h_r$  is equal to 0.13 for the surface of macropores. Solute transport in the macropore domain can then be simulated using Equations (6.3) and (6.12). For that purpose, a computer program, called Modeljo.pro, was developed in the PV-WAVE language.

Modeling results in the macropore domain at depths 200, 350 and 550 mm are shown in Figure 6.14. The model describes the overall tendency of the breakthrough in macropores with R-squared values between 0.58 and 0.85. Figure 6.14 suggests that the relative concentrations computed with Modeljo.pro are greater than that of the observed



values. This indicates that (1) the model overestimates the breakthrough time/concentrations, (2) the observed breakthroughs in the macropore domain tend to underestimate breakthrough in macropores or, a combination of (1) and (2). As mentioned above, the macropore domain in our study was defined in terms of macropore geometry instead of a combination of geometry/functionality. This may result in an underestimation of observed breakthrough in the macropore domain.

Figures 6.14b and 6.14c were obtained using an additional algorithm to account for the presence of macropore necks. Necks (also known as throats) are an important feature of macropore geometry which directly affects percolation rates. It is defined as the

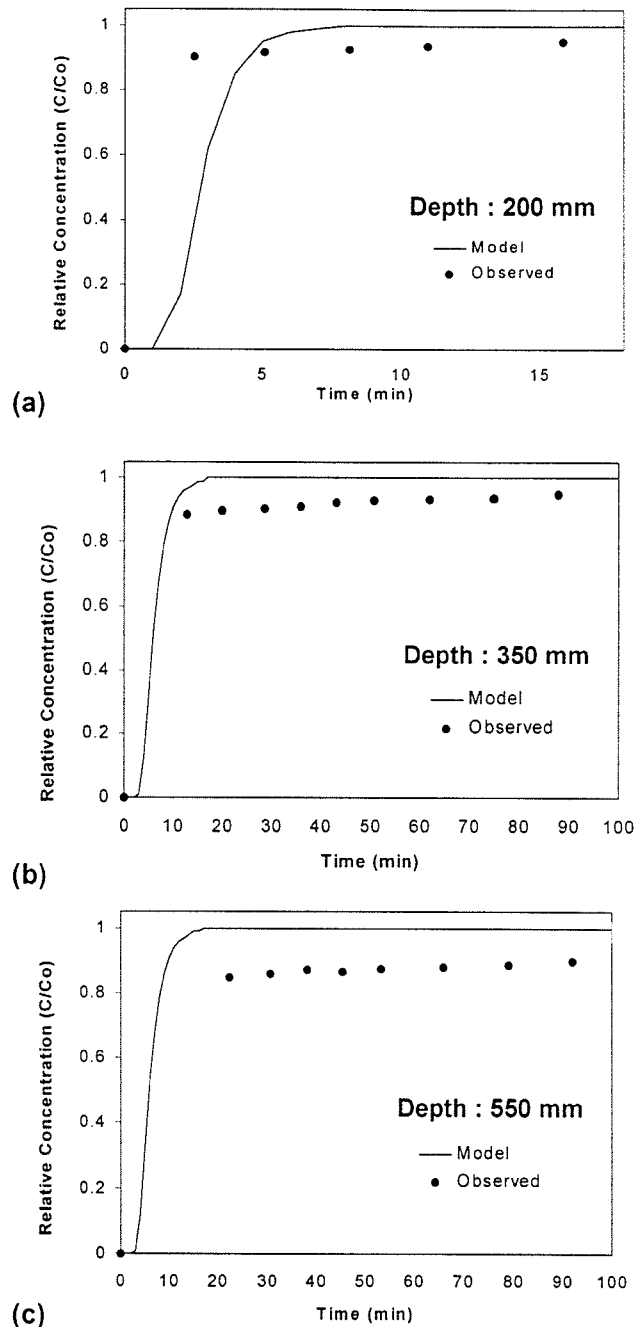


Figure 6.14: Observed and modeled breakthrough in the macropore domain at (a) depth=200 mm, (b) depth=350 mm and (c) depth=550 mm.

local minimum in pore space size (Kwiecien et al., 1990). Since necks restrict and control flow rate in continuous macropores, their presence should be accounted for. The soil column was divided into 7 sections. The minimum flow rate or flow rate in macropore necks was used in Equation 6.3 for every section. It should be mentioned, however, that necks control flow when macropore networks show a great degree of continuity. Therefore, this algorithm was considered in the lower section of the soil column where most of the continuous macropores are. In the upper section of the column, there was no need to apply this algorithm since networks are small and discontinuous (Figure 6.2a).

Although the model provides an acceptable estimate of the breakthrough of non-reactive solute in fully saturated conditions, there are several adjustments that could be made in order to improve the model. Presently, the model averages the macropore volume for every 2 mm section and does not consider the continuity of networks. A macropore network is defined as a set of macropores that are interconnected such that there is a passage from any part of the set to every other part (Scott et al., 1988a). In a previous study (Perret et al., 1998b), every macropore network were isolated. Instead of volume averaging macropores for every section, calculations can be made at a network level to compute flow rates. The minimum flow rate in each branch should then be isolated in order to consider flow restriction caused by the macropore necks. This approach has the advantage of taking into account macropore continuity.

Another improvement can be made by considering the interactions between the matrix domain and the macropore domain (Figure 6.15). Perret et al. (1998b) have presented an approach to evaluate the macropore wall-area. This provides a good insight

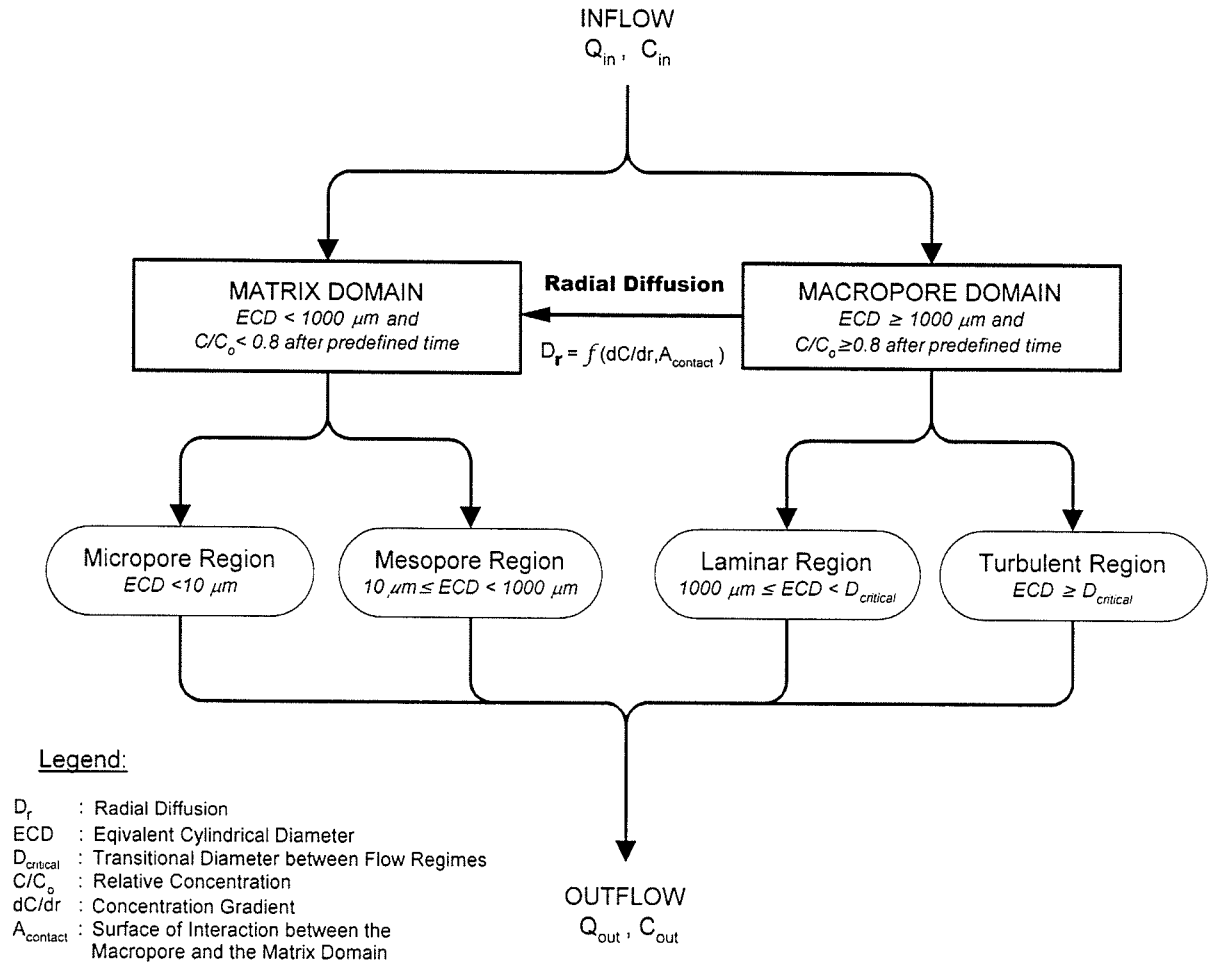


Figure 6.15: Schematic representation of the improved multi-regions system.

on the interactions between the two domains. In saturated conditions, solute will diffuse from macropores to the matrix in radial fashion, following Fick's second law, as the main driving force is induced by concentration gradient (i.e., diffusion). Moreover, the macropore domain should be thresholded based on geometry (i.e.,  $ECD \geq 1000 \mu m$ ) and on capacity to transport solute (i.e., predefined time to reach  $C/C_o = 0.8$ ). These modifications will be more representative of the actual solute transport in a macroporous soil. They will be implemented in a modified version of Modeljo.pro in the future.

## 6.5 Summary and Conclusions

Although macropore occupy only a fraction of total soil porosity, they have a great effect on water movement and chemical transport. Research efforts have been made to determine and model the dynamics of macropore flow. Stochastic methods and deterministic approaches have been developed for this purpose. However, it is still not possible to quantitatively predict water and chemical movement in soil containing macropores. Several researchers have pointed out the potential offered by multi-region modeling. This modeling approach relies on the simplification of the flux into several regions. Until now, the criteria used to define boundaries between flow regions were indeterminate and arbitrarily selected. To explore the full potential of multi-region modeling, the development of a reliable method for isolating and characterizing flow domains is needed.

An X-ray CAT scanner was used in this study to monitor breakthrough of a non-reactive solute in a macroporous soil. More precisely, the spatial distribution of solute was measured at thirteen depths along an undisturbed soil column. Several computer programs were written in the PV-WAVE language to quantify the three-dimensional geometry of macropore. With the knowledge of the macropore structure and the spatial distribution of the solute, breakthrough in the macropore and matrix flow domains was evaluated. Not only this innovative approach allowed us to isolate flow regions but also to monitor solute breakthrough in a non-destructive manner and in real-time at different depths in soil.

A visual inspection of the tracer spatial distribution at different times and depths indicates regions of high concentrations. These regions depict flow in macropores. Very

soon after the tracer application, the occurrence of macropore flow was detected. It took approximately 2.75 pore volumes to reach the inflow concentration in the effluent. However, after 2.75 pore volumes the mobile fraction of the water throughout the soil column did not yet reach more than 75 percent of the inflow concentration. This suggests that the solute has moved preferentially in the macropore domain of the soil. Flow in the matrix domain suggested that part of the matrix contains small pores that are connected to macropore networks. These pores contribute to a rapid tracer build up in the matrix domain. They were identified as mesopores. This suggests that the matrix domain should be sub-divided into two regions: the mesopores and the micropores.

Flow in the macropore domain strongly indicated the presence of preferential flow. It also suggested that a fraction of the flow in macropores was relatively slow. This was due to the presence of dead-end branches or cavities, which, from a geometrical point of view, belong to the macropore domain but do not behave as macropores since they do not contribute to preferential flow. Therefore, the question of effective flow in the macropore domain arises. This suggests that the macropore domain should be defined both in terms of the geometry of macropores and of their ability to convey tracer preferentially. With the approach presented in this paper, the macropore domain could be isolated by considering pores with an equivalent cylindrical diameter greater or equal to 1000  $\mu\text{m}$  and by thresholding macropores which reach a relative concentration of 0.8 after a predefined time.

The breakthrough curves measured in the matrix domain were fitted using the convection dispersion equation (CDE) with CXTFIT 2.0. The high regression coefficients obtained suggest that the CDE model describes breakthrough in the matrix

domain quite well. Solute transport in the macropore domain was modeled using the analogy between macropore flow and pipe flow. The macropore domain was divided into two regions, namely, the laminar and the turbulent regions. A modified version of Poiseuille's law was used to model solute breakthrough in the laminar region. For the turbulent region, a formula was derived based on Manning's equation. The modifications were done so that these simple models would take into account the distribution density functions of macropore size and hydraulic radius. Modeling results suggest that this approach provides a reasonable approximation of the overall tendency of the breakthrough in the macropore domain. Several improvements could be made. As mentioned above, the macropore domain should be thresholded based on geometry (i.e.,  $ECD \geq 1000 \mu m$ ) and on capacity to transport solute (i.e., predefined time to reach  $C/C_0 = 0.8$ ). Moreover, the model should work at a network level to take into account macropore continuity. Considering radial diffusion from the macropores to the matrix domain could lead to another improvement.

## 6.6 Acknowledgements

The authors wish to thank Daniel Marentette for his help and suggestions in the technical part of this work. The authors also gratefully acknowledge the financial support provided by the Natural Sciences and Engineering Research Council of Canada (NSERC) and ESTAC (Environmental Science and Technology Alliance Canada).

## PREFACE TO CHAPTER 7

The analysis of soil macropores and preferential flow, presented in chapters 3 through 6, was based on the data generated by CAT scanning. X-ray CAT is primarily designed for the visualization of an object's structure. Another non-invasive imaging technique is Single Photon Emission Computer Tomography (SPECT). SPECT scanning can be seen as a complementary approach to CAT imaging since it allows for the visualization of a dynamic process or organ function at a sub-second level. Single Photon Emission Computer Tomography is based on the detection of nuclear radiation injected into an object. It provides a powerful tool for visualizing and characterizing temporal and spatial changes of radionuclide concentrations. This technique allows for the detection of functional changes, occurring within minutes to hours, that may otherwise be difficult to investigate in static images. As a result, SPECT scanning is an ideal tool for visualizing and quantifying tracer displacement, in a non-destructive manner, in dynamic flow studies.

Although SPECT imaging has been commonly used in hospitals, it has rarely been applied to engineering and has never been introduced to a discipline such as soil physics. The primary objective of Chapter 7 is to investigate the capabilities of SPECT scanning for visualizing preferential flow in soil.

The basic principle of SPECT scanning and its applications are reviewed in this chapter. The methodology and results of tracer breakthrough in four soil columns is also presented. Visualization and analysis of radioactive tracer flow patterns in 2-D, using

planar imaging, and in 3-D, with the tomographic capabilities of the SPECT scanner, are also discussed. Our results suggest that SPECT scanning can bring a new dimension to 2-D and 3-D dynamic tracer studies in soils.

Several computer programs were developed in PV-WAVE for this study. These programs are included in the attached CD-ROM. This chapter has been submitted for publication. For the sake of completeness, some material in this chapter is repeated from previous chapters so that this paper can stand on its own. (Perret J.S., S.O. Prasher, A. Kantzas, K. Hamilton and C. Langford. 1998. Soil-core breakthrough in intact soil columns measured by SPECT scanning. Submitted to the Soil Science Society of America Journal). The candidate was responsible for designing and conducting the research experiments, developing computer codes for the visualization and analysis of data and finally, preparation of this manuscript. Dr. Shiv O. Prasher, professor at the Agricultural and Biosystems Engineering Department of McGill University, contributed in all aspects of this research project. He provided the necessary funds and assistance for this research, including the supervisory guidance and revision of this paper before its submission for publication. Dr. A. Kantzas, Director of the Tomographic Imaging and Porous Media (TIPM) Laboratory in Calgary, Alberta, and associate professor at the University of Calgary's Department of Chemical and Petroleum Engineering, provided access to SPECT scanning facilities of the TIPM laboratory. Dr. Kantzas also made invaluable suggestions during SPECT scannings. Ms. K. Hamilton, nuclear research technologist at TIPM laboratory, provided help and guidance at the experimental stage of this research. Dr. C. Langford, University of Calgary's vice-president research and



professor at the Department of Chemistry, was the principal investigator for the NSERC Collaborative Project Grant.

## CHAPTER 7

# SOIL-CORE BREAKTHROUGH IN INTACT SOIL COLUMNS MEASURED BY SPECT SCANNING

---

### 7.1 Abstract

Single photon emission computed tomography (SPECT) is an imaging technique widely used in medical diagnosis. This technique has never been applied to soils. The objective of this study was to investigate the capabilities of SPECT scanning for visualizing preferential flow in soil. This paper describes the principle of SPECT scanning and its application to tracer breakthroughs in four large undisturbed soil columns (800 mm x 77 mm diameter). This new approach allows real-time analysis of flow patterns of radioactive tracers in 2-D, using planar imaging, and in 3-D, with the tomographic capabilities of the SPECT scanner. Not only does SPECT scanning provide qualitative data, but it also allows for quantification of the tracer's spatial distribution. Our results characterized preferential flow very clearly in soil columns. SPECT scanning opens new avenues for 2-D and 3-D tracer studies in porous media such as soil.

## 7.2 Introduction

Water and solutes transport through soil macropores can be quite significant and is now well documented (Perret et al., 1997, Perret et al., 1998a; Beven and Germann, 1982; Bouma, 1990; Hamblin, 1985; Logsdon, 1995; McCoy et al., 1994; Steenhuis et al. 1990; Singh and Kanwar, 1991; White, 1985). Macropore flow results in rapid movement of water and solutes through the soil profile with important implications for groundwater quality. Short travel time may not allow contaminants, such as pesticides, to be adsorbed on and into soil particles. Consequently, most solutes in the water will be quickly delivered to the drains or groundwater aquifers without being degraded by chemical and biological actions. However, quantification and prediction of preferential flow has been difficult due to the complexity of the inference of soil structure.

Knowledge of soil structure, along with a suitable technique for measurement of water and associated solutes flow characteristics through soil, is essential to understanding the mechanisms of preferential flow. Unfortunately, progress in this area has been severely limited by difficulties in obtaining direct and non-destructive measurements of the preferential flow in a structured soil. CAT scanning offers a powerful approach to study preferential flow (Perret et al. 1998c). However, whereas CAT scanning provides high resolution cross-sectional images in usually more than a second, Single photon emission computed tomography (SPECT) allows for longitudinal views at a sub-second level. SPECT has never been applied to soil studies and may provide a new and exciting approach for visualization and characterization of preferential flow phenomenon. The primary objective of this paper is to investigate the capabilities of SPECT scanning for visualizing preferential flow in soil during solute breakthrough.

### 7.3 Single Photon Emission Computed Tomography

Single photon emission computed tomography (SPECT) is based on detecting nuclear radiation emitted from the body or an object in which a very small amount of radioactive material, called radiopharmaceuticals, has been introduced. A special type of camera, known as a scintillation or gamma camera, is used to transform these radioactive emissions into images or data which describe the location and intensity of these emissions.

SPECT scanning is widely used as a diagnostic technique in nuclear medicine. 10 to 12 million nuclear medicine imaging and therapeutic procedures are performed each year in the US alone (SNM, 1998). Today, nearly all cardiac patients in developed countries receive a SPECT scan to detect arterial diseases or a damaged heart. Investigation of the liver, kidneys, thyroid gland and many other organs are, similarly, leading applications of SPECT (Coleman et al., 1986). It is used routinely to help diagnose restriction of blood flow to parts of the brain, cancer, stroke, lung disease and many other physiological abnormalities.

Scintillation camera technology has been used in the industrial applications since the mid 1980s. For instance, photon emission imaging has been used to perform visual and radiometric scans of nuclear facilities. Sedaghat et al. (1988) developed a technique to characterize cross flow in a two sub-channel nuclear fuel assembly using a gamma camera. Gamma camera technology has also been adapted to conduct contamination surveys inside buildings connected with nuclear production (Chesnokov et al., 1997; Mottershead and Orr, 1996).

The gamma camera has also brought a new dimension to disciplines such as particle tracking and flow analysis in mixing reactor vessels. Castellana and Dudley (1984) were among the first researchers to visualize particle motion in fluid-solid systems using a gamma camera. With a similar approach, Lin et al. (1985) measured the solid motion of radioactive particles, in gas fluidized beds, with a series of photomultiplier tubes. Still today, radioactive particle tracking offers great potential for measurement of recirculating phase velocities in gas-fluidized beds and bubble columns (Hamilton et al., 1997). Scintillation cameras have also been used in determining the hydrodynamics and radial distributions of velocity in vertical riser reactors and mixing reactor vessels (Castellana et al., 1984; Berker and Tulig, 1986; Legoupil et al., 1997). The potential of SPECT scanning for imaging a gas-flow fluidization test rig and fluid flow in a gasification unit is discussed by Jonkers et al. (1990). Other applications to the field of engineering include measurements of liquid film thickness on the surface of a rotating disk (Castellana and Hsu, 1984) and analysis of the radioactive ball trajectories within the charge of a rotary grinding mill (Powell and Nurick, 1996).

Nuclear technology has also been utilized in oil recovery fields to visualize dynamic oil displacement in porous media. For instance, Huang and Gryte (1988) used a gamma camera to observe immiscible displacement of oil in thin slabs of a porous medium saturated with water. In their study, Technitium-99m was used as a tracer for the water phase. The authors showed that photon emission imaging provides a powerful approach to determining local fluid saturations in quantitative terms. Lien et al., (1988) studied the one-dimensional distribution of saturation in 0.75 m long sandstone cores, operating at reservoir pressure and temperature. Information on one-dimensional fluid

saturation distributions was obtained by labeling fluid phases with nuclear tracers and detecting radiation with a gamma camera. They reported that the apparatus fulfilled its objective, i.e., imaging displacement processes at reservoir conditions. Charlier et al. (1995) applied gamma ray absorption techniques in order to determine the permeability of oil during a tertiary gas gravity drainage experiment. Using this technique, they were able to visualize fluid saturation distribution in the core as a function of the injected gas' volume.

Although the power of non-invasive and *in situ* SPECT scanning has been demonstrated for dynamic industrial processes, and for oil recovery, this technique has never been applied to soil studies, nor to the visualization and characterization of preferential flow. This approach opens new avenues, both in 2-D and in 3-D, for tracer studies in porous media, such as soil.

## **7.4 Materials and Methods**

As stated earlier, this study is the first of its kind dealing with the application of SPECT scanning in soil hydrology. Therefore, the materials and methods section includes some introductory material on the SPECT scanning process. This section is divided into five sub-sections. The first sub-section presents the extraction and preparation of the column. The second sub-section describes breakthrough measured by SPECT scanning while the third one deals with the basic principles and operation of the SPECT scanner. The following sub-section presents the radioactive tracer. Finally, the last sub-section discusses the processing data generated by SPECT scanning.

#### **7.4.1 Soil core extractions and column preparation**

Four undisturbed soil columns, 800 mm in length and 77 mm in diameter, were taken from a field site at the Macdonald Campus of McGill University in Quebec, Canada. The soil cores were obtained by driving a polyvinyl chloride (PVC) pipe into the soil with a backhoe. The lower end of the PVC pipe was the shape of a thin cutting edge in order to reduce compaction inside the column and to facilitate pipe insertion into the soil. PVC caps were installed so as to create an empty space at the end of the column. This space allows water and tracers to penetrate uniformly through the column cross-section. A plastic screen was placed on both ends of the soil column to prevent the soil from collapsing. One of the soil columns was drilled from top to bottom in order to verify the gamma camera's ability to portray preferential flow in this pore. This artificial macropore consisted of a polyethylene tube, 1 mm in inner diameter. Air inside the soil columns was removed by diffusing CO<sub>2</sub> through the soil columns for a period of 24 hours. Since CO<sub>2</sub> dissolves in water, empty spaces were easily saturated. After filling the soil cavities with CO<sub>2</sub>, undisturbed soil cores were slowly saturated by gradually increasing the water level over a period of 3 days. Prior to core saturation, the water was de-aerated in a 25-L vessel that was connected to a vacuum pump.

#### **7.4.2 Breakthrough measured by SPECT scanning**

The breakthrough experiment was performed on four saturated soil columns. A hydraulic gradient of 0.1 m was maintained at the upstream face of the soil columns in order to reach steady-state flow. A simple system was constructed for this purpose and is described in Perret et al. (1998c). A thin layer of mineral oil was maintained on top of the water so as to minimize gas exchange between air and de-aerated water. A tracer

pulse (i.e., 60 ml of radioactive solution at approximately 11.5 mCi) was initiated at the upstream end of the soil columns. Samples were collected in the effluent every 30 seconds. The radioactivity level was evaluated with the gamma camera at the end of the breakthrough experiments. Sampling time was carefully taken in order to account for radioactive decay and to estimate flow rate. During the tracer breakthrough, the spatial distribution of radioactivity was monitored in the soil column with a SPECT scanner. A small cotton thread, saturated with a radioactive solution, was taped around the soil columns to delimit their boundaries.

#### **7.4.3 SPECT scanning**

A Siemens Orbiter was used for this study (Figure 7.1). This equipment is located at the Tomographic Imaging and Porous Media (TIPM) laboratory in Calgary, Alberta, Canada. It consists of three main components: the Orbiter detector stand assembly, the operator's console and the NucLear MAC computer. The latter is a Power PC with



Figure 7.1: Siemens Orbiter Gamma Camera at the TIPM laboratory in Calgary (Alberta).



NucLear software for displaying and processing SPECT data installed on it. This computer is used to acquire, display, store and post-process data generated by the gamma camera. To understand the basic concepts of SPECT scanning, let us follow the process from emission of gamma radiation to images/matrices generated by the NucLear MAC computer. The radioactive source emits gamma rays in all directions. The first task is to detect radiation. This is achieved by the gamma camera of the Orbiter stand assembly. The main components of the gamma camera are the collimator, the NaI crystal and the photomultiplier tubes. Their functions are briefly discussed below.

#### 7.4.3.1 Collimator

The collimator's purpose is to mechanically confine the direction of incident photons and to localize the site of the emitting source (Cho et al., 1993). Collimation has the greatest effect on determining the SPECT system's spatial resolution and sensitivity. Sensitivity of a SPECT scanner relates to how many photons per second are detected. The spatial resolution relates to the size of each picture element. The collimator contains thousands of hexagonal parallel channels through which gamma rays are allowed to pass. The gamma camera used in this study has a spatial resolution of approximately 4 mm.

#### 7.4.3.2 NaI crystal and photomultiplier tubes

Gamma rays, traveling along a path that coincides with one of the collimator channels, pass through the collimator unabsorbed and interact with a large NaI crystal, creating light. These photons are then guided toward photocathodes on an array of photomultiplier tubes (light sensitive), where they are converted into electrons, multiplied and finally, converted into an electrical signal (Cho et al., 1993). In other words, behind

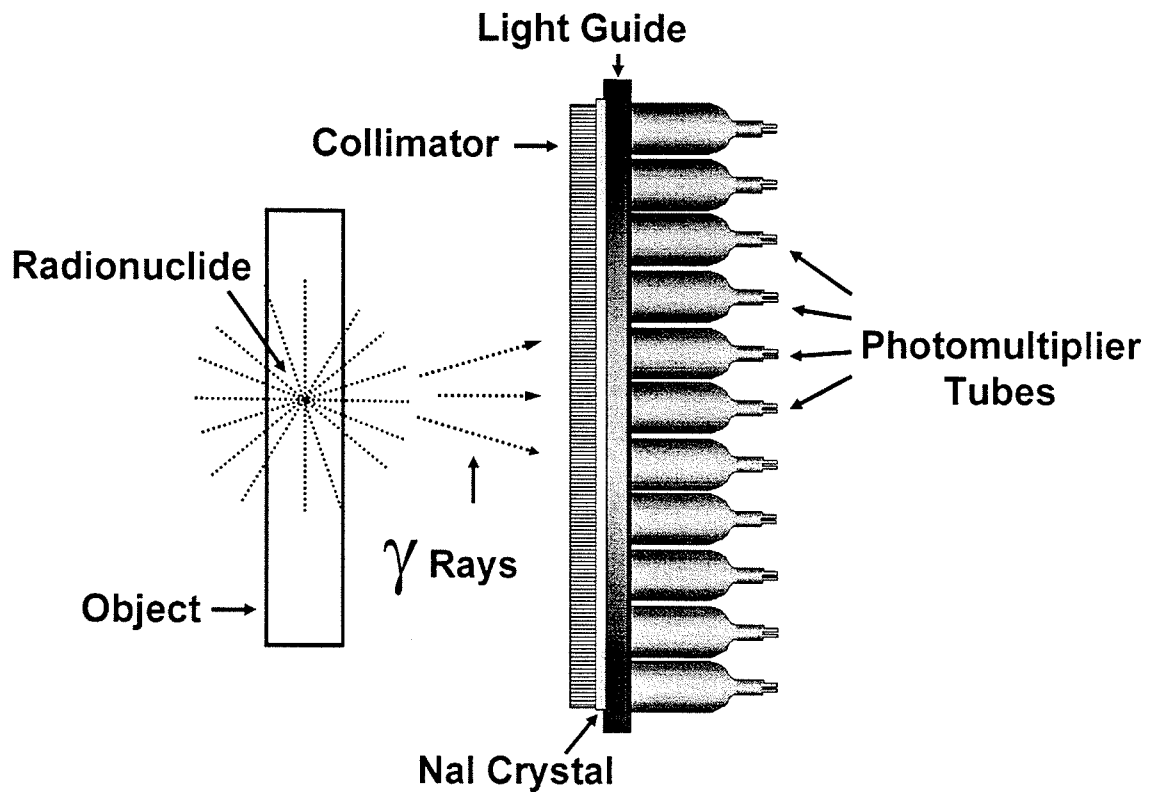


Figure 7.2: Basic principles and components of a gamma camera.

the crystal, a grid of photomultiplier tubes collect light for processing. The Siemens Orbiter has a NaI crystal with a diameter of 0.375 m and a total of 37 photomultiplier tubes. The principle components of the gamma camera are presented in Figure 7.2.

The brightness of each flash is proportional to the amount of energy deposited in the crystal, which is proportional to the energy of the incident photon. Thus, both the number and energy of incident photons can be recorded. Moreover, the collimator, attached to the NaI crystal, and position logic circuits relate the position of each scintillation to the X, Y coordinates of a two-dimensional projection image. The

electrical pulse generated by each of the photomultiplier tube is then discriminated to retain only the pulse that lies within a prescribed energy window. This task is achieved by pulse-height analyzer circuits. A retained pulse is known as a count. The output of the gamma camera corresponds to the count rates generated by the pulse-height analyzer circuits.

#### 7.4.3.3 Transformation of the output signal

The output from the gamma camera is analog and must, therefore, be converted to digital form by an analog-to-digital converter. After the X (horizontal) and Y (vertical) position signals of the gamma camera are digitized, their position values are used to generate matrices. The numeric value of each pixel represents the counts recorded at that particular location. In this study, count rates were stored in a 160x160 matrix. Once the digital form is memorized, images can be displayed with various contrasts and brightness, or stored for further and more detailed analysis on the NucLear MAC computer.

#### 7.4.3.4 Dynamic scanning

The Siemens Orbiter is capable of generating matrices in a dynamic mode. Dynamic investigation of sequential matrices is similar to the analysis of time-lapse photography. As soon as acquisition of the first matrix is completed, it immediately begins to collect a second matrix, and so on. The time interval between acquisition of matrices is set at the beginning of the acquisition process. It is possible to acquire matrices at a sub-second level. This allows for real-time detection of the tracer's spatial distribution and provides a powerful approach to visualizing and quantifying tracer displacement in dynamic flow studies. However, an acquisition time of 1 second per

matrix was sufficient to monitor breakthrough in the four soil columns. The breakthrough for certain soil columns was monitored for a period of over 3 hours. Matrices produced during the acquisition process are two-dimensional and can be recorded either as planar projection images or in a tomographic fashion.

#### 7.4.3.5 Planar imaging

A planar single photon images is a pictorial representation of the radioactive decay that emanates from within the patient or the object of interest. More precisely, it is a two-dimensional representation of a three-dimensional object. It depicts the radiopharmaceutical's three-dimensional distribution onto a planar two-dimensional surface producing a projection matrix. A planar single photon image is very similar to a standard radiograph, however, the photons do not pass through the object, but are emitted from within it. Planar imaging was performed on Columns 1, 2 and 3.

#### 7.4.3.6 Tomographic imaging

Tomographic single photon images are acquired by detecting radioactive decay activities from different angles around the object. This is accomplished by rotating the camera head around the object and recording data from multiple projections. The stand of the Orbiter supports and counterbalances the gamma camera to accomplish this task. The Orbiter is designed to allow the camera head to orbit around an object as shown in Figure 7.3. During its rotation, the gamma camera stops at predefined angles to record spatial distribution of the radioactive decay within the object's volume. These multiple planar single photon images are then stored in a computer until the entire object has been viewed from multiple angles. A series of cross-sectional images or matrices of the object

are then generated on the NucLear MAC computer using a filtered back-projection reconstruction algorithm. Tomographic imaging could be performed only on 0.4 m length at a time, due to the size of the gamma camera head. More precisely, nine SPECT sequences were performed to monitor the three-dimensional breakthrough at different times. The time required for SPECT acquisition was approximately 6 minutes. During that period, 64 planar matrices were recorded around the soil column. There should be no tracer

displacement during SPECT acquisition in order to accurately reconstruct the radioactive tracer's spatial distribution. For this purpose, the tracer was allowed to move during a period of 2 minutes prior to SPECT scanning. Then, the flow was interrupted in order to "freeze" convection through macropores. At that time, the scanning sequence was initiated. This operation was repeated nine times. Each time, 64 planar views of the tracer distribution were recorded by the NucLear MAC computer.

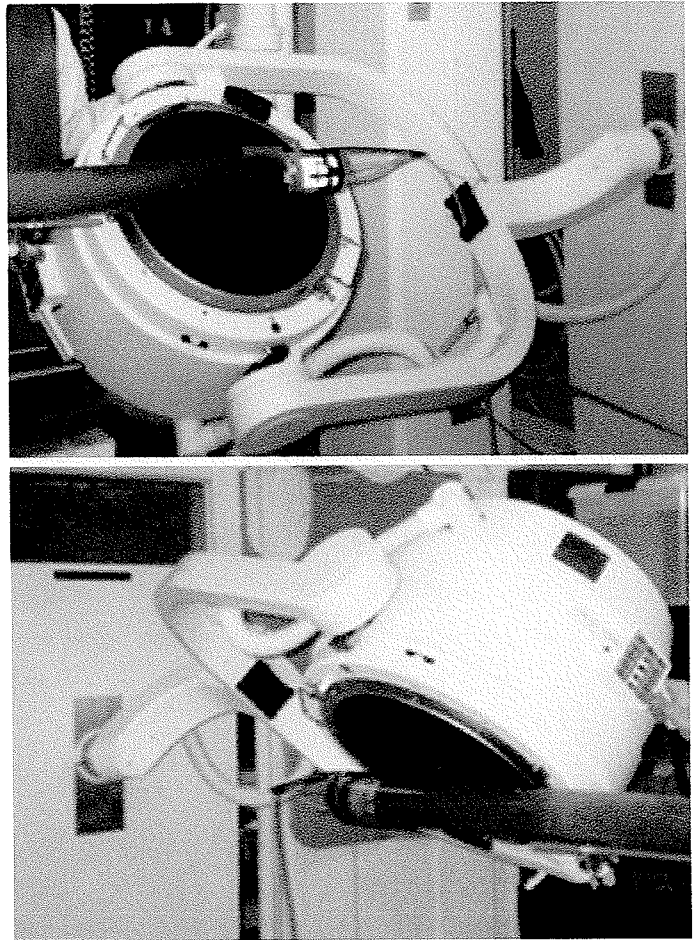


Figure 7.3: Rotation of the gamma camera around a column of soil.

#### 7.4.4 Radiopharmaceutical

As mentioned above, SPECT scanning involves the detection of gamma rays emitted from radioactive tracers called radiopharmaceuticals. Most radiopharmaceuticals consist of two parts: a radioactive label (i.e., radionuclides) and a molecule whose physical or chemical properties define the location on which the radiopharmaceutical will be adsorbed (Palmer et al., 1992). One or more atoms in the molecular structure of the radiopharmaceutical is, therefore, unstable. This instability results in emission of alpha, beta and gamma particles (Early and Sodee, 1995). As long as the photons emanating from the radionuclide have sufficient energy to escape, in significant numbers, from the object, images, that depict the spatial distribution of the radiopharmaceutical, can be generated.

Most common radiopharmaceuticals have short half-lives measured in hours or days. For instance, Technetium-99m ( $^{99m}\text{Tc}$ ) has a half-life of 6.02 hours (Hamilton et

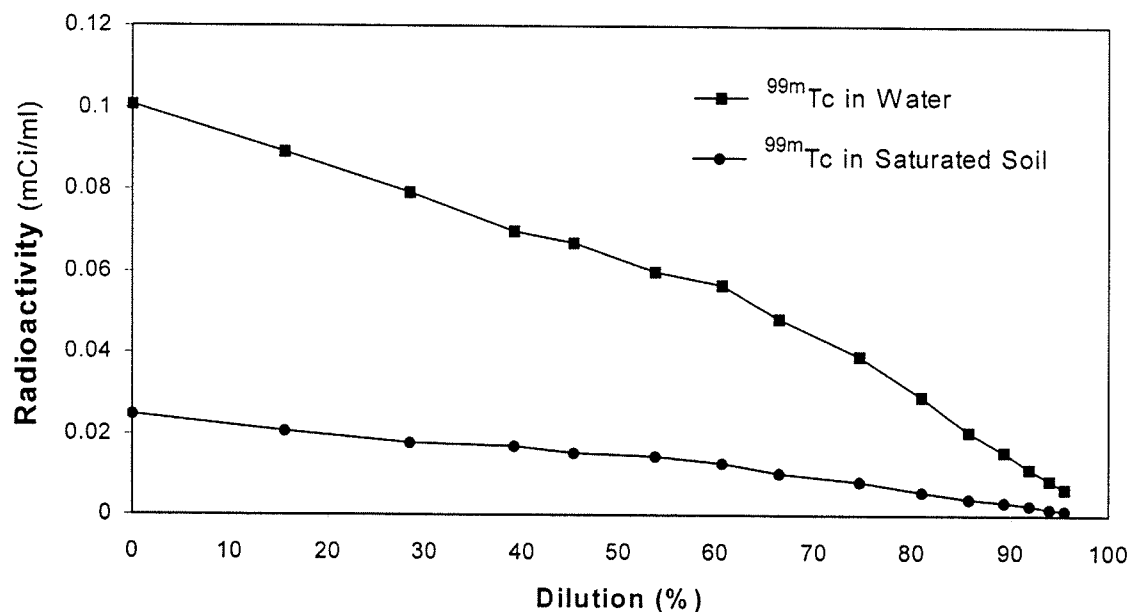


Figure 7.4: Comparison of the radioactivity level of Technetium in water and in soil at different concentrations.

al., 1997). Tc-99m is by far the most important radionuclide in current medical practice (Palmer et al., 1992). Technetium is usually generated in the form of sodium pertechnetate,  $\text{Na}^{99\text{m}}\text{TcO}_4^-$ . The pertechnetate ion is similar to iodide in its size and charge and is commonly used in dynamic flow studies for acquiring rapid sequential images. Moreover,  $\text{Na}^{99\text{m}}\text{TcO}_4^-$  is easily available, water soluble and requires no special preparation. Therefore,  $\text{Na}^{99\text{m}}\text{TcO}_4^-$  was selected for the present study. Several tests were conducted to evaluate the gamma camera's ability to pick up radioactive emissions from  $^{99\text{m}}\text{Tc}$  in saturated soil. A saturated soil column (0.1 m long x 0.1 diameter) was used for this purpose. A 2 ml vial containing the radioactive solution was placed in the center of the column. The radioactivity emitted from the vial (i.e.,  $^{99\text{m}}\text{Tc}$  in water) and from the core (i.e.,  $^{99\text{m}}\text{Tc}$  in saturated soil) was measured at several concentrations. The corrected radioactivity was calculated to account for radioactive decay. Results are shown in Figure 7.4. The linear relationship between concentration and corrected radioactivity level was verified for saturated soil. However, the reduction in radioactivity was found to be higher for  $^{99\text{m}}\text{Tc}$  in water. This suggests that saturated soil absorbs more gamma radiation at higher concentrations.

#### **7.4.5 Preprocessing of gamma camera output**

As mentioned above, the NucLear MAC computer is a high performance system for acquisition, display and post-processing data generated by the gamma camera. The NucLear MAC software follows standard user interface guidelines. After acquisition of the gamma camera output, the NucLear MAC was used to generate files containing 1000 matrices of 160x160 elements. Each matrix portrays 1 second of breakthrough in the soil columns. These files were saved in 8-bit Tagged Image File Format (TIFF). A program

called "Readg.pro" was written in the PV-WAVE language to read the TIFF files and to export them in ASCII format for further analysis on a Pentium II 300 MHz, equipped with 128 Mb of RAM.

The NucLear MAC software has a special module which allows reconstruction of cross-sectional matrices from planar views acquired in tomographic mode. This module was used to reconstruct the spatial distribution of  $^{99m}\text{Tc}$  in Column 4. More precisely, 160 cross-sections were generated for the nine times Column 4 was scanned in tomographic mode. Each cross-sectional matrix had a thickness of approximately 2.4 mm and contained 160x160 pixels. For each SPECT acquisition, the module stored the cross-sections in a three-dimensional matrix of 160x160x160 pixels. These matrices were then converted from TIFF to ASCII format using "Readg.pro". A second program (SPECTjo.pro) was developed for selection of a region of interest (ROI). Only part of the 160x160 cross-sectional matrices is actually used to investigate tracer distribution. The resulting matrix requires only 35 kilobytes of disc space and is composed of an array of 40 by 40 elements. "SPECTjo.pro" also contains a filtering subroutine to remove noise, created by the radioactive string that was used to delimit the boundaries of the columns. Two additional programs were developed in PV-WAVE to generate three-dimensional reconstructions of the tracer distribution in the soil Column. The first program (SPECT\_3-D.pro) combines the 40x40 matrices into 3-D arrays and stores them in binary I/O format. The second program (SPECT\_3-Dview.pro) produces a list of vertices and polygons that describes the three-dimensional distribution of technetium. The list of vertices and polygons is then used to generate 3-D images for visualization of the breakthrough.



## 7.5 Results and Discussion

### 7.5.1 Visualization of macropore flow

Most studies on the characterization of macropore flow consider the soil system to be a “black-box”. Knowledge of flow behavior in macropores has been inferred by analyzing tracer variations in one or more detection sites of a soil column or a field plot. Visual inspection of the tracer breakthrough would be a new and exciting step towards analysis of the preferential flow phenomenon.

Figure 7.5 shows a schematic representation of the tracer breakthrough in the top 0.4 m of one of the soil columns. As mentioned earlier, the inside diameter of the columns is 77 mm. The three-dimensional rendered surface represents the tracer’s spatial distribution. The vertical axis indicates the level of radioactivity.

Similar 3-D surfaces are shown in Figure 7.6. These surfaces represent tracer distributions in Column 1 at different times. The progression of the tracer front can be observed in chronological order from Figure 7.6(a) to 7.6(l). The breakthrough in Column 1

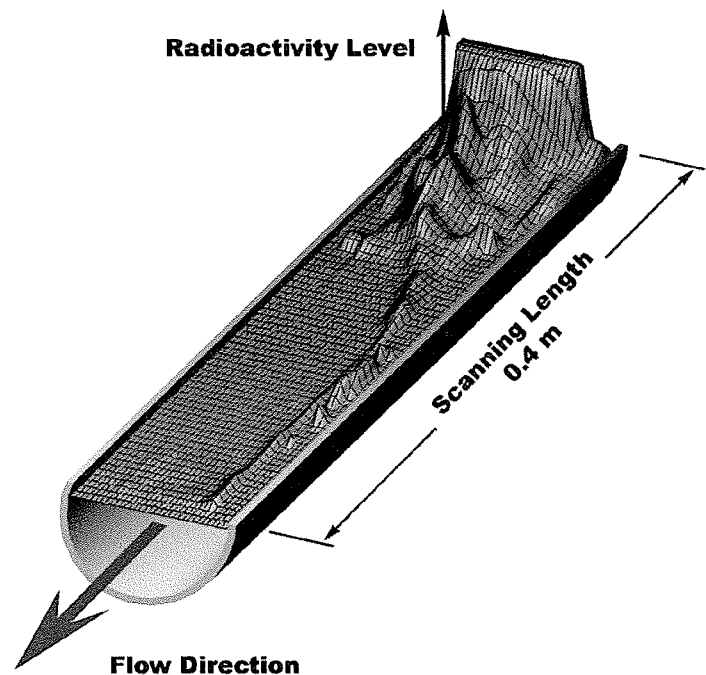


Figure 7.5: Schematic representation of the breakthrough of the radioactive tracer in the top region of one of the soil columns.

was monitored for a period of approximately 1 hour and 50 minutes. Only results for the first 1000 seconds (i.e., 16.6 minutes) of the breakthrough are presented here.

The flow rate was maintained at approximately 218 ml/min during the entire breakthrough in Column 1. The presence of technetium was detected 15 seconds after injection. Figure 7.6b shows that 50 seconds after injection, the very top section of the soil is nearly saturated with  $^{99m}\text{Tc}$ . Flux through a continuous macropore appears at time 75s (Figure 7.6c). The rise in radioactivity through that macropore is even clearer in Figure 7.6d and 7.6e. The region around it does not indicate the presence of radioactivity. This ascertains the occurrence of preferential flow. The plateau in the upstream section of the column slowly progresses in the flow direction.

In Figure 7.6f, radioactivity in the macropore has build up significantly. Moreover, it seems that flux through that macropore is branching out to the left, to another network. The tracer front in Figure 7.6f has moved down substantially. This suggests that between 125 and 150 seconds, the tracer reached a region of high macroporosity, where the tracer moves rapidly by convection or diffusion. 200 seconds after injection, radioactivity in the top 0.4 m of Column 1 reaches a maximum.

The tracer is flushed from the column after that time and the radioactivity level decreases. It is interesting to note that after 300 seconds, the large plateau in the top 1/3 of the column does not seem to progress anymore. In fact, it appears to be draining away from that region through the continuous macropore. From 400 to 1000 seconds after injection (Figure 7.6i to 7.6l), the tracer diffuses slowly through the soil matrix.

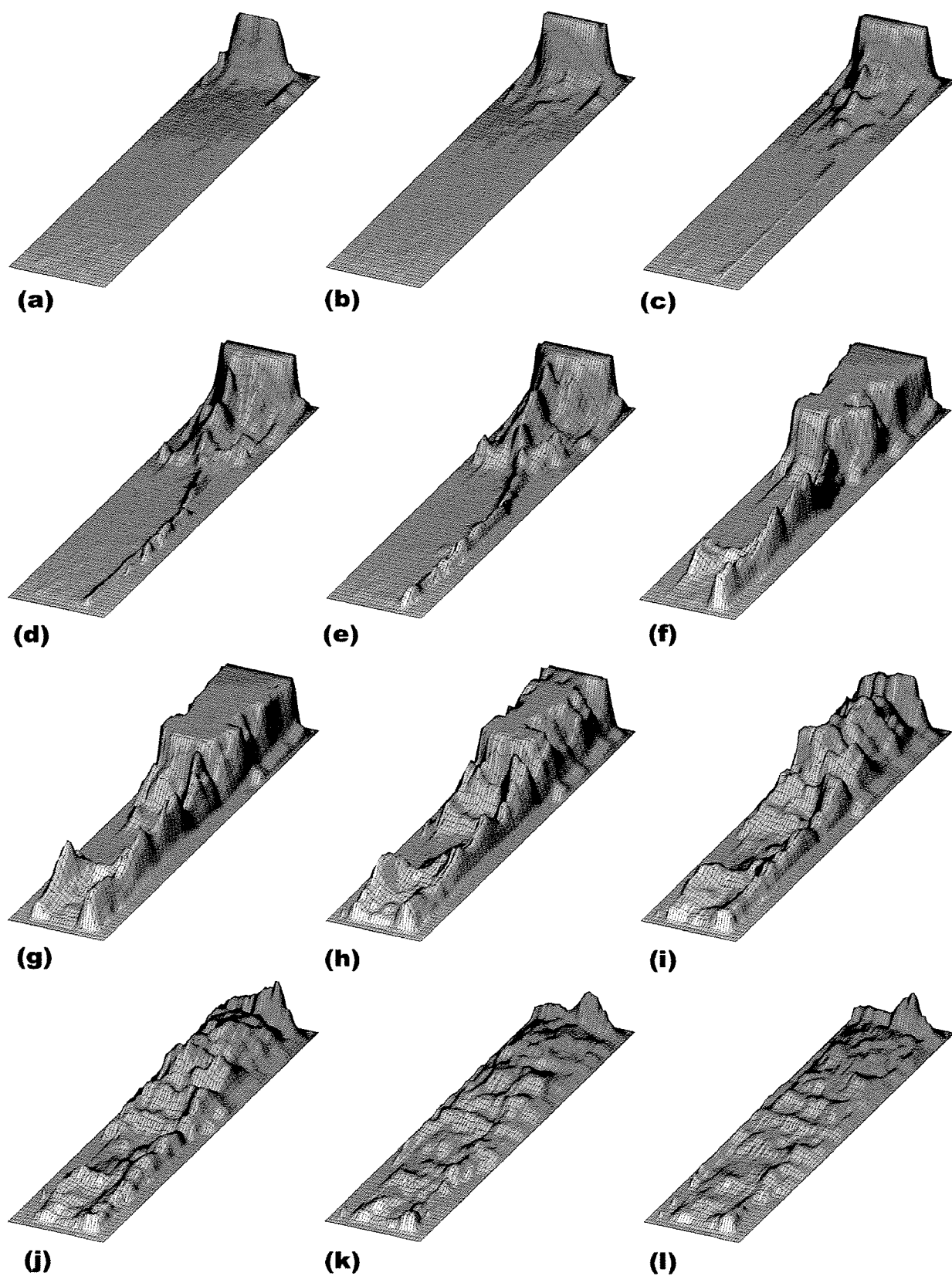


Figure 7.6: Three-dimensional representation of  $^{99m}\text{Tc}$  flux at different times after injection; (a) 25s, (b) 50s, (c) 75s, (d) 100s, (e) 125s, (f) 150s, (g) 200s, (h) 300s, (i) 400s, (j) 500s, (k) 750s and (l) 1000s in Column 1.

Figure 7.7 shows the relationship between macropore structure and tracer flux in Columns 1 (Fig. 7.7a,b) and 4 (Fig. 7.7c,d). Figures 7.7a and 7.7c show three-dimensional reconstructions of macropores, based on the CAT scan data (Perret et al. 1997, 1998b). Several macropores are displayed as orange, vertical, descending structures. Figures 7.7b and 7.7d show the tracer distribution in soil. These images were generated using a Gamma-II color palette in PV-WAVE, where dark blue represents low radioactivity and bright yellow indicates tracer saturation. If we compare the macropore structure to breakthrough in Column 1, it is quite obvious that the tracer moves preferentially

through a continuous macropore. Moreover, it is interesting to notice that not all macropores contribute to flow. The top region of Column 1 shows high macroporosity. Since the activities of arthropods, oligochaetes and plant roots tend to be more important



Figure 7.7: Relation between 3-D macropore space and tracer flux. 3-D reconstructions of macropore networks are shown for (a) Column 1 and (c) Column 4; the spatial distributions of tracer were evaluated at (b) 165 seconds in Column 1 and (d) 80 seconds in Column 4 after tracer injection.

close to the soil surface, this observation was anticipated. Figure 7.7b indicates clearly that this region of high macroporosity, organized in a complex network of interconnected macropores, allows the tracer to move rapidly.

As mentioned earlier, one of the soil columns was drilled from top to bottom in order to verify the gamma camera's ability to portray preferential flow. This artificial macropore can be seen in Column 4. Figure 7.7d clearly shows that breakthrough in Column 4 is occurring through the artificial macropore.

Three-dimensional reconstructions of the breakthrough in the top 0.4 m of Column 4 are shown for different times in Figure 7.8. There are 2 minutes separating each 3-D reconstruction. Figure 7.8a shows breakthrough 2 minutes after injection; 7.8b, 4 minutes after injection; 7.8c, 6 minutes after injection and so on.

In Figure 7.8a through 7.8i, the tracer is clearly visible in the artificial macropore.

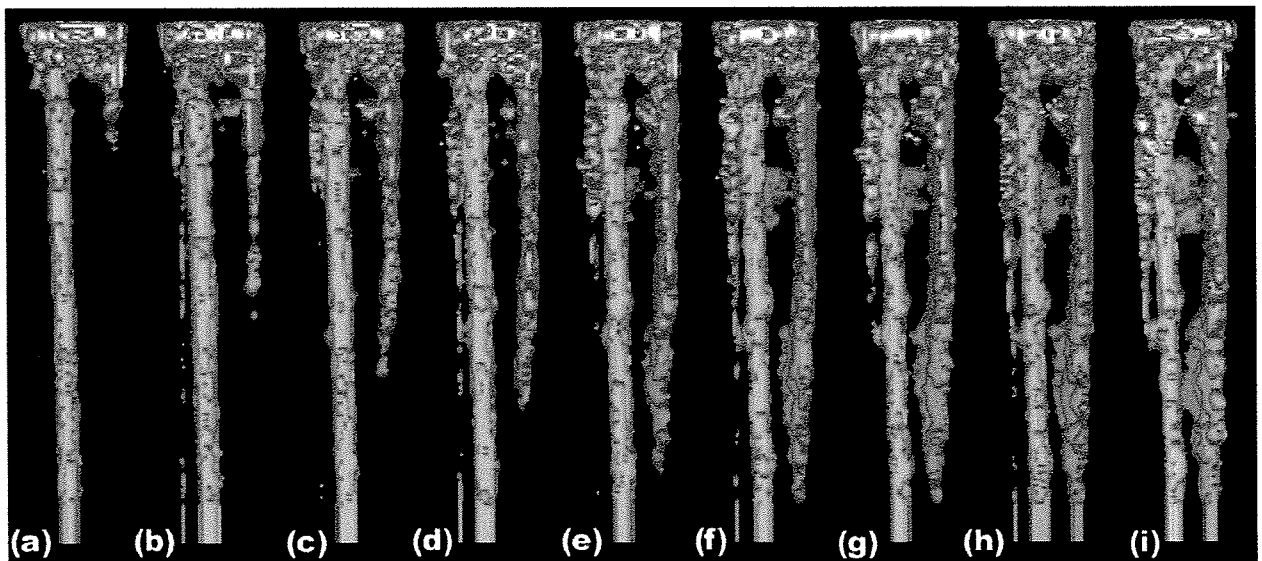


Figure 7.8: Three-dimensional reconstructions of the breakthrough in Column 4 obtained by SPECT scanning. The reconstructions represent 3-D tracer distribution at different time after injection: (a) 2 min; (b) 4 min; (c) 6 min; (d) 8 min; (e) 10 min; (f) 12 min; (g) 14 min; (h) 16 min; (i) 18 min.

Moreover, breakthrough can be seen along the side of the column. Although the tracer front in that region moves only a few centimeters per minute, this shows that edge flow has an impact on overall tracer transport.

### 7.5.2 Effluent breakthrough

Figure 7.9 shows breakthrough in the effluent for Columns 1, 2 and 3. The shape of the breakthrough curves are quite different from one column to another. Column 1 shows a maximum concentration before 1 pore volume. Czapar et al. (1992), Bouma (1991), and Singh and Kanwar (1991) pointed out that a breakthrough before a pore volume of one in an undisturbed soil column was an indication of macropore flow. The kurtosis of breakthroughs was calculated to characterize their degree of flatness. Kurtosis values of 0.9, -1.2, -1.5 were obtained for Columns 1, 2 and 3, respectively. The negative

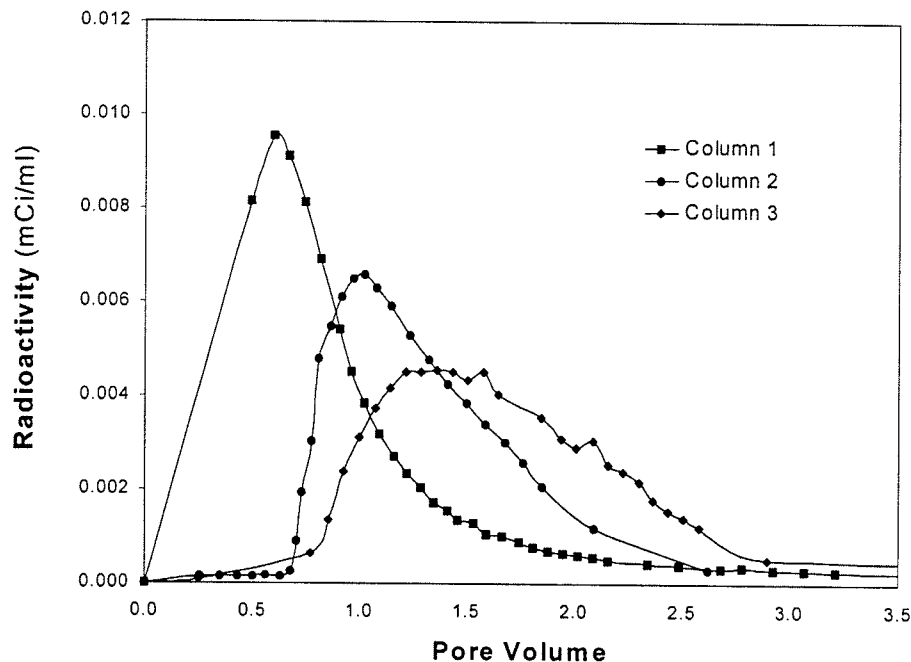


Figure 7.9: Breakthrough curves observed in the effluent of Columns 1, 2 and 3.

values for Column 2 and 3 indicate that the breakthroughs are more spread out. This explains why the maximum radioactivity level is lower in Columns 2 and 3 than that in Column 1. This also suggests that flow is occurring through pores of different shapes and sizes and that there has been substantial mixing and diffusion before the tracer reached the effluent. It took approximately 1.15 pore volumes to reach maximum radioactivity in the effluent of Column 2 and about 1.5 pore volumes for Column 3. Therefore, this suggests that the mobile pore-water fraction of soil did not move preferentially. Macropores observed in the three-dimensional reconstructions of Columns 2 and 3 (Perret et al., 1997) are very discontinuous as compared to those of Column 1. This may explain the differences obtained for breakthroughs in Columns 1, 2 and 3.

## **7.6 Summary and Conclusions**

We have demonstrated that SPECT scanning is a very powerful technique for studying flow through soil. This new approach allows analysis of flow patterns for radioactive tracers in 2-D, using planar imaging, and in 3-D, with the tomographic capabilities of SPECT devices. This technique not only provides qualitative data but also quantitative information on the spatial distribution of the tracer. Our results clearly depict preferential flow in large undisturbed soil columns. SPECT scanning opens new avenues for visualization and characterization of the preferential flow phenomenon.

## **7.7 Acknowledgements**

The authors wish to thank Dr. L. Hahn for initiating access to  $^{99m}\text{Tc}$  from the Foothills Medical Center, Calgary; Ingrid Koslowsky, for providing radioactive materials; and Barry Gulck, for the preparation of the radioactive tracer. The authors also

gratefully acknowledge the financial support provided by the Natural Sciences and Engineering Research Council of Canada (NSERC) and ESTAC (Environmental Science and Technology Alliance Canada).



## CHAPTER 8

### SUMMARY AND OVERALL CONCLUSIONS

---

The primary goal of this research project was to characterize, visualize and quantify soil macropores and preferential flow using X-ray CAT scanning and Single Photon Emission Computed Tomography (SPECT). The study was divided into three parts: ① 2-D and 3-D visualization and quantification of macropores using X-ray CAT scanning, ② breakthrough experiments in soil columns measured by X-ray CAT scanning and SPECT scanning, and ③ modeling of preferential flow and conservative solute transport in the macropore domain. A summary and conclusions is presented below for each of these three sections.

#### **8.1 2-D and 3-D Visualization and Quantification of Macropores using X-ray CAT Scanning**

In July of 1995, four undisturbed soil columns, 800 mm in length and 77 mm in diameter, were taken from a field site at the Macdonald Campus of McGill University in Ste-Anne-de-Bellevue, Québec. Column size was selected based on the need for a large enough sample to represent macropore distribution, yet small enough to be easily handled when full of soil. During the summers of 1995, 1996 and 1997, the soil columns were scanned under dry conditions. X-ray CAT scanning was used to reconstruct the complex three-dimensional arrangement of soil macropores in a non-destructive manner. During

CAT scanning, each soil column was fractionated in more than 94,000,000 pixels of  $195 \times 195 \mu\text{m}$ . This data was used to quantify and visualize soil macropores in both 2-D and 3-D. Based on the findings of this study, the following conclusions were drawn:

1. X-ray computed tomography is a very useful technique in estimating soil macroporosity of undisturbed soil columns. The ability of CAT scanning to visualize soil pore structure offers considerable potential for reliable characterization of soil macropores. In soil studies, the integration of computer programming in the PV-WAVE language and X-ray CAT scanning has given us the ability to investigate the interconnected pore space of large undisturbed soil columns to an unprecedented level.
2. Pores larger or equal to 1.0 mm in equivalent diameter were readily detected, visualized and quantified. The artificial network installed in one of the soil column was easily identified. Both the number of macropores and the surface area occupied by soil macropores decrease with depth. It was also observed that distance from the soil surface does not affect macropore size.
3. It was found that the average macroporosity of four soil columns varied between 2.1 and 3.8 %. Moreover, the macroporosity was found to decrease significantly with depth. Similarly, the number of macropores was decreasing by 0.7 % to 2.5 % over the entire depth of the soil columns.
4. It was observed that the soil profile exhibited two distinct regions. The first region (0 to 200 mm) showed a rapid decrease in number of macropores (i.e., from 3.8 to 12.9 %), whereas in the second region (200 to 720 mm), the number of macropores was not changing significantly with depth, having an average macropore count of 1400

per square meter. Moreover, it was found that macropore-size distributions exhibited a peak for all soil columns and at all depths, for macropores having an equivalent cylindrical diameter ranging from 2 mm to 4 mm. The number of macropores falling into this category decreased with depth.

5. From the hydraulic radius distribution, it was inferred that about 20 % of macropore throats have a diameter of 1.6 mm.
6. It was noted that the relative percentage of circular macropores increased with depth.
7. The spatial continuity of pixels in cross-sections of one soil column was studied using geostatistical analysis. Semi-variograms showed spatial dependency for most soil sections up to 17 mm. This limit on spatial dependence indicates the degree of spatial continuity. Moreover, geostatistical analysis indicates greater spatial variability in cross-sections of the topsoil.
8. The geometry and topology of macropore networks were determined using three-dimensional reconstruction techniques. Programs in PV-WAVE were developed to visualize the complex three-dimensional network of interconnected pore space. These 3-D reconstructions are unique. Our results suggest that the numerical density (i.e., number of networks per unit volume) varies between 13,421 to 23,562 macropore networks per cubic meter of soil. No direct relationship was observed between numerical density and macroporosity.
9. The position, length, volume and wall area of macropore networks were evaluated. It was found that the majority of macropore networks had a length of 40 mm, a volume of  $60 \text{ mm}^3$  and a wall area of  $175 \text{ mm}^2$ . However, some macropore networks,

although representing a small percentage, reached a length of 750 mm, a volume of  $10,000 \text{ mm}^3$  and a wall area of  $50,000 \text{ mm}^2$ .

10. The hydraulic radius, in three-dimensions, was also assessed as an indication of the networks' ability to convey water. It was found that the greater the network length, the greater their hydraulic radii. On average, macropore networks had a hydraulic radius of 0.13 mm.
11. Our results suggest that macropore inclination ranges from vertical to an angle of about 55 degrees from the vertical. The overall tendency of network inclination distributions suggests that the smaller the inclination, the greater the number of macropores.
12. Results for tortuosity indicate that the majority of networks had a tortuosity between 1 and 1.4. The mode of tortuosity distributions suggests that most macropore networks had a three-dimensional tortuous length 15% greater than the distance between its extremities. It was found that some macropore networks had a tortuosity as high as 2.4.
13. More than 60% of the networks are made up of 4 branches. The connectivity was assessed for one of the columns. Our results suggest that 82% of the networks had a connectivity of zero. The connectivity density was equal to 4772 non-redundant loops per cubic meter.

## **8.2 Breakthrough Experiments in Soil Columns Measured by X-ray CAT Scanning and SPECT Scanning**

Breakthrough of potassium iodide was monitored with the CAT scanner at thirteen depths in one of the soil columns, leaving a 50 mm interval between consecutive scans.

Before scanning, the soil column was placed vertically in the scanner unit and a hydraulic gradient of 0.1 m was maintained at the upstream face of the soil column to reach steady-state flow. The column was scanned at one of the thirteen positions every 45 seconds. 10 ml of effluent were sampled every 3 minutes to evaluate breakthrough in the effluent. This approach allows for real-time examination of flow mechanisms through soil macropores at various depths along the soil column length. Several computer programs were written in the PV-WAVE language to quantify the three-dimensional geometry of macropores and to characterize the spatial distribution of solute at thirteen depths in the soil column. With knowledge of macropore structure and spatial distribution of the solute, breakthrough in the macropore and matrix flow domains was evaluated.

SPECT scanning was also used for the real-time analysis, both in 2-D and in 3-D, of radioactive tracer flow patterns, in four soil columns. This technique has never been applied to soil. Thus, the objective of this study was to investigate the capabilities of SPECT scanning for visualizing preferential flow in soil. Our results characterized preferential flow very clearly in soil columns. SPECT scanning opens new avenues for tracer studies, both in 2-D and in 3-D, in porous media such as soil.

Based on the findings of these studies, several conclusions were drawn. They are listed below:

14. X-ray CAT scanning offers tremendous potential for non-destructive quantification of tracer volume concentrations inside soil columns during breakthrough experiments using potassium iodide. Not only does this innovative approach allow us to isolate flow regions, but it also allows us to monitor solute breakthrough in a non-destructive manner and in real-time at different soil depths.

15. SPECT scanning is a very powerful technique used to study solute movement through soils. This new approach allows for the analysis of radioactive tracer flow patterns in 2-D, using planar imaging, and in 3-D, with the tomographic capabilities of SPECT devices. This technique not only provides qualitative data but also quantitative information on the spatial distribution of the tracer. Our results clearly illustrate the occurrence of preferential flow in large undisturbed soil columns. SPECT scanning opens new avenues for visualization and characterization of the preferential flow phenomenon.
16. Flow in the matrix domain suggests that part of the matrix contains small pores that are connected to macropore networks. These pores contribute to rapid tracer build up in the matrix domain. They were identified as mesopores. This suggests that the matrix domain should be sub-divided into two regions: mesopores and micropores.
17. Flow in the macropore domain strongly indicates the presence of preferential flow. It also suggests that a fraction of the flow in macropores was relatively slow. This was due to the presence of dead-end branches or cavities which, from a geometrical point of view, belong to the macropore domain but do not behave as macropores since they do not contribute to preferential flow. This suggests that the macropore domain should be defined both in terms of macropore geometry and its ability to convey the tracer preferentially.

### **8.3 Modeling of Preferential Flow and Conservative Solute Transport**

Several researchers have pointed out the potential offered by multi-region modeling. However, the criteria used to define boundaries between flow regions have

been, till now, arbitrarily defined. Using the CAT scanner, a reliable technique to isolate and characterize flow domains was developed. Breakthroughs in the macropore and matrix flow domains were evaluated. The breakthrough curves measured in the matrix domain were fitted using the convection dispersion equation (CDE) with CXTFIT 2.0. The high regression coefficients obtained suggest that the CDE model describes breakthrough in the matrix domain quite well. Solute transport in the macropore domain was modeled using the analogy between macropore flow and pipe flow. The macropore domain was divided into two regions, namely the laminar and turbulent regions. A modified version of Poiseuille's law was used to model solute breakthrough in the laminar region. For the turbulent region, a new formula was derived, based on Manning's equation. Modifications were made so that these simple models would take into account the distribution density functions of macropore size and hydraulic radius. This approach appears to provide a reliable approximation of the overall tendency for breakthrough in the macropore domain. From this study, the following conclusions were drawn:

18. X-ray CAT scanning provides a reliable technique for isolating flow domains in soil.
19. Simulation results suggest that our new multi-region approach provides a fair approximation of the overall tendency for breakthrough in the macropore domain.

## **CHAPTER 9**

# **RECOMMENDATIONS FOR FUTURE RESEARCH**

---

In light of the findings and shortcomings encountered during the course of this study, several areas for further investigation have been identified. They are presented in four sections. The first section deals with improvements that should be made during extraction, preparation and scanning of large undisturbed soil columns. The second section presents several aspects of the CAT and SPECT data analysis and visualization that were found to be important and, therefore, that should be kept in mind for future research. In the ensuing section, several improvements to the modeling approach developed in this study are discussed. And finally, the last section opens discussion to new areas of research that would be interesting to explore after this study.

### **9.1 Recommendations for Extraction, Preparation and CAT**

#### **Scanning of Large Undisturbed Soil Cores**

1. In this study, soil cores were obtained by driving polyvinyl chloride (PVC) pipes into the soil with a backhoe. The lower end of the PVC pipe was shaped like a thin cutting edge in order to reduce compaction. In the future, it is recommended to apply grease inside the pipes to facilitate their insertion into the soil.



2. Due to the presence of small rocks, some PVC pipes were damaged and broken during their insertion. These rocks also created some cavities along the sides of the soil columns, resulting in edge-effect problems. In order to remedy this situation, a new extraction technique is proposed. This method is based on the use of a steel core barrel, designed to spring apart after core extraction. The core barrel will be hydraulically pressed into the soil during extraction and the intact soil column will be dislodged from the steel core barrel after it has been moved out of the soil. Once the soil column has been extracted, it will be placed in thermo-retractable plastic that will fit exactly over the soil by adapting its shape to the external irregularities of soil column surface. To strengthen the soil core, it could be encased in a PVC pipe. This new technique will significantly reduce the problems associated with the edge-effect.
3. During the summer of 1995, macroporosity in the soil columns was investigated by leaving a 20 mm space between consecutive scans. Information, such as macropores' tortuosity and connectivity, was, therefore, difficult to extract. In 1996 and 1997, no space was left between two consecutive scans and the analysis of 3-D macropore characteristics became unambiguous. It is recommended to follow this approach in future investigations.

## **9.2 Recommendations for Working with CAT and SPECT Data**

4. Both CAT scanning and SPECT scanning generate an overwhelming amount of information. For instance, more than 94,000,000 voxels were obtained with the CAT scanner for each soil column to describe their dry state. Thus, large storage space and a high level programming language, on a powerful computer, are essential for post-processing and manipulation of CAT scan and SPECT data. It was found that the use

of CD-ROMS is ideal for storage and working with data directly from a CD-ROM drive.

5. It is recommended that the programming language used for analysis of CAT and SPECT data has the ability to convert the 3-D ASCII array into Binary I/O format. The Binary I/O format is the simplest and most efficient form of I/O. Images and large data sets are usually stored and manipulated using Binary I/O in order to minimize the processing load on the computer. In this study, the PV-WAVE language was found to be adequate for this purpose.

### **9.3 Recommendations for Improving the Modeling Approach**

6. Flow in the matrix domain suggests that part of the matrix contains small pores that are connected to macropore networks. These pores contribute to rapid tracer build up in the matrix domain. They were identified as mesopores. Therefore, for modeling water flow and solute transport in the matrix domain, it is recommended that it be sub-divided into two regions: mesopores (i.e., equivalent cylindrical diameter (ECD) between 1000 and 10  $\mu\text{m}$ ) and micropores (i.e.,  $\text{ECD} < 10 \mu\text{m}$ ).
7. Flow in the macropore domain strongly indicates the presence of preferential flow. It also suggests that a fraction of the flow in macropores was relatively slow. This was due to the presence of dead-end branches or cavities which, from a geometrical point of view, belong to the macropore domain, but do not behave as macropores since they do not contribute to preferential flow. Therefore, it is recommended to define macropores both in terms of their geometry and of their ability to convey water and solute preferentially. In future research, the macropore domain should be thresholded

based on geometry (e.g.,  $ECD \geq 1000\mu m$ ) and on capacity to transport solute (i.e., predefined time to reach  $C/C_0=0.8$ ).

8. Solute transport in the macropore domain was modeled using the analogy between macropore flow and pipe flow. The macropore domain was divided into two regions, namely the laminar and turbulent regions. A modified version of Poiseuille's law was used to model solute breakthrough in the laminar region. For the turbulent region, a formula was derived based on Manning's equation. Modifications were made so that these simple models took into account the distribution density functions of macropore size and hydraulic radius. These density functions were obtained for every soil column cross-sections. However, no consideration was given to the relationship between distribution density functions of macropore size and the hydraulic radius between any two consecutive cross-sections. Therefore, it is recommended to modify the model so that it takes into account 3-D macropore parameters, such as connectivity and continuity. This can be achieved by obtaining the distribution density functions of macropore size and hydraulic radius for every macropore network that was isolated during the 3-D quantification of macroporosity.
9. The model developed in this study does not take into account solute transfer from the macropore domain to the matrix domain due to a concentration gradient. Considering radial diffusion from macropores to the matrix domain could lead to another improvement.
10. Since it is possible to isolate regions of interests in soil cross-sections, the outer column edges could be isolated and removed while analyzing flow through the

macropores. By considering only an inner core, the edge effect problems can be greatly reduced.

## 9.4 New Research Areas

10. In this study, the effect of preferential flow paths on water movement and non-reactive solute transport was evaluated in saturated conditions. When the soil is saturated, macropores have a dominant effect on water and solute transport. However, unsaturated soils below an infiltrating surface will behave differently since the soil matrix exerts capillary forces on water. Therefore, it would be quite interesting to use X-ray CAT scanning and SPECT scanning to study water and solute movement under unsaturated flow conditions.
11. Soil is a dynamic environment and its structure changes with time. In the present study, vegetation was removed from the top of the soil columns. The saturation and drying process removed or killed most earthworms and ants from the soil. Soil activities affecting macroporosity were restrained so that only little differences in soil structure were noticed from one year to another. However, the CAT scanning approach used in this research project can be extended to studies that also incorporate soil structural changes over time.
12. The analysis of macroporosity was performed for one soil type from a field site at the Macdonald Campus of McGill University in Ste-Anne-de-Bellevue. Our results are, therefore, site and soil specific. It would be quite interesting to investigate different types of soils from various locations so as to develop a relationship between macroporosity and soil physical properties, climatic factors, geographical location, and land use.

13. The presence of fractal geometry in geophysical systems is now well recognized by the research community. It would be useful to investigate fractal geometry of 3-D macropore networks and to see how it can provide a quantitative summary of the overall macropore structure.

## CHAPTER 10

## REFERENCES

---

- Ahuja, L.R., D.G. DeCoursey, B.B. Barnes and K.W. Rojas. 1993. Characteristics of macropore transport studied with the ARS root zone water quality model. *Transactions of the ASAE*, 36(2):369-379.
- Ahuja, L.R., K.E. Johnsen, and G.C. Heathman. 1995. Macropore transport of a surface - applied bromide tracer: model evaluation and refinement. *Soil Sci. Soc. Am. J.*, 59:1234-1241.
- Aley, T. 1977. A model for relating land use and ground water quality in southern Missouri. P. 232-332. In R.R. Dialmarter and S.C. Csallany (ed.). Hydraulic problems in karst regions. Western Kentucky University, Bowling Green, Kentucky, USA.
- Amin, M.H., R.J. Choley, K.S. Richards, B.W. Bache, L.D. Hall and T.A. Carpenter. 1993. Spatial and temporal mapping of water in soil by magnetic resonance imaging. *Hydro. Proc.*, 7:279-286.
- Anderson, J.L. and J. Bouma. 1977. Water movement through pedal soils: I. Saturated flow. *Soil Sci. Soc. Am. J.*, 41:413-418.
- Anderson, S.H., C.J. Gantzer, J.M. Boone and R.J. Tully. 1988. Rapid non-destructive bulk density and soil-water content determination by computed tomography. *Soil Sci. Soc. Am. J.*, 52:35-40.
- Anderson, S.H., R.L. Peyton, and C.J. Gantzer. 1990. Evaluation of constructed and natural soil macropores using X-ray computed tomography. *Geoderma*, 46:13-29.

- Anderson, S.H., R.L. Peyton, J.W. Wigger, and C.J. Gantzer. 1992. Influence of aggregate size on solute transport as measured using computed tomography. *Geoderma*, 53:387-398.
- Andreini, M.S. and T.S. Steenhuis. 1988. Preferential flow under conservation and conventional tillage. Paper 88-2633. *Am. Soc. Agr. Engr.*, St. Joseph, MI, USA.
- Asare, S.N., R.P. Rudra, W.T. Dickinson, and A. Fentser. 1995. Investigating soil macropores using a volume CT scanner. Presented at the 1995 CSAE annual meeting, Ottawa, Ontario, Canada. Paper No.95-110.
- Atkinson, D. 1991. *Plantgrowth: an ecological perspective*. Blackwell Scientific Publications. Oxford, London. UK.
- Aylmore, L.A.G. 1993. Use of computer-assisted tomography in studying water movement around plant roots. *Adv. Agron.*, 49:1-54.
- Bennie, A.T. 1991. Growth and mechanical impedance. P. 393-414. In Y Waisel, A. Eshel, U. Kafkafi (ed.). *Plant roots: the hidden half*. Marcel Dekker, Inc., New York, USA.
- Berker, A. and T.J. Tulig. 1986. Hydrodynamics of gas-solid flow in a catalytic cracker riser: implications for reactor selectivity performance. *Chem. Eng. Sci.*, 41(4):821-827.
- Beven, K. and P. Germann. 1981. Water flow in soil macropores, 2, a combined flow model. *J. Soil Sci.*, 32: 15-29.
- Beven, K. and P. Germann. 1982. Macropores and water flow in soils. *Water Resour. Res.*, 18: 1311-1325.
- Beven, K.J. 1981. Micro-, meso-, macroporosity and channeling flow in soil. *Soil Sci. Soc. Am. J.*, 45:1245.
- Beven, K.J. and P.C. Young. 1988. An aggregate mixing zone model of solute transport through porous media. *J. Contam. Hydrol.*, 3:128-143.
- Booltink, H.W. and J. Bouma. 1991. Physical and morphological characterization of bypass flow in a well-structured clay soil. *Soil Sci. Soc. Am. J.*, 5:1249-1254.
- Bottomley, P.A., H.H. Rogers and T.H. Foster. 1986. NMR imaging shows water distribution and transport in plant root systems in situ. *Proc. Natl. Acad. Sci.*, 83:87-89.

- Bouma, J. 1990. Using morphometric expressions for macropores to improve soil physical analyses of field soils. *Geoderma*, 46:3-11.
- Bouma, J. 1991. Influence of soil macroporosity on environmental quality. *Adv. Agron.*, 46:1-37.
- Bouma, J. 1981. Comments on " Micro-, meso-, and macroporosity of soil ". *Soil Sci. Soc. Am. J.*, 45:1244-1245.
- Bouma, J., A. Jongerius, O. Boersma, A. Jager and D. Schoonderbeek. 1977. The function of different types of macropores during saturated flow through four swelling soil horizons. *Soil Sci. Soc. Am. J.*, 41:945-950.
- Bouma, J., C.F. Belmans and L.W. Dekker. 1982. Water infiltration and redistribution in a silt loam sub-soil with vertical worm channels. *Soil Sci. Soc. Am. J.*, 46:917-921.
- Breve, M.A. 1994. Modeling movement and fate of nitrogen in poorly drained soils. Ph.D. Thesis, North Carolina State University, North Carolina, USA.
- Brewer, R. 1964. *Fabric and mineral analysis of soils*. Wiley, New York, USA.
- Brown, G.O., M.L. Stone, J.E. Gazin, and S.R. Clinkscale. 1994. Gamma ray tomography measurements of soil density variations in soil cores. p. 87-98. In S.H. Anderson, and J.W. Hopmans (ed.). Special publication no. 36. *Proceeding of Symposium on Tomography of soil-water-root processes*. Soil Sci. Soc. of Am. Inc. 677 South Segoe Road, Madison, WI, USA.
- Brown, L. R. 1989. Reexamining the World Food Prospect. p. 41-58. In: *State of the world*. W.W. Norton and Company, New York, USA.
- Bullock, P. and A.J. Thomansson. 1979. Rothamsted studies of soil structure. *J. Soil Sci.*, 30:391-414.
- Burges, A. and F. Raw. 1967. *Soil biology*. Academic Press, New York, USA.
- Carsel, R.F., C.N. Smith, L.A. Mulkey, J.D. Dean. 1995. PRZM-2, A model for predicting pesticide fate in the crop root and unsaturated soil zones. User manual for release 2.0 U.S. EPA, Athens, USA.
- Castellana, F.S. and B.A. Dudley. 1984. Imaging of particle motion in fluid-solid systems using a gamma camera. *Chem. Eng. Commun.*, 29:113-123.



- Castellana, F.S. and H.R. Hsu. 1984. Measurement of liquid film thickness on the surface of a partially immersed vertical rotating disc using a gamma camera. *Chem. Eng. Commun.*, 26:111-115.
- Castellana, F.S., M.I. Friedman, and J.L. Spencer. 1984. Characterization of mixing in reactor through analysis of regional tracer dilution data obtained with gamma camera. *AIChE J.*, 26:207-13.
- Chalier, G., S. Sakthikumar, V. Giry and Ph. Maquignon. 1995. Dual energy gamma-ray absorption technique applied to oil relative permeability determination during a tertiary gas gravity drainage experiment. SCA Conference, Paper Number 9510, San Francisco, USA.
- Chatzis I. and F. A. Dullien. 1977. Modelling pore structure by 2-D and 3-D networks with application to sandstones. *J. Can. Pet. Technol.*, 16:97-108.
- Chen, C. and R.J. Wagenet. 1992. Simulation of water and chemicals in macropore soils. Part 1. Representation of the equivalent macropore influence and its effect on soilwater flow. *J. of Hydrology*, 130:105-126.
- Chen, C., D.M. Thomas, R.E. Green and R.J. Wagenet. 1993. Two-domain estimation of hydraulic properties in macropore soils. *Soil Sci. Soc. Am. J.*, 57:680-686.
- Chesnokov, A.V., S.M. Ignatov, V.N. Potapov, S.B. Shcherbak and L.I. Urutskoev. 1997. Determination of surface activity and radiation spectrum characteristics inside buildings by a gamma locator. *Nuc. Inst. Meth. Phys. Res.*, 401(2-3):414-420.
- Cho, Z.H., J.P. Jones and M. Singh. 1993. Foundations of medical imaging. John Wiley & Sons, Inc., New York, USA.
- Clemente, R.S., S.O. Prasher and S.F. Barrington. 1993. PESTFADE, a new pesticide fate and transport model: Model development and verification. *Transactions of the ASAE*, 36(2):357-367.
- Coleman, R.E., R.A. Blinder and R.J. Jaszczak. 1986. Single Photon Emission Computed Tomography (SPECT) Part II: Clinical Applications. *Inv. Radiol.*, 21(1):1- 11.
- Constantinides G. N. and A. C. Payatakes. 1989. A three-dimensional network model for consolidated porous media. Basic studies. *Chem. Eng. Comm.*, 81:55-81.

- Crestana, S., R. Cesareo and S. Mascarenhas. 1986. Using a computed tomography mini-scanner in soil science. *Soil Sci.*, 142:56-61.
- Crestana, S., S. Mascarenhas, and R.S. Pozzi-Mucelli. 1985. Static and dynamic three-dimensional studies of water in soil using computed tomographic scanning. *Soil Sci.*, 140:326-332.
- Curry, J.P. 1994. *Grassland invertebrates*. Chapman and Hall, London, UK.
- Czapar, G.F., R. Horton, and R.S. Fawcett. 1992. Herbicide and tracer movement in soil columns containing an artificial macropore. *J. Environ. Qual.*, 21:110-115.
- Davis, J.R., M.J. Morgan, P. Wells, P. Shadbolt, and B. Suendermann. 1986. X-ray computed tomography. 1: A non-medical perspective. *Aust. Phys.*, 23:245-247.
- Dipietro, L. and F. Lafolie. 1991. Water flow characterization and test of a kinetic-wave model for macropore flow in a highly contrasted and irregular double-porosity medium. *J. Soil Sci.* 42:551-563.
- Dullien, F. A. L. 1979. *Porous media - Fluid transport and pore structure*. Academic Press, New York, USA.
- Dullien, F. A. L. 1992. *Porous media - Fluid transport and pore structure*. 2nd Ed. Academic Press, New York, USA.
- Dunn, G. H. and R. E. Phillips. 1991a. Macroporosity of a well-drained soil under no-till and conventional tillage. *Soil Sci. Soc. Am. J.*, 55:817-823.
- Dunn, G. H. and R. E. Phillips. 1991b. Equivalent diameter of simulated macropore systems during saturated. *Soil Sci. Soc. Am. J.*, 55:1244-1248.
- Dutilleul, P. and P. Legendre. 1993. Spatial heterogeneity against heteroscedasticity: an ecological paradigm versus a statistical concept. *Oikos*, 66:152-171.
- Early, P.J. and D.B. Sodee. 1995. Principles and practice of nuclear medicine. 2nd Ed., Mosby-Year book, Inc., St Louis, Missouri, USA.
- Edwards W.M., M.J. Shipitalo, L.B. Owens and L.D. Norton. 1990. Effect of lumbricus terrestris L. burrows on hydrology of continuous no-till corn fields. *Geoderma*, 46:73-84.
- Ehlers, W. 1975. Observations on earthworm channels and infiltration on tilled and untilled loess soil. *Soil Sci.*, 119:242-249.

- Englund, E. and A. Sparks. 1992. *Geo-EAS documentation*. U.S. Environmental Protection Agency, Las Vegas, Nevada, USA.
- Everts, C.J. and R.S. Kanwar. 1993. Interpreting tension-infiltrometer data for quantifying soil macropores: some particle considerations. *Transactions of the ASAE*, 36(2):423-428.
- Fish, A.N. and A.J. Koppi. 1994. The use of a simple field air permeameter as a rapid indicator of functional soil pore space. *Geoderma*, 63:255-264.
- Floyd, C.E., R.J. Jaszczak, C.C. Harris and R.E. Coleman. 1984. Energy and spatial distribution of multiple order Compton scatter in SPECT: a Monte Carlo investigation. *Phys. Med. Biol.*, 29(10):1217-1230.
- Follett, R. F. and D.J., Walker. 1989. Ground water quality concerns about nitrogen. *Dev. Agric. Managed-For. Ecol.*, 21:1-22.
- Germann, P. and K. Beven. 1981. Water flow in soil macropores, 1, Experimental approach. *J. Soil Sci.*, 32: 1-13.
- Germann, P.F. 1990. Preferential flow and the generation of runoff: 1. Boundary layer flow theory. *Water Resour. Res.*, 26:3055-3066.
- Germann, P.F., W.M. Edwards and L.B. Owens. 1984. Profiles of bromide and increased soil moisture after infiltration into soils with macropores. *Soil Sci. Soc. Am. J.*, 48:237-244.
- Gibbons, B. and S.C. Wilson. 1984. Do we treat our soil like dirt? *National Geographic*, 166:350-389.
- Glinski, J. and W. Stepniewski. 1985. *Soil aeration and its role for plants*. CRC Press, Inc. Boca Raton, Florida, USA.
- Greenberg, M., B. Greenberg and I. Greenberg. 1983. *Essentials of body computed tomography*. W.B. Saunders Compagny, Philadelphia, USA.
- Greenland, D.J. 1977. Soil damage by intensive arable cultivation: temporary or permanent ? *Philos. Trans. R. Soc. London*, Ser.B, 281:193-208.
- Grevers, M.C.J. and E. de Jong. 1994. Evaluation of soil-pore continuity using geostatistical analysis on macroporosity in serial sections obtained by computed tomography scanning. p. 73-86. In S.H. Anderson, and J.W. Hopmans (ed.). Special publication no. 36. *Proceeding of Symposium on Tomography of soil-*

*water-root processes*. Soil Sci. Soc. of Am. Inc. 677 South Segoe Road, Madison, WI, USA.

- Grevers, M.C.J., E. de Jong, and R.J. St. Arnaud. 1989. The characterization of soil macropores with CT scanning. *Can. J. Soil Sci.*, 69:629-637.
- Griffiths, F., J. Joshi and C. Ramesh. 1991. Change in pore size distribution owing to secondary consolidation of clays. *Can. Geotechnical J.*, 28(1):20-24.
- Grochulska, J. and E.J. Kladvko. 1994. A two-region model of preferential flow of chemicals using a transfer function approach. *J. of Environ. Qual.*, 23:498-507.
- Haaga, J.R., C.F. Lanzieri, D.J. Sartoris, and E.A. Zerhouni. 1994. *Computed tomography and magnetic resonance imaging of the whole body*. 3rd edition. Mosby Ed. St. Louis, USA.
- Hainsworth, J.M. and L.A.G. Aylmore. 1983. The use of computer-assisted tomography to determine spatial distribution of soil water content. *Aust. J. Soil Res.*, 21:435-443.
- Hamblin, A.P. 1985. The influence of soil structure on water movement, crop root growth, and water uptake. *Adv. Agron.*, 38:95-158.
- Hamilton, K., I. Wright, T. Zarabi, A. Kantzas and J. Perret. 1997. Applications of Single Photon Emission Computer Tomography (SPECT) in Flow Visualization and Particle Tracking. presented at the 47th Canadian Chemical Engineering Conference. October 5-8, 1997. Westin Hotel, Edmonton, Alberta, Canada.
- Hanson, J. E., L. K. Binning, R. A. Drieslien, D. E. Stoltenberg, M. A. Gehring, and M. A. Bonanno. 1991. A new method of validating pesticide preferential flow through three-dimensional imagery of soil pore structure and space using computed tomography. In T. J. Gish and A. Shirmohammadi (ed.). *Preferential flow Proceedings of the national symposium*. Am. Soc. of Agr. Engr., St Joseph, MI, USA.
- Harley, J.L. and R.S. Russell. 1979. *The soil-root interface*. Academic press. London, UK.
- Heijs, A.W.J., C.J. Ritsema and L.W. Dekker. 1996. Three-dimensional visualization of preferential flow patterns in two soils. *Geoderma*, 70:101-116.

- Heinze, D.J. 1994. Undisturbed soil core breakthrough analysis using X-ray computed tomography. M.S. Thesis, Dept. of Civil Engineering, University of Missouri, Columbia, MO, USA.
- Hendershot, W.H., H. Lalande and M. Duquette. 1993a. Ion exchange and exchangeable cations. P. 167-175. In M.R. Carter (ed.). *Soil sampling and methods of analysis*. Lewis Publishers, Boca Raton, USA.
- Hendershot, W.H., H. Lalande and M. Duquette. 1993b. Soil reaction and exchangeable acidity. P. 141-145. In M.R. Carter (ed.). *Soil sampling and methods of analysis*. Lewis Publishers, Boca Raton, USA.
- Hillel, D. 1980. *Fundamentals of soil physics*. Academic Press, Inc. New York, USA.
- Hillel, D. 1982. *Introduction to soil physics*. Academic Press, Inc. New York, USA.
- Hornberg, G.M., K.J. Beven and P.F. Germann. 1990. Inferences about solute transport in macroporous forest soils from time series models. *Geoderma*, 46: 249-262.
- Huang, Y.B. and C.C. Gryte. 1988. Gamma camera imaging of oil displacement in thin slabs of porous media. *J.Petrol Tech.*, 40:1355-1360.
- Huffman, R.L. and E.J. Monke. 1989. Dual porosity modeling in agricultural soils: theory. Paper 89-2095. *Am. Soc. Agr. Engr.*, St. Joseph, MI, USA.
- Hursh, C.R. 1944. Report of the subcommittee on subsurface flow. *Eos Trans. AGU*, 25:743-746.
- Hutson, J.L. and R.J. Wagenet. 1989. LEACHM (Leaching estimation and chemistry model). A user's guide. Department of Agronomy, Cornell University, Ithaca, NY, USA.
- Hutson, J.L. and R.J. Wagenet. 1995. A multi-region model describing water flow and solute transport in heterogeneous soils. *Soil Sci. Soc. Am. J.*, 59:743-751.
- Jabro, J.D., J.M. Jemison, R.H. Fox, and D.D. Fritton. 1994. Predicting bromide leaching under field conditions using SLIM and MACRO. *Soil Sci.*, 157:215-223.
- Jaszczak, R.J. 1988. Tomographic radiopharmaceutical imaging. *Proc. IEEE*, 76(9):1079-1094.
- Jessen, P.D. and P.H. Heyerdahl. 1988. Soil column descriptions from X-ray computed tomography density images. *Soil Sci.*, 146:102-107.

- Johnson, W.M., J.E. McCelland, S.B. McCaleb, R. Ulrich, W.G. Harper and T.B. Hutchings. 1960. Classification and description of soil pores. *Soil Sci.*, 89:319-321.
- Jones, A. 1982. X-ray fluorescence spectrometry in methods of soil analysis. In A. Page (ed.). *Methods of soil analysis, Part 2. Chemical and microbiological properties*. 2nd Edition. Series of Agronomy No. 9. American Society of Agronomy Inc. and Soil Science Society of America Inc. Madison, Wisconsin, USA.
- Jongnerius, A. 1957. *Morphologic investigation of the soil structure*. Meded. Stricht. Bodemkartering. Wageningen, The Netherlands, Bodem Stud., 2pp.
- Jonkers, G., E.A. Van Den Bergen and P.A. Vermont. 1990. Industrial applications of a gamma camera system. 1. Qualitative studies. *Appl. Rad. Iso.*, 41(10-11):1023-1031.
- Journel, A.G. and C.J. Huijbregts. 1978. *Mining geostatistics*. Academic Press, New York, USA.
- Jury, W. A. and G. Sposito. 1985. Field calibration and validation of solute transport models for unsaturated zone. *Soil Sci. Soc. Am. J.*, 45:671-672.
- Jury, W. A. and H. Flühler. 1992. Transport of chemicals through soil: mechanisms, models, and fields applications. *Adv. Agron.*, 47:141-201.
- Jury, W.A., W.R. Gardner. And W.H. Gardner. 1991. *Soil Physics*. 5th Edition. John Wiley and Sons ,Inc. New-York, USA.
- Kantzas, A. 1990. Investigation of physical properties of porous rocks and fluid flow phenomena in porous media using computer assisted tomography. *In-Situ*. 14(1):77-132.
- Kantzas, A. 1991. Determination of sulphur saturation in dolomitic sour gas reservoir using computer assisted tomography. *In-Situ*. 15(3):215-246.
- Kantzas, A. and I. Chatzis. 1988. Network simulation of relative permeability curves using a bond correlated-site percolation model of pore structure. *Chem. Eng. Comm.*, 69:191:214.
- Koppi, A. J. and A. B. McBratney. 1991. A basis for soil mesomorphological analysis. *Journal of Soil Sci.*, 42:139-146.

- Kumar, A. and R.S. Kanwar. 1997. Incorporating preferential flow and herbicide fate and transport into the DRAINAGE model. *Transactions of the ASAE*, 40(4):977-985.
- Kwiecien, M.J. 1987. Determination of pore size distributions of berea sandstone through three-dimensional reconstruction. M.S. Thesis. University Waterloo. Ontario, Canada.
- Kwiecien, M.J., I.F. Macdonald, and F.A.L. Dullien. 1990. Three-dimensional reconstruction of porous media from serial section data. *J. of Microscopy*, 159:343-359.
- Lajoie, P. and R. Baril. 1954. *Soil Survey of Montreal, Jesus and Bizard Islands in the Province of Quebec*. Queen's Printer. Ottawa, Canada.
- Lal, R. and B.A. Stewart. 1994. *Soil processes and water quality*. Lewis Publishers, Boca Raton, Florida, USA.
- Legoupil, S., G. Pascal, D. Chambellan and D. Bloyet. 1997. An experimental single photon emission computed tomograph method for dynamic 2-D fluid flow analysis. *Appl. Rad. Iso.*, 48(10-12):1507-1514.
- Li, Y. and M. Ghodrati. 1994. Preferential transport of Nitrate through soil columns containing root channels. *Soil Sci. Soc. of Am. J.*, 58:653-659.
- Li, Y. and M. Ghodrati. 1995. Transport of nitrate in soils as affected by earthworm activities. *J. Environ. Qual.*, 24:432-438.
- Liaghat, M. 1997. Use of soil and vegetative filter strips for reducing pesticide and nitrate pollution. Ph.D. Thesis. McGill University. Montreal, Quebec, Canada.
- Lien, J.R., A. Graue and K. Kolltveit. 1988. A nuclear imaging technique for studying multiphase flow in a porous medium at oil reservoir conditions. *Nuc. Inst. Meth.*, A271:693-700.
- Lin, J.S., M.M. Chen and B.T. Chao. 1985. A novel radioactive particle tracking facility for measurement of solids motion in gas fluidized beds. *AIChE J.*, 31:465-473.
- Logsdon, S. D. 1995. Flow mechanisms through continuous and buried macropores. *Soil Sci.*, 160:237-242.

- Logsdon, S. D., R. R. Allmaras, L. Wu, J. B. Swan and G. W. Randall. 1990. Macroporosity and its relation to saturated hydraulic conductivity under different tillage practices. *Soil Sci. Soc. of Am. J.*, 54:1096-1101.
- Logsdon, S.D., E.L. McCoy, R.R. Allmaras, and D.R. Linden. 1993. Macropore characterization by indirect methods. *J. Soil Sci.*, 155:316-324.
- Luxmoore, R.J. 1981. Micro-, meso-, and macroporosity of soil. *Soil Sci. Soc. Am. J.*, 45:671-672.
- Luxmoore, R.J., P.M. Jardine, G.V. Wilson, J.R. Jones and L.W. Zelazny. 1990. Physical and chemical controls of preferred path flow through a forested hillslope. *Geoderma*, 46:139-154.
- Ma, L. and H.M. Selim. 1994. Tortuosity, mean residence time, and deformation of tritium breakthroughs from soil columns. *Soil Sci. Soc. Am. J.*, 58:1076-1085.
- Ma, L. and H.M. Selim. 1997. Physical non-equilibrium modeling approaches to solute transport in soils. *Adv. Agron.*, 58: 95-153.
- Macdonald, I.F., P. Kaufmann, and F.A.L. Dullien. 1986. Quantitative image analysis of finite porous media: I. Development of genus and pore map software. *J. of Microscopy*, 144:277-296.
- Mallants, D., B.P. Mohanty, D. Jacques, and J. Feyen. 1995. Spatial variability of hydraulic properties in a multi-layered soil. *Soil Sci.*, 161(3):167-181.
- Marshall, T. J. and J. W. Holmes. 1988. *Soil Physics*. 2<sup>nd</sup> Ed. Cambridge University Press. Cambridge, UK.
- Marshall, T.J. 1959. Relations between water and soil. *Tech. Comm. 50*, Commonwealth Bur. Soils, Harpenden, U.K.
- Matheron, G. 1970. Quoted by J.R. Philip. *Annual Review of Fluid Mechanics*, Vol. 2, p.177.
- Mazziota, J.C. and S. Gilman. 1992. *Clinical brain imaging: principles and applications*. F.A. Davis Company, Philadelphia, USA.
- McCoy, E.L., C.W. Boast, R.C. Stehouwer and E.J. Kaldivko. 1994. Macropore hydraulics: taking a sledgehammer to classical theory. p. 303-348. In R. Lal, and B.A. Stewart (ed.). *Soil processes and water quality*. Lewis Publishers, Boca Raton, Florida, USA.



- McIntyre, D.S. 1974. Pore space and aeration determinations. p. 67-74. In J. Loveday (ed.). *Methods for analysis of irrigated Soils*. Common. Agric. Bur., Farnham Royal, Bucks, UK.
- Mehuys, G.R. 1995. *Soil Physics 372-331B. Laboratory Manual*. 5th Edition. Department of natural resources sciences. McGill University, Montreal.
- Moore, I.D., G.J. Burch and P.J. Wallbrink. 1986. Preferential flow and hydraulic conductivity of forest soils. *Soil Sci. Soc. Am. J.*, 50:876-881.
- Moran, C. J. and A. B. McBratney. 1992. Acquisition and analysis of three component digital images of soil pore structure. I. Method. *Journal of Soil Sci.*, 43:541-549.
- Moran, C. J., A. B. McBratney and A.J. Koppi. 1989. A rapid method for analysis of soil macropore structure. I. Specimen preparation and digital binary image production. *Soil Sci. Soc. Am. J.*, 53:921-928.
- Morgan, C.L., 1983. *Basic principles of computed tomography*. University Park Press. Baltimore, Maryland.
- Mottershead, G. and C.H. Orr. 1996. Gamma scanner for pre-decommissioning monitoring and waste segregation. *J. Inst. Nuc. Eng.*, 37(1):4-8.
- Munyankusi, E., S.C. Gupta, J.F. Moncrief, and E.C. Berry. 1994. Earthworm macropores and preferential transport in a long-term manure applied typic Hapludalf. *J. Environ. Qual.*, 23:773-784.
- Nelson, D.W. and L.E. Sommers. 1982. Total carbon, organic carbon, and organic matter. In A. Page (ed.). *Methods of soil analysis, Part 2. Chemical and microbiological properties*. 2nd Edition. Series of Agronomy No. 9. American Society of Agronomy Inc. and Soil Science Society of America Inc. Madison, Wisconsin, USA.
- Nielsen, D.R., M.T. Van Genuchten and J.W. Biggar. 1986. Water flow and solute transport in the unsaturated zone. *Water Resour. Res.*, 22:89-108.
- Office for Technology Assessment. 1990. *Beneath the bottom line : Agricultural approaches to reduce agricultural contamination of ground water*. Summary. U.S. Govt. Printing Office, Washington, DC, USA.
- Palmer, E., J.A. Scott and H.W. Strauss. 1992. *Practical nuclear medicine*. Saunders Company, Philadelphia, USA.

- Perret J.S., H. Pizarro, S.O. Prasher, A. Kantzas and C. Langford. 1996a. Quantification of soil macropores by computer assisted tomography. p 446-467. *In : Proceedings of the International Conference on Porous Media and its Applications*. K. Vafai and P. Shivakumar (ed.). Columbus, Ohio, USA.
- Perret J.S., H. Pizarro, S.O. Prasher, A. Kantzas and C. Langford. 1996b. Imaging and analysis of the pore structure of undisturbed soil columns by X-ray computed tomography. CSAE paper No: 96-106 presented to the 1996 *Annual Conference of the Canadian Society For Engineering in Agricultural, Food, and Biological Systems*. July 7-10, 1996 - Lethbridge, Alberta, Canada.
- Perret J.S., S.O. Prasher, A. Kantzas and C. Langford. 1997. 3-D visualization of soil macroporosity using X-ray CAT scanning. *J. Can. Agr. Eng.*, 39(4):249-261.
- Perret J.S., S.O. Prasher, A. Kantzas and C. Langford. 1998a. Characterization of macropore morphology in a sandy loam soil using X-ray computer assisted tomography and geostatistical analysis. *Can. Water Res. J.*, 23(2):143-165.
- Perret J.S., S.O. Prasher, A. Kantzas and C. Langford. 1998b. Three-dimensional quantification of macropore networks in undisturbed soil cores. Submitted to the *Journal of Agricultural Engineering Research*.
- Perret J.S., S.O. Prasher, A. Kantzas and C. Langford. 1998c. Development of a two-domain simulation approach using X-ray CAT scanning to model solute transport in a soil with preferential flow pathways. Submitted to the *Journal of Environmental Quality*.
- Perroux, K.M. and I. White. 1988. Designs for disc permeameters. *Soil Sci. Soc. of Am. J.*, 52:1205-1215.
- Petrovic, A.M., J.E. Siebert, and P.E. Rieke. 1982. Soil bulk density analysis in three-dimensions by computed tomographic scanning. *Soil Sci. Soc. of Am. J.*, 46:445-450.
- Peyton, L.R., S.H. Anderson, C.J. Gantzer, J.W. Wigger, D.J. Heinze, and H Wang. 1994a. Soil-core breakthrough measured by X-ray computed tomography. p. 59-71. *In* S.H. Anderson, and J.W. Hopmans (ed.). Special publication no. 36. *Proceeding of Symposium on Tomography of soil-water-root processes*. Soil Sci. Soc. of Am. Inc. 677 South Segoe Road, Madison, WI, USA.

- Peyton, L.R., C.J. Gantzer, S.H. Anderson, B.A. Haeffner and P. Pfeifer. 1994b. Fractal dimension to describe soil macropore structure using X-ray computed tomography. *Water Resour. Res.*, 30:692-700.
- Peyton, R.L., B.A. Haeffner, S.H. Anderson, and C.J. Gantzer. 1992. Applying X-ray CT to measure macropore diameters in undisturbed soil cores. *Geoderma*, 53:329-340.
- Phogat, V. K. and L. A. G. Aylmore. 1989. Evaluation of soil structure by using computer assisted tomography. *Aust. J. Soil Res.*, 27:313-323.
- Potter, M.C., D.C. Wiggert and M. Hondzo. 1997. *Mechanics of fluids*. 2<sup>nd</sup> Edition. Prentice Hall, Inc. Upper Saddle River. USA.
- Powel, M.S. and G.N. Nurick. 1996. Study of charge motion in rotary mills. Part 2 – experimental work. *Minerals Eng.*, 9(3):343-350.
- Prapaharan, S., D.M. White and A.G. Altschaeffl. 1991. Fabric of field- and laboratory-compacted clay. *J. of Geotechnical Engineering*. 117(12):1934-1940.
- Quisenberry, V.L. R.E. Philips and J.M. Zeleznik. 1994. Spatial distribution of water and chloride macropore flow in a well structured soil. *Soil Sci. Soc. Am. J.*, 58:1294-1300.
- Radulovich, R., E. Solorzano and P. Sollins. 1989. Soil macropore size distribution from water breakthrough curves. *Soil Sci. Soc. Am. J.*, 53:556-559.
- Reeves, M.J., D.G. Hall and P. Bullock. 1980. The effect of soil composition and environmental factors on shrinkage of some clayey British soil. *J. Soil Sci.*, 31:429-442.
- Ren, G.L., B. Izadi, B. King and E. Dowding. 1996. Preferential transport of bromide in undisturbed cores under different irrigations methods. *Soil Sci.* 161(4):214-225.
- Richter, J. 1987. *The soil as a reactor*. Catena Verlag. Cremlingen, Germany.
- Rogers, H.H. and P.A. Bottomley. 1987. In situ magnetic resonance imaging of roots: influence of soil type, ferromagnetic particle content, and soil water. *Agron. J.*, 79:957-965.
- Roseberg, R. J. and E. L. McCoy. 1990. Measurement of soil macropore air permeability. *Soil Sci. Soc. Am. J.*, 54:969-974.

- Roseberg, R. J. and E. L. McCoy. 1992. Tillage and traffic induced changes in macroporosity and macropore continuity: air permeability assessment. *Soil Sci. Soc. Am. J.*, 56:1261-1267.
- Roth, k., W.A. Jury, H. Flühler and W. Attinger. 1991. Field scale transport of chloride through an unsaturated field soil. *Water Resour. Res.*, 27:2533-2541.
- Russel, E.W. 1973. *Soil conditions and plant growth*. 10<sup>th</sup> ed. Longmans, London, UK.
- Sahimi, M. 1993. Flow phenomena in rocks: from continuum models to fractals, percolation, cellular automata, and simulated annealing. *Reviews of Modern Physics*, 65:1393-1534.
- Sahimi, M. 1995. *Flow and transport in porous media and fractured rock*. Weinheim. New-York, USA.
- Schumacher, W. 1864. *Die physik des bodens*. Berlin, Germany.
- Scott G.J.T., R. Webster and S. Nortcliff. 1988a. The topology of pore structure in cracking clay soil. I. The estimation of numerical density. *J. Soil Sci.*, 39:303-314.
- Scott G.J.T., R. Webster and S. Nortcliff. 1988b. The topology of pore structure in cracking clay soil. II. Connectivity density and its estimation. *J. Soil Sci.*, 39:315-326.
- Sedaghat, A., F. Castellana, R.H. Hsu and R.B. Macduff. 1988. Noninvasive technique for the evaluation of dispersion cross-flow at the inlet of a simulated fuel rod bundle. *Nuc. Tech.*, 80(3):360-370.
- Shepard, J. S., 1993. Using fractal model to compute the hydraulic conductivity function. *Soil Sci. Soc. Am. J.*, 57:300-306.
- Shipitalo, M.J. and W.M. Edwards. 1996. Effects of initial water content on macropore/matrix flow and transport of surface-applied chemicals. *J. Environ. Qual.*, 25:662-670.
- Singh, P. and R.S. Kanwar. 1991. Preferential solute transport through macropores in large undisturbed saturated soil columns. *J. Environ. Qual.*, 20:295-300.
- Singh, P., R.S. Kanwar and M.L. Thompson. 1991. Macropore characterization for two tillage systems using resin-impregnation techniques. *Soil Sci. Soc. Am. J.*, 55:1674-1679.

- Skopp, J. 1981. Comments on " Micro-, meso-, and macroporosity of soil ". *Soil Sci. Soc. Am. J.*, 45:1246.
- Smith, W.N., S.O. Prasher and S.F. Barrington. 1991. Evaluation of PRZM and LEACHMP on intact soil columns. *Transactions of the ASAE*, 34(6):2413-2420.
- Society of Nuclear Medicine (SNM). 1998. Internet address: <http://www.snm.org>.
- Steenhuis T.S., T.L. Richard, M.B. Parlange, S.O. Aburime and J.Y. Parlange. 1986. Preferential flow influences on drainage of shallow sloping soils. Paper No. 86-2551. *Am. Soc. Agr. Engr.*, St. Joseph, MI, USA.
- Steenhuis, T.S., J.Y. Parlange and M.S. Andreini. 1990. A numerical model for preferential solute movement in structured soils. *Geoderma*, 46:193-208.
- Steenhuis, T.S., S. Pacenka and K.S. Porter. 1987. MOUSE. A Management model for evaluating ground water contamination from diffuse surface sources aided with computer graphics. *Appl. Agric. Res.*, 2:277-289.
- Stewart, R.R. 1992. *Exploration seismic tomography: Fundamentals*. Vol. 3. S.N. Domenico Ed. University of Calgary. Alberta, Canada.
- Sutton, R.F. 1991. *Soil properties and root development in forest trees: a review*. *Forestry Canada*,. Information report O-X-413. Sault Ste. Marie, Ontario, Canada.
- Swift, M.J., O. W. Heal and J.M. Anderson. 1979. *Decomposition in terrestrial Ecosystems*, Blackwell Scientific Publications, Oxford, UK.
- Thomas, G.W. and R.E. Phillips. 1979. Consequences of water movement in macropores. *J. Environ. Qual.*, 8:149-152.
- Timlin, D.J., L.R. Ahuja and M. D. Ankeny. 1994. Comparison of three field methods to characterize apparent macropore conductivity. *Soil Sci. Soc. Am. J.*, 58:278-284.
- Tollner, E. W., D. E. Radcliffe, L. T. West, and P. F. Hendrix. 1995. Predicting hydraulic transport parameters from X-ray CT analysis. Paper: 95-1764. *Am. Soc. Agr. Engr.* St Joseph, MI, USA.
- Toride, N., F.J. Leij and M.Th. Van Genuchten. 1995. *The CXTFIT code for estimating transport parameters from laboratory or filed tracer experiments*- Version 2.0. Research Report No. 137. U.S. Salinity Laboratory. USDA, Riverside, California, USA.

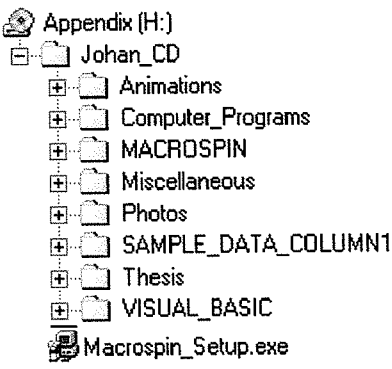
- Trojan, M.D. and D.R. Linden. 1992. Microrelief and rainfall effects on water solute movement in earthworm burrows. *Soil Sci. Soc. Am. J.*, 56:727-733.
- Van Genuchten, M.Th. 1990. Transport of water and solutes in macropores - preface. *Geoderma*, 46:1.
- Van Genuchten, M.Th. and P.J. Wierenga. 1976. Mass transfer studies in sorbing porous media. I. Analytical solutions. *Soil Sci. Soc. Am. J.*, 40:473-480.
- Vermeul, V. R., J. D. Istok, A. L. Flint, and J. L. Pikul. 1993. An improved method for quantifying soil macroporosity. *Soil Sci. Soc. Am. J.*, 57:809-816.
- Visual Numerics. 1994. *PV-WAVE personal edition for windows™ - User's Guide*. Boulder, Colorado, USA.
- Wagenet, R.J. and J.L. Germann. 1989. Concepts and models of water flow in macropore soils. Bull. 876. *Conn. Agric. Exp. Stn.*, New Haven, USA.
- Warner, G. S. 1990. Characterization of soil macropores by computed tomography. Ph.D. Thesis. University of Minnesota. Michigan, USA.
- Warner, G. S. and J. L. Nieber. 1988. CT scanning of macropores in soil columns. Paper No. 88-2632. *Am. Soc. Agr. Engr.*, St. Joseph, MI, USA.
- Warner, G. S., J. L. Nieber, I. D. Moore, and R. A. Geise. 1989. Characterizing macropores in soil by computed tomography. *Soil Sci. Soc. Am. J.*, 53:653-660.
- Watson, K.W. and R.J. Luxmoore. 1986. Estimating macroporosity in a forest watershed by use of a tension infiltrometer. *Soil Sci. Soc. Am. J.*, 50:578-582.
- White, R.E. 1985. The influence of macropores on the transport of dissolved and suspended matter through soil. *Adv. Soil Sci.*, 3:95-120.
- Wigger, J. 1991. Breakthrough analysis using X-ray computed tomography. M.S. Thesis, Dept. of Civil Engineering, University of Missouri, Columbia, MO, USA.
- Wilson, G.V. and R.J. Luxmoore. 1988. Infiltration, macroporosity, and mesoporosity distribution on two forested watersheds. *Soil Sci. Soc. Am. J.*, 52:329-335.
- Wood, M. 1989. *Soil biology*. Blackie and Son Ltd. London, UK.
- Wu, L., J. B. Swan, J. L. Nieber, and R. R. Allmaras. 1993. Soil macropore and layer influences on saturated hydraulic conductivity measured by borehole permeameters. *Soil Sci. Soc. Am. J.*, 57:917-923.

Zeng, Y., C.J. Gantzer, R.L. Peyton, and S.H. Anderson. 1996. Fractal dimension and lacunarity of bulk density determined with X-ray computed tomography. *Soil Sci. Soc. Am. J.*, 60:1718-1724.

# APPENDIX

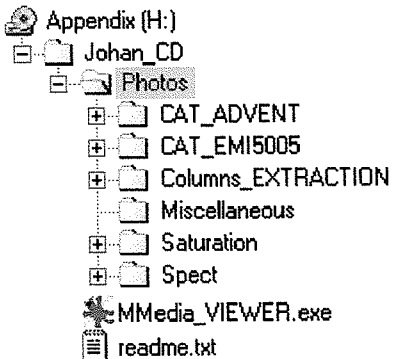
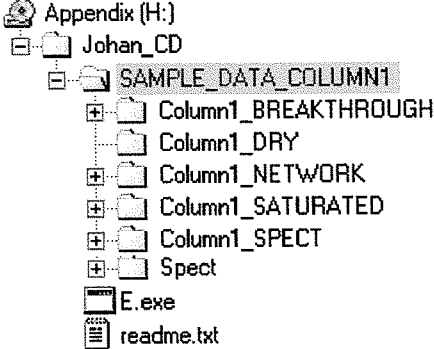
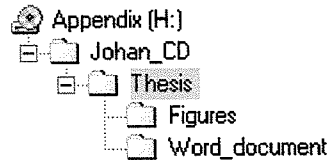
## CD content:

This table briefly presents the contents of the CD-ROM.

<b><i>Illustrations of the Subdirectories</i></b>	<b><i>Overview</i></b>
 <p>Appendix (H:)  Johan_CD  ├── Animations  ├── Computer_Programs  ├── MACROSPIN  ├── Miscellaneous  ├── Photos  ├── SAMPLE_DATA_COLUMN1  ├── Thesis  ├── VISUAL_BASIC  └── Macrospin_Setup.exe</p>	<p>The root directory of the CD-ROM contains a subdirectory called JOHAN_CD and several files necessary to install the MACROSPIN program on your PC. MACROSPIN is a small program which allows a user to visualize macropores in a soil column interactively. To run MACROSPIN, simply execute the Macrospin_setup.exe file. It will copy Visual Basic run-time and Macrospin.exe on your hard drive (less than 2 MB). After installation, you will be able to run the program from the WINDOW's Program menu. Make sure to insert the CD-ROM in the CD drive. To remove MACROSPIN go in the add/remove program section in the WINDOW's SETTING. It will remove all the MACROSPIN's components.</p> <p>In addition to MACROSPIN, the CD_ROM contains a lot of information (animations, computer programs, sample data, etc...) in the JOHAN_CD subdirectory. It is composed of 8 subdirectories that are presented below:</p>
	<p><u><i>Subdirectory ANIMATIONS</i></u></p> <p>Several computer animations generated in PV-WAVE language are presented here to display macropores in 2D (cross-sectional views and longitudinal views) and in 3D. In addition, animations of preferential flow in soil can be found</p>



<p>Appendix (H:)  Johan_CD  Animations  2D_Visualization  3D_Visualization  Introduction  Miscellaneous  SPECT_scanning  Tracer_Breakthrough  MMedia_VIEWER.exe  readme.txt</p>	<p>in the subdirectories SPECT_scanning (breakthroughs evaluated with the SPECT scanner) and Tracer_Breakthrough (breakthroughs measured with the CAT scanner). Some animations generated in 3-D STUDIO® show the CAT scan process and some introductory material (subdirectories Introduction and Miscellaneous).</p> <p><u>Note:</u> All of the animations are in AVI format. To view the animations, you can use the multimedia viewer by executing the file Mmedia_Viewer.exe</p>
<p>Appendix (H:)  Johan_CD  Computer_Programs  2D_Quantification  3D_Quantification  Breakthrough  Calibration_conversion  Geostats  Modeling  Spect  Visualization</p>	<p><u>Subdirectory COMPUTER PROGRAMS</u></p> <p>This subdirectory contains 8 subdirectories. Each subdirectory contains the computer programs (PV-WAVE code in ASCII format) developed in this research project. The names of the subdirectories describe the program category.</p>
<p>Appendix (H:)  Johan_CD  Animations  Computer_Programs  MACROSPIN  Miscellaneous  Photos  SAMPLE_DATA_COLUMN1  Thesis  VISUAL_BASIC</p>	<p><u>Subdirectories MACROSPIN and VISUAL BASIC</u></p> <p>These subdirectories contain the input files to run the program MACROSPIN (subdirectory MACROSPIN) and the visual basic code (subdirectory VISUAL_BASIC).</p>
<p>Appendix (H:)  Johan_CD  Miscellaneous  breakthrough  Cat_scanner_Calibration  CD_label  Geostatistics  Modeling  Quantification2D  Quantification3D  SOIL_ANALYSIS  Spect  Utilities  Visio  readme.txt</p>	<p><u>Subdirectory MISCELLANEOUS</u></p> <p>This subdirectory contains 11 subdirectories. The subdirectories Breakthrough, CAT scanner Calibration, Geostatistics, Modeling, Quantification2D, Quantification3D, Soil Analysis and SPECT contain Excel worksheets showing the data and the graphs presented in the thesis dissertation.</p> <p>The other subdirectories contain the CD label (subdirectory CD_label), the MS-Office service pack (subdirectory Utilities) and some figures generated in Visio (subdirectory Visio).</p>

 <p>Appendix (H:)</p> <ul style="list-style-type: none"> <li>Johan_CD <ul style="list-style-type: none"> <li>Photos <ul style="list-style-type: none"> <li>CAT_ADVENT</li> <li>CAT_EMI5005</li> <li>Columns_EXTRACTION</li> <li>Miscellaneous</li> <li>Saturation</li> <li>Spect</li> </ul> </li> <li>MMedia_VIEWER.exe</li> <li>readme.txt</li> </ul> </li> </ul>	<p><u><i>Subdirectory PHOTOS</i></u></p> <p>This subdirectory contains pictures of the experimental setup and scanning equipment (in BMP and JPEG format); the names of the subdirectories describe the categories of the pictures.</p> <p><u>Note:</u> <i>To view these photos, you can used the multimedia viewer by executing the file Mmedia_Viewer.exe</i></p>
 <p>Appendix (H:)</p> <ul style="list-style-type: none"> <li>Johan_CD <ul style="list-style-type: none"> <li>SAMPLE_DATA_COLUMN1 <ul style="list-style-type: none"> <li>Column1_BREAKTHROUGH</li> <li>Column1_DRY</li> <li>Column1_NETWORK</li> <li>Column1_SATURATED</li> <li>Column1_SPECT</li> <li>Spect</li> </ul> </li> <li>E.exe</li> <li>readme.txt</li> </ul> </li> </ul>	<p><u><i>Subdirectory SAMPLE DATA_COLUMN1</i></u></p> <p>This subdirectory contains sample data obtained by CAT and SPECT scanning for one of the soil columns (<i>column 1</i>).</p> <p><u>Note:</u> <i>The files are in ASCII format. To view these files, you can used the E-editor by executing the file E.exe</i></p>
 <p>Appendix (H:)</p> <ul style="list-style-type: none"> <li>Johan_CD <ul style="list-style-type: none"> <li>Thesis <ul style="list-style-type: none"> <li>Figures</li> <li>Word_document</li> </ul> </li> </ul> </li> </ul>	<p><u><i>Subdirectory THESIS</i></u></p> <p>This subdirectory contains the thesis document in MS-WORD format and the figures (in Gif and Jpeg format).</p>